

TOWARD SAFER, HIGH-PERFORMING PRODUCTS USING WELL-DEFINED  
NANOPARTICLES AND DELIBERATE FORMULATIONS

by

AURORA LEE GINZBURG

A DISSERTATION

Presented to the Department of Chemistry and Biochemistry  
and the Graduate School of the University of Oregon  
in partial fulfillment of the requirements  
for the degree of  
Doctor of Philosophy

September 2019

DISSERTATION APPROVAL PAGE

Student: Aurora Lee Ginzburg

Title: Toward Safer, High-Performing Products Using Well-Defined Nanoparticles and Deliberate Formulations

This dissertation has been accepted and approved in partial fulfillment of the requirements for the Doctor of Philosophy degree in the Department of Chemistry and Biochemistry by:

Victoria J. DeRose	Chairperson
James E. Hutchison	Advisor
Ramesh Jasti	Core Member
Kevin Van Den Wymelenberg	Institutional Representative

and

Janet Woodruff-Borden      Vice Provost and Dean of the Graduate School

Original approval signatures are on file with the University of Oregon Graduate School.

Degree awarded September 2019

© 2019 Aurora Lee Ginzburg

## DISSERTATION ABSTRACT

Aurora Lee Ginzburg

Doctor of Philosophy

Department of Chemistry and Biochemistry

September 2019

Title: Toward Safer, High-Performing Products Using Well-Defined Nanoparticles and Deliberate Formulations

The success of sustainable products in commerce relies on enhancing performance while minimizing environmental impacts. Avoiding the selection of alternatives that have unrealized negative consequences is of the utmost importance. Achieving these goals relies on understanding the fundamental relationships between material structure, function, and toxicity. Since innovation is often needed to access viable alternatives, novel materials that have established and controllable underlying chemistries are the most beneficial for preparing alternatives with desired properties. Nanomaterials are promising candidates for revolutionizing many technologies; they can impart sophisticated functionality with minimal material. However, they haven't seen widespread commercialization due to various roadblocks in harnessing their potential. Advances in synthetic and analytical methods that allow for rapid iteration and screening are poised to alleviate some of these challenges. This dissertation focuses on the development of adaptable synthetic methods to generate well-defined nanoparticles capable of fulfilling commercial needs.

This dissertation first introduces sustainable product design, particularly as it pertains to the development of nanomaterials. The synthetic and characterization

challenges faced at the nanoscale are highlighted, followed by advances in adaptable syntheses and high-throughput analysis. Additionally, the importance of evaluating nanomaterial performance and safety in environments representative of their commercial use is discussed. The following two chapters present novel single-step syntheses for accessing mixed-ligand gold nanoparticles with well-defined and tunable structures. The first study accesses gold nanoparticles that act analogously to traditional molecular reagents because of their clickable ligand shell, and the second study accesses partially cationic gold nanoparticles that have significantly reduced toxicity compared to nanoparticles with entirely cationic shells. The following two chapters demonstrate the importance of evaluating nanoparticle safety in formulas. The first study shows that a synergistic toxicity is produced by combining food-grade surfactants and non-toxic gold nanoparticles, and the second study shows that zinc oxide particles induce sunscreen toxicity upon UV irradiation. Finally, the last chapter of this dissertation presents a framework for teaching chemistry students to design sustainable products that offer both environmental and performance benefits.

This dissertation includes previously published and unpublished co-authored material.

## CURRICULUM VITAE

NAME OF AUTHOR: Aurora Lee Ginzburg

### GRADUATE AND UNDERGRADUATE SCHOOLS ATTENDED:

University of Oregon, Eugene OR  
California State University Channel Islands, Camarillo CA

### DEGREES AWARDED:

Doctor of Philosophy, Chemistry, 2019, University of Oregon  
Master of Science, Chemistry, 2015, University of Oregon  
Bachelor of Science, Chemistry, 2014, California State University Channel Islands

### AREAS OF SPECIAL INTEREST:

Nanomaterial Development  
Nanoparticle Synthesis  
Nanoparticle Toxicity

Green Chemistry  
Formulation Hazards and Toxicity  
Systems Thinking  
Product Design

### PROFESSIONAL EXPERIENCE:

Graduate Research Fellow, Hutchison Laboratory, University of Oregon, 2015-2019

Green Chemistry Consultant, WAYB, April-October 2018

Graduate Teaching Assistant, Department of Chemistry and Biochemistry, University of Oregon, 2014-2015

### GRANTS, AWARDS, AND HONORS:

Student Leadership in Sustainability, University of Oregon, 2019

Graduate Research Fellowship, National Science Foundation, 2016

Chemistry Department Honors, California State University Channel Islands, 2014

PUBLICATIONS:

Ginzburg, A. L.; Check, C. E.; Hovekamp, D. P.; Sillin, A. N.; Brett, J.; Eshelman, H.; Hutchison, J. E. Experiential Learning To Promote Systems Thinking in Chemistry: Evaluating and Designing Sustainable Products in a Polymer Immersion Lab. *J. Chem. Educ.* **2019**, ASAP.

Ginzburg, A. L.; Truong, L.; Tanguay, R. L.; Hutchison, J. E. Synergistic Toxicity Produced by Mixtures of Biocompatible Gold Nanoparticles and Widely Used Surfactants. *ACS Nano* **2018**, *12*, 5312–5322.

Elliott, E. W.; Ginzburg, A. L.; Kennedy, Z. C.; Feng, Z.; Hutchison, J. E. Single-Step Synthesis of Small, Azide-Functionalized Gold Nanoparticles: Versatile, Water-Dispersible Reagents for Click Chemistry. *Langmuir* **2017**, *33*, 5796–5802.

Wirth, R.; White, J. D.; Moghaddam, A. D.; Ginzburg, A. L.; Zakharov, L. N.; Haley, M. M.; Derosé, V. J. Azide vs Alkyne Functionalization in Pt(II) Complexes for Post-Treatment Click Modification: Solid-State Structure, Fluorescent Labeling, and Cellular Fate. *J. Am. Chem. Soc.* **2015**, *137*, 15169–15175.

Ginzburg, A. L.; Baca, N. A.; Hampton, P. D. The Isomerization of (-)-Menthone to (+)-Isomenthone Catalyzed by an Ion-Exchange Resin. *J. Chem. Educ.* **2014**, *91*, 1748–1750.

## ACKNOWLEDGEMENTS

I owe my deepest gratitude to my advisor, Dr. Jim Hutchison. I feel so grateful that through Jim's mentorship I was able to tailor my PhD and develop a skill set representative of my innate passions. I appreciate Jim's unwavering support of students irrespective of what career they are pursuing. Additionally, Jim has an uncanny ability to foresee the long-term potential of a science project and ask the nonobvious questions; regularly experiencing his thought process has improved my own scientific analysis greatly. Needless to say, working under his guidance has been an experience I will cherish for the rest of my life. I would like to thank the rest of my committee members, Dr. Vickie DeRose, Dr. Ramesh Jasti, and Dr. Kevin Van Den Wymelenberg, for making me feel supported and offering their insightful feedback. Vickie has given me great career advice and helped me to be less timid about networking, Ramesh's encouraging and approachable nature had a profound effect on me during my first year of graduate school, and Kevin's interest in sustainable products and technologies has helped me to see the importance and applications of this field beyond chemistry.

This dissertation was made possible through fruitful collaborations with incredibly talented people. I am thankful to have been a part of the toxicity collaboration with Dr. Robert Tanguay's group at OSU; working with him, Dr. Lisa Truong and Claudia Santillan has been a joy. I am so appreciative that Dr. Richard Blackburn from the University of Leeds wanted to work with me to develop the sunscreen project. Finally, working with Dr. Casey Check, WAYB and the 2018 master's students on the foam project was a huge learning experience and I am very proud of what a great team we all were.

I want to acknowledge some of my past mentors. I have had the fortune of not only having an exceptional graduate school advisor, but also an incredible undergraduate advisor, Dr. Phil Hampton. Phil made me fall in love with chemistry and research. He has helped me in times of uncertainty and has always offered the perfect balance of support and advice. During my REU at UCSB I worked in Dr. Javier Read de Alaniz's lab under Dr. Sameh Helmy's mentorship. They both taught me so much and prepared me for working in a graduate research lab.

The UO chemistry community has enhanced my graduate school experience significantly. Thanks to the incredible Hutch lab members who have made my time here so rich. Dr. Justin Barry provided significant assistance with the 2D NMR experiments. So many of the students here have incredible qualities that have influenced me professionally and personally. Additionally, I am so appreciative of the talented CAMCOR staff who are all so knowledgeable and friendly.

I couldn't have done this without my family's support. They have always taught me about the importance of education while giving me the freedom to choose my own path. My mom never let the Oregon-California distance feel too far with our frequent communications. Over the past five years Forrest has become part of my family too, and I am forever thankful that we both decided to come to UO in 2014.

I would like to acknowledge the significant financial support I received from the NSF Graduate Research Fellowship Program under Grant DGE-1309047. This research was also supported by a grant from the NSF (1512755) and NSF Partnerships for Innovation: Building Innovation Capacity program (IIP- 1237890). The NMR instrument facility at the University of Oregon is supported by the NSF (CHE-1427987).

## TABLE OF CONTENTS

Chapter	Page
I. INTRODUCTION .....	1
Development of a New Class of Materials .....	1
The Evolution of Nanotechnology .....	3
Challenges in Deliberate Nanomaterial Development.....	5
Relating Nanoparticle Architecture to Performance.....	5
Influence of Mixture Composition on Nanomaterial Performance. ....	10
Dissertation Overview .....	12
Bridge to Chapter II .....	13
II. SINGLE-STEP SYNTHESIS OF SMALL, AZIDE-FUNCTIONALIZED GOLD NANOPARTICLES: VERSATILE, WATER-DISPERSIBLE REAGENTS FOR CLICK CHEMISTRY .....	15
Introduction.....	15
Experimental .....	19
Materials .....	19
Synthesis of N <sub>3</sub> -EG <sub>3</sub> -BS Ligand.....	20
Synthesis of N <sub>3</sub> -EG <sub>3</sub> -AuNP-EG <sub>3</sub> .....	20
Click Reactions with N <sub>3</sub> -EG <sub>3</sub> -AuNP-EG <sub>3</sub> .....	21
Characterization .....	21
Instrumentation .....	21
NMR Spectroscopy- Analysis of NP Purity and Analysis of Decomposed NPs for Estimating Mixed Ligand Composition .....	22
Nanoparticle Core Size Determination Using SAXS .....	23
TEM of Purified N <sub>3</sub> -EG <sub>3</sub> -AuNP-EG <sub>3</sub> and 1-triazole-EG <sub>3</sub> -AuNP-EG <sub>3</sub> for Analysis of Morphology .....	23

Chapter	Page
UV-Visible Spectroscopy of Purified N <sub>3</sub> -EG <sub>3</sub> -AuNP-EG <sub>3</sub> and 1-triazole-EG <sub>3</sub> -AuNP-EG <sub>3</sub> .....	23
Fluorescence Spectroscopy of Purified N <sub>3</sub> -EG <sub>3</sub> -AuNP-EG <sub>3</sub> and 1-triazole-EG <sub>3</sub> -AuNP-EG <sub>3</sub> to Verify the Efficacy of the Strain Promoted AAC Reaction .....	24
Results and Discussion .....	24
AuNP Design and Synthesis .....	24
Characterization of N <sub>3</sub> -EG <sub>3</sub> -AuNP-EG <sub>3</sub> .....	27
Characterization of Clicked AuNPs.....	29
Conclusions.....	32
Bridge to Chapter III.....	34
<b>III. PROTECTIVE EFFECT OF PEG LIGANDS ON CATIONIC GOLD NANOPARTICLE TOXICITY .....</b>	<b>35</b>
Introduction.....	35
Results and Discussion .....	38
Nanoparticle Preparation .....	38
Toxicity Analysis of TMAT/MEEE-AuNPs .....	39
Effect of a shorter PEG chain on Mixed-Ligand AuNP toxicity .....	41
Interactions Between TMAT/MEEE-AuNPs and a Model Protein.....	43
Conclusions.....	45
Methods.....	47
AuNP Synthesis .....	47
Quantification of AuNP ligand shell components .....	48
Zebrafish Toxicity Testing.....	49
Assessment of BSA/AuNP Interactions.....	50

Chapter	Page
Bridge to Chapter IV .....	51
<b>IV. SYNERGISTIC TOXICITY PRODUCED BY MIXTURES OF BIOCOMPATIBLE GOLD NANOPARTICLES AND WIDELY USED SURFACTANTS .....</b>	<b>53</b>
Introduction.....	53
Results and Discussion .....	57
AuNP and PS20 exhibit a synergistic toxicity <i>in vivo</i> .....	59
PS20 and MEEE-AuNPs interact to form assemblies .....	62
Examining potential mechanisms for synergistic toxicity .....	69
Other common surfactants have synergistic interactions with MEEE-AuNPs.....	71
Conclusions.....	73
Methods.....	75
Chemicals.....	75
Preparation and Characterization of MEEE-AuNPs.....	76
Zebrafish Care and Husbandry .....	77
Nanoparticle delivery.....	77
Developmental toxicity screen.....	78
2D NMR spectroscopy on AuNPs plus surfactant.....	79
Gold tissue concentration.....	80
Bridge to Chapter V .....	81
<b>V. ZINC OXIDE INDUCED CHANGES TO SUNSCREEN EFFICACY AND TOXICITY UNDER UV IRRADIATION.....</b>	<b>83</b>
Introduction.....	83
Methods.....	86
Materials .....	86

Chapter	Page
Sun Filter Mixture Formulation .....	87
UV-Exposure .....	87
Absorbance Measurements .....	88
Preparation of Solutions for Animal Exposure.....	88
Zebrafish Husbandry/Developmental Exposures .....	88
Results.....	89
Sun Filter Mixtures Containing Small-Molecules .....	89
Sun Filter Mixtures Containing Small-Molecules and ZnO.....	95
Conclusions.....	99
Bridge to Chapter VI.....	102
<b>VI. EXPERIENTIAL LEARNING TO PROMOTE SYSTEMS THINKING IN CHEMISTRY: EVALUATING AND DESIGNING SUSTAINABLE PRODUCTS IN A POLYMER IMMERSION LAB.....</b>	<b>103</b>
Introduction.....	103
Systems Thinking to Guide Green Chemistry .....	108
Overview and Impact of Workshops .....	110
Implementation of Workshops.....	115
Workshop I.....	115
Workshop II. ....	117
Workshop III.....	121
Findings and Future Outlook .....	125
Bridge to Chapter VII .....	129
<b>VII. CONCLUSION .....</b>	<b>130</b>
Concluding Remarks.....	130
<b>APPENDICES .....</b>	<b>134</b>

Chapter	Page
A. SUPPORTING INFORMATION FOR CHAPTER II: SINGLE-STEP SYNTHESIS OF SMALL, AZIDE-FUNCTIONALIZED GOLD NANOPARTICLES: VERSATILE, WATER-DISPERSIBLE REAGENTS FOR CLICK CHEMISTRY .....	134
B. SUPPORTING INFORMATION FOR CHAPTER III: PROTECTIVE EFFECT OF PEG LIGANDS ON CATIONIC GOLD NANOPARTICLE TOXICITY .....	157
C. SUPPORTING INFORMATION FOR CHAPTER IV: SYNERGISTIC TOXICITY PRODUCED BY MIXTURES OF BIOCOMPATIBLE GOLD NANOPARTICLES AND WIDELY USED SURFACTANTS .....	163
D. SUPPORTING INFORMATION FOR CHAPTER V: ZINC OXIDE INDUCED CHANGES TO SUNSCREEN EFFICACY AND TOXICITY UNDER UV IRRADIATION.....	179
E. SUPPORTING INFORMATION FOR CHAPTER VI: EXPERIENTIAL LEARNING TO PROMOTE SYSTEMS THINKING IN CHEMISTRY: EVALUATING AND DESIGNING SUSTAINABLE PRODUCTS IN A POLYMER IMMERSION LAB.....	182
REFERENCES CITED.....	198

## LIST OF FIGURES

Figure	Page
Figure 1.1 Architectural features on a NP that are important for understanding properties.....	7
Figure 1.2 Key parameters for consideration when designing or interpreting NP toxicity assays. ....	9
Figure 2.1 Schematic of the one-step flow-based synthesis of azide-terminated, mixed monolayer AuNPs.....	26
Figure 2.2 Characterization of 1-triazole-EG <sub>3</sub> -AuNP-EG <sub>3</sub> .....	30
Figure 2.3 NMR spectra of N <sub>3</sub> -EG <sub>3</sub> -AuNP-EG <sub>3</sub> and 7-triazole-EG <sub>3</sub> -AuNP-EG <sub>3</sub> .....	32
Figure 3.1. AuNPs with varying ratios of cationic ligand (TMAT) to PEG ligand (MEEE) studied in this work. ....	37
Figure 3.2. Mortality caused by each set of AuNPs over 5 days.....	41
Figure 3.3. MEEE/TMAT-AuNP versus MEE/TMAT-AuNP.....	42
Figure 3.4. Extent of BSA/AuNP Aggregation. ....	44
Figure 4.1 Structure of the nanoparticles, mercaptoethoxyethoxyethanol (MEEE) stabilized gold nanoparticles (AuNPs), and primary surfactant, Polysorbate 20 (PS20), studied in this work.....	56
Figure 4.2 Mortality profiles of 1.0 nm AuNPs at 24 hpf in embryonic zebrafish.....	60
Figure 4.3 2D DOSY spectrum for MEEE-AuNP <sub>1.0 nm</sub> in D <sub>2</sub> O. ....	65
Figure 4.4 Summary of DOSY data tracking MEEE-AuNP <sub>1.0 nm</sub> growth in the presence of varying concentrations PS20 over 18 hrs. ....	67
Figure 4.5 Concentration of PS20 versus zebrafish mortality.....	68
Figure 4.6 Tissue concentration after exposure to gold, as determined by ICP-MS. ....	71
Figure 4.7 Structures of additional surfactants studied <i>in vivo</i> .....	72
Figure 5.1. UV-Vis spectra showing photodegradation of Mixtures 1-5 measured in 99:1 IPA/DMSO. ....	92

Figure	Page
Figure 5.2. Summary toxicity changes of Mixtures 1-5 phototoxicity following UV irradiation. ....	94
Figure 5.3. UV-Vis spectra of Mixture 1 + ZnO particles before and after 2 hrs of UV irradiation. ....	96
Figure 5.4. Changes in zebrafish development over five days at ten different endpoints. ....	98
Figure 6.1 Complementary lenses to practical sustainable product design. ....	104
Figure 6.2 The interplay between the three lenses introduced in Fig. 6.1: Green chemistry, life cycle and systems thinking. ....	109
Figure 6.3 Summary of Workshop Activities. ....	112
Figure 6.4 Student-generated data measuring foam rigidity. ....	120
Figure A1. <sup>1</sup> H-NMR (300 MHz), D <sub>2</sub> O, spectrum of N <sub>3</sub> -EG <sub>3</sub> BS .....	136
Figure A2. UV-vis of AuNPs before (N <sub>3</sub> -EG <sub>3</sub> -AuNP-EG <sub>3</sub> ) and after (1-triazole-EG <sub>3</sub> -AuNP-EG <sub>3</sub> ) coupling reactions. ....	137
Figure A3. UV-vis of N <sub>3</sub> -EG <sub>3</sub> -AuNP-EG <sub>3</sub> immediately following purification. ....	138
Figure A4. Raw SAXS patterns and overlaid LSQ model fits for AuNPs. ....	139
Figure A5. <sup>1</sup> H-NMR (600 MHz), CD <sub>3</sub> CN, stacked spectra of EG <sub>3</sub> -BS and N <sub>3</sub> -EG <sub>3</sub> -BS. ....	140
Figure A6. <sup>1</sup> H-NMR (600 MHz), CD <sub>3</sub> CN/D <sub>2</sub> O (99:1), N <sub>3</sub> -EG <sub>3</sub> -AuNP-EG <sub>3</sub> before decomposition. ....	140
Figure A7. <sup>1</sup> H-NMR (600 MHz), CD <sub>3</sub> CN/D <sub>2</sub> O (99:1), spectra after AuNP decomposition. ....	141
Figure A8. XPS survey spectrum of 17-month-old N <sub>3</sub> -EG <sub>3</sub> -AuNP-EG <sub>3</sub> (stored dry) on a chromium coated silicon substrate. ....	142
Figure A9. A sulfur 2p XPS spectrum with peaks fit as the blue and purple traces (same sample as in Figure A8). ....	142
Figure A10. Copper-free 1,3-dipolar cycloadditions of N <sub>3</sub> -EG <sub>3</sub> -AuNP-EG <sub>3</sub> and strained alkynes (1-3). ....	143

Figure	Page
Figure A11. <sup>1</sup> H-NMR (600 MHz), D <sub>2</sub> O, characterization of 1-triazole-EG <sub>3</sub> -AuNP-EG <sub>3</sub> before and after I <sub>2</sub> decomposition.....	144
Figure A12. <sup>1</sup> H-NMR (600 MHz), D <sub>2</sub> O, characterization of 2-triazole-EG <sub>3</sub> -AuNP-EG <sub>3</sub> before and after I <sub>2</sub> decomposition. ....	145
Figure A13. <sup>1</sup> H-NMR (600 MHz), D <sub>2</sub> O/DMSO-d <sub>6</sub> (80:20) characterization of 3-triazole-EG <sub>3</sub> -AuNP-EG <sub>3</sub> before and after I <sub>2</sub> decomposition.....	146
Figure A14. Copper catalyzed 1,3-dipolar cycloadditions involving N <sub>3</sub> -EG <sub>3</sub> -AuNP-EG <sub>3</sub> and various terminal alkynes (4-7).....	147
Figure A15. <sup>1</sup> H-NMR (600 MHz), D <sub>2</sub> O/DMSO-d <sub>6</sub> (80:20), characterization of 4-triazole-EG <sub>3</sub> -AuNP-EG <sub>3</sub> following I <sub>2</sub> decomposition.....	148
Figure A16. <sup>1</sup> H-NMR (600 MHz), CD <sub>2</sub> Cl <sub>2</sub> , characterization of 5-triazole-EG <sub>3</sub> -AuNP-EG <sub>3</sub> following I <sub>2</sub> decomposition. ....	148
Figure A17. <sup>1</sup> H-NMR (600 MHz), CDCl <sub>3</sub> , characterization of 6-triazole-EG <sub>3</sub> -AuNP-EG <sub>3</sub> AuNPs following I <sub>2</sub> decomposition.....	149
Figure A18. <sup>1</sup> H-NMR (600 MHz), D <sub>2</sub> O/DMSO-d <sub>6</sub> (91:9), characterization of 7-triazole-EG <sub>3</sub> -AuNP-EG <sub>3</sub> following I <sub>2</sub> decomposition. ....	150
Figure B1. TEM images showing spherical AuNP <sub>31% MEEE</sub> morphology. ....	157
Figure B2. <sup>1</sup> H-NMR spectrum of AuNP <sub>31% MEEE</sub> indicating successful column purification.....	158
Figure B3. XPS spectra (black trace) and background subtractions (blue trace) of AuNP <sub>31% MEEE</sub> on boron doped diamond.....	158
Figure B4. Small-angle X-ray scattering pattern of AuNP <sub>31% MEEE</sub> .....	159
Figure B5. UV-Vis stability study of AuNP <sub>31% MEEE</sub> at 50 ppm. ....	159
Figure B6. Developmental effects caused by AuNP <sub>100% TMAT</sub> .....	160
Figure B7. Developmental effects caused by mixed-ligand MEEE/TMAT-AuNPs (AuNP <sub>X% MEEE</sub> ), MEE(E)-AuNPs (AuNP <sub>100%MEE(E)</sub> ), and MEE/TMAT-AuNPs(AuNP <sub>45% MEE</sub> ).....	161
Figure B8. Control of centrifuged AuNPs without BSA. ....	162
Figure B9. Extent of BSA/AuNP Aggregation for AuNPs with shortened PEG chains. ....	162

Figure	Page
Figure C1. Assay Set-up. ....	163
Figure C2. Representative results of the entire set of endpoints examined for all toxicity assays. ....	164
Figure C3. Summary of zebrafish developmental endpoints in the presence of each size of AuNPs, and the free ligand, when dispensed with the BioPrinter. ....	165
Figure C4. UV-Vis measurements demonstrating the stability of the smallest AuNPs. ....	166
Figure C5. SAXS of smallest AuNPs (AuNP <sub>1.0 nm</sub> ) in (a) water and (b) with PS20 after 18 hours. ....	167
Figure C6. Structure of MEEE-AuNPs differentiating the core size ( $D_{core}$ ) from the solvation size ( $D_h$ ). ....	168
Figure C7. Comparison of <sup>1</sup> H-NMR spectra of PS20 and the two smallest sizes of AuNPs. ....	169
Figure C8. 2D spectrum of PS20 (0.3%) in D <sub>2</sub> O. ....	170
Figure C9. 2D spectrum of AuNPs before 0.3% PS20 is added. ....	170
Figure C10. 2D spectrum of AuNPs + PS20 (0.3%) after 30 mins. ....	171
Figure C11. 2D spectrum of AuNPs + PS20 (0.3%) after 2 hours. ....	171
Figure C12. 2D spectrum of AuNPs + PS20 (0.3%) after 13 hours. ....	172
Figure C13. 2D spectrum of AuNPs + PS20 (0.3%) after 18 hours. ....	172
Figure C14. Structural comparison of MEEE-AuNPs to polyethylene glycol dendrimers. ....	174
Figure C15. Summary of zebrafish developmental endpoints in the presence of a PEG dendrimer and PS20/dendrimer mixtures. ....	175
Figure C16. 2D spectrum of dendrimers alone in D <sub>2</sub> O; dendrimers are 1.6 nm in hydrodynamic diameter at 1000 µg/mL. ....	175
Figure C17. 2D spectrum of dendrimers (1000 µg/mL) + PS20 (0.3%) after 30 minutes. ....	176

Figure	Page
Figure C18. Summary of zebrafish developmental endpoints in the presence of various surfactants, and the corresponding surfactant/AuNP mixtures. ....	177
Figure C19. Bright-field and dark-field TEM images of AuNPs corroborating the 1.0 nm core size. ....	178
Figure D1. UV-Vis spectra of a moderately stable sun filter mixture formulated with just neat actives in DMSO versus actives into a lotion.....	179
Figure D2. Irradation of a moderately stable sun filter mixture over 2 hrs. ....	179
Figure D3. UV-Vis spectra showing photodegradation of Mixtures 1-5.....	180
Figure D4. UV-Vis spectra showing photodegradation of Mixtures 1 + ZnO. ....	180

## LIST OF TABLES

Table	Page
Table 3.1 Summary of the MEEE/TMAT-AuNPs studied.....	39
Table 4.1 Chemical influence on the incidence of mortality at 24 hpf (MO24) in embryonic zebrafish.....	61
Table 5.1. Sun filter mixture formulations with a calculated SPF of 15. ....	90
Table 6.1 Student generated data ranking foam effectivity at energy dissipation from instantaneous impact. ....	119
Table A1. Multiple batches of N <sub>3</sub> -EG <sub>3</sub> -AuNP-EG <sub>3</sub> , core size determined by SAXS. ....	137
Table C1. Definition of particle notation and corresponding core sizes determined by SAXS. ....	163
Table D1. Concentrations used for <i>in vivo</i> toxicity testing.....	181

## LIST OF SCHEMES

Scheme	Page
Scheme 2.1 Approaches to the synthesis of azide-terminated mixed monolayer-protected AuNPs. ....	17
Scheme 2.2 The direct synthesis of azide/EG <sub>3</sub> AuNPs and subsequent functionalization using the Cu-free or Cu-catalyzed Azide-Alkyne Cycloaddition (CuAAC) reaction. ....	25
Scheme A1. Synthetic route to a EG <sub>3</sub> tethered azide-functionalized Bunte salt 1-azido-2-(2-(2-chloroethoxy)ethoxy)ethane (8). ....	134

## LIST OF CHARTS

Chart	Page
Chart 2.1 Alkyne containing species used to demonstrate the scope of the N <sub>3</sub> -EG <sub>3</sub> -AuNP-EG <sub>3</sub> reactivity. ....	31

## CHAPTER I

### I. INTRODUCTION

#### **Development of a New Class of Materials**

Chemists are uniquely positioned to bring novel materials into commerce that can improve the quality of life in ways previously unimaginable. In the past decade alone we have seen advancements in 3D printing chemistry that enable customized medical and athletic parts to be grown from a liquid bath in minutes,<sup>1,2</sup> and advancements in solid-state reflective displays that enable colored (but pigment-free), energy-efficient electronic displays.<sup>3,4</sup> Chemists work at the frontiers of technology and develop fundamental knowledge that continuously helps humanity adapt to the challenges of an ever-changing world. The advancement of new chemistries and materials doesn't just bring about positive change though; there are always inherent tradeoffs and consequences when the status quo is altered. Some of the most unfortunate examples of this, such as the adoption of the insecticide DDT, are well-recognized<sup>5</sup> and have provoked public scrutiny over the implementation of new chemicals.<sup>6,7</sup> While the scientific community recognizes that caution must be taken to prevent the dissemination of unsafe chemicals,<sup>8</sup> assessing hazard and anticipating tradeoffs among alternatives remains a practical challenge.<sup>9,10</sup> For many new chemicals, a thorough understanding of properties and toxicological impacts is precluded by lengthy experimentation, high costs, and incomplete data sets.<sup>11-13</sup> Even for established chemicals there are often deficiencies in the understanding of how their structural features relate to observed performance and risks; in turn, it is challenging to use established chemicals as a basis for the design of enhanced new chemicals.<sup>14-16</sup>

Systematic studies that develop robust structure/property relationships are useful for constructing chemical libraries and predictive models that can allow for the rational design of next generation chemicals.<sup>10,13,17</sup> These tools can help prevent many iterations and allow for rapid property enhancement but remain underdeveloped for many classes of chemicals.<sup>11,12,16,18</sup>

This dissertation details advances I have made towards understanding and controlling the structure of nanoparticles (NPs), thereby enabling enhancements in their technological performance and minimization of their hazards. NPs have been studied as the materials of interest for most of this work because their translation from the benchtop into applications has been delayed by challenges such as unadaptable syntheses, ill-defined structures, and poorly understood toxicities. The last chapter of this dissertation incorporates lessons learned from the sustainable design of NPs and expands them to a generalized framework for designing high-performing sustainable products.

NPs have received extensive attention because of their potential to revolutionize many applications including drug delivery,<sup>19</sup> medical imaging,<sup>20</sup> optical sensing,<sup>21</sup> environmental remediation,<sup>22</sup> and catalysis.<sup>23</sup> Since NPs, which are generally defined as materials being 1-100 nm in at least one dimension, exist in a size regime between that of small-molecules and bulk material they have unique size-dependent properties. Like a bulk material they have a surface area that can be utilized for multi-functionalization and many simultaneous interactions with molecules, but they also have the volumetric advantage of small-molecules wherein they don't take up much space or require much material. This combination is often referred to as a 'surface-to-volume ratio' and describes many of the unique benefits of the nano size-regime. The high surface-to-

volume ratio makes NPs especially useful for functions where material conservation is important, such as precious-metal catalysis. It also gives them the ability to be designed with sophisticated surface chemistries that enable multiple functionalities such as biological targeting and drug delivery to be present, in a high surface density, on a single small 3D structure.<sup>24-26</sup> Other applications depend on the confined electrons present in NPs, which yield interesting properties, such as localized surface plasmon resonances and high contrast in X-ray application. These properties yield NPs that are useful for functions like biological imaging,<sup>27,28</sup> optical sensing,<sup>21,29</sup> and light-to-heat tumor ablation treatment.<sup>30</sup> Despite the immense promise and proof-of-concept reports of NPs acting as sophisticated materials, translating NPs from the discovery phase to commercialized applications is an ongoing challenge.<sup>31-34</sup>

To understand the current state of nanotechnology research, where countless materials of interest have been made on the benchtop, but relatively few have materialized into industrial products, it is helpful to give context regarding how the field has evolved.

### **The Evolution of Nanotechnology**

Richard Feynman is credited as the father of modern nanotechnology because of his 1959 lecture titled “There’s Plenty of Room at the Bottom” wherein he motivated the atomic-level manipulation of matter.<sup>35</sup> Although NPs and other nanostructures have been unintentionally produced by humans for centuries,<sup>36</sup> Feynman was the first scientist to suggest deliberately studying chemicals at this scale. Inspired by biochemical processes, he introduced the potential of a new scientific field where ‘machines’ could be miniaturized down to the atomic scale and perform unusual functions, like acting as a

surgeon. The ideas he presented began to materialize in the 1980s when the scanning tunneling microscope and atomic force microscope were invented enabling direct visualization of materials at the nanoscale.<sup>37</sup> Around this same time, buckyballs were discovered by Kroto, Smalley, and Curl who showed that carbon atoms can exist in surprising caged architectures that possess unusual properties.<sup>38</sup> This convergence of newly realized nanoscale materials with unique properties, and new instruments capable of studying them, ushered in a field of research on nanoscale materials. Then in 2000 U.S. president Bill Clinton enacted the National Nanotechnology Initiative (NNI), a multi-agency research program that has since funded billions of dollars of nanomaterials research.<sup>39,40</sup> The NNI gave nanotechnology an identity and a vision outside of specialized research labs; it was regarded as the next industrial revolution wherein scientists would be able to use ‘exact’ manufacturing to design materials atom-by-atom.<sup>41,42</sup>

In the early 2000s the scientific community and public alike were excited about the rapid advancements promised by the NNI, especially emphasized were the expected impacts on the medical and electronics industries. Indeed, some products in the electronics industry, such semiconductor chips, have seen major improvements due to the advancement of nanotechnology. At large though, much of the ambitious promise of nanotechnology remains unfulfilled.<sup>33,43</sup> Some of this can be attributed an initial narrative around nanotechnology with goals and timelines that failed to consider product lifecycle development, such as predicting the elimination of cancer-caused deaths by the year 2015.<sup>39</sup> Nonetheless, even relatively straight-forward applications have been challenging in moving nanomaterials from benchtop synthesis to commercialization.<sup>32,43</sup> The delays

in commercial fulfillment emphasize the challenge of developing a new research field from infancy where theory, standardized production, characterization methods, and defined safety metrics were initially absent. While the field has seen significant advances in these areas over the past twenty years, it remains challenging to synthesize nanomaterials with deliberate compositions, performance, and toxicity.<sup>32,43</sup>

## **Challenges in Deliberate Nanomaterial Development**

### Relating Nanoparticle Architecture to Performance.

The lack of robust NP structure/property relationships have made it difficult to enhance NP performance in a strategic manner.<sup>19,44,45</sup> Ideally, scientists would be able to predict what structural changes need to occur to alter a specific property without many successive iterations. Currently though, very few syntheses are adaptable enough to allow for fine-tuning of individual structural features, further, even with an adaptable synthesis it is often unclear what the target NP architecture should be for a given function. This section will go on to give specific examples about the state of the field, and while some of this is broadly applicable to all NPs, it was written in the context of inorganic NPs which have been the focus of this dissertation.

NPs have complex architectures that are difficult to control and study. Figure 1.1 describes a generic NP architecture and some of the features that can affect overall performance. First, there is a core material that yields a 3D structure on the order of  $10^{-9}$  m. The *core* can vary in metal/metal-oxide composition, size, shape, phase, dopant levels, and dopant distribution. A NP core is often coated with organic molecules to stabilize the NPs from fusion or dissolution, and to enable dispersibility in solution. The structure

surrounding the core material is often termed the NP shell. A shell can be composed of polymers, small molecules, macromolecules, or even inorganic material. For the purposes of this thesis, we will focus on shells that consist of defined molecules bound to the NP surface, which are referred to as ligands. Shell chemistry, though sometimes overlooked by descriptions of NP cores, is important and can determine solvent dispersibility, solvation size, NP stability, toxicity and functionality.<sup>46,47</sup> These types of agglomerated, incidental coatings are usually referred to as coronas, and will be distinguished separately from shells in this work. The two most commonly studied types of coronas are those composed of proteins,<sup>48</sup> which are acquired from biological media, or natural organic matter,<sup>49</sup> which are acquired from surface waters. Finally, nanomaterial structure is further complicated by the inherent dispersion of products; a single synthesis will produce some range of NP architectures with the range in core size typically being the only reported value. Most NP syntheses generally aim to minimize product dispersity, but the success of this, and the standard of success, varies greatly depending on the materials used. Some features, such as the range in surface-chemistry on mixed-ligand particles, remain ill-defined due to limitations in experimental techniques.<sup>50</sup>

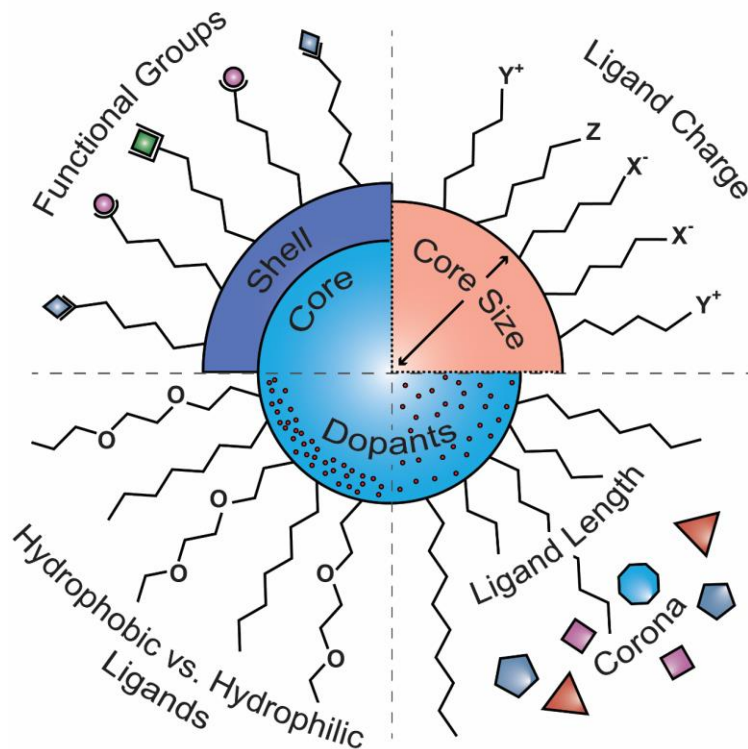


**Figure 1.1 Architectural features on a NP that are important for understanding properties.**

The complexity of NP architectures has contributed to incomplete characterization and nonstandard reporting; consequently, there are conflicting accounts of the relationship between structural characteristics and functional properties.<sup>51</sup> These disparities in structure/property relationships have hindered the ability to target structures with enhanced performance for a range of applications. For instance, magnetic iron oxide NPs are promising materials for MRI imaging,<sup>52</sup> but the magnetic properties are influenced by a combination of size, surface structure, phase, and shape, and most studies do not thoroughly analyze all of these parameters. Therefore, there are large variations in magnetic properties among NPs that are reported to be the same.<sup>53</sup> Another application of NPs is their use in thin films; tin-doped indium oxide NPs are transparent and conducting which makes them important materials for electronic devices.<sup>54</sup> Until recently,

inconsistencies in dopant incorporation and NP surface chemistry among literature reports had convoluted the relationship between NP size and the resulting thin film optoelectronic properties.<sup>55</sup> Although the specific challenges faced for each application vary, overall lack of NP synthetic control and incomplete structural elucidation has led to many instances of structure/property relationships that don't correlate across studies.

Ultimately, the field would benefit from the ability to rationally design particles that perform a specific function with a predictable toxicity. The challenges associated with incompletely characterized NPs discussed above complicate the evaluation of nanotoxicity. Besides having NPs with incomplete characterization, there are added challenges with toxicity assay design (*e.g.*, using solvents that cause slow sedimentation of NPs) that bias results and yield confusing data.<sup>46</sup> Complicating this further is the fact that nanotoxicology is a new field where there was no prior precedent for dosing metrics<sup>56</sup> (*e.g.*, dosing can be determined by number of particles, mass, or surface area) and exposure conditions (*e.g.*, use of dispersants, solvent system, or pH);<sup>46,57,58</sup> both of which can affect the outcome. Figure 1.2 shows some of the important variables for NP toxicity assays.

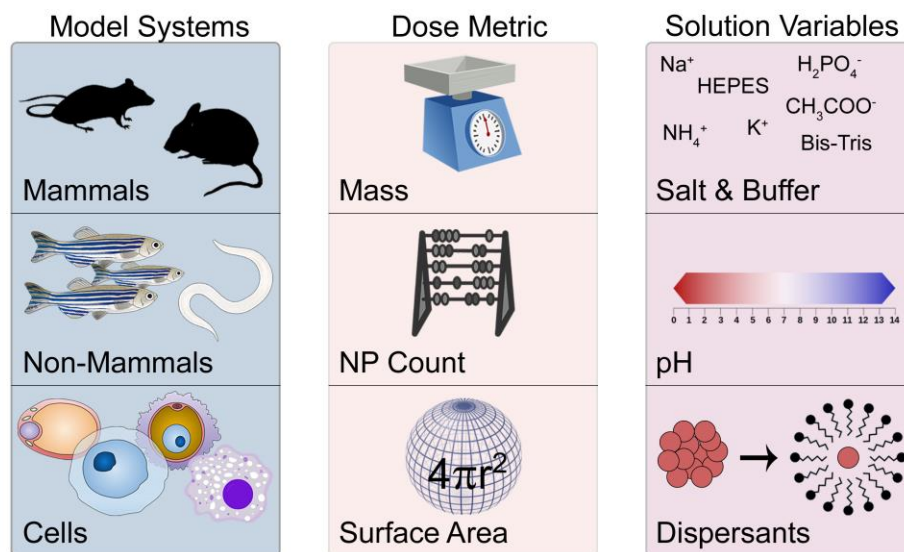


**Figure 1.2 Key parameters for consideration when designing or interpreting NP toxicity assays.**

Generalized NP synthesis and property screening methods are needed to overcome the described challenges and develop reliable NP structure-property-toxicity relationships. To address these needs, microfluidic NP syntheses are emerging as promising alternatives to traditional batch syntheses; often enabling access to NPs with improved tunability, precision and reproducibility.<sup>59,60</sup> A microfluidic synthesis of gold NPs<sup>61</sup> was used throughout much of the work in this dissertation and proved to be beneficial in terms of accessing specific gold nanoparticle (AuNP) sizes and ligand shell compositions with high degrees of control and reproducibility. Batch syntheses remain the standard method for NP discovery because a practical batch synthesis enables quick iteration and variation of structural parameters without any reengineering or reprogramming that might be necessary to modify a microfluidic synthesis. The most useful batch syntheses allow for independent control over multiple structural parameters. Towards this front, our lab has developed a continuous growth synthesis of metal oxide NPs that enables simultaneous control over size, core metal, dopant metal, and dopant

distribution.<sup>53,62,63</sup> While these types of generalizable NP syntheses are important for generating the NPs, there is still a need for sophisticated property screening methods capable of quickly and accurately comparing NP performance in specific functions, such as electrocatalytic activity<sup>64</sup> or heavy metal adsorptivity.<sup>65</sup> Automated approaches have proven useful for toxicity screening (discussed below) and may be a promising route for improving the accuracy and speed of performance assessments.

In recent years, advances in high-throughput technologies have offered increasingly expediated screening of NPs in biological environments.<sup>59,66</sup> Biomimetic microfluidic technologies have shown exciting new possibilities for assessing how NPs interact with organs that are not possible using conventional *in vitro* systems. Using this approach, cells have been grown on silicone membranes and used in microfluidic devices to assess the effects of flow and cyclic strain on NP/organ interactions.<sup>59</sup> Zebrafish and nematodes have proven to be informative animal models for quickly learning about the *in vivo* effects induced by NPs without the high cost, material requirements and ethical issues associated with mammal testing.<sup>66-68</sup> The work in this dissertation uses a combination of tunable NP design methods and high-throughput toxicity analysis to develop well-defined NPs with structures that are related to specific properties/toxicity.

#### Influence of Mixture Composition on Nanomaterial Performance.

While NP properties are now recognized to be highly influenced by all aspects of their architecture, the influence of surrounding chemicals remains largely unappreciated. In most applications, NPs exist in mixtures with other molecules, not as isolated species. For example, surfactants are often added to NPs to enhance their stability and dispersibility for biological studies,<sup>69</sup> and in sunscreens the NPs are one ingredient in a

complex lotion formulation.<sup>70</sup> The highly dynamic nature<sup>71,72</sup> of NPs emphasizes the importance of considering the chemical environment and potential intermolecular interactions. The high surface-to-volume ratio on NPs makes them especially prone to transformations in the presence of surrounding chemicals (*e.g.*, protein corona formation) due to the abundant NP surface area that will readily adsorb molecules.<sup>11</sup> Similarly, the properties of NPs relating to the NP core can facilitate chemistry on surrounding molecules (*e.g.* through generation of reactive oxygen species).<sup>73,74</sup> Further, surrounding molecules can induce catastrophic NP degradation via mechanisms such as ligand shell oxidation, ligand displacement, or core ion dissolution.<sup>75,76</sup> Consequently, even when isolated NPs can be synthesized with ideal properties, the surrounding chemical environment for their target application can cause unexpected performance.

Mixture effects have been noted for certain NPs in specific studies but are not broadly considered by the field yet. Macromolecule corona formation has been the main area studied for mixture effects.<sup>48,49,77,78</sup> These coronas have been documented to change NP properties and biological impacts. For instance, cationic NPs that acquired a dense natural organic matter corona were observed to have a charge reversal that prevented interactions with biological membranes.<sup>49</sup> Outside of corona studies, a few other examples of mixture effects have been reported. For example, when zinc oxide NPs were mixed with fatty acids, synergistic toxicity was observed on human colon epithelial (Caco-2) cells, thereby raising concerns over the biological impacts of zinc oxide NPs upon oral ingestion.<sup>79</sup> There is sufficient evidence that when NPs are combined with other chemicals in applications their performance and hazards can be altered in ways not predicted by their behavior as isolated ingredients. Therefore, consideration of mixture

effects is critical for developing robust strategies of NP property enhancement and hazard minimization.

To gain meaningful information on NP properties they need to be studied in environments relevant to their intended application. Since there are few studies like this, it would be beneficial to have more fundamental work done where NPs are examined in the presence of other chemicals and the structural features of all components are carefully analyzed using complementary and corroborative techniques.<sup>32,47</sup> This type of thorough analysis can form the foundation for developing predictivity of NP mixture behavior. An important target for the field is to be able to predict mixtures that are at high-risks for displaying non-additive behavior (*i.e.*, synergies).<sup>80,81</sup> Since the work in this dissertation is focused on developing structural understanding, mixture effects were examined in controlled environments where NPs were intentionally combined with other pure chemicals in known quantities. Therefore, mixtures where chemicals were added intentionally in controlled amounts will be referred to as *formulas*. Uncontrolled mixtures containing NPs and other chemicals in environmental settings like surface waters and soils are also important to consider but contain complexities beyond the scope of this work.

### **Dissertation Overview**

This dissertation focuses on some major challenges at the forefront of NP development, with the goal of helping expediate the advancement of safe and high-performing NPs. AuNPs have been used for much of this work because of their biomedical promise coupled with their well-developed syntheses that allow for fine-tuning of structure. Many of the strategies from this dissertation for bridging the gap

between benchtop and commercialization can be expanded beyond AuNPs to other types of NPs. Chapters 2 and 3 focus on the precise design of NPs with sophisticated architectures. In Chapter 2, a streamlined technique was developed to access easily-conjugated AuNPs that act analogously to traditional molecular reagents. These NPs are fully water-dispersible, even when conjugated with hydrophobic moieties, and can be used by non-specialists for a variety of biomedical or imaging purposes. In Chapter 3 a tunable synthesis for AuNPs with mixed-charge cationic/poly ethylene glycol shells was developed. Using these mixed-ligand AuNPs, deleterious effects of homogenous ligand-shell cationic NPs, including high incidences of animal mortality and biological aggregation, were significantly reduced. Chapters 4 and 5 examine NP performance and safety in formulations. Chapter 4 shows that mixing AuNPs with food-grade surfactants alters the NP structure and toxicity in surprising ways. Chapter 5 demonstrates that zinc oxide NPs significantly affect the toxicity and performance of commercially inspired sunscreen mixtures once they are exposed to sunlight. Finally, in chapter 6 materials innovation and sustainable design is discussed from a pedagogical perspective, and a framework is developed for preparing chemistry students to make meaningful market contributions. Taken together, this dissertation serves to push sustainable technologies forward by coupling the use of materials chemistry for performance enhancement with strategies for minimizing health and environmental impacts.

## **Bridge to Chapter II**

Chapter I has motivated the need for generalizable syntheses that allow for facile tuning of NP architecture. The work in Chapter II presents an approach to generating

AuNPs that act analogously to molecular reagents in that they can be stored for long periods of time then readily conjugated.

Mixed-ligand AuNPs were generated that contain water-solubilizing ligands and a small amount of azide-functionalized ligand. The hydrophilic ligands allow for the AuNPs to stay dispersed in aqueous environments for extended periods of time, while the azide-containing ligands provide a handle for easy conjugation through the use of click chemistry. This approach was developed to enable non-specialists to generate hybrid AuNPs customized for their application of choice; our hope is that it inspires the development of additional NP syntheses that yield easily modified products.

## CHAPTER II

### II. SINGLE-STEP SYNTHESIS OF SMALL, AZIDE-FUNCTIONALIZED GOLD NANOPARTICLES: VERSATILE, WATER-DISPERSIBLE REAGENTS FOR CLICK CHEMISTRY

Reproduced with permission from Elliott, E. W.; Ginzburg, A. L.; Kennedy, Z. C.; Feng, Z.; Hutchison, J. E. Single-Step Synthesis of Small, Azide-Functionalized Gold Nanoparticles: Versatile, Water-Dispersible Reagents for Click Chemistry. *Langmuir* **2017**, 33, 5796–5802. Copyright 2017 American Chemical Society.

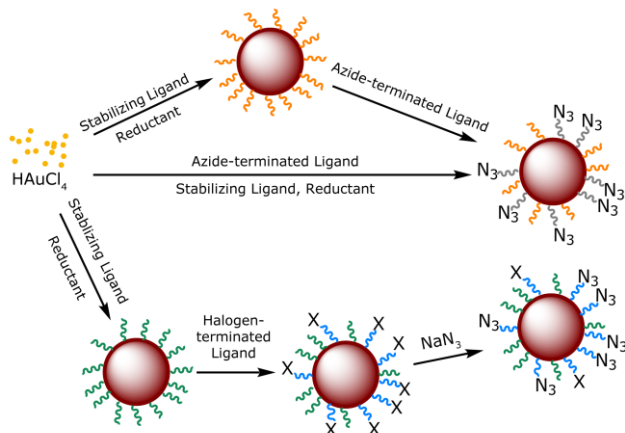
#### **Introduction**

Functionalized monolayer protected nanoparticles (NPs) are of interest in a wide range of biomedical<sup>1</sup> and environmental<sup>2</sup> applications including: biological imaging,<sup>3</sup> targeted drug delivery,<sup>4</sup> photothermal therapy,<sup>3</sup> nano-toxicity studies,<sup>5</sup> detection of analytes,<sup>1</sup> environmental remediation,<sup>6</sup> and environmental fate and transport.<sup>2</sup> Typically, a mixture of functional groups on the NP surface is needed to tailor the NP properties for each application.<sup>7,8</sup> In addition, specific sizes (and size distributions) are often required.<sup>7,9</sup> Multifunctional NPs with specific core sizes have been shown to offer high levels of performance tailored to defined applications;<sup>7,10</sup> however, their use has been limited by the lack of synthetic control over size, composition and structure.<sup>11</sup> In addition, the synthesis and production of such functionalized nanoparticles has proven time-consuming and expensive.<sup>10,12</sup>

Ideally NPs would be readily prepared with controlled core structures and possess defined ligand shells consisting of reactive, stabilizing and targeting ligands for use as NP reagents. Such reagents could be efficiently coupled to yield more complex building blocks such as hybrid nanomaterials.<sup>13</sup> The development of NP reagents would enable convergent syntheses wherein parallel syntheses can be used rather than a linear strategy.<sup>14</sup> An attractive strategy towards versatile NP reagents is the incorporation of clickable functional groups<sup>13,15</sup> within the ligand shell to facilitate highly efficient coupling reactions. Gold NPs (AuNPs) are well-suited to develop as clickable NP reagents because the core material it is biocompatible<sup>4</sup> and the surface chemistry is well-defined.<sup>8</sup>

Clickable AuNPs possessing terminal azide groups have been previously reported to produce nanoparticles that are dispersible in either organic solvents or water.<sup>16–20</sup> Despite the number of applications for NPs in aqueous media, there are comparatively fewer examples of clickable AuNPs that readily disperse in water. As noted above, water-dispersible NPs are of particular interest in environmental and biomedical applications. Syntheses of NPs tailored for these applications present a number of challenges<sup>21</sup> and the NPs often suffer from poor colloidal stability.<sup>22</sup> In addition to producing AuNPs that form stable dispersions, methods are needed to permit precise control over the dimensions of the nanoparticle. For example, it has been reported that for small EG functionalized AuNPs the core size determines cellular uptake. 16 nm and larger AuNPs did not enter cells, 5.5 and 8.2 nm NPs were delivered into the cytoplasm, while 2.4 nm AuNPs localized in the nucleus.<sup>23</sup> Although a few approaches have been developed to produce non-

covalently coated NPs with azide-containing polymers;<sup>24,25</sup> here we focus on syntheses that yield a gold-thiol interface as it is known to provide stability in biomedical applications.<sup>4</sup>



**Scheme 2.1 Approaches to the synthesis of azide-terminated mixed monolayer-protected AuNPs.**

To harness the potential of azide-functionalized AuNP reagents for the broad range of possible applications, approaches are needed that result in precise control of core size and surface functionality in a reliable, reproducible fashion. Scheme 2.1 presents approaches to the synthesis of azide-terminated mixed monolayer-protected AuNPs. The top and bottom routes summarize previously reported syntheses where the AuNPs are first synthesized with a stabilizing ligand, followed by ligand exchange. In the top route AuNPs are synthesized in the presence of a stabilizing ligand that, after isolation and purification, is partially exchanged by an azide-terminated ligand.<sup>18,19,26,27</sup> In the bottom route, the second step involves ligand exchange to introduce some proportion of a commercially available halogen ligand. In a third step, azide reacts with the halogenated ligand through a covalent modification reaction.<sup>16,20</sup> The top and bottom approaches take advantage of previously established nanoparticle formation chemistry that produces AuNPs with

a narrow size dispersity,<sup>28,29</sup> however, this ease is offset by the challenges associated with each subsequent modification step. It is difficult to control the extent of these ligand exchanges and ligand-modification reactions and the reactions and associated purifications can be time-consuming. As a result, controlling the nanoparticle architecture and reproducibly forming specific compositions are difficult. In cases where the stabilizing ligands make the AuNPs soluble in organic solvents, additional modifications, such as click-chemistry modification of a portion of the azide ligands, are necessary to make the NPs dispersible in water.<sup>19,20</sup>

The use of ethylene glycol-based stabilizing ligands is an attractive approach to producing AuNPs that readily disperse in water. Workentin's group employed methyl-terminated ethylene glycol (EG) ligands to produce aqueous azide-AuNPs via a route represented by the top set of arrows in Scheme 2.1.<sup>26,27</sup> Our experience with AuNPs stabilized with these and other short methyl-terminated EG chains is that they can only be dispersed in water at low concentrations, presumably due to the presence of the more hydrophobic terminal methyl group.<sup>30</sup> Further, we found that AuNPs that are minimally dispersible in water tend to agglomerate when hydrophobic molecules such as drugs or targeting groups are appended to the ligand shell surface.

Herein, we demonstrate a synthesis of uniform, small (3.5 nm core diameter) mixed-ligand azide-functionalized AuNPs that react with a large scope of alkynes to produce highly stable and water-dispersible NPs. Our approach utilizes a minimalist synthetic strategy, shown as the middle route in Scheme 2.1, to make

water-dispersible clickable AuNPs in a single step. The mixed-ligand AuNPs were prepared directly in water, needing no subsequent modification steps following particle formation. These AuNPs are readily prepared, isolated and purified, and have a narrow size dispersity (<15%) at a biologically useful size. They are stable for months in solution at high concentrations ( $\geq 1$  mg/mL concentrations) or as dried powders (Figure A3) and their syntheses are highly reproducible even when conducted by different chemists (Table A1).<sup>31</sup> The approach is amenable to producing AuNPs with other core dimensions.<sup>31</sup> These AuNP reagents are modular building blocks that demonstrate the envisioned benefits of click chemistry applied to nanoparticles.

## Experimental

### Materials

All materials were used as received: HAuCl<sub>4</sub>·H<sub>2</sub>O (99.9%) (Strem); 2-[2-(2-chloroethoxy)-ethoxy]ethanol (99%), sodium borohydride (98%, caplets), Copper(I) bromide (99.999%), 1-ethynyl-1-cyclohexanol (99%), (Aldrich); sodium hydroxide, sodium thiosulfate (anhydrous), (Mallinckrodt); sodium L-ascorbate (powder, Bioreagent), dibenzocyclooctyne-PEG<sub>4</sub>-Fluor 545 (DBCO-EG<sub>4</sub>-Fluor 545), phenylacetylene (98%), ethynylferrocene (97%), (Sigma-Aldrich); thionyl chloride (99.5%) (Acros), sodium azide (95%) (J.T. Baker); benzyltriethylammonium chloride (BTEAC, 99%) (TCI America); DBCO-PEG<sub>4</sub>-OH, DBCO-NHS ester (Click Chemistry Tools). The Bunte salt analog of 2-[2-(2-mercaptoethoxy)-ethoxy]ethanol (EG<sub>3</sub>-BS) was synthesized as previously reported.<sup>32</sup> Deionized water (18.2 M $\Omega$ ·cm) was obtained using

a Barnstead Nanopure Diamond system. Flow nanoparticle syntheses were driven using Kloehn syringe pumps (P/N 54022) and Kloehn 10 and 25 mL syringes. The flow system was created using IDEX Teflon tubing (0.030 in. i.d., WO# 0554152) and Teflon T-mixers.

### Synthesis of N<sub>3</sub>-EG<sub>3</sub>-BS Ligand

Synthetic details can be found in the SI. Briefly, 2-(2-(2-chloroethoxy)ethoxy)ethanol was converted to 1-azido-2-(2-(2-chloroethoxy)ethoxy)ethane in two steps using a literature preparation without the need for any chromatographic purification.<sup>33</sup> The chloro group was transformed to Bunte salt by substitution using sodium thiosulfate, and excess salts were removed by precipitation and filtration to yield the final product, S-(2-(2-(2-azidoethoxy)ethoxy)ethyl)sulfathioate (N<sub>3</sub>-EG<sub>3</sub> BS) as an oily pale yellow solid. <sup>1</sup>H-NMR (300 MHz, D<sub>2</sub>O):  $\delta$  = 3.78 (t, 2H), 3.57-3.65 (m, 6H), 3.39 (t, 2H), 3.18 (t, 2H).

### Synthesis of N<sub>3</sub>-EG<sub>3</sub>-AuNP-EG<sub>3</sub>

Mixed monolayer-protected AuNPs with a core diameter of 3.5 nm (by small angle X-ray scattering (SAXS)) were synthesized using our previously described mesofluidic reactor with minor modifications.<sup>31</sup> Aqueous solutions of each reagent were prepared in quantities to enable three successive syntheses using a single T-mixer. Thus, 1 mM stock solutions of EG<sub>3</sub> BS and N<sub>3</sub>-EG<sub>3</sub> BS were prepared and used in a volumetric ratio of 95:5, for a total volume of 30 mL. Then, 30 mL of 5 mM HAuCl<sub>4</sub> was prepared and 320  $\mu$ L of 1 M NaOH was added, raising the pH to 5. Finally, 505  $\mu$ L of 1 M NaOH was added to 60 mL of 1 mM NaBH<sub>4</sub>. Reagents

were mixed in Teflon T-mixers at a total flow rate of 60 mL / minute and the reaction mixture was purified using 30 volume equivalents of 18.2 MΩ water passed through a 10 kDa Pall Minimate tangential flow filtration capsule. The AuNPs were then lyophilized and isolated as a black powder before use in click reactions. *N<sub>3</sub>-EG<sub>3</sub>-AuNP-EG<sub>3</sub>* yields were typically ~5.1 mg per synthesis after purification, corresponding to a 69% yield of gold. It is worth noting that this yield is reduced as the first 5 secs of the flow output (i.e. ~ 1/8 of the synthesis) is discarded to allow reagent mixing to stabilize.

#### Click Reactions with *N<sub>3</sub>-EG<sub>3</sub>-AuNP-EG<sub>3</sub>*

Conditions specific to each alkyne are detailed in the SI. Generally, ~15 mg of lyophilized azide/EG<sub>3</sub> AuNPs were dissolved in 1 mL of water. A 10-fold excess of alkyne substrate was dissolved (in water, t-BuOH, or DMSO) and stirred with the NPs at room temperature for 48 hours to ensure the reaction went to completion. Terminal alkynes also had catalytic quantities of copper bromide and sodium ascorbate added to the reaction. The click products were purified by tangential flow filtration (samples with organic solvents were diluted 100x to avoid damage to the membrane) and then lyophilized.

#### **Characterization**

##### Instrumentation

NMR spectroscopy of the AuNPs, both before and after decomposition, was carried out on a Bruker Avance III-HD 600 MHz Spectrometer. NMR of the Bunte salt ligands was recorded on a Varian INOVA-300 NMR Spectrometer. An Anton Paar SAXSess mc<sup>2</sup> instrument, operating in line collimation mode, was used to

obtain SAXS patterns. Transmission electron microscopy (TEM) was performed on a FEI Tecnai G2 Spirit TEM operating at 120 kV. All UV-vis measurements were performed using an HP 8453 UV-visible spectroscopy system. Fluorescence measurements were performed using a Horiba Jobin Yvon Fluoromax-4 spectrofluorometer.

#### NMR Spectroscopy- Analysis of NP Purity and Analysis of Decomposed NPs for Estimating Mixed Ligand Composition

Following purification, approximately 7-10 mg of purified lyophilized nanoparticles were dispersed in 0.6 mL D<sub>2</sub>O or a CD<sub>3</sub>CN/D<sub>2</sub>O mixture, as specified in the SI. An initial spectrum was acquired at 600 MHz with 64 scans, and a relaxation delay of 1 s, to confirm that all free ligands and small molecules were removed during purification. The absence of sharp peaks (due to free ligands), and the presence of the characteristically broadened peaks,<sup>34</sup> indicated that all of the ligands were bound to the surface. Characterization of the bound mixed ligands before and after coupling reactions was initiated by adding approximately 2 mg of iodine (I<sub>2</sub>)<sup>35</sup> or 2.5 molar eq. of potassium cyanide (KCN) (per Au atom)<sup>36</sup> to the NMR tube. The mixture was shaken vigorously and allowed to react in ambient conditions for ~10-15 min. For samples with I<sub>2</sub>, excess solid I<sub>2</sub> was then removed from the NMR tube prior to acquiring another spectrum at 600 MHz with 512 scans. Samples with KCN went to completion within 5 minutes so no additional sample treatment was necessary. All decomposed AuNP NMR spectra indicated the ligands had been released into solution, forming disulfides with various forms of EG<sub>3</sub> chain fragmentation. The success of a click reaction was verified by identification of characteristic peaks attributed to the coupled product (Figures A11-A18).

## Nanoparticle Core Size Determination Using SAXS

Nanoparticle sizes resulting from the direct syntheses performed were determined in solution using SAXS. NP samples were exposed to monochromated X-rays from a Long Fine Focal spot (LFF) sealed X-ray tube (Cu 1.54 Å) powered by a generator at 2 kW focused by multilayer optics, measured with a Roper CCD in a Kratky camera. The Anton Paar SAXSess was set to average a minimum of 50 scans of 40 s exposures. The corresponding dark current and background scans were subtracted from the data before desmearing using the beam profile in Anton Paar SAXSQuant software. The size distribution of the sample was then determined by using the size distribution macro in the IRENA package for Igor Pro.<sup>37</sup> The SAXS patterns were fit using the modeling II macro and best model fits were determined using a nonlinear least squares method, assuming spherical particles (confirmed with TEM), to yield a Gaussian size volume distribution binned by core diameter. For each sample, percent polydispersity was then also determined relative to the average core size. Representative SAXS patterns are provided in the SI (Figure A4).

## TEM of Purified N<sub>3</sub>-EG<sub>3</sub>-AuNP-EG<sub>3</sub> and 1-triazole-EG<sub>3</sub>-AuNP-EG<sub>3</sub> for Analysis of Morphology

AuNP samples were prepared for analysis by floating holey carbon TEM grids (Ted Pella) on top of a drop of diluted AuNP solution of either **N<sub>3</sub>-EG<sub>3</sub>-AuNP-EG<sub>3</sub>** or **1-triazole-EG<sub>3</sub>-AuNP-EG<sub>3</sub>** for ~5 minutes. The grids were lifted from the drop and excess solution wicked away using a Kim wipe before being allowed to dry in ambient conditions prior to imaging.

## UV-Visible Spectroscopy of Purified N<sub>3</sub>-EG<sub>3</sub>-AuNP-EG<sub>3</sub> and 1-triazole-EG<sub>3</sub>-AuNP-EG<sub>3</sub>

Absorbance of purified AuNP solutions were measured in a quartz cuvette cleaned with aqua regia and rinsed copiously with nanopure water between all measurements.

#### Fluorescence Spectroscopy of Purified N<sub>3</sub>-EG<sub>3</sub>-AuNP-EG<sub>3</sub> and 1-triazole-EG<sub>3</sub>-AuNP-EG<sub>3</sub> to Verify the Efficacy of the Strain Promoted AAC Reaction

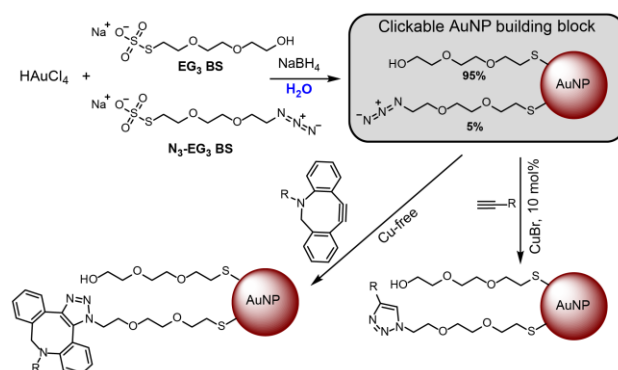
Nanoparticle solutions were first diluted with nanopure water to an absorbance at  $\lambda_{\text{max}}$  of 0.6. The fluorimeter was set to excite at 525 nm and collect emission from 540-700 nm, slit widths were set to 5 nm. The quartz cuvette was cleaned with aqua regia and rinsed copiously with nanopure water in between all measurements.

## **Results and Discussion**

### AuNP Design and Synthesis

We aimed to develop a design strategy for azide-functionalized AuNPs that was not only facile, but will enable their use in a range of environmental, biological and biomedical applications. These applications require nanoparticles that are stable in biological media, possess specific core sizes and can be reproducibly prepared with a controlled number of reactive groups on the periphery of the ligand shell. To ensure colloidal stability as well as biocompatibility, we employed hydroxy-terminated triethylene glycol (EG<sub>3</sub>), to compose the majority of the ligand shell.<sup>38-40</sup> Previous work has shown that a ligand shell containing only a small amount of azide-terminated ligand (relative to stabilizing ligand) achieves the most efficient click coupling reactions, therefore we chose to use 1:19 molar equivalents of the ligands, respectively.<sup>41</sup> Moreover, we have observed that higher azide content (greater than a 1:9 ratio) results in NPs that aren't as

dispersible (further highlighting the need for a controlled ligand-shell composition). The azide units were introduced via terminally modified triethylene glycol-Bunte salts (**N<sub>3</sub>-EG<sub>3</sub> BS**). We employed identical tethering chains (**EG<sub>3</sub>**) to promote even incorporation of ligands into the shell, leading to compositions controlled by the ligand feed ratio.<sup>40</sup> The azide group is unreactive during nanoparticle synthesis under these mild synthetic conditions (in water at room temperature).<sup>42</sup>



**Scheme 2.2 The direct synthesis of azide/EG<sub>3</sub> AuNPs and subsequent functionalization using the Cu-free or Cu-catalyzed Azide-Alkyne Cycloaddition (CuAAC) reaction.**

The synthesis in Scheme 2.2 illustrates our approach to yield water-dispersible, clickable AuNPs. Azide-functionalized AuNPs with a mixed-monolayer ligand shell (azide/EG<sub>3</sub> AuNPs) were prepared in a single step using Bunte salt ligand precursors in a mesofluidic reactor,<sup>31,32</sup> modified to allow for the incorporation of the second ligand type. The mesofluidic reactor was assembled using commercially available parts. Technical details regarding the set-up are provided in Appendix A along with codes used to carry out the synthesis. Core size can be controlled over a range of 2-6 nm by adjusting the pH of the gold precursor

solution.<sup>31</sup> In this work 3.5 nm AuNPs were prepared by using a precursor solution pH of 5. The Bunte salt ligands were readily prepared on the gram scale in one or three steps (for the **EG<sub>3</sub>-BS** and **N<sub>3</sub>-EG<sub>3</sub> BS**, respectively (Scheme A1)) from commercially available alkyl halides, and purified without any chromatography. Typical AuNP syntheses require only a few milligrams of ligand. During AuNP synthesis in the reactor, the two BS ligands were first mixed in a 1:19 ratio (**N<sub>3</sub>-EG<sub>3</sub> BS/EG<sub>3</sub> BS**), followed by addition of the NaBH<sub>4</sub> solution and, finally, by the addition of the pH-adjusted HAuCl<sub>4</sub> (Figure 2.1).

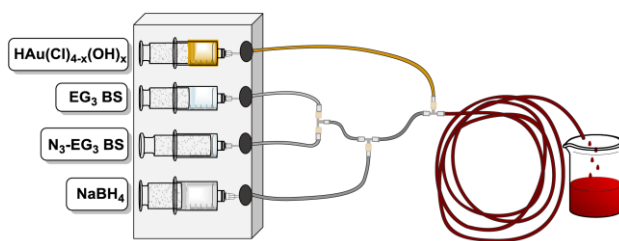


**Figure 2.1 Schematic of the one-step flow-based synthesis of azide-terminated, mixed monolayer AuNPs.**

Computer-controlled pumps deliver reagents that are combined with T-mixers; check valves are utilized between the outlet of each syringe and the inlet to the T-mixers to prevent backflow; and the length of the reaction tubing leaving the final mixer is sufficient to provide at least a 2 s residence time.

Attempts to prepare the desired AuNPs in a batch reaction using the same reagents, but in a round-bottomed flask, were unsuccessful. Formation of AuNPs occurs so rapidly that mixing in the flask creates an inhomogeneous reaction mixture that does not permit reproducible control over ligand shell composition, core size, and core size distribution. During a flow synthesis employing high flow rates (60 mL/min) and narrow tubing (0.030 in. inner diameter), turbulent mixing results in mixing times that are on the order of reaction time.<sup>31,43,44</sup> We observed

that synthesis of AuNPs using a mesofluidic reactor affords excellent reproducibility (SD of core diameter < 0.1 nm) across multiple batches as well as low (< 15%) polydispersity of the AuNPs produced (Tables A1 and A2). All AuNP samples were purified using only tangential flow filtration,<sup>45</sup> as described in the experimental, and isolated as easily redispersible powders following lyophilization. Using this direct synthetic approach, ~5 mg of AuNPs are synthesized in < 30 minutes, purified in 3 hours where they are ready for immediate use, or they may be dried overnight to store as a powder for future use.

#### Characterization of N<sub>3</sub>-EG<sub>3</sub>-AuNP-EG<sub>3</sub>

The azide/EG<sub>3</sub> AuNP composition, size, and stability were thoroughly characterized (Figures A2-A9). The size of the AuNPs was determined by SAXS and corroborated by TEM. Unlike TEM, SAXS can rapidly determine NP size information with higher statistics because SAXS probes a large volume of a given sample, analogous to optical measurements in solution. Additionally, because SAXS measurements are performed in solution, the results are not influenced by drying effects that often complicate analysis of TEM data.<sup>46</sup> The compositions of the AuNPs were determined by X-ray photoelectron spectroscopy (XPS) and proton NMR (<sup>1</sup>H-NMR). The ligand shell coverage determined by XPS was consistent with our previous characterization on AuNPs made using the same stabilizing ligand (EG<sub>3</sub> Bunte salt) in a flow synthesis.<sup>31</sup> To determine the amounts of azide functional groups in the mixed ligand shell we turned to <sup>1</sup>H-NMR (vide infra) because quantifying the amount of nitrogen by XPS is unreliable given that nitrogen comprises only 0.8 atomic % of the sample. Quantification of XPS signals

near the detection limits for nitrogen would be difficult even if adventitious carbon and oxygen were absent.<sup>47</sup>

The use of the hydroxyl-terminated EG ligand significantly enhanced the water-dispersibility of these AuNPs. We found that as long as  $\leq 10$  mol% azide BS ligand (relative to stabilizing ligand) was used during NP synthesis, the resulting azide/EG<sub>3</sub> AuNPs remained completely dispersed in water for extended periods of time. During NMR studies we observed that solutions could be concentrated up to 17 mg/mL without any visible changes; additionally, our 1 mg/mL stock solutions did not have any changes over the course of three months. This was in stark contrast to the methyl terminated EG synthesis,<sup>26,27</sup> where we observed AuNPs precipitated out of solution immediately at  $\sim 0.1$  mg/mL. The increased stability of the azide-functionalized AuNPs reported herein demonstrates that the novel AuNP composition directly impacts the particle performance.

We monitored the long-term stability of the azide/EG<sub>3</sub> AuNPs by UV-visible spectroscopy. Samples were stored either as dried powders or dispersed in water. The UV-vis spectra remain unchanged over the course of 17 months (Figure A3) and the samples remained readily dispersible in water without any signs of aggregation using either storage method. XPS was used to assess the extent of thiolate oxidation during storage as a dried powder (Figure A8-A9). The presence of a thiolate linkage binding the ligands to the NP at  $\sim 163$  eV was seen in the S 2p region. Over the course of 17 months, some oxidation of the sulfur occurs, as evidenced by the peak at  $\sim 169$  eV (Figure A9), but even after prolonged storage

less than 26% of the sulfur was oxidized. This degree of oxidation does not appear to diminish the stability of these AuNPs.

Successful incorporation of the azide into the ligand shell was confirmed by  $^1\text{H}$ -NMR spectroscopy. When attached to AuNP surfaces, the  $^1\text{H}$ -NMR signals of the ligands are significantly broadened due to varying magnetic susceptibility at the ligand-NP interface.<sup>34</sup> Therefore, the ligands were released into solution by decomposing the AuNPs using  $\text{I}_2$  or KCN.<sup>35,36</sup> Although both react with the  $\text{EG}_3$  chains, making quantification of the  $\text{N}_3\text{-EG}_3$  to  $\text{EG}_3$  ligand ratio challenging, it was still possible to estimate the composition of the ligand shell.  $^1\text{H}$ -NMR spectra of the free ligands suggested that there was a unique signal for the methylene protons  $\alpha$  to the azide unit (Figure A5) in  $\text{N}_3\text{-EG}_3$ . In  $\text{D}_2\text{O}$  the ligands freed by decomposing the particles with KCN could not be quantified due to overlap of nearby signals. However, the signals resulting from fragmented azide signal were distinct (at 3.4 ppm) in  $\text{CD}_3\text{CN}/\text{D}_2\text{O}$  (99:1), (as confirmed by the decomposition of AuNPs containing only stabilizing ligand). The ratio of the integral of the peaks at 3.4 ppm to the methylene signal observed for the hydroxyl terminus at 3.5 ppm (Figure A7) yielded a ligand shell composition close to the feed ratio (~7% azide as compared to 5% in the feed).

#### Characterization of Clicked AuNPs

To examine the reactivity of the azide/ $\text{EG}_3$  AuNPs, both strain promoted alkyne-azide cycloaddition (SPAAC) reactions and copper catalyzed alkyne-azide cycloaddition (CuAAC) reactions were investigated. The resulting AuNP click products were analyzed using a suite of complementary techniques:  $^1\text{H}$ -NMR

spectroscopy, fluorimetry, thin layer chromatography, SAXS, TEM, and UV-vis spectroscopy.  $^1\text{H-NMR}$  spectroscopy of the purified clicked products was used to verify that any unreacted alkyne was removed during purification.

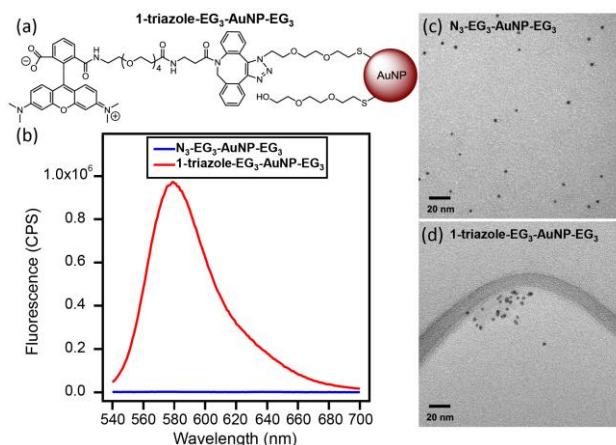


**Figure 2.2 Characterization of 1-triazole-EG<sub>3</sub>-AuNP-EG<sub>3</sub>.**

(a) The product of the SPAAC reaction between  $\text{N}_3\text{-EG}_3\text{-AuNP-EG}_3$  and **DBCO-PEG<sub>4</sub>-Fluor 545** (b) Fluorescence measurements of **1-triazole-EG<sub>3</sub>-AuNP-EG<sub>3</sub>** and the azide-containing reagent (c) TEM micrograph of  $\text{N}_3\text{-EG}_3\text{-AuNP-EG}_3$  (d) TEM micrograph of the click product, **1-triazole-EG<sub>3</sub>-AuNP-EG<sub>3</sub>**.

DBCO-PEG<sub>4</sub>-Fluor 545 (**1**) was selected as a model reactant because the terminal fluorophore made it easy to characterize the success of the click reaction. Fluorescent AuNPs (**1-triazole-EG<sub>3</sub>-AuNP-EG<sub>3</sub>**, Figure 2.2a) were obtained by reacting 15.6 mg of  $\text{N}_3\text{-EG}_3\text{-AuNP-EG}_3$  with 1.40 mg (3 eq. based upon a 5% azide shell) of DBCO-PEG<sub>4</sub>-Fluor 545 in 2 mL of H<sub>2</sub>O. The nanoparticle solution was then purified and isolated as a black powder as detailed in the experimental. Subsequent TLC, NMR and fluorescence measurements indicated successful attachment of the fluorophore (Figure 2.2b and A11) and complete removal of unreacted DBCO-PEG<sub>4</sub>-Fluor 545.

The reactant ( $\text{N}_3\text{-EG}_3\text{-AuNP-EG}_3$ ) and product (**1-triazole-EG<sub>3</sub>-AuNP-EG<sub>3</sub>**) AuNP solutions were visualized by TEM under identical experimental conditions

(Figure 2.2c-d). Images of the product AuNPs show agglomeration of the intact AuNPs, whereas the reactant AuNPs are evenly distributed. The behavior of the nanoparticles as deposited is indicative of the change in surface chemistry following the coupling reaction. SAXS analysis confirms that agglomeration seen in the TEM micrographs following drying is not present in solution. The product AuNPs retain the same average core size ( $3.4 \pm 0.7$  nm) as the reactant AuNPs ( $3.4 \pm 0.4$  nm).

The versatility of these azide/EG<sub>3</sub> AuNPs was further demonstrated by coupling them to a variety of both hydrophobic and hydrophilic moieties with alkyne functionalities (Chart 2.1). We selected alkynes that demonstrate the promise of these NPs within a range of their potential applications. The fluorescent properties of **1** yield AuNPs capable of dual (fluorescence/TEM) imaging,<sup>48</sup> the extended EG

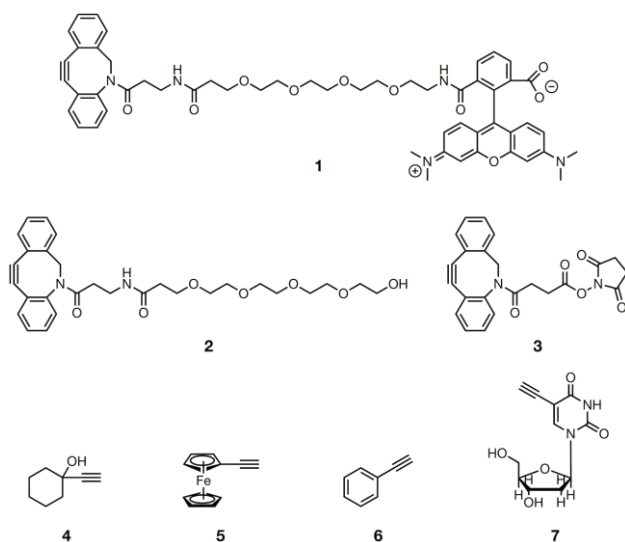


**Chart 2.1 Alkyne containing species used to demonstrate the scope of the N<sub>3</sub>-EG<sub>3</sub>-AuNP-EG<sub>3</sub> reactivity.**

chain in **2** may increase blood circulation time of the NPs,<sup>49</sup> the activated carboxylic acid in **3** can be coupled to a biomacromolecule, the alcohol group in **4**

can be used in subsequent covalent derivatization reactions, the ferrocene unit in **5** is an electrochemical probe, the phenyl group in **6** was used to test NP stability with a hydrophobic group, and **7**, a thymidine analogue, is used to label cellular DNA.<sup>50</sup> In all cases, even when the incoming species was hydrophobic, the AuNPs remained water-dispersible, making the **N<sub>3</sub>-EG<sub>3</sub>-AuNP-EG<sub>3</sub>** reagent of potential interest for biomedical applications such as the delivery of hydrophobic drug molecules.<sup>51</sup> The coupling reactions with terminal alkynes were carried out using low loadings of a simple copper catalyst (~10 mol% CuBr, relative to azide content) in air. The success of the reactions was verified using <sup>1</sup>H-NMR. AuNP ligands were removed by oxidizing them to disulfides with I<sub>2</sub> and then verifying the appearance of signals in diagnostic regions of the NMR spectrum for each alkyne. A representative spectrum is shown in Figure 2.3; all other spectra are in the SI.

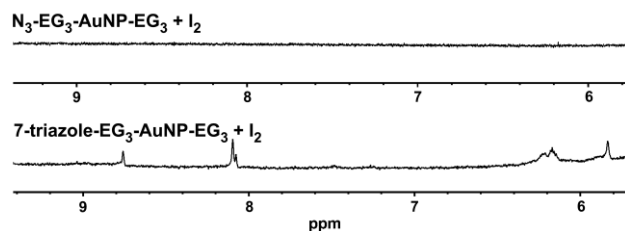


**Figure 2.3** NMR spectra of **N<sub>3</sub>-EG<sub>3</sub>-AuNP-EG<sub>3</sub>** and **7-triazole-EG<sub>3</sub>-AuNP-EG<sub>3</sub>**. <sup>1</sup>H-NMR (600 MHz), D<sub>2</sub>O/DMSO-d<sub>6</sub> (91:9), characterization of **N<sub>3</sub>-EG<sub>3</sub>-AuNP-EG<sub>3</sub>** versus **7-triazole-EG<sub>3</sub>-AuNP-EG<sub>3</sub>** following I<sub>2</sub> decomposition. The diagnostic region showing successful coupling is enlarged for clarity.

## Conclusions

This work describes a new approach towards clickable AuNPs that have controlled dimensions, are readily dispersible in water, and are produced from a

gold salt in a single step. The traditional need for subsequent modifications (following AuNP synthesis) to install azide functionality and increase dispersibility was bypassed by synthesizing mixed-ligand AuNPs directly in water. The typical loss of size control resulting from a water-based synthesis was mitigated by employing a mesofluidic reactor. AuNP purification was rapid with low environmental impacts:<sup>45</sup> tangential flow filtration allowed for removal of small-molecule impurities without the need for any organic solvents. The stability of the NP reagent was demonstrated by the ability to store the azide/EG<sub>3</sub> AuNPs either in water (nanopure or buffered) or as a dehydrated powder for months without noticeable changes. The NPs were amenable to both CuAAC and SPAAC reaction conditions, while maintaining core diameter and water dispersibility, making them promising candidates for biomedical applications.

The azide-functionalized AuNPs presented here are versatile building blocks for accessing hybrid nanomaterials through click reactions. Because they can be readily made in large quantities and stored until their time of use, they are analogous to traditional molecular reagents. NP reagents can provide the opportunity for a broad range of scientists to access and employ sophisticated nanomaterials. Although azide-functionalized AuNPs were highlighted here as an example of a clickable NP reagent, numerous additional AuNP reagents can be envisioned. Since these AuNPs have a ligand-shell that is controlled to be primarily composed of hydroxyl-terminated EG<sub>3</sub>, it is easy to maintain water dispersibility even after being clicked to hydrophobic moieties. Moreover, matching both ligands with EG<sub>3</sub> linkers allows for homogenous mixing of

reagents. These attributes of the synthesis suggest that other functional groups could be appended in place of an azide. For example, an obvious extension of this work would be to replace the  $N_3$ -EG<sub>3</sub> ligands with COOH-EG<sub>3</sub> ligands to make AuNPs for peptide coupling chemistry.

### **Bridge to Chapter III**

Chapter II showed that AuNPs can be generated with mixed-ligand shells to access structures with multiple functionalities. The study in Chapter III also develops a novel synthesis to access well-defined mixed-ligand AuNPs, but now the ratio of ligands is incrementally varied to understand how toxicity changes as a function of shell composition. What we found was that the biological response did not correlate linearly with ligand composition; a small amount of non-toxic ligand had a substantial impact on overall AuNP toxicity. This chapter explores the protective effect of a polyethylene glycol diluent ligand on cationic AuNPs that are toxic in the absence polyethylene glycol ligands.

Both Chapters II and III show that by using deliberate mixed-ligand shell compositions the overall AuNP performance can be significantly enhanced. In Chapter II having  $\leq 10\%$  azide ligand in the shell was vital for maintaining AuNP solution stability, and in Chapter III having a small amount of polyethylene glycol as a diluent ligand significantly reduces the toxicity of cationic AuNPs.

## CHAPTER III

### III. PROTECTIVE EFFECT OF PEG LIGANDS ON CATIONIC GOLD NANOPARTICLE TOXICITY

This chapter is expected to appear in an upcoming publication authored by Aurora L. Ginzburg, Lisa Truong, Tatiana Zaikova, Peregrine D. Painter, Robert L. Tanguay, and James E. Hutchison. A.L.G performed the majority of AuNP synthesis, characterization and data interpretation. L.T. and R.L.T. performed toxicity assays. T.Z. and P.D.P. assisted with development of AuNP syntheses. J.E.H and R.L.T. provided project mentorship. This chapter was written by A.L.G. with editorial assistance provided by J.E.H.

#### **Introduction**

For nanoparticles (NPs) to fulfill their potential in biomedical predictive relationships between NP structure and toxicity are needed.<sup>1,2</sup> Multifunctional gold nanoparticles (AuNPs) have received a substantial amount of medical interest due to their synthetic tunability, general core stability, and plasmonic properties.<sup>3</sup> To achieve multiple functionalities two or more ligand-types are typically employed within a single NP shell; for example, polyethylene glycol (PEG) ligands are used to increase systemic circulation time,<sup>4</sup> and antibodies are used for active targeting.<sup>5</sup> Studies on the toxicity of mixed-ligand NPs have been scarce though; likely due to the synthetic and characterization challenges associated with incremental variations in NP ligand structure.<sup>6</sup> Understanding mixed-ligand NP toxicity is critical for the design of sophisticated nanoparticle-based

medicines, wherein the ligand shell is rarely composed of only one type of molecule.<sup>3,5,7</sup> Our group has previously found that AuNP toxicity can be influenced by the ligand shell in surprising ways.<sup>8-10</sup> We have observed instances of AuNPs being rendered toxic by both chemically bound and adsorbed molecules, including: when synthesized using a cationic ligand that is non-toxic on its own,<sup>8</sup> in the presence of residual (non-toxic) ligand from incomplete ligand-exchange,<sup>9</sup> and when a small amount of non-toxic surfactant is added.<sup>10</sup> Given the influence of even trace non-toxic molecules on the resulting AuNP toxicity, it is essential to study the toxicity of mixed-ligand NPs, particularly those containing ligands with significant differences in their biological behavior.

In this study, mixed-ligand AuNPs were examined that contain two commonly employed ligands used for different biological functions. A short polyethylene glycol (PEG) chain, mercaptoethoxyethoxyethanol (MEEE), was selected as a nonionic and benign ligand because this ligand has been well-documented to yield biocompatible and water-dispersible AuNPs. Moreover, PEG chains are frequently used to produce NPs that escape surveillance by the reticuloendothelial system and have long blood circulation times (often referred to as “stealth” properties);<sup>11,12</sup> we aimed to probe the extent to which “stealth” properties can be imparted on mixed-ligand AuNPs. In contrast to MEEE, our second ligand, a short cationic chain, N,N,N-trimethylammoniumethanethiol (TMAT), contains a quaternary amine, which will typically yield NPs with high cellular uptake, short blood circulation times, and high toxicity.<sup>13,14</sup>

The facile uptake of cationic NPs has made them promising materials for the delivery of therapeutics, such as genes<sup>15,16</sup> or anticancer drugs.<sup>17</sup> However, the toxicity induced by cationic NPs makes separating therapeutic efficacy from cytotoxicity an

ongoing challenge.<sup>15,18–20</sup> PEGylation has been demonstrated as a successful strategy for reducing cationic polymer toxicity,<sup>4,21–23</sup> and we hypothesized some of the benefits PEG imparts to polymers could be extended to cationic AuNPs. We began this study intending to investigate the relationship between TMAT/MEEE ligand ratio and overall NP toxicity. What we found was more remarkable than anticipated; the “stealth” properties imparted by a PEG ligand (MEEE) always overwhelmed the toxicity imparted by TMAT, even in cases where MEEE was significantly underrepresented compared to TMAT.

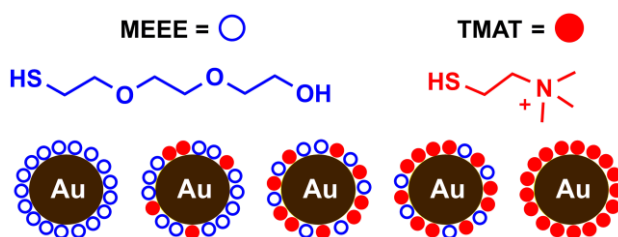


**Figure 3.1. AuNPs with varying ratios of cationic ligand (TMAT) to PEG ligand (MEEE) studied in this work.**

Herein, we have synthesized a series of mixed-ligand TMAT/MEEE AuNPs where the amount of MEEE was varied incrementally. Using a flow AuNP synthesis enabled simple tuning of the stoichiometric ratio of ligands to access a suite of mixed-ligand AuNPs with similar core sizes (~3 nm), despite differences in ligand charge (Figure 3.1). TMAT and MEEE were selected as the ligands of focus for this study because they yield water-dispersible AuNPs with well-known toxicities, and their charge remains the same regardless of local pH. We have previously studied various sizes of MEEE-AuNPs and TMAT-AuNPs and have found TMAT-AuNPs to induce mortality within 18 hours *in vivo*, whereas MEEE-AuNPs are non-toxic for the duration of the assay (5 days).<sup>8</sup> Zebrafish were used as the animal model because of their utility in high-throughput toxicity screening and their good gene homology to humans.<sup>24</sup>

Three sets of mixed-ligand TMAT/MEEE-AuNPs were prepared ranging from 26-77% MEEE and all three sets of the mixed-ligand AuNPs were found to be non-toxic at all concentrations tested (up to 75 ppm). In contrast, the 100% TMAT-AuNPs caused mortality at concentrations as low as 30 ppm. The effect of using a shorter PEG chain, 2-mercaptoethoxyethanol (MEE) was also examined, and the TMAT/MEE-AuNPs were found to be non-toxic as well. The extent of AuNP/protein aggregation was assessed by combining the AuNPs with bovine serum albumin (BSA) which resulted in significant aggregation for the 100% TMAT-AuNPs and relatively little aggregation for all of the mixed TMAT/MEE(E)-AuNPs. The results of this study suggest that incorporating small amounts of PEG into a cationic NP ligand-shell may enable new technologies wherein cationic NPs are desired, but their toxicity must be minimized.

## **Results and Discussion**

### Nanoparticle Preparation

A mesofluidic flow synthesis yielded a suite AuNPs with varying MEEE/TMAT ratios using a slightly modified version of a synthesis that has been previously described in detail.<sup>25,26</sup> Here, instead of Bunte salt ligands, thiol ligands were used due to their ease of synthetic accessibility. Briefly, thiol ligands were made from commercially available chemicals using established 1-3 step procedures.<sup>27,28</sup> To synthesize the ligand-passivated AuNPs, a gold salt precursor solution was prepared and then reacted with thiol ligands and sodium borohydride (adjusted to pH 12 with NaOH) in a ligand to gold to reducing agent ratio of 1:5:2, at room temperature in water.<sup>25</sup> The AuNPs were then dried using lyophilization to concentrate them for column purification. Following drying, a fresh

size-exclusion column was prepared in water and AuNPs were rehydrated in ~1 mL of water to load onto the column. Successful column purification was determined using <sup>1</sup>H-NMR to verify that all free ligand signals were absent (signals due to ligands attached to AuNPs are characteristically broadened).<sup>29</sup>

The pure AuNPs were stored in water and characterized using a suite of complementary techniques.<sup>30</sup> Their core size was determined using small angle X-ray scattering and their morphology was verified to be spherical using transmission electron microscopy (representative data are provided in Figures B1 and B4).<sup>31</sup> AuNP stability was assessed using UV-Vis spectroscopy to monitor changes in their absorbance over the five days (duration of toxicity studies) (Figure B5). All AuNPs described herein had sufficient solution stability to rule out the possibility that AuNP precipitation was responsible for the outcomes of the toxicity studies. AuNP ligand composition was quantified using XPS wherein the sulfur and nitrogen regions were scanned extensively to develop strong signals (Figure B3). The ratio of nitrogen to sulfur is representative of the ratio of TMAT/(TMAT + MEEE). This XPS quantification method was validated by verifying the absence of nitrogen and sulfur contamination and analyzing the pure

**Table 3.1 Summary of the MEEE/TMAT-AuNPs studied.**

Name	Core diameter (nm)	TMAT (%)	MEEE (%)	Range (uncertainty) in XPS results (%)
AuNP <sub>100%</sub> MEEE	3.6 +/- 0.7	0	100	-
AuNP <sub>77%</sub> MEEE	3.5 +/- 1.1	23	77	6
AuNP <sub>31%</sub> MEEE	3.7 +/- 1.1	69	31	13
AuNP <sub>26%</sub> MEEE	2.8 +/- 0.4	74	26	11
AuNP <sub>100%</sub> TMAT	3.1 +/- 0.7	100	0	-

ligands. A summary of the characterization data is provided in Table 3.1.

#### Toxicity Analysis of TMAT/MEEE-AuNPs

Each purified set of AuNPs was tested *in vivo* using a 96-well plate with each well containing one zebrafish embryo. The embryos were fertilized 6 hours before study, and the effects of the NPs on embryo development were monitored over the course of five days. Determination of an appropriate dose/response range was accomplished by first performing a broad range-finding study with a given set of NPs, where 12 animals were tested at each concentration. AuNP concentrations never exceeded 75 ppm because concentrations higher than this are not relevant for applications, and by 75 ppm all of the fish have died with AuNP<sub>100% TMAT</sub>. Following the range-finding study, a larger number of animals (16-48, depending on sample quantity and concentration step size) were exposed to each concentration of AuNPs to determine the AuNP effects on morphological development and mortality. The key findings are provided in Figure 3.2; additional endpoints and concentrations are provided in Appendix B.

In summary, only AuNP<sub>100% TMAT</sub> induced mortality in the zebrafish, and none of the mixed-ligand AuNPs caused any statistically meaningful effects. A range of concentrations were explored for the mixed-ligand AuNPs (shown in Appendix B), including over double the ED<sub>50</sub> concentration observed for AuNP<sub>TMAT 100%</sub>. Figure 3.2 shows the observed zebrafish mortality over five days for 0-50 ppm of AuNPs. While we didn't expect a linear response between the percent TMAT and the observed mortality, the complete lack of response was surprising. We hypothesized that MEEE's increased length compared to TMAT may be effectively burying the positive charge thereby mitigating toxic effects.

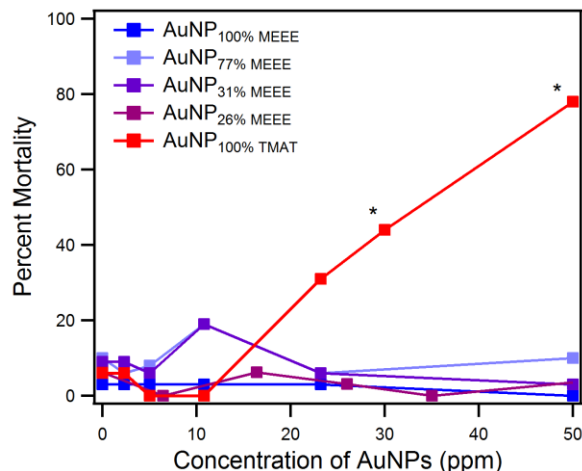


**Figure 3.2. Mortality caused by each set of AuNPs over 5 days.**

Each percentage was calculated by taking the total number of animal hits and dividing it by the total number of viable animals studied (n= 16-48, per data point). A \* indicates mortality that is statistically significant as determined by Fischer's exact test.

It is worth noting that although there is a 0.9 nm range in core size (Table 3.1), the difference between the largest and smallest particle set was not expected to result in significant differences in toxicity based upon our previous study that examined the toxicity of a size ladder of TMAT-AuNPs.<sup>32</sup> Further, the smallest TMAT-AuNPs should be the most toxic (on a mass basis),<sup>8,32</sup> therefore had the mixed-ligand AuNPs induced toxicity, AuNP<sub>26% MEEE</sub> (the smallest set) would have had exacerbated effects due to its small size. Since that did not happen, it is fair to conclude that the size differences between the sets of AuNPs had a negligible effect on toxicity within this study.

#### Effect of a shorter PEG chain on Mixed-Ligand AuNP toxicity

Cationic NPs can induce toxicity by having increased biological interactions and uptake, compared to nonionic or anionic NPs.<sup>19,33,34</sup> We hypothesized that MEEE's increased length, compared to TMAT, may be weakening TMAT's interactions with negatively charged biological species, thus reducing toxicity. To investigate this

possibility, a set of mixed-ligand AuNPs with a shorter PEG chain, MEE and TMAT were synthesized (Figure 3.3). These AuNPs were determined to have a ligand shell composition of 55% TMAT/45% MEE and a core size of 4.1 +/- 1.6 nm (this AuNP set is referred to as “AuNP<sub>45% MEE</sub>”).

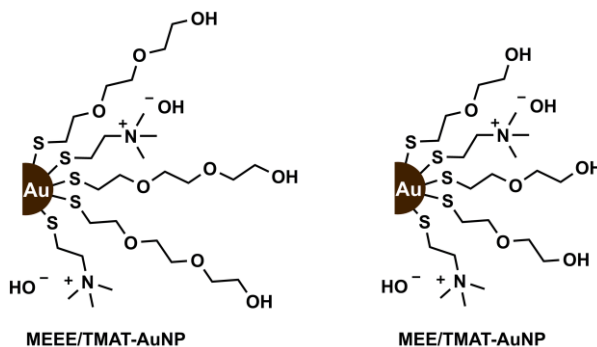


**Figure 3.3. MEEE/TMAT-AuNP versus MEE/TMAT-AuNP.**

MEE is one ethoxy unit shorter than MEEE and is therefore expected to expose more of the cationic charge at the surface of the particle.

If TMAT/MEEE-AuNP toxicity was being precluded due to the positive charge being buried within the ligand shell, then employing MEE instead of MEEE should result in an increase in toxicity. However, AuNP<sub>45% MEE</sub> did not show any toxicity. It seemed unlikely given the similar length of the TMAT and MEE ligands, and the significant portion of the shell containing TMAT, that quaternary amines weren't exposed at the NP surface of AuNP<sub>45% MEE</sub>.

We then considered the possibility that simply diluting TMAT in the ligand shell with MEE(E) ligands was affecting the multivalent presentation of TMAT, and that an unobstructed multivalent TMAT presentation is responsible for the characteristic biological behavior of cationic NPs. However, previous studies have found instances where cationic ligands were diluted with nonionic or anionic ligands within a NP ligand shell (of note, the diluent ligands were not PEG), and in those cases the NPs still

predominantly behaved as cationic NPs in biological systems, even when the net surface charge was neutral or slightly negative.<sup>35,36</sup> Taking results from previous studies and this one together, the data suggest that the chemical properties of PEG itself are imparting a protective effect on the cationic AuNPs and precluding their usual biological interactions.

### Interactions Between TMAT/MEEE-AuNPs and a Model Protein

NP/protein interactions are often the first step in a cascade of biological recognition events that ultimately determine NP circulation time, biodistribution, and toxicity.<sup>4,21,37,38</sup> Previous studies have used *in vitro* methods to evaluate how minor differences in NP ligand shells influence NP/protein interactions;<sup>12,39,40</sup> inspired by past work, we designed a series of experiments for comparing the AuNP/protein interactions between AuNP sets. BSA was selected as the model protein because it is commonly used for *in vitro* NP/protein studies due to its biological relevance;<sup>12,39</sup> albumin is typically the most abundant protein in serum and is therefore likely to impact the biological fate of NPs.<sup>12</sup> AuNPs with homogenous charged ligand shells have been observed to bind with BSA and sediment out of solution when centrifuged,<sup>39</sup> whereas densely-packed PEG shells have been observed to minimize NP interactions with BSA.<sup>12</sup>

The goal of our experiment was to assess the extent of aggregation between BSA and the mixed-ligand AuNPs and determine if PEG was disproportionately affecting NP/protein interactions. To do this, each set of AuNPs was centrifuged with BSA, as well as a complementary control tube of AuNPs without BSA, and then the supernatant absorbance was measured. The results were obvious with the naked eye, there was a purple pellet formed and the supernatant was visibly colorless when AuNP<sub>100%</sub> TMAT was

centrifuged with the BSA, but for all other AuNP sets the supernatant retained a dark purple color. A summary of the UV-Vis results is shown in Figure 3.4.

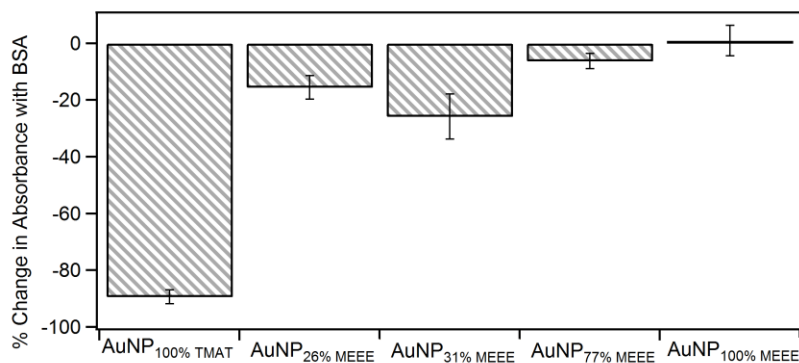


**Figure 3.4. Extent of BSA/AuNP Aggregation.**  
Error bars represent the range of three triplicate measurements.

AuNPs containing even a small amount of MEEE in the mixed-ligand shell have a dramatic reduction in protein agglomeration. Even for AuNP<sub>26%</sub> MEEE, the NP/protein interactions more closely resemble that of AuNP<sub>100%</sub> MEEE than AuNP<sub>100%</sub> TMAT. It is important to note that we ensured the AuNPs were mostly stable to these centrifugation conditions in the absence of BSA by measuring the change in absorbance caused by centrifugation of the pure AuNPs versus a non-centrifuged sample. For all NPs there was <9% change in absorbance caused by centrifugation (Figure B8). Additionally, the original absorbance values used for generating the “% change” on the y-axis of Figure 3.4 were obtained by spinning each set of AuNPs without BSA, to help account for small differences in centrifugation stability between AuNP sets.

The differences between AuNP<sub>26%</sub> MEEE and AuNP<sub>31%</sub> MEEE BSA aggregation aren't likely to be so pronounced based on NP surface chemistry alone. We suspect that the differences observed between the two sets are likely a result of their differences in

core size, which is well-known to influence protein adsorption,<sup>38,41</sup> and particle stability (AuNP<sub>31% MEEE</sub> was the least stable to centrifugation; Figure B8). Even with the minor complexity of AuNP<sub>31% MEEE</sub>, it is clear that the ligand-shell composition plays a dominant role in determining protein interactions. This is evident because AuNP<sub>100% TMAT</sub> lies between AuNP<sub>31% MEEE</sub> and AuNP<sub>26% MEEE</sub> in size, is entirely stable to centrifugation (Figure B8), and yet experiences substantial aggregation with BSA.

Since AuNP<sub>100% MEEE</sub> remained entirely in solution but AuNP<sub>100% TMAT</sub> nearly entirely aggregated out of solution, this experiment served as a method for evaluating the PEG protective effect, or “stealth”, of the mixed-ligand AuNPs. The stealth nature of a PEG shell has been well-documented, and it is known to decrease NP/protein interactions.<sup>38</sup> Nevertheless, because no studies (to the best of our knowledge) have systematically evaluated metal NPs containing PEG/cationic ligand shells, we were surprised just how efficient the MEE(E) partial shells were at preventing aggregation with BSA. Although BSA is a model protein and does not represent the proteins contained in the zebrafish toxicity analysis, understanding the relative propensities of mixed-ligand NPs to bind with proteins helps to inform how different ligands influence NP interactions at biological interfaces.<sup>38</sup> This experiment was also performed on AuNP<sub>45% MEE</sub> and those particles only had in a 20% loss in absorbance (Figure B9), suggesting that the shortened MEE length still provides “stealth” properties.

## Conclusions

By developing a tunable mixed-ligand AuNP synthesis and selecting ligands that can be reliably quantified using an elemental analysis technique, we were able to systematically study the relationship between mixed-ligand composition and *in vivo*

toxicity. Herein, we used two model ligands to explore a suite of mixed-ligand AuNPs with varying cationic/PEG shell compositions. We found that for all AuNPs studied herein, any amount of PEG in a cationic ligand shell was sufficient to turn off toxicity and diminish AuNP aggregation with a model protein. This remained true even for AuNPs containing a small amount of PEG in the ligand shell (26%), and when the PEG ligand was shortened to match the length of the cationic ligand. This is the first study to find that the deleterious effects of cationic AuNPs can be mitigated by incorporating PEG into the ligand shell.

Previous work has established that incorporating PEG ligands into cationic polymers can increase biocompatibility,<sup>4,21–23</sup> but using this strategy with cationic metal-based NPs has not been reported. Conjugating PEG ligands onto cationic NPs has been shown to impart PEG's unique "stealth" properties, such as reduction of non-specific interactions with biological structures.<sup>42</sup> PEG's protective properties are not simply a result of diluting the multivalent presentation of toxic ligand; we observed major reductions in toxicity even at relatively low PEG densities. Additionally, previous work has examined mixed-ligand cationic/alkane-AuNPs which retain their toxicity despite the mixed-ligand shell.<sup>36</sup> PEG's hydrophilicity, lack of ionic character, and conformational flexibility all contribute to its unique ability to minimize NP interactions with biological components.<sup>4</sup> Our research here expands on past cationic polymer studies and demonstrates that incorporation of PEG into a cationic ligand shell can also decrease the toxicity of metal-core NPs. To further widen the toolbox for methods of minimizing cationic NP toxicity, other diluent ligands that possess similar properties to PEG, such as polyglycolic acid and dextran,<sup>4,38</sup> are worth future study.

NPs have many proposed applications in medicine but fulfilling their potential requires tunability of NP localization, accumulation, and toxicity. For example, although cationic NPs have demonstrated the ability to act as gene delivery vectors, their high cytotoxicity has limited commercialization.<sup>21-23</sup> Since therapeutics must balance efficacy against toxicity,<sup>43</sup> our results suggest that partial PEGylation of NPs with toxic ligand-shells may be an effective strategy for increasing therapeutic potential. An additional benefit of using this strategy is that PEG ligands will also increase water-solubility and biological recirculation times, thereby aiding in more efficient drug delivery as well.<sup>44</sup> Herein, we have examined structure/toxicity relationships for mixed-ligand cationic/PEG-AuNPs, and we hope the promising results of these architectures inspire future studies to probe their biomedical properties, such as gene encapsulation efficiency.

## **Methods**

### AuNP Synthesis

AuNPs were prepared we used a modified version of the flow synthesis reported by Elliot et al.<sup>26</sup> The two notable modifications were: rather than using three meters of resonance tubing we used one meter (the data showed an undetectable difference in NP product), and rather than using Bunte salt ligand precursors we used thiols. 1 mM thiol solutions were prepared immediately prior to synthesis from the neat ligands, which were stored under Ar in the freezer. The pH of the gold salt precursor was not adjusted in order to produce small particles with high surface-to-volume ratios.<sup>25</sup> Typically, six synthesis were done in quick succession of one another to yield ~5 mg of crude AuNPs. Two hours after synthesis AuNPs were dehydrated via lyophilization. Following drying, they were

rehydrated in a small amount of nanopure water and purified on a freshly prepared Sephadex LH20 column. Success of the purification was verified by drying a small portion of the product and rehydrating it in D<sub>2</sub>O to ensure that no signals were observed in the proton NMR spectrum. The pure AuNPs were stored in water, except for 1-2 mL which were dried for weighing. Because we were typically weighing out ~1 mg of AuNPs, the stock solution concentration was corroborated using UV-Vis. Since the pure AuNPs weren't entirely stable to lyophilization, only a sacrificial amount was used for weighing and this dried aliquot did not undergo any further testing. The pure stock solutions (concentrations ranged 0.9-1.6 mg/mL) were fully characterized using a suite of complementary techniques (XPS, TEM, UV-Vis and SAXS) before undergoing *in vivo* testing.

#### Quantification of AuNP ligand shell components

Since TMAT is the only nitrogen-containing species within these AuNP architectures we were able to use XPS to quantify the ratio of ligands. To ensure no sulfur or nitrogen contamination was present on the substrate we prepared XPS films on boron-doped diamond that was rigorously cleaned using aqua regia and piranha prior to film deposition. AuNPs were deposited as thin films by pipetting 5  $\mu$ L of stock solution onto the diamond substrate in a nitrogen drying chamber, and then allowing the sample to fully dry before adding another 5  $\mu$ l aliquot. This process was repeated until there was an opaque purple spot on the substrate; around 25  $\mu$ L deposited total. Elemental composition was then measured using a ThermoScientific ESCALAB 250 X-ray Photoelectron Spectrometer with an Al K $\alpha$  monochromated source (150 W, 20 eV pass energy, 500  $\mu$ m spot size). The spectra were analyzed in ThermoScientific Avantage 4.75 software by

performing a linear background subtraction and calibrating to the Au4f peak (83.95 eV). Within both the S and N regions, we observed only one chemical environment. The N1s peak appeared at 402.9 eV and the S2p doublet appeared at 162.4 eV. Representative spectra are shown in Figure B3. Each set of AuNPs has three different spots examined, with each spot containing extensive scans of both the N and S regions (scanning was terminated only when additional scans did not improve spectral resolution, typically 30-50 scans). The N/S ratio was calculated for each spot and an average of the three values was reported in Table 3.1, with the uncertainty representing the range in values.

Control experiments with just the free TMAT and MEEE ligands, and no AuNPs, showed that the program's sensitivity factor was incorrect for the quaternary N. For a pure TMAT ligand the ratio of N to S should be 1, but Advantage calculated it as 0.800. We then performed controls on AuNP<sub>100%TMAT</sub> to see if this difference in sensitivity could be confirmed for ligands attached to an Au surface; indeed we found that the N/S ratio was 0.807 for AuNP<sub>100% TMAT</sub>. Therefore, all of the calculated N/S values for the mixed-ligand AuNPs were divided by 0.807 to correct the sensitivity factor during processing.

### Zebrafish Toxicity Testing

The night prior to zebrafish exposure testing spawning funnels were attached to adult 5D zebrafish tanks and embryos were collected and staged.<sup>45</sup> At 4 hours post-fertilization (hpf) zebrafish embryos were enzymatically dechorionated.<sup>46</sup> AuNPs were stored as concentrated stock solutions ranging 900-1600 ppm. Prior to animal exposure, the AuNP solutions underwent serial dilutions to formulate solutions ranging 2-75 ppm in ultrapure water. At 6 hpf, the dechorionated embryos were manually loaded into microplate wells prefilled with 100  $\mu$ L of AuNPs or water for control animals. To ensure

uniform mixing of the AuNPs, the plates were stored overnight on a custom-built shaker, in a temperature-controlled room. The plates were covered with parafilm and foil to prevent evaporation and any potential degradation to AuNPs. For each AuNP set an initial range-finding experiment was conducted with 12 animals at each concentration of AuNPs. Once an appropriate dose-response range was determined 5-7 concentrations of AuNPs were selected to test development effects at, with 16-48 animals exposed to each concentration of AuNPs.

The zebrafish had 22 developmental endpoints analyzed at 18 hpf and 120 hpf using a custom laboratory information management system, the Zebrafish Acquisition and Analysis Program (ZAAP).<sup>47,48</sup> These endpoints included mortality and morphological effects; a representative figure displaying all endpoints is included in Appendix B (Figure B6). The control animals that were only exposed to water were used to ensure that the background response was below previously established thresholds.<sup>10</sup> To meet this criteria the number of affected subjects must be below 20% for all measured end points combined (and less than 10% for mortality alone) at 120 hpf. To differentiate background response from real signal statistical analysis was performed as we have previously described.<sup>49</sup>

#### Assessment of BSA/AuNP Interactions

A 20 $\mu$ M stock BSA solution was made in 10 mM NaCl. AuNP stocks were standardized to 1 mg/mL solutions and then BSA/NaCl or NaCl controls were added for a combined ratio of 100:15 AuNPs/NaCl(BSA) v/v in Eppendorf tubes. The 100:15 solutions were then vortexed before being centrifuged for 20 minutes at 7000 rpm. AuNPs were also tested for stability to centrifugation by preparing tubes which were not

centrifuged. Following centrifugation small aliquots of supernatant were carefully removed from the tubes and diluted into water for UV-Vis measurements. All UV-Vis measurements were performed in triplicate on a microplate reader, with 200  $\mu\text{L}$  of solution in each well. Measurements were taken on a BioTek Synergy 2, using Gen5 1.11 software to set the experimental parameters scanning from 290 to 750 nm in 2 nm steps. Water was background subtracted from all traces.

### **Bridge to Chapter IV**

Understanding the toxicity and biological effects of NPs, particularly as they relate to specific NP structural features, is critically important for enabling the rational design of NPs. Unfortunately, even when NPs are designed with specific properties, they can behave in unexpected ways when introduced into their application environment. Therefore, understanding how NP structure and activity changes within an intended application environment is also quite important.

The work discussed in Chapter IV was an accidental finding; there wasn't prior literature precedent establishing just how susceptible NPs can be to mixture effects, despite the routine use of surfactants in toxicity assays. Our toxicity analysis setup had just been upgraded to allow for automated syringe dispensing of materials. In this setup, a small amount of non-toxic surfactant was used during syringe dispensing of aqueous solutions in order to break the surface tension. We tested this automated process using AuNPs we knew to be biocompatible and were surprised to find that the mixture of the two non-toxic components induced rapid animal mortality. Chapter IV is a detailed investigation into the concentration-dependent mixture synergy between AuNPs and

surfactants, with a focus on structural changes that occur in solution. The findings emphasize the importance of considering all solution components when evaluating NPs.

## CHAPTER IV

### IV. SYNERGISTIC TOXICITY PRODUCED BY MIXTURES OF BIOCOMPATIBLE GOLD NANOPARTICLES AND WIDELY USED SURFACTANTS

Reproduced with permission from Ginzburg, A. L.; Truong, L.; Tanguay, R. L.; Hutchison, J. E. Synergistic Toxicity Produced by Mixtures of Biocompatible Gold Nanoparticles and Widely Used Surfactants. *ACS Nano* **2018**, *12*, 5312–5322. Copyright 2018 American Chemical Society.

#### **Introduction**

Inorganic nanoparticles (NPs) have emerged as promising materials with properties that advance a wide range of applications including: electronic displays,<sup>1</sup> water purification,<sup>2</sup> cosmetics,<sup>3</sup> textiles,<sup>4</sup> medical imaging,<sup>5</sup> and drug delivery.<sup>6</sup> Despite their enhanced properties, NPs are rarely used as individual components within applications. NP-containing products and technologies often combine NPs with molecular species, either by chemically linking the two (*e.g.*, a hybrid nanostructure)<sup>7,8</sup> or by mixing them freely in solution.<sup>9,10</sup> Examples of these approaches include mixing UV-scattering NPs with lithium stearate in sunscreen to help NPs adhere to skin,<sup>11</sup> and using tethering ligands to link silver NPs to clothing to yield an anti-bacterial coating that is durable through repeated laundering.<sup>8</sup> Although the use of mixtures to enhance nanomaterial performance has been demonstrated, it remains unclear how the molecular components of these mixtures will influence any health or environmental impacts of the NPs. Thus,

understanding the effects of NPs in combination with other species is important to avoid negative impacts and to design safer materials.

Studies on mixture toxicity are important complements to studies of individual compounds because chemicals can influence one another's toxicity.<sup>12,13</sup> When a mixture is more toxic than the combination of individual components the interaction is classified as *synergistic*. Historically, synergism was thought to be rare, and considered negligible for low-dose mixtures typically encountered in nature.<sup>14</sup> While this is generally true for the classically studied pesticide mixtures, recent reviews of the literature suggest that mixtures in other environmentally relevant contexts, like biocide formulations, have a much higher incidence of synergy (26% incidence reported in tested biocide mixtures in contrast to 7% of pesticide mixtures).<sup>13</sup> Synergistic toxicities have been observed between mixtures of mycotoxins at compositions and concentrations typically found in foods,<sup>15</sup> and between metals and polycyclic aromatic hydrocarbons, which are ubiquitous contaminants in both freshwater and coastal environments.<sup>16</sup> The European Union has reviewed concerns that current risk assessments may be inadequate for predicting outcomes of exposures to mixtures and, thus, have prioritized further studies on mixture toxicity.<sup>17,18</sup> Traditional assessments of mixture hazards are based on data collected on the individual components, as opposed to measurements of the mixtures. When the components are expected to have different modes of action, an *Independent Action* model considers the likelihood of each independent chemical causing mortality. On the other hand, a *Concentration Addition* model is used when components have similar modes of action. In this approach chemicals are treated as additive and the impacts are summed together to assess mixture hazards.<sup>3,19</sup> When these models work, they are convenient

because they decrease the time and expense of testing the toxicity of a staggering number of possible combinations and concentrations of components in mixtures.<sup>20</sup> Unfortunately, these convenient models can be misleading because they assume that no chemical interactions and/or reactions occur, both of which can lead to synergistic or antagonistic effects.<sup>12</sup>

Mixture synergies are especially relevant in the case of NPs because their surface properties increase their propensity for interacting with other species.<sup>21-23</sup> NPs often have catalytic activity and high surface area that maximize their interactions with molecules.<sup>24</sup> Even when solution components are not covalently bound or undergoing chemical transformations at the NP surface, they are often readily adsorbed onto the ligand shell. Examples include protein corona formation when NPs are immersed in biological media, and the acquisition of natural organic matter coatings when NPs enter environmental systems.<sup>23,25-27</sup> Such interactions compromise the application of some general axioms of NP hazard, such as smaller NPs tend to be more lethal than larger ones per mass-based dose<sup>21</sup> and uncoated toxic metal cores often leach toxic ions.<sup>28</sup> The addition of additives can alter NP biological reactivity, toxicity, stratum corneum penetration depth, and biodistribution, thereby making it difficult to predict NP safety in mixtures.<sup>27,29</sup> To date, little is known about how mixture-induced changes to NPs (notably ones that do not alter NP dispersibility, core size, or charge) will affect their toxicity.

We recently observed that a series of gold nanoparticles (AuNPs) possessing a ligand shell known to produce some of the safest AuNPs<sup>30,31</sup> exhibits up to 83% increased toxicity when dispensed with a digital dispensing system rather than standard manual hand pipetting. The digital dispensing system, a Hewlett-Packard D300 (referred to as the

BioPrinter), uses inkjet printing technology to precisely dispense picoliter-sized droplets of materials for biological assays. The only substantive difference between this method of dispensing and hand pipetting is the presence of a small amount of surfactant (Polysorbate 20) used to control surface tension within the narrow channels in the BioPrinter printhead. The fact that this non-toxic surfactant,<sup>32</sup> often used as a food additive,<sup>33</sup> dramatically affected the toxicity of the AuNPs, led us to question how the

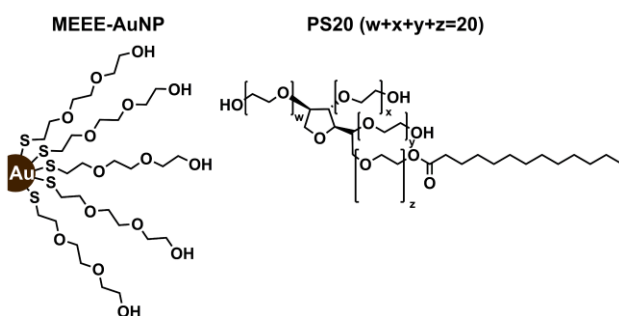


**Figure 4.1 Structure of the nanoparticles, mercaptoethoxyethoxyethanol (MEEE) stabilized gold nanoparticles (AuNPs), and primary surfactant, Polysorbate 20 (PS20), studied in this work.**

surfactant influences the NP toxicity and whether common surfactants might alter the toxicity of AuNPs. Although surfactants have been widely used to disperse nanoparticles,<sup>11,34</sup> and are even used as stabilizing ligand shells on NP surfaces, studies that investigate how free surfactant molecules affect NP properties are sparse. In fact, a review of the literature shows that only a few studies have investigated the effects of mixture components on NP toxicity. The work that has been done is largely focused on how the toxicity of zinc oxide NPs is influenced by components encountered in food and during digestion, such as vitamin C<sup>9</sup> or fatty acids.<sup>35</sup>

Herein, we combined toxicological assays with detailed structural analysis to develop an understanding of how additives influence NP toxicity. We studied the biological

effects of polyethylene glycol-stabilized gold nanoparticles (a class of NPs known to be some of the least toxic),<sup>31</sup> in the presence of a non-ionic, non-toxic<sup>32</sup> surfactant, Polysorbate 20 (PS20); chemical structures are shown in Figure 4.1. Biological assays performed using embryonic zebrafish showed that mixtures of these two chemicals result in a synergistic toxicity. We examined the structural basis for this synergy using a combination of 2D-NMR, small-angle X-ray scattering, and UV-vis. We found that the surfactant assembles on the NP surface, effectively increasing the hydrodynamic particle size, but does not disrupt the metallic core. Mass spectrometry measurements show that PS20 increases the biological uptake of the AuNP/PS20 assemblies. However, the higher quantity of gold accumulated within the zebrafish embryos (*i.e.*, tissue burden), alone, does not account for the increased toxicity. These results suggest that the assembled structures themselves are more toxic. Two other common surfactants were investigated, and both increased the NP toxicity, although to varying extents and on different timeframes.

## **Results and Discussion**

In the initial BioPrinter experiments, we observed that even a small amount (0.003% v/v) of PS20 yielded an AuNP mixture with synergistic toxicity. This result was surprising because both the PS20 and AuNPs showed statistically negligible background mortality when tested individually at these concentrations, and synergistic effects are thought to be essentially nonexistent at the concentrations we were studying (low  $\mu\text{g}/\text{mL}$ ).<sup>20,36</sup> Because our preliminary results suggested that NP toxicity may be susceptible to mixture effects in ways not yet reported, we aimed to investigate (i) at what concentrations do these effects occur, (ii) what is the structural basis for the synergy, and

(iii) can these effects be avoided through the use of alternative surfactants. Ligand-stabilized AuNPs were selected as the NP model because of their well-defined chemical composition and structure, well-studied toxicity, and dispersibility as discrete structures without additional dispersal agents (that would cloud the interpretation of the data by producing a more complex mixture). The AuNPs herein were stabilized by covalently bound mercaptoethoxyethoxyethanol (MEEE) ligands, which have been shown to increase AuNP safety and biological circulation time.<sup>30,31</sup>

These AuNPs were tested *in vivo* using embryonic zebrafish as an animal model for rapid screening. Embryonic zebrafish were used to perform whole-animal investigations because they develop externally and a female is able to produce hundreds of eggs, thereby allowing for large sample sizes.<sup>37</sup> The zebrafish assay is also time and material-efficient, only requiring a few milligrams of AuNPs to perform a rigorous broad test concentration range study in just a few days.<sup>38</sup> We performed extensive testing of a range of surfactant concentrations, AuNP concentrations, and AuNP sizes, to observe how surfactant/AuNP mixtures affect zebrafish development. Inductively coupled plasma mass spectrometry (ICP-MS) was employed to analyze changes in biological uptake of the AuNPs in the presence of surfactant. We primarily focused on studying AuNPs with PS20, but also examined Polysorbate 80 (PS80) and sodium dodecyl sulfate (SDS) as potential alternatives for minimizing mixture synergies. All of the surfactants selected for study are recognized as safe by the U.S. Environmental Protection Agency,<sup>39</sup> and approved for direct addition to foods by the U.S. Food and Drug Administration.<sup>40</sup> These particular surfactants were selected for their ubiquity in consumer products and high production volumes.<sup>41,42</sup>

### **AuNP and PS20 exhibit a synergistic toxicity *in vivo***

Toxicity assays were performed by exposing zebrafish embryos (8 hours post fertilization (hpf)) to AuNPs and monitoring embryo development over the course of five days. Embryos were exposed to five sizes of AuNPs with core diameters ranging from 1.0 to 3.9 nm (sizes and distributions listed in Table C1). Each size was exposed at five concentrations ranging from 2.32 to 50  $\mu\text{g/mL}$ , a concentration range that is typical for examining the biocompatibility of nanomaterials.<sup>43</sup> Our previous work studying the toxicity of MEEE-AuNPs examined concentrations ranging 1-250  $\mu\text{g/mL}$  and, although the particles are stable even at those high concentrations, we focused here on the lower concentrations that are closer to those used in applications. AuNPs were delivered to the embryos using one of two mechanisms, traditional hand-loading with micropipettes or digital dispensing with the BioPrinter. As shown in Figure 4.2, the results of the hand pipetting experiments (Figure 4.2b) were strikingly different than those obtained from the BioPrinter (Figure 4.2a). For example, 50  $\mu\text{g/mL}$  of 1.0 nm AuNPs dispensed using the BioPrinter resulted in 88% mortality; while hand-loading of the same AuNPs only resulted in 3% mortality (background mortality for non-exposed animals is  $\leq 10\%$ ). The only substantive difference between dispensing methods is that the BioPrinter requires a small amount of PS20 to break solution surface tension of aqueous samples. The stock sample in the printhead (containing 0.3% PS20 + AuNPs) is diluted 100X when dispensed into embryo-containing wells, resulting in a final well concentration of 0.003% PS20. This concentration of PS20 does not cause any mortality individually (see 0  $\mu\text{g/mL}$  condition in Figure 4.2a). A schematic of the BioPrinter setup is included in Appendix C (Figure C1).

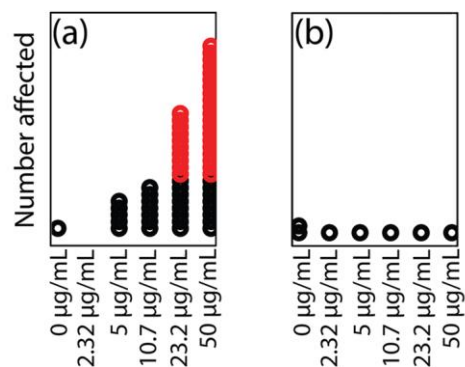


**Figure 4.2 Mortality profiles of 1.0 nm AuNPs at 24 hpf in embryonic zebrafish.**

Graphs display the number of zebrafish embryos affected under each condition (numbers also provided in Table 4.1, N=32 per exposure condition). The red data indicate statistically significant incidents. Embryos were exposed to AuNPs either by (a) digital dispensing using the BioPrinter in the presence of PS20 or (b) without PS20 (by hand-pipetting). The complete data sets with 22 endpoints are shown in Fig. C2.

In the toxicity profiles shown in Figure 4.2, each circle represents one embryo experiencing the endpoint of interest (mortality at 24 hpf in Figure 4.2, other endpoints are included Figure C2). Fisher's exact test is used to determine if a null hypothesis is supported, if not, the treatment affected the incidence and that response is statistically significant. We indicate responses above this statistically significant threshold by coloring those data points red. Figure 4.2 shows that in the absence of PS20, 1.0 nm AuNPs have low toxicity, which is consistent with what we<sup>31</sup> and others<sup>44</sup> have previously observed for polyethylene glycol coated AuNPs in this size range (1-4 nm). The significant toxicity observed when AuNPs are dispensed with the BioPrinter was a consistent trend for all sizes of AuNPs tested (Figure C3).

**Table 4.1 Chemical influence on the incidence of mortality at 24 hpf (MO24) in embryonic zebrafish**

[AuNP <sub>1.0 nm</sub> ] (µg/mL)	[PS20] (% v/v)	MO24(%)
2.3	0	3
5.0	0	3
10.7	0	3
23.2	0	3
50.0	0	3
0	0.0003	3
0	0.003	0
0	0.03	13
0	0.3	81*
2.3	0.003	0
5.0	0.003	16
10.7	0.003	22
23.2	0.003	56*
50	0.003	88*
23.2	0.0003	9
23.2	0.003	53*
23.2	0.03	94*
23.2	0.3	100*

32 zebrafish embryos were exposed to each treatment. Asterisks indicate significance as determined by Fisher's exact test, \* $p < 0.01$ . Background mortality for non-exposed controls is  $\leq 10\%$ .

Table 4.1 lists the toxicity caused by 1.0 nm AuNPs individually, PS20 individually, and mixtures of the two. The AuNPs have low, statistically insignificant, mortality through 50 µg/mL. PS20 has insignificant mortality until a concentration of 0.3% is reached. Comparing these individual toxicities to the results from initial studies using the BioPrinter for dispersal (where PS20 concentration is always 0.003% and AuNP concentration is varied, Figures C2 and C3), shows that the extent of mixture synergism depends on AuNP concentration. For AuNP<sub>1.0 nm</sub>, the onset of synergy occurs at 23.2 µg/mL of AuNPs. Thus, we used this concentration of AuNPs to assess the extent of mixture synergism when the amount of PS20 is varied.

The synergistic effects of the AuNP/PS20 mixtures depend upon not only the concentration of AuNPs, but also the amount of PS20 in solution. When the AuNP concentration is held constant and 0.0003% PS20 is added, there is no increased mortality in the zebrafish (the 9% mortality observed is consistent with background incidence). Mixtures of AuNPs and either 0.003 or 0.03% PS20 exhibit significant mixture toxicity even though the components alone do not cause toxicity. Since the 0.3% PS20/AuNP mixture kills the whole zebrafish cohort, and 0.3% PS20 induces toxicity on its own, it is not feasible to determine the extent of synergism under these conditions. Collectively, these data show that synergistic effects are modulated based upon chemical composition of the mixture; changing the amount of PS20 in the mixture can decrease mortality incidence from 94% to 9%, despite both concentrations of PS20 only causing background mortality when tested without AuNPs.

The observed synergy, with respect to zebrafish mortality, suggests that there may be an interaction between the PS20 and the AuNPs. It is well established that the toxicities of NPs can be altered due to the free ions, released ligands, unpassivated NP surface, or the change in core<sup>45,46</sup> that occurs when NPs dissolve or agglomerate in solution. Therefore, we examined whether PS20 was altering the structure of the AuNPs, which could lead to the observed synergy.

### **PS20 and MEEE-AuNPs interact to form assemblies**

The types of structural changes that might occur include AuNPs agglomerating or forming assemblies with PS20, PS20 displacing MEEE ligands, or PS20 etching/dissolving the AuNP core. UV-vis was used to monitor the stability of the AuNP cores and their dispersion in the presence of PS20, for each core diameter. UV-vis is an

informative technique for AuNPs in this size range because changes of just a few atoms in the core, either by dissolution or agglomeration, will result in a different optical signature.<sup>47,48</sup> Comparing the absorption spectra of the AuNPs with and without PS20 shows no differences between the two, suggesting that PS20 is not destabilizing the AuNPs (representative results are shown in Figure C4, this stability was consistent for all five AuNP sizes). However, the smallest AuNPs studied herein (AuNP<sub>1.0 nm</sub>) do not have a localized surface plasmon resonance peak so UV-vis may not detect small changes in NP size or dispersity. Therefore, we collected small-angle X-ray scattering (SAXS) data on AuNP<sub>1.0 nm</sub> in the presence of PS20 to confirm the UV-vis results. The scattering patterns measured by SAXS depend upon NP size; dissolution of NPs leads to changes in the scattering pattern and/or a comparatively lower scattering intensity, while agglomeration will cause a Bragg peak at a low  $q$  value.<sup>48,49</sup> The measured SAXS patterns showed that the AuNPs exist as a single size population and retain the same average core size after combination with PS20 (Figure C5). There is no evidence of NP agglomeration in the SAXS patterns. Because SAXS and UV-vis measurements are sensitive to small changes related to the NP cores at this lengthscale, we thought it was unlikely that the increased toxicity was the result of changes that were too small to detect by these techniques. The combined results from SAXS and UV-vis suggest that enhanced toxicity might be the result of interactions between the PS20 and AuNP ligand shell, as opposed to AuNP core dissolution or agglomeration.

If PS20 interacts with the AuNP's ligand shell *in solution* it is likely through weak, non-covalent interactions, resulting in an AuNP/PS20 assembly, analogous to protein corona formation. Techniques to investigate the formation and structure of such

assemblies typically rely on diffusion-based measurement such as dynamic light scattering (DLS) or Diffusion-Ordered Spectroscopy (DOSY) NMR.<sup>50</sup> These techniques provide information about the diffusion coefficient of a species or assembly, which is related to hydrodynamic radius *via* the Stokes-Einstein equation, and the radius can be converted to a hydrodynamic diameter ( $D_h$ ).<sup>50,51</sup> For clarity, Figure C6 illustrates the structural difference between an AuNP  $D_h$  and a core diameter ( $D_{core}$ ).

DOSY is a powerful tool for measuring hydrodynamic size and, as opposed to DLS, can be used to determine the chemical composition of different populations in the mixture. From the DOSY data it is possible to determine the  $D_h$ , relative proportion, and chemical make-up of each diffusing population.<sup>50</sup> In our studies, it is beneficial that DOSY displays the protons composing each diffusion population because it enables differentiation between populations of AuNPs, PS20 micelles, and AuNP/PS20 assemblies.

Although the benefits of DOSY seemed clear, we wanted to evaluate the appropriateness of the technique for this application. One challenge with DOSY is the need for sharp peaks in the 1D-NMR spectrum. This limits its use for many NP systems, because ligand peaks are characteristically broadened due to their reduced molecular tumbling.<sup>52</sup> Fortunately, our smallest size of AuNPs ( $D_{core} = 1.0$  nm) rotate fast enough to have well-resolved peaks, thus allowing for tracking of the AuNP proton signals in the 2D spectra (Figure C7). A second concern we had was whether the calculated diffusion coefficients would be influenced by small differences in temperature and viscosity, two important variables in the Stokes Einstein equation.<sup>50,51</sup> We examined the influence of these variables by computing  $D_h$  with the largest variation expected, as well as testing the

viscosity changes experimentally with a mannose standard. The amount of variation calculated was smaller than the experimental error of the measurements in each case (see SI for details). The last challenge we anticipated for the DOSY experiment was obtaining sufficient signal/noise for the MEEE-AuNP peaks of interest. Since the purpose of this study was to correlate structural changes with toxicity profiles, it was necessary to mimic the same parameters used in toxicity assays. Therefore, increasing the AuNP concentration was not a feasible method of increasing the signal. Increasing the number of scans could increase signal, but would limit our ability to study what we anticipated would be a dynamic system once PS20 was added.

To determine the best experimental parameters for obtaining accurate data from the relatively small MEEE-AuNP peaks, we first performed DOSY studies on AuNP<sub>1.0 nm</sub> alone in D<sub>2</sub>O. Using this sample we determined a set of experimental parameters<sup>53</sup> (*e.g.*, number of scans (NS), range of gradient strength (**g**), diffusion time ( $\Delta$ ), and diffusion gradient length ( $\delta$ )) that provided a  $D_h$  value consistent with what is expected based upon

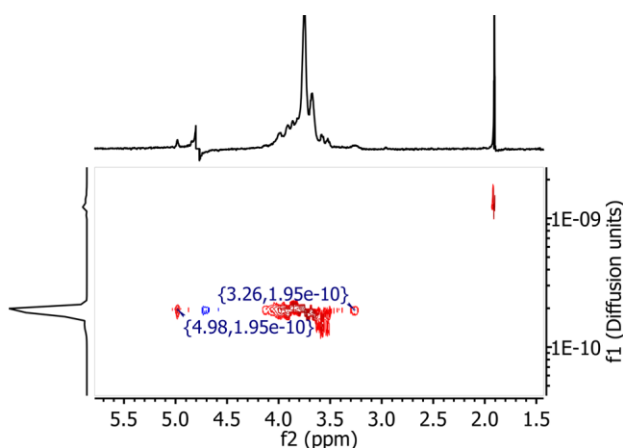


**Figure 4.3 2D DOSY spectrum for MEEE-AuNP<sub>1.0 nm</sub> in D<sub>2</sub>O.**

The peak at 4.98 ppm was used to track the size of the AuNPs throughout experiments, and confirmed by the peak at 3.26 ppm.

a 1.0 nm core and MEEE ligands. Despite our initial concerns that detecting the whole decay function properly would require multiple hours of acquisition, we identified experimental parameters that allow for a 35 min acquisition time with results that show no difference in the MEEE-AuNP 2D spectrum compared to a 4.5 hr acquisition time.

The 2D DOSY spectrum for pure MEEE-AuNPs is shown in Figure 4.3 The horizontal spectrum displays the  $^1\text{H-NMR}$  peaks and the vertical spectrum displays the diffusion populations, which are just residual HDO and one population of AuNPs in this case. The peak at 4.98 ppm was used as the unique signal for tracking AuNPs in solution with PS20, and a second AuNP peak, at 3.26 ppm was used to confirm that the peak at 4.98 was not affected by the HDO signal that results from proton impurities in the  $\text{D}_2\text{O}$  solvent. The 3.26 and 4.98 ppm AuNP peaks do not overlap with PS20 signals (Figure C7), making it possible to attribute the measured diffusion coefficients to the AuNPs, not PS20 micelles. The maximum of the MEEE-AuNP diffusion population is  $1.95 \times 10^{-10} \text{ m}^2\text{s}^{-1}$ , corresponding to a  $D_h$  of  $2.5 \pm 0.1 \text{ nm}$  (reported uncertainty is the experimental variation in the peak maximum, as determined by triplicate measurements).

DOSY NMR was used to monitor the evolution of AuNPs over time in the presence of varying concentrations of PS20. Samples contained  $1000 \mu\text{g/mL}$  of AuNPs to mimic BioPrinter stock solution conditions (*i.e.*, conditions the NPs were exposed to prior to dispersal with zebrafish, set-up details are included in Figure C1). Importantly, both DOSY and SAXS data demonstrated that even at this relatively high concentration of  $1000 \mu\text{g/mL}$ , AuNPs remain a single, non-aggregated, population in the absence of PS20. Samples were monitored for 18 hrs: 18 hrs is the amount of time between the initiation of embryo exposure and the first endpoint assessment. At the start of each study

samples had 0.3, 0.03, 0.003 or 0.0003% (v/v) PS20 added. The AuNP/PS20 mixtures were monitored closely for the first two hours, as that is when most of the changes in AuNP size occurred. A control sample, containing only AuNPs and no PS20, remained unchanged over the course of 18 hours.

New AuNP-containing species with lower diffusion coefficients appear almost immediately after PS20 addition, suggesting rapid assembly of PS20 onto the AuNPs. Because each of these populations contains proton signals from both the MEEE-AuNPs and the PS20, the data provide further evidence for MEEE-AuNP/PS20 assemblies. The

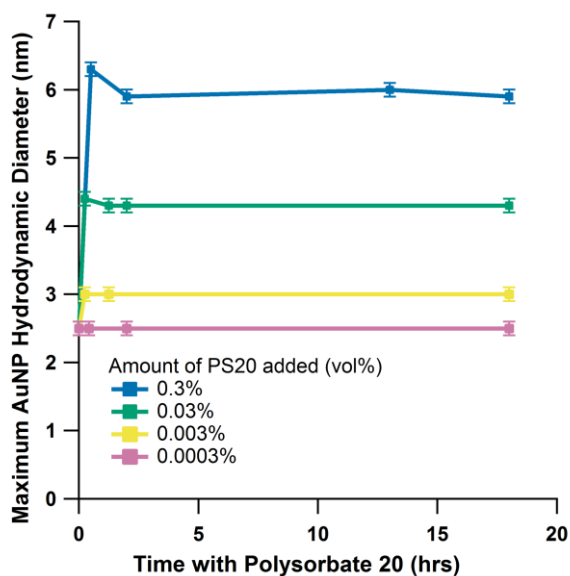


**Figure 4.4 Summary of DOSY data tracking MEEE-AuNP<sub>1.0 nm</sub> growth in the presence of varying concentrations PS20 over 18 hrs.**

Error bars (+/- 0.1 nm) represent the experimental variation in the MEEE-AuNP size, as determined by triplicate measurements on a sample of pure AuNPs. In the absence of PS20, MEEE-AuNP<sub>1.0 nm</sub> have the same response as the 0.0003% PS20 trendline, exhibiting no change in Dh.

diffusion coefficients for both the AuNPs and PS20 micelles are different in the mixture than when measured as single components (Figures C8 and C9), suggesting that the solvation sphere of both the PS20 and the AuNPs are affected by one another. We

monitored the interactions between PS20 and MEEE-AuNPs by collecting DOSY spectra over 18 hours and determining the maximum intensity for each AuNP/PS20 diffusion population. The diffusion coefficients from the slowest moving assembly at each time point were converted to a  $D_h$  and plotted in Figure 4.4. It is important to note that as the concentration of PS20 increased, so did the distribution of AuNP/PS20 assembly sizes. In all cases the largest assembly size was tracked because that population is expected to have toxicity that deviates the most from unassembled AuNPs. The data showed that the diffusion coefficients and relative proportions of the AuNP/PS20 assemblies are dynamic for the first two hours of mixing, but tend to stabilize for the remaining 16 hours of the study (representative DOSY spectra are included in Figures C10-C13).

Figure 4.4 shows that the MEEE-AuNP/PS20 assembly size depends on the concentration of PS20. Only the smallest concentration of PS20, at 0.0003%, did not induce a change in AuNP size. All other mixtures (>0.0003% PS20) formed assemblies within 20 minutes. Comparing the assemblies at 18 hours to the initial MEEE-AuNPs

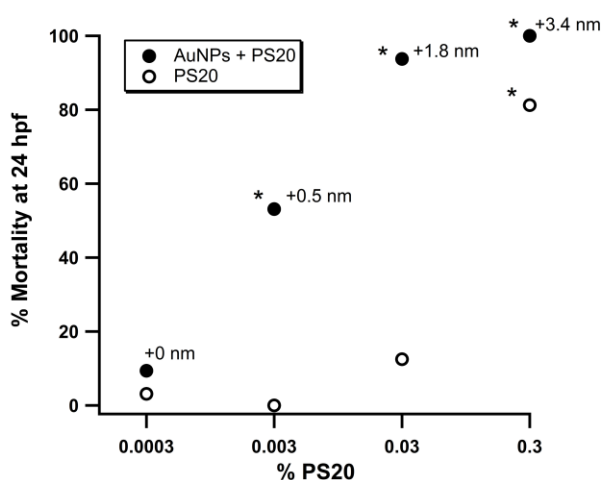


**Figure 4.5 Concentration of PS20 versus zebrafish mortality.**

Solid markers are AuNPs (23.2  $\mu\text{g/mL}$ ) + PS20. Labels next to the solid markers indicate the influence of PS20 on the assembly size (all AuNPs began with  $D_h = 2.5$  nm). Hollow markers show the toxicity due to PS20 individually. Asterisks indicate significance as determined by Fisher's exact test, \* $p < 0.01$ .

reveals that 0.3% PS20 caused 3.4 nm of growth in  $D_h$ , whereas 0.03% and 0.003% PS20 resulted in 1.8 nm and 0.5 nm growth, respectively. The size changes observed are consistent with a model where the PS20 forms a sub-monolayer or interdigitates into the covalently attached MEEE ligand shell. The data do not suggest that PS20 is forming a complete monolayer around the MEEE, because those particles would include sizes between 7 and 16 nm depending upon the structure and conformation of PS20 (see SI for calculations).

Figure 4.5 displays the mortality data as a function of the percent PS20 added (from Table 4.1), along with the assembly size data determined by DOSY. The influence that a given amount of PS20 has on AuNP size is labeled with the relative increase in hydrodynamic diameter ( $\Delta D_h$ ) next to each data point. The plot shows that the formation of assemblies coincides with the onset of mixture synergism. Further, the figure demonstrates that AuNP/PS20 assemblies have different biocompatibility than the individual components, and this is particularly evident for the middle points on the graph (0.003% and 0.03% PS20). At these concentrations of PS20, the toxicity of the mixture is amplified by over 3-fold compared to that of the individual components.

### **Examining potential mechanisms for synergistic toxicity**

There are multiple mechanisms that could render PS20/MEEE-AuNPs more toxic than the sum of their components. One hypothesis for the observed toxicity is that the oligo-ethylene glycol coated AuNPs serve as a template for assembly of the PS20, and that the surfaces of these PS20 assemblies are responsible for increased toxicity. Alternatively, PS20, through interaction with the AuNP, might render the NPs themselves more toxic. We examined nanostructures that were similar to the 1 nm AuNPs, but

lacking a metal core, so as to isolate the possible effects of the surface coating and the metal core. We aimed to find a metal-free structure with approximately the same dimensions and surface chemistry as our AuNPs. A commercially available dendrimer containing hydroxyl-terminated polyethylene glycol ligands, similar in length to the MEEE ligands, met these criteria (structures in Figure C14). The measured  $D_h$  for the dendrimer was 1.5 nm (compared to 2.5 nm for the AuNPs). The dendrimers were then evaluated, alone and in combination with PS20, in zebrafish embryos, employing the same conditions as the manually-dispensed AuNP assays. The isolated dendrimers did not cause any developmental toxicity and mixtures of the dendrimers with PS20 produced only additive effects (Figure C15). Further, DOSY NMR studies show that the dendrimers and PS20 form assemblies (Figures C16 and C17) like those found for the AuNPs with PS20. The formation of assemblies, but lack of synergism for these mixtures, suggests that PS20-coated oligo-ethylene glycol nanostructures are not the direct cause of the synergism, and implies that the mechanism of toxicity is not due to MEEE-AuNPs enhancing the delivery of PS20. Instead, the PS20/AuNP assemblies may have synergistic toxicity because of differences in AuNP bioavailability.

To evaluate whether MEEE-AuNP/PS20 assemblies have enhanced uptake compared to AuNPs alone, we used inductively coupled plasma mass spectrometry (ICP-MS) to measure the mass of gold in zebrafish (n=3, 4 biological replicates) in the presence and absence of PS20 (Figure 4.6). The results showed that in the presence of PS20, 44% more gold enters the embryos. While this clearly demonstrates that PS20 increases the gold tissue burden, an increase in the dose of AuNPs, alone, should not have

increased toxicity at these concentrations based upon the data shown in Table 4.1 (in Table 4.1, both 23  $\mu\text{g}/\text{mL}$  and 50  $\mu\text{g}/\text{mL}$  of AuNPs cause only 3% toxicity). Instead, the 53% toxicity that is observed for the mixture of 23  $\mu\text{g}/\text{mL}$  AuNPs and 0.003% PS20 suggests that the AuNP/PS20 assemblies are more toxic structures on a molar basis. Although the increased uptake of the assemblies (compared to the AuNPs alone) exacerbates the synergism, these results suggest that the assemblies have a different mechanism of toxicity than the AuNPs or PS20 alone. In previous work,<sup>54,55</sup> we were able to use behavioral and developmental endpoints to assess differences in the

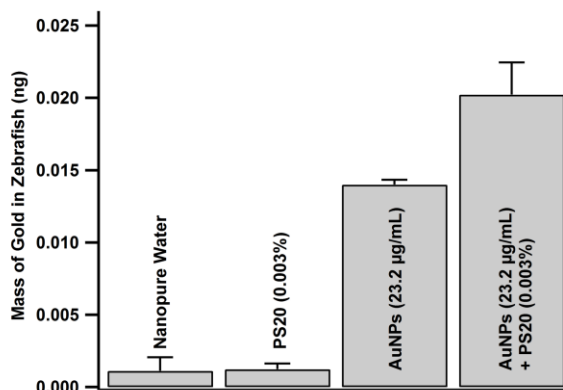


**Figure 4.6 Tissue concentration after exposure to gold, as determined by ICP-MS.**

mechanisms of toxicity. For the materials studied herein, however, this was prohibited by the high level of mortality caused by the mixtures and the low level of effects caused by the individual components (see Figure C2).

#### **Other common surfactants have synergistic interactions with MEEE-AuNPs**

We evaluated two other common surfactants, Polysorbate 80 (PS80) and sodium dodecyl sulfate (SDS) (Figure 4.7), to examine whether the synergistic toxicity found in the PS20/AuNP mixture might be a more general phenomenon. PS80 was selected to

compare a surfactant chemically similar to PS20 but with increased hydrophobicity, and SDS was examined to compare an ionic surfactant to the nonionic polysorbates. Both PS20 and PS80 are derived from polyethoxylated sorbitan and a hydrophobic acid; in PS20 the hydrophobic chain is 11 carbons long and saturated, whereas in PS80 the hydrophobic chain is 17 carbons long and contains an internal double bond. In contrast, SDS is anionic, and consists of a 12-carbon alkane chain attached to a sulfate head group.

In the presence of MEEE-AuNPs, the toxicity profile for PS80 is similar to that of PS20, although the magnitude of the synergistic effects is somewhat lower (Figure C18). For example, for 0.03% PS80/AuNPs at 24 hpf there is a measurable synergy, whereas a measurable synergy is observed down to 0.003% in the case of PS20. The similarity between mixture effects for PS80 and PS20 might be predicted based on their similar structures. The reduction in mortality rates in the case of PS80 may be due to structural differences between PS tails, changing the interaction with the MEEE ligands.

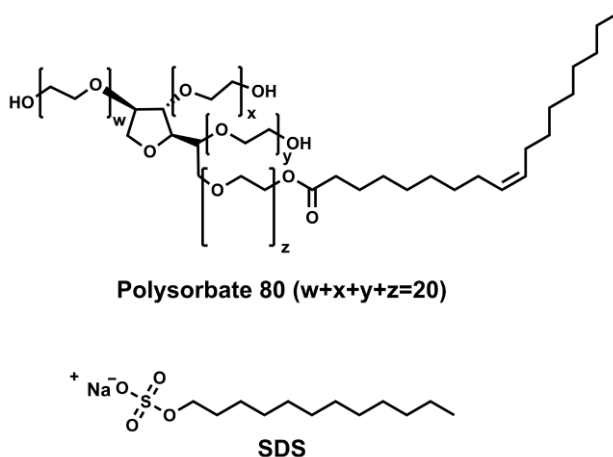


**Figure 4.7 Structures of additional surfactants studied *in vivo*.** Developmental endpoints are shown in the SI.

In the presence of the anionic surfactant (SDS) at 24 hpf the toxicity is additive and essentially no synergy is observed; however, by day five, (see Figure C18) there is a notable synergistic increase in toxicity for the samples containing MEEE-AuNPs and either 0.03 or 0.003% SDS. The delayed onset of the synergistic effects suggests that the mechanism of synergy is different for SDS than with the Polysorbate surfactants. These results demonstrate that surfactants, as a class of compounds, may exhibit synergistic increases in toxicity with NPs, but the magnitude of these effects and the mechanisms causing them depend upon the surfactant structure.

## Conclusions

*In vivo* studies were performed with five MEEE-AuNP sizes in the presence of Polysorbate 20 (PS20). Although the AuNPs and PS20 both exhibit low toxicity alone, any concentration of PS20 sufficiently high to produce an assembly with the AuNPs resulted in significantly increased toxicity for the mixture. Synergistic toxicity at low concentrations, 23  $\mu\text{g/mL}$  of AuNPs and as low 0.003% (v/v) of PS20 is especially surprising because synergies generally occur at higher concentrations.<sup>13</sup> NMR studies confirmed that PS20 assembles onto the periphery of the AuNPs under the biological exposure conditions. Studies on dendrimers with similar dimensions to the AuNPs show that they, too, form assemblies with PS20, but those assemblies do not cause increased toxicity. Those results suggest that PS20 increases the toxicity of the AuNPs, as opposed to the NPs inducing a toxic assembly of PS20. ICP-MS studies show that PS20 increases the uptake of AuNPs in the organisms compared to AuNPs alone. However, these differences in uptake do not account the observed synergy, suggesting that the assemblies are also more toxic per mole than the individual components. Lastly, we studied other

surfactants and found that the AuNP/surfactant synergy is not exclusive to PS20; synergistic toxicity also occurred with Polysorbate 80 and sodium dodecyl sulfate.

Our findings that the presence of surfactants can increase the hazards of a NP mixture are important for the nanotechnology community. Surfactants are often added to NP solutions to disperse nanomaterials or enhance the stability of dispersions,<sup>34</sup> reduce the formation of free radicals,<sup>56</sup> and improve the texture of cosmetic formulations.<sup>11</sup> For example, NPs in sunscreens are often coated with dimethicone to decrease agglomeration and increase photostability,<sup>56</sup> and NP toxicity studies sometimes employ PS80 in the media to promote solution dispersion.<sup>34,57</sup> Moreover, when NPs enter surface waters or sewage systems they are likely to come in contact with surfactants, and understanding the conditions that promote these types of NP transformations will be important for evaluating environmental risks.<sup>58,59</sup> For nearly a century the rarity of documented synergies, along with the combinatorial nature of mixture toxicology, have motivated a standard practice of treating mixture toxicity as the sum of individual components.<sup>12,13,20</sup> Based upon our findings, the synergistic role of surfactants on NP toxicity should be considered in the design of investigations or products. It is not safe to assume that a mixture of “non-toxic” ingredients, such as surfactants and NPs, will produce a benign mixture. In addition, these findings should be considered when interpreting previous studies that have employed NP/surfactant mixtures, such as those assessing nanomaterial safety or the formulation of cosmetic formulations, where the outcomes may have been influenced by the surfactants used.

Given the widespread use of surfactants both industrially and academically, it is important to identify strategies for selecting safe NP/surfactant combinations. By

combining toxicological analysis with a molecular design approach,<sup>60</sup> NP/surfactant mixtures can be formulated with the desired properties without the introduction of undesired hazard. Our studies suggest this is possible because even among chemically similar Polysorbates, there are differences in synergistic effects. It will be important to identify or design alternative chemicals that do not result in a loss of function or performance.<sup>61</sup> Recent advancements in high-throughput technologies and computing may ease the process of identifying mixtures that deviate from additive dosimetry models.<sup>62-64</sup> To enable deliberate chemical selection, there first needs to be studies conducted that form foundational design rules. Our recommendations for maximizing the impact of these studies are to: select NP mixtures with known composition and a minimal number of components, prioritize mixtures by the relevance of the components, and compare chemicals of similar function against one another.

## **Methods**

### Chemicals

All materials were used as received.  $\text{HAuCl}_4 \cdot \text{H}_2\text{O}$  (99.9%) was purchased from Strem, 2-[2-(2-chloroethoxy)ethoxy]ethanol (99%) was from TCI America, sodium thiosulfate (anhydrous) was from Mallinckrodt, pronase was from Roche, sodium dodecyl sulfate was from J.T. Baker, thiourea was from Aldrich, and Tween 20 (*i.e.*, Polysorbate 20) was from Acros. Tween 80 (*i.e.*, Polysorbate 80), triphenylphosphine and glycerol ethoxylate (average  $M_n \sim 1,000$ ) were from Sigma-Aldrich. Deuterium oxide was purchased from Cambridge Isotope Laboratories and stored in the dark. Nanopure water

(18.2 M $\Omega$ ·cm resistivity) was obtained using a Barnstead Nanopure filtration system and used for all syntheses and assays.

#### Preparation and Characterization of MEEE-AuNPs

Mercaptoethoxyethoxyethanol (MEEE) is synthesized *via* a substitution reaction with the chlorinated precursor, 2-[2-(2-chloroethoxy)ethoxy]ethanol, and thiourea.<sup>65</sup> MEEE-AuNPs that are 1.0 nm in metal-core diameter ( $(D_{\text{core}})$ ) as measured by SAXS), and 2.5 nm in hydrodynamic diameter ( $(D_{\text{h}})$ ) as measured by DOSY) were synthesized according to previously reported methods.<sup>31</sup> Briefly, phosphine-stabilized AuNPs were prepared as intermediates and then underwent a biphasic ligand-exchange with MEEE.<sup>66</sup> AuNP<sub>1.0 nm</sub> were purified via size-exclusion chromatography, as confirmed by <sup>1</sup>H-NMR. The <sup>1</sup>H-NMR spectrum was collected in 500  $\mu$ L of D<sub>2</sub>O (residual HDO referenced at 4.79 ppm) on a Bruker Avance III-HD 600 MHz Spectrometer. The other AuNP sets with core diameters ranging from 2.8 to 3.9 nm (sizes and distributions are detailed in Table C1) were synthesized using a mesofluidic reactor where the pH of the gold salt precursor was varied to control core size,<sup>67</sup> and then purified using diafiltration.<sup>68</sup> Following purification, all sets of AuNPs underwent lyophilization and were stored as dried powders.

The AuNP core size and distribution was determined by SAXS and corroborated by TEM to confirm size and shape. SAXS measurements were performed on an Anton Paar SAXSess instrument in in-line collimation mode. SAXS measures AuNP core size in solution, therefore it was possible to measure changes to gold core in the presence of Polysorbate 20 (PS20). Samples for analysis of PS20 effects were prepared at 1000  $\mu$ g/mL of AuNP<sub>1.0 nm</sub>, and 50 scans were collected at 70-second exposure times. In the

SAXSquant software, the raw NP scattering pattern was background and dark subtracted and desmeared using the beam profile generated by the transmitted beam (patterns are shown in Figure C5). TEM confirmed that the sizes obtained by SAXS were valid and that the particles were indeed spherical. TEM measurements were collected on a FEI Titan (S)TEM equipped with an  $C_s$  aberration corrector at 300kV. TEM samples were prepared by floating a copper grid on a dilute solution of AuNPs for ~2 mins, then floating the grid on water for ~2 mins, and then wicking away excess liquid with a Kimwipe. Select dark-field and bright-field images are provided in the SI (Figure C19). Dispersion stability of the AuNPs was assessed with UV-vis. Spectra were collected using an Ocean Optics USB2000 spectrometer with samples in a quartz cuvette (1 cm path length). There was no change in the absorbance of the particles (both with and without PS20) within the time frame and concentrations of the toxicity assays (Figure C4). The dispersion stability was also assessed using SAXS and the average core size was unchanged over 18 hrs in the presence of PS20 (Figure C5b).

### Zebrafish Care and Husbandry

Tropical 5D adult zebrafish were housed at Oregon State University Sinnhuber Aquatic Research Laboratory on a recirculating system at 28°C on a 14h light:10h dark photoperiod. Spawning funnels were placed into the tank the night prior and embryos were collected and staged.<sup>69</sup> The chorion was enzymatically removed using pronase (90  $\mu$ L of 25.3 units/ $\mu$ l) at 4 hpf using a custom built dechorionator.<sup>70</sup> Adult care and reproductive techniques were conducted according to the Institutional Animal Care and Use Committee protocols at Oregon State University (OSU).

### Nanoparticle delivery

For these studies, the MEEE-AuNPs were stored as dried powder in various masses. To standardize all solutions made, each sample used was brought to a stock concentration of 1000  $\mu\text{g/mL}$  by adding an appropriate volume of ultrapure water. Two techniques for delivering the AuNPs were employed: manual pipetting, or the use of Hewlett-Packard D300 digital dispenser (referred to as the BioPrinter).<sup>71</sup> The BioPrinter uses inkjet technology to digitally dispense chemicals. This technology eliminates the need for serial dilution and increases accuracy.<sup>62</sup> For manual hand pipetting, concentrated stock of AuNPs (1000  $\mu\text{g/mL}$ ) were transferred into sterile glass tubes, and brought to the specified concentrations using ultrapure water. Five-point serial dilutions of the AuNPs were made ranging from 2.32 to 50  $\mu\text{g/mL}$ .

#### Developmental toxicity screen

For manual hand pipetting experiments, dechorionated embryos were manually loaded into the wells prefilled with 100  $\mu\text{L}$  of the various concentrations of AuNPs and/or PS20. The experiments using the BioPrinter required embryos to be loaded into individual wells prefilled with 100  $\mu\text{L}$  of ultra pure water. After the embryos were loaded, a stock concentration of AuNPs (1000  $\mu\text{g/mL}$ ) with 0.3% PS20 was dispensed using the BioPrinter to achieve the desired test concentration of AuNPs and 0.003% PS20 in one step (BioPrinter set-up and schematic in Figure C1). After dispensing of the chemicals, to ensure uniform mixing, the plates were moved to a temperature-controlled room with a custom modified shaker and shook overnight.<sup>62</sup> For each AuNP size, six concentrations (a control without any AuNPs, and five concentrations of AuNPs) were assessed, with a total of 32 animals exposed to each concentration. During the

experiments, all plates were covered in parafilm and foil to prevent evaporation and protect against potential AuNP degradation.

In manual hand pipetting experiments where one concentration of the AuNP was used with a varying percentage of PS20, a 50 mL solution of AuNPs at 23.2  $\mu\text{g/mL}$  was made. PS20 was diluted and added to 23.2  $\mu\text{g/mL}$  AuNP aliquots to make 3 separate solutions with final concentrations of 0.3, 0.03, 0.003 and 0.0003% PS20.

At 24 and 120 hpf, 22 morphological endpoints were evaluated and collected in a custom laboratory information management system, the Zebrafish Acquisition and Analysis Program (ZAAP).<sup>62,72</sup> These 22 endpoints include mortality, developmental progression, and eye/jaw defects. The control group (non-exposed animals) were assessed to determine if the number of affected subjects is below 20% for all measured endpoints combined (and less than 10% for mortality alone) at 120 hpf. These thresholds were established statistically from historical data and based upon various large chemical screens. Because developmental testing involves numerous complex series of steps, there is variability in background incidence between experiments. To differentiate background from real signal, statistical analysis was performed as previously described by Truong *et al.*<sup>73</sup> A representative figure displaying the data from all endpoints is included in the supplemental information (Figure C2).

### 2D NMR spectroscopy on AuNPs plus surfactant

The diffusion NMR experiments were performed at an AuNP concentration of 1000  $\mu\text{g/mL}$ . Although toxicity studies only go through 50  $\mu\text{g/mL}$  of AuNPs, we chose to use 1000  $\mu\text{g/mL}$ , as this is the initial concentration of AuNPs present in the BioPrinter incubator prior to dilution in the embryos. The NMR data suggest that the PS20 and

AuNPs associate almost immediately upon addition, therefore changes to the AuNPs will happen during the incubation period and we wanted NMR studies to reflect those changes. Stock solutions of PS20 in D<sub>2</sub>O were made such that 8  $\mu$ L of diluted PS20 was added to 492  $\mu$ L of AuNPs in D<sub>2</sub>O for a total volume of 500  $\mu$ L, where the final PS20 concentrations ranged 0.3-0.0003% by volume.

All <sup>1</sup>H NMR experiments were performed on a Bruker Avance III-HD 600 MHz NMR Spectrometer and acquired at 298.2 K. Data was collected in the TopSpin software and processed in MestReNova version 10.0.2. During acquisition, each DOSY sample first had a 1D spectrum collected with 4 dummy scans and 32 scans. The line broadening was set to 1.00 and the acquisition time to 1 s, then the 1D spectrum was solvent suppressed. The pulse sequence was set to ledbpgppr2s with diffusion time ( $\Delta$ ) equal to 0.1 s and diffusion gradient length ( $\delta$ ) equal to 3400 ms, 4 dummy scans and 32 scans, and a varying gradient power from 5-55% collected over 30 spectra. This gradient range was determined to be appropriate for properly sampling the data points along the whole decay curve from the MEEE-AuNP peaks of interest.<sup>53</sup> Each 2D NMR spectra took about 35 minutes of acquisition time. All spectra were collected in D<sub>2</sub>O and referenced to residual HDO at 4.79 ppm. It is important to note that since quantification of DOSY data is relatively uncommon, we first validated this method using a mannose standard. Additional information about processing the DOSY data is provided in the SI.

#### Gold tissue concentration

Zebrafish embryos that were 8 hpf were statically exposed to 0 (ultrapure water), 0.003% PS20, 23.2  $\mu$ g/mL AuNPs, and 23.2  $\mu$ g/mL AuNPs + 0.003% PS20. It was not feasible to conduct these experiments at 50  $\mu$ g/mL exposures because most of the

population dies within 18 hpf, making the exposure times uncertain. The populations were sampled at 24 hpf to quantify tissue concentration of gold as previously published,<sup>74</sup> with a modification of the wash step. Embryos were washed in the 96-well plate by adding 100  $\mu$ L of ultrapure water, and quickly removed using a Rainin liquidator. This was repeated 10 times. Three embryos were transferred to 14 mL round bottom plastic centrifuge tubes and excess water was removed. There were four biological replicates per exposure group, with a biological replicate made up of three animals. Collected samples were stored in -80 °C until time to sample. Using a Thermo X-Series II Inductively Coupled Plasma-Mass Spectrometer (ICP-MS), gold concentrations were measured in the samples. For each sample, internal standards (indium, rhenium and bismuth) were added with a final concentration of 2 ppb in a total volume of 5 mL. A 5 point standard curve was created using a purchased gold standard (0.01, 0.1, 1, 5, and 10 ppb) and had a R<sup>2</sup> value of 0.997.

### **Bridge to Chapter V**

The synergism produced by mixing food-grade surfactants and biocompatible NPs highlighted the need for studying mixture toxicity. Put simply, using chemicals that are safe individually does not mean the mixture of them is safe because chemicals can transform one another. NPs in particular are especially prone to undergoing transformations, as well as generating reactive oxygen species that can affect the molecules surrounding them. Since one of the most common commercial applications of NPs is their use in sunscreens, we decided to investigate mixture toxicity of sunscreens. When researching this area, it became clear that an important consideration for sunscreen safety is formula photostability. Sunscreens are not only subject to changes in toxicity

due to mixture formulation, but their composition can also be altered through absorption of high energy light. Therefore, Chapter VI investigates the phototoxicity of some common commercial sunscreen mixtures with and without the presence of inorganic particles.

## CHAPTER V

### V. ZINC OXIDE INDUCED CHANGES TO SUNSCREEN EFFICACY AND TOXICITY UNDER UV IRRADIATION

This chapter is expected to appear in an upcoming publication authored by Aurora L. Ginzburg, Claudia Santillan, Lisa Truong, Richard S. Blackburn, Robert L. Tanguay, and James E. Hutchison. A.L.G determined experimental plans, formulated mixtures, performed spectroscopic analysis and data interpretation. C.S., L.T. and R.L.T. performed toxicity assays. R.S.B provided expertise on the cosmetics industry. A.L.G, R.S.B. and J.E.H. conceptualized this study. R.S.B., R.L.T and J.E.H. provided project mentorship. This chapter was primarily written by A.L.G, the toxicity methods section written by C.S. and editorial assistance was provided by R.S.B and J.E.H.

#### **Introduction**

Sunscreen safety and efficacy is of paramount importance for both humans and the environment. The limited list of ingredients available for use as sun protecting actives is concerning, especially considering the emerging public scrutiny of ingredients. Within the past few years there have been multiple highly publicized studies regarding the potential hazards of small-molecule based sunscreens on human health and aquatic environments.<sup>1-4</sup> As of May 2018, the US FDA sunscreen monograph listed only 16 UV filters (the active ingredients in sunscreens) approved for inclusion in cosmetic products: eight organic compounds that absorb primarily in the UVB region (280-315 nm); four

organic compounds that absorb in the UVB and short-wave UVA (315-340 nm) regions; but only two organic compounds that absorb primarily in the full UVA region (315-400 nm).<sup>5</sup> Filters that provide coverage of the UVA region are particularly important as up to 95% of UV radiation reaching the Earth's surface is UVA.<sup>6,7</sup> The FDA also approves the use of two inorganic 'filters', titanium dioxide (TiO<sub>2</sub>) and zinc oxide (ZnO), that provide wide spectrum scattering of UV light.<sup>5</sup>

Public perception of sunscreen safety has driven the market to use certain ingredients in abundance, while limiting others, based upon relatively little data. Two trends have emerged in recent years because of public perception. First, oxybenzone has been essentially discontinued due to concern over its hazards to coral reefs;<sup>2</sup> beginning January 1<sup>st</sup> 2021 the State of Hawaii will prohibit the sale and use of sunscreen formulations that contain either oxybenzone or octinoxate.<sup>8</sup> Second, inorganic sunscreens TiO<sub>2</sub> and ZnO have become favored due to their marketing as safer alternatives to "chemical-based" sunscreens.<sup>1,9</sup> This marketing is misleading given the well-documented instances of UV-irradiated metal oxides generating reactive oxygen species (ROS)<sup>10,11</sup> and degrading organic compounds.<sup>12</sup>

In contrast to the US, the EU approves 28 UV filters for inclusion in cosmetic products: nine UVB-absorbing organic compounds; seven organic compounds that absorb UVB and short-wave UVA; four UVA-absorbing organic compounds; and four organic compounds that provide broad spectrum UV absorbance. The EU approves the use of both TiO<sub>2</sub> and ZnO, including their use as nanoparticles (with certain specification and concentration restrictions).<sup>13</sup> The EU also allows two organic compounds, bisoctrizole and *tris*-biphenyl triazine, that are used as physical-chemical hybrids

providing UVA and UVB absorbance and UV scattering; both are also permitted in a nanoparticulate form. The greater chemical palette available to formulators in the EU motivated us to study the safety of both US and EU ingredients, with the goal of determining strategies for minimizing formula hazard.

While consumers have become aware of the potential hazards of sunscreen ingredients, an area of importance that has yet to receive public attention is the photodegradation of sunscreens. Sunscreen formulations have been documented to UV-induced degradation; however, the extent and time-frame of these reactions is highly dependent upon formula composition.<sup>14-18</sup> The most common UV filters have undergone photostability testing and strategies have been developed to prevent their rapid decomposition.<sup>14</sup> UVA filters in particular are generally not photo-stable and rapidly degrade upon UV exposure, resulting in a marked reduction in their efficacy.<sup>19,20</sup> For example, avobenzene, one of the few FDA approved UVA filters, is known to undergo photodegradation but another UV filter, octocrylene, can help stabilize it when a sufficient amount is added.<sup>21,22</sup> The effect that photodegradants have on formula toxicity is not well-understood.<sup>14</sup> When a sunscreen ingredient is determined to be non-toxic and safe for formulations the assessment is only based on an evaluation of the pure chemical, and not any photochemically generated species. Considering that there are a number of studies demonstrating that sunscreens can quickly react under UV-exposure,<sup>14,18,21-24</sup> the specifically intended environment for use, it is surprising that very little toxicity testing has been done on the photodegradants.<sup>14,23</sup>

Herein our aim was to study the phototoxicity of commercially inspired formulas from both the EU and US. We acknowledge that degradation products will vary based

upon formula compositions, moreover, as with all studies on mixture toxicity, the complex and combinatorial nature of mixtures can be limiting. However, using zebrafish as a model organism, we were able to perform a use-inspired *in vivo* study that tested a range of mixture formulas in a statistically significant manner. We selected zebrafish because they have good gene homology to humans, but unlike mammalian studies, high-throughput screening is readily achievable.<sup>25</sup> We complemented the toxicity data with spectroscopic analysis to understand how the UV protection offered by the formulas was changing as well.

## **Methods**

### Materials

All chemicals purchased were of cosmetic-grade or above. Homosalate, octocrylene, oxybenzone, and avobenzone were purchased from makingcosmetics.com. Octisalate was purchased from TCI Chemicals. The ZnO purchased (referred to as ZnO microparticles herein) was purchased from makingcosmetics.com; it is described as free of other metal impurities, with particle sizes ranging 200-1000 nm, and prepared by a high-temperature vaporization of zinc. It is recommended to be added to products in 5-25% *w/w* concentrations, with a maximum US limit of 25%. The nanoparticle sized ZnO (referred to as ZnO nanoparticles herein), purchased from makingcosmetics.com, has a commercial name of “micronized ZnO” but is described as having particles < 100 nm in size, with a mean size of 85 nm; it is recommended to be added in 3-6% *w/w* to organic sunscreens or 3-20% *w/w* when used alone. Both types of ZnO particles are uncoated.

### Sun Filter Mixture Formulation

We recorded the ingredients for ~40 commercial sunscreens from both the US and EU markets. From these data we identified trends in commonly combined sun filters and designed five commercially-inspired mixtures (Table 5.1). We determined the concentration of each filter by using BASF's online sunscreen simulation tool<sup>26</sup> to generate formulas that were predicted to have an SPF of 15 ( $\pm 0.4$ ) and achieve a PASS for UVA protection (with *in vitro* test ISO 24443). To formulate mixtures the raw chemicals were weighed and solvated into concentrated DMSO stock solutions. The solutions were then combined and an appropriate amount of DMSO was added to bring the final concentrations of chemicals to the amounts stated in Table 5.1, with a total of 3 g of each mixture. Mixtures were stored in the dark at room temperature. To formulate the ZnO containing mixtures, small aliquots of the 3 g "Mixture 1" stock were combined with 6% (*w/w*) of ZnO particles (microparticles or nanoparticles). Addition of ZnO resulted in thick suspensions, so solutions were vortexed immediately prior to pipetting. The ZnO-containing mixtures were irradiated and diluted as described above.

### UV-Exposure

All mixtures were freshly vortexed before use to promote homogeneity, then 3  $\mu\text{L}$  aliquots were removed and placed into small glass vials without any tapering. The vials were then opened and exposed to a solar simulator (Newport Oriel Sol3A) at 104  $\text{mW cm}^{-2}$  (~1 sun) for 120 minutes. Following exposure, 97  $\mu\text{L}$  of DMSO was added to the vials and vortexed. These solutions were then used for toxicity and spectroscopic

analysis. Control samples, not exposed to UV irradiation, were prepared in an identical manner except they were open in the dark during the irradiation period.

#### Absorbance Measurements

Aliquots of irradiated and control mixtures were removed from the 100  $\mu$ L vials and diluted into 99% water or IPA. 200  $\mu$ L of the 99:1 solutions were placed into UV-STAR® microplates for measuring the absorbance. A BioTek Synergy 2 microplate reader was used with Gen5 1.11 software. Scans were run between 280 and 700 nm in 2 nm steps, and the 99:1 solvents were background subtracted. Only the UV region (280-400 nm) is displayed within the included spectra because longer wavelengths had no absorbance, even following degradation.

#### Preparation of Solutions for Animal Exposure

Glass vials containing 50  $\mu$ L of each concentrated mixture in DMSO were placed in 50 mL falcon tubes and centrifuged at 64 x g for 3 minutes and then tapped to mix the solutions. The samples were added into ultra pure (UP) water and DMSO to achieve a concentration of 10% DMSO to create a 10x exposure solution. 10  $\mu$ L of each 10x exposure solution was then added to 90  $\mu$ L of UP water in each individual well to reach a final concentration of 1% DMSO and the mixture concentrations listed in Table D1.

#### Zebrafish Husbandry/Developmental Exposures

Tropical 5D wild type zebrafish were housed at the Sinnhuber Aquatic Research Laboratory (Corvallis, OR) at Oregon State University under a 14 h light/10 h dark cycle. Adult care and reproductive techniques were conducted according to the Institutional Animal Care and Use Committee protocols at Oregon State University (OSU). Fish were

raised in tanks with ~500 fish/50-gal tank filled with RO water supplemented with Instant Ocean (0.6%) and kept at 28°C. Their diet consisted of appropriately-sized Gemma Micro (Skretting Inc, Tooele, France) fed to them two times a day. Zebrafish were group spawned in tanks with spawning funnels placed in the tanks the night before, and embryos collected the next morning. The embryos were staged according to a previously described procedure<sup>27</sup> and kept in an incubator at 28°C in embryo media (EM). Embryo media's composition was 15 mM NaCl, 0.5 mM KCl, 1 mM MgSO<sub>4</sub>, 0.15 mM KH<sub>2</sub>PO<sub>4</sub>, 0.05 mM Na<sub>2</sub>HPO<sub>4</sub> and 0.7 mM NaHCO<sub>3</sub>.<sup>28</sup> At 4 hours post-fertilization (hpf), the chorions were removed with the use of an automated dechorionator and 83 µL of 25.3 U/µL of pronase (Roche, Indianapolis, IN, USA).<sup>29</sup> The embryos were transferred to individual wells of 96-well plates containing 100 µL of the exposure solution where they were statically exposed until 120 hpf (N=12). The plates were sealed with parafilm and shaken overnight at 235 rpm. The embryos were assessed for a total of 22 endpoints at 24 and 120 hpf.<sup>30</sup>

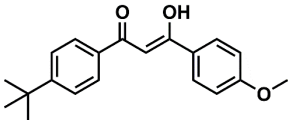
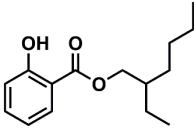
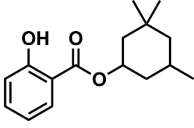
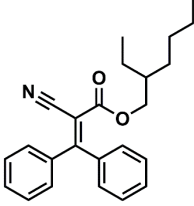
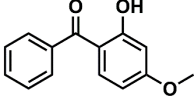
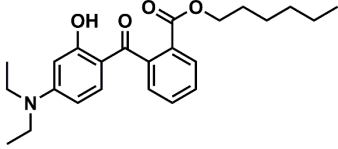
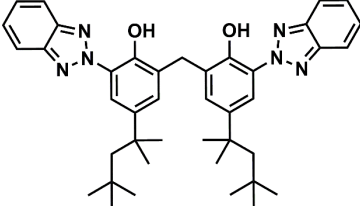
## **Results**

### Sun Filter Mixtures Containing Small-Molecules

Five different small-molecule based sun filter mixtures were formulated to have an SPF of 15 (formulations are detailed in Table 5.1). These mixtures were commercially-inspired and served to represent both *status quo* and next-generation sunscreen products. Mixture 1 represents a formulation used commercially for “sport” applications and is very commonly found on the market. Mixtures 2 and 3 represent a “sport” lotion that also incorporates next-generation sun filters approved in the EU but

not the US, bisoctrizole and DHHB, respectively. Mixture 4 represents a typical sunscreen lotion that combines many sun filters (usually to achieve a high SPF, but here their concentrations were intentionally low to normalize SPFs between mixtures). Mixture 5 represents a next-generation EU formulation for allergy-sensitive skin.

**Table 5.1. Sun filter mixture formulations with a calculated SPF of 15.**

UV filter (INCI name if different)	Structure	UV absorbance	% w/w of UV filter in mixture				
			1	2	3	4	5
Avobenzene (Butyl methoxy dibenzoylmethane)		UVA	1.8	1.0	2.0	2.0	0.0
Octisalate (Octyl salicylate)		UVB	4.0	4.0	3.0	3.0	3.0
Homosalate		UVB	7.0	0.0	3.0	6.0	0.0
Octocrylene (2-ethylhexyl ester)		UVB and short-wave UVA	5.0	3.0	4.0	3.0	2.0
Oxybenzone (benzophenone-3)		UVB and short-wave UVA	0.0	0.0	0.0	2.5	0.0
DHHB (Diethylamino hydroxybenzoyl hexyl benzoate)		UVA	0.0	0.0	5.0	0.0	0.0
Bisocetrizole (methylene bis- benzotriazolyl tetramethylbutylphenol)		UVB and UVA	0.0	3.0	0.0	0.0	5.0

All mixtures were formulated in DMSO to enable the solvation of chemicals and because it is one of the only organic solvents that can be used in small quantities for *in vivo* toxicity testing. It is worth noting that past studies have found that the extent of sun filter photodegradation is highly solvent dependent, with polar solvents generally reported as more stabilizing than non-polar solvents, therefore degradation results may have been more dramatic had we used a non-polar solvent.<sup>14</sup> DMSO's polarity, we found that with these concentrations of chemicals and 120 minutes of UV irradiation, there was still significant photodegradation when the mixtures were not formulated with ample stabilizers (Figure D2).

Mixtures 1-5 were irradiated with a solar simulator using a solar irradiance representative of the energy at sea level on a clear day. The irradiated mixtures, and non-irradiated controls, were diluted in DMSO then mixed with 99 parts of IPA or water. UV-Vis spectra were collected in both 99:1 IPA/DMSO (Figure 5.1) and 99:1 Water/DMSO (Figures D3-D4). The photodegradation was examined in two solvent systems because they each provided different information. IPA solubilized all of the mixture components, thus giving a complete picture of the chemical degradation, while the 99:1 Water/DMSO system showed the chemical exposure zebrafish embryos experienced during the toxicity assays. The water/DMSO mixture did not fully solubilize all chemicals, and this can be seen by the high baseline trace which is characteristic of scattering. Overall, the two solvent systems agreed that the mixtures were mostly photostable, but the results were less reliable in water/DMSO because of mixture inhomogeneity. This was alleviated some when the mixtures were formulated into lotions (D1) and emulsifiers helped to suspend the components in water.

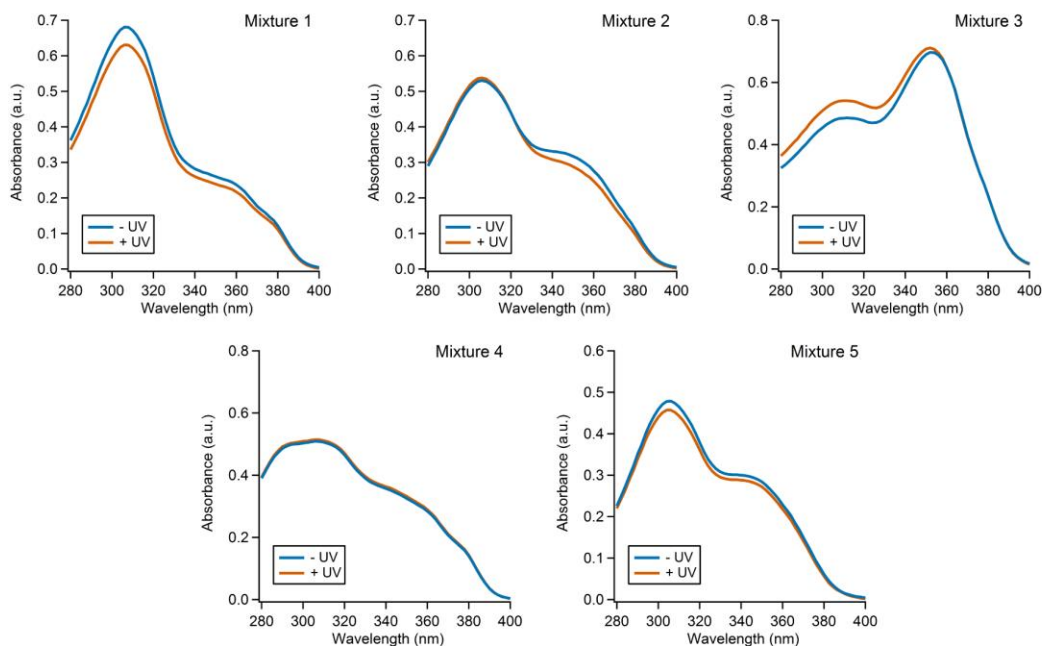


**Figure 5.1. UV-Vis spectra showing photodegradation of Mixtures 1-5 measured in 99:1 IPA/DMSO.**

UV-Vis absorbance spectra are informative for assessing sun filters because they not only provide data on ingredient degradation, but also on product performance. The efficacy of a small-molecule based sunscreen can be determined by its UV-Vis absorbance. A sunscreen mixture should have good absorbance throughout the entire UVA and UVB regions (280-400 nm) and if the mixture is photostable then the absorbance spectrum should not decrease or change shape after exposure to UV irradiation.

The UV-Vis data collected on Mixtures 1-5 show that these mixtures are mostly photostable despite containing avobenzene, which is known to undergo photolysis individually.<sup>14,24</sup> This suggests that the small-molecule based formulas available commercially, which the recipes for these mixtures have been inspired by, are formulated

with ratios of ingredients that minimize photodegradation. The presence of octocrylene in each of the five mixtures likely plays a key role in stabilizing formula stability, as it has been documented to quench excited-state triplets that can otherwise lead to photolysis.<sup>22</sup> We did not initially expect octocrylene to have such a dramatic stabilizing effect, as past work has shown that even when adequately stabilized, a modest amount of photolysis still occurs (e.g. ~16% for avobenzone in the presence of octocrylene);<sup>14</sup> however, it is hard to draw direct comparisons when all other studies use highly varied irradiation conditions and solvents.

The individual sun filters were screened *in vivo* at various concentrations to determine appropriate doses for eliciting an effect on animal development. This informed the mixture dosing, we used between 0.00142% and 0.003% (*weight of sun filters/ weight of solution*) depending on mixture. Each irradiated mixture was always tested at the same concentration as its non-irradiated analog.

The zebrafish animal models were exposed to each mixture for five days and 22 developmental endpoints were monitored. Because photodegradation, and consequent degradant toxicity, was so minor for these mixtures, the developmental results have been aggregated into a single endpoint in Figure 5.2. The y-axis represents the difference in toxicity between the irradiated and non-irradiated mixtures. In this case, the “toxicity” is a single endpoint which is the summation of all morphological and mortality effects experienced by the fish. We aggregated the data because the difference was so low overall that looking at one morphological or mortality endpoint was not informative.

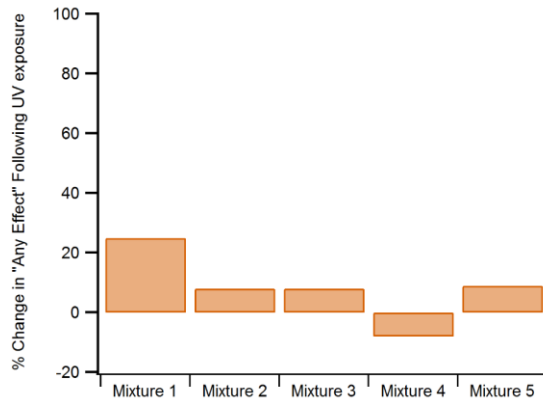


**Figure 5.2. Summary toxicity changes of Mixtures 1-5 phototoxicity following UV irradiation.**

The standard error for the aggregated “any effect” endpoint ranged 8-15%.

The toxicity data are in good agreement with the spectroscopic data; UV irradiation of Mixtures 1-5 elicits minimal differences in formula efficacy and safety. The only mixture with a statistically meaningful difference in toxicity following irradiation is Mixture 1. Although it appears that Mixtures 2-5 have minor differences in their response, they are within the standard error. Even for Mixture 1, the differences in toxicity are minimal considering this is an aggregated endpoint.

It is important to note that these experiments were simplified to just look at mixtures of the neat chemical sun filters and did not include the non-active ingredients found in lotions such as emollients, surfactants and preservatives. We initially set out to formulate complementary lotions as well, but preliminary results suggested that obtaining reliable photodegradation data from the lotions would not be possible within the scope of this work. The challenge with formulating lotions is that their degradation is highly dependent upon film thickness. We formulated a generic body lotion base and added the organic actives to the oil phase prior to heating.<sup>31</sup> The lotion was spread into a film of 1.5 mg cm<sup>-2</sup> thickness, which falls at the high end of average consumer use but below the 2

mg cm<sup>-2</sup> standard that SPF is determined with.<sup>32</sup> The film was exposed to UV irradiation for 2 hours before being solvated in DMSO and diluted to measure the UV-Vis spectrum. Using this method, we were able to reproduce the results obtained in neat DMSO (Figure D1) but obtaining sufficient sample quantity for a full toxicity assay, and reproducibly spreading the films uniformly was a challenge. Knowing that the neat-DMSO degradation was a reasonable way to measure the photodegradation, we decided to focus our efforts on just the sun filters for this study.

### Sun Filter Mixtures Containing Small-Molecules and ZnO

A small-molecule based sunscreen can interact with ZnO particles both due to intentional mixing in hybrid sunscreens (containing both chemical and physical UV-absorbers), and incidental mixing when cosmetics and/or different sunscreens are used in combination. While metal oxide particles have been documented to generate ROS and induce small-molecule degradation,<sup>10-12</sup> little attention has been paid to how this may affect sunscreen toxicity. To investigate this, one small-molecule based sunscreen formula was examined with two different kinds of ZnO particles added. Of the five small-molecule based formulas examined in this work, Mixture 1 was the most representative of current commercial formulations, with relevance in both US and EU markets, so we used this mixture as the model for studies with ZnO particles.

Two different sizes of ZnO particles were examined with Mixture 1: microparticles with sizes ranging 200-1000 nm and nanoparticles with sizes < 100 nm. Both sets of ZnO were reported to be prepared *via* a high-temp vaporization synthesis and neither had any type of added coating. The particles were added to Mixture 1 in 6% (*w/w*) quantities, which is a typical amount for a hybrid sunscreen. Following particle addition,

the mixtures were exposed to 120 minutes of UV irradiation and then their UV-Vis spectra were measured (Figure 5.3). Since the particles do not form a homogenous solution with either IPA or water, minor differences in the baseline can be attributed to the solution heterogeneity imparted by the particles.

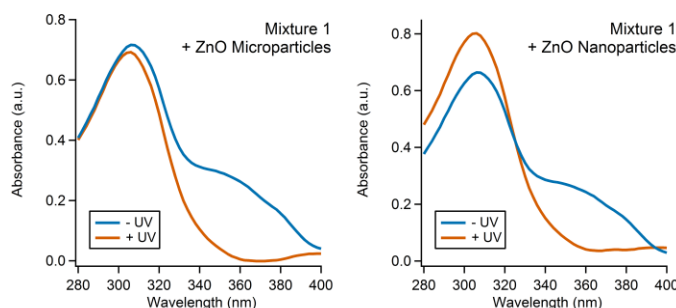


**Figure 5.3. UV-Vis spectra of Mixture 1 + ZnO particles before and after 2 hrs of UV irradiation.**

Following UV irradiation the lower energy absorbance peak (350-400 nm) is nonexistent, which is consistent with avobenzone degrading.<sup>12,14</sup> Avobenzone was the only longwave UVA absorbing small-molecule present in Mixture 1 so there was clearly a change in avobenzone's structure that resulted in the mixture's loss in UVA absorbance. Avobenzone is known to undergo keto-enol tautomerization wherein its enol-form (UVA absorber) converts to the diketo-form (UVC absorber) and then can undergo various lysis reactions.<sup>14,21</sup> It is possible that we just observed avobenzone tautomerization rather than any molecular cleavage, but it seems unlikely this is the case when the spectroscopic data and toxicity data (below) are considered together. Since we didn't observe major changes in the photostability until the ZnO was added, it is likely that the UV irradiation produced electron-hole pairs in the ZnO, leading to the generation of ROS<sup>11</sup> and subsequent oxidative degradation of avobenzone. Other Mixture 1 sun

filters may have also been degraded by ROS, but their overlapping spectroscopic signatures preclude the ability to draw any conclusions from this data.

The results presented in Figure 5.4 show that ZnO + Mixture 1 induces phototoxicity. The experimental design and controls make it clear that this toxicity is not the result of the pure inorganic particles or UV light. Since the mixtures were exposed to UV light days before encountering the zebrafish, there is no chance that ROS generated due to UV irradiation is still present in solution during animal exposure. Instead, we can definitively state that ZnO induces the production of toxic photodegradations. This is supported by the control experiments that show only minor amounts of phototoxicity observed for the organic and ZnO components alone (Figure 5.4 C and D). Panel C in Figure 5.4 suggests there is a slight increase in toxicity following UV irradiation, which was mentioned in the prior section. Panel D shows that the UV light may have induced a small amount of damage to the ZnO particles that made them more toxic; this could happen by etching them and/or leaching toxic Zn ions.<sup>33</sup> The results from panels A and B in Figure 5.4 are not additive from panels C and D though, there is clearly an increase in toxicity due to photodegradation of small-molecules that is induced by ZnO. This is further suggested by the dramatic change in the UV-Vis spectra (Figure 5.3).

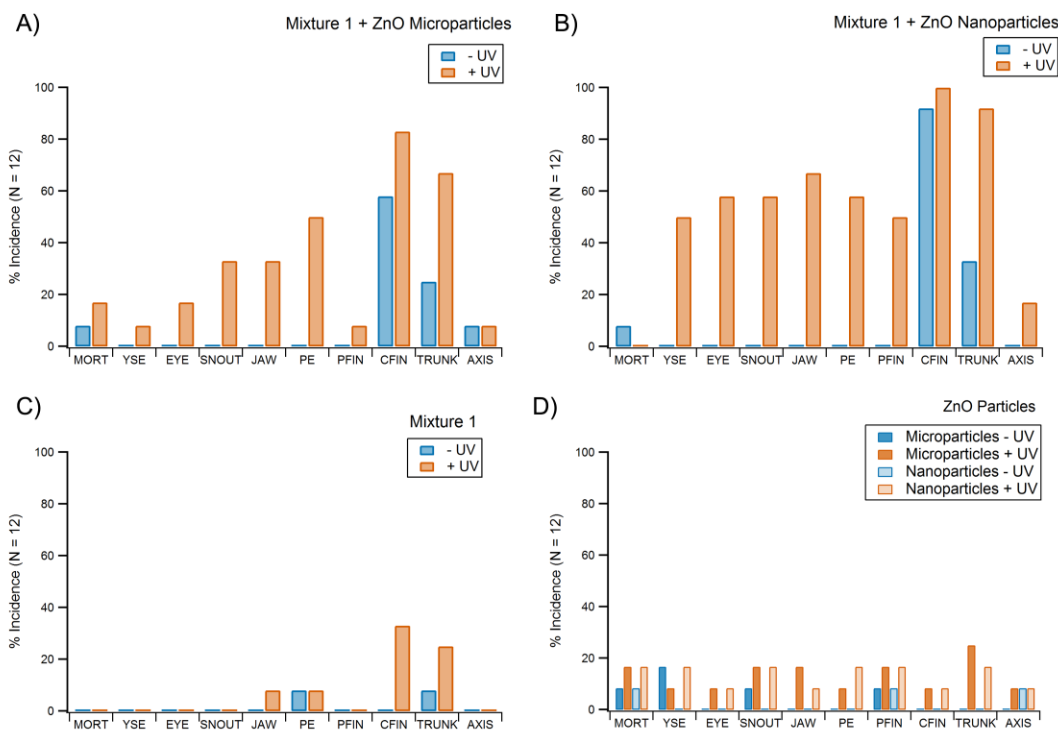


**Figure 5.4. Changes in zebrafish development over five days at ten different endpoints.**

Animals were exposed to 99:1 Water/DMSO solutions containing 0.0014% (w/w) organic filters (Mixture 1; panels A-C) and 0.0005% (w/w) ZnO (panels A,B and D).

Key to endpoints: Mortality (MORT), excess fluid accumulation around yolk sac (YSE), abnormal eye placement or size (EYE), visibly malformed snout (SNOUT), jaw (JAW), excessive fluid accumulation around pericardial edema (PE), under developed or malformed pectoral fin (PFIN), under developed or malformed caudal fin (CFIN), body length shorter than normal (TRUNK), and body axis curvature (AXIS).

The 22 endpoints monitored *in vivo* provide a comprehensive method of identifying developmental effects in an integrated system. The morphological malformations observed provide insight into the biological targets of these mixtures. These targets are useful for motivating future molecular investigations that inform on the mechanism(s) of toxicity. Because we observed a high incidence of morphological effects but not mortality, the mechanism(s) of toxicity is likely linked to changes in biological signaling systems.

It is important to highlight the fact that both nanosized ZnO particles and non-nano ZnO particles caused toxicity upon UV irradiation. This is notable to mention because, although there is evidence of size-effects, toxicity was not precluded by the “non-nano” sized particles. As a team that specializes in studying nanoparticle toxicity, these results are not surprising to us. We suspect though, that they would surprise many consumers who are misled by “nano free” labels on mineral-based sunscreens. The reality is that any metal oxide particle can have reactive surface sites, whether it is less than 100 nm (generally determined to be “nano” sized) or not. More important than metal particle size, is the metal identity, crystal structure, and any surface coatings.<sup>10</sup> We acknowledge that including these properties on a product label is not practical, but the scientists who formulate the products should advise against the use of misleading marketing tactics that perpetuate broad sweeping concerns over nanoparticles.

## **Conclusions**

The aim of this study was to establish if certain sunscreen ingredients or formulations undergo photodegradation that can be harmful to humans and/or the environment. We were surprised to find that all five of the commercially inspired small-molecule containing sunscreen mixtures were mostly photostable. These results suggest that the ability of the small-molecule formulas to protect against UV-damage is not altered under normal use conditions. This may be because the ratios of actives have been industrially optimized to minimize photodegradation, but the findings were just never published. This small-molecule mixture stability was further observed during *in vivo* analysis, which indicated there were minimal differences in biological impacts following

UV irradiation. However, when the most commercially-relevant small-molecule formulation was studied in combination with a modest amount of ZnO particles, significant differences in photostability and phototoxicity were observed. Both the nano-sized and the micro-sized ZnO particles degraded the organic mixture and caused a loss in UVA protection. Additionally, the ZnO induced photodegradation caused significant increases in zebrafish morphological defects. These results suggest that ZnO particles may increase sunscreen hazards in ways not currently well-recognized by the community.

The results show that ZnO-containing sunscreens can undergo two different types of photochemistry that result in deleterious effects; they can have significantly decreased UVA protection due to degradation of the organic sun filters, and they can generate toxicity-inducing ROS. Loss of UVA protection is especially problematic in US sunscreens where there are only two absorbers regularly used in commercial formulations, avobenzene and zinc oxide.<sup>34</sup> The only other US-approved UVA absorber, oxybenzone, is being continually outlawed due to concerns over its hazard to coral reefs.<sup>2,4,8</sup> There is a significant need for additional UVA absorbers to be approved in the United States. Some of the European ingredients such as bisoctrizole and DHHB show promising photostability<sup>13,35</sup> and have no reported phototoxicity currently. This information is currently only documented within the primary literature, perhaps more widespread media communication explaining the promise of these next-generation actives would help pressure US industry and regulatory agencies to expediate their study.

Hopefully, the pipeline of sun filters can be strengthened through continued study of promising chemicals. Even in a best-case scenario where next-generation filters end up being better performing and safer than current options, the reality is that obtaining

regulatory approval is time-consuming and expensive.<sup>36</sup> In the meantime, further work should be done exploring the phototoxicity of various architectures of coated ZnO. Prior work has indicated that the photocatalytic activity of titanium dioxide particles can be minimized by coating them with silica or aluminum hydroxide,<sup>14</sup> so similar strategies may be helpful for precluding ZnO photocatalysis. Overall, much more work studying sunscreen formula photostability and phototoxicity is needed in order for there to be certainty that the products put into mass production are safe and effective.

Widespread skin cancer prevention education has supported growth in the global sunscreen market which is now worth over 12 billion US dollars.<sup>37</sup> As the market has grown, so have consumer concerns over ingredient safety and effectivity.<sup>9</sup> In some instances these concerns have led to positive improvements, such as broad-spectrum protection labeling,<sup>38</sup> but they have also enabled misleading marketing like the promotion of “chemical-free” sunscreens. Moreover, SPF isn’t just put into sunscreen lotion; it is now regularly found in an array of cosmetic products that are intended for daily use in combination such as, facial moisturizer, liquid foundation and powder foundation. Currently, there is no awareness that mixing products may increase health hazards. We fear that the increasing ubiquity of sun filters (in particular metal oxide particles), coupled with the lack of studies on sunscreen phototoxicity, is likely to result in products that have unintended consequences (*e.g.*, production of reactive oxygen species in sunlight and insufficient UVA protection). We hope that this work can bring awareness to some of the hazards of sun filters and caution against their widespread incorporation into products where sun protection isn’t crucial, especially until there is more information on how to design sunscreens for safe degradation.

## Bridge to Chapter VI

Although scientists and the public alike have put great effort into reducing chemical hazards over the past few decades, little attention has been paid to the mixing safety of formula components. Only recently has there been an emerging recognition that chemicals can interact in non-additive ways, and certain exposure conditions can dramatically change mixture safety. While regulatory agencies have made some efforts to consider these effects (*e.g.*, by prohibiting certain nanoparticle/organic sun filter combinations in a single product), no widespread efforts have been made to inform formulation scientists or consumers about the potential hazards of mixing multiple products. Further, the advertised usage of many of these products, such as SPF-containing cosmetics, involves specifically layering them with other cosmetics. This oversight in legislation and product design emphasizes the need for systems thinking when designing safer products. A systems perspective encourages a designer to ask questions such as, “how is this product likely going to be used by consumers and how does that change the hazards?” Chapter VII presents a framework for teaching chemistry students how to use systems thinking and integrate it with green chemistry principles and life cycle thinking to design sustainable products.

## CHAPTER VI

### VI. EXPERIENTIAL LEARNING TO PROMOTE SYSTEMS THINKING IN CHEMISTRY: EVALUATING AND DESIGNING SUSTAINABLE PRODUCTS IN A POLYMER IMMERSION LAB

Reproduced with permission from Ginzburg, A. L.; Check, C. E.; Hovekamp, D. P.; Sillin, A. N.; Brett, J.; Eshelman, H.; Hutchison, J. E. Experiential Learning To Promote Systems Thinking in Chemistry: Evaluating and Designing Sustainable Products in a Polymer Immersion Lab. *J. Chem. Educ.* **2019**, ASAP. Copyright 2019 American Chemical Society.

#### **Introduction**

Green chemistry has gained considerable acceptance in both industry and academia.<sup>1-4</sup> As the world has grown more environmentally conscious, greener products and processes have become the focus of innovation and product development in industry.<sup>5</sup> In academia, green chemistry has improved laboratory safety and taught students strategies and techniques to reduce the environmental impacts of chemicals and chemical transformations.<sup>4</sup> Regardless of the setting, green chemistry solutions are intended to reduce environmental impacts while simultaneously maintaining, or even improving, performance. Yet, in many cases, changes made to green a product or process introduce unintended problems.<sup>6</sup> For example, products have been modified to use renewable carbon sources, and claims have been made that this change in feedstock inherently reduces environmental impacts. While there are certain circumstances in

which impacts are reduced, there are often net increases in environmental impacts when upstream effects (*e.g.*, water and energy input) or functional sacrifices (*e.g.*, decreased product performance) are not taken into consideration or fully evaluated.<sup>7</sup> Unintended consequences are not only detrimental because they can increase environmental impacts, but also because unsubstantiated sustainability claims can lead to consumer distrust of green technologies.

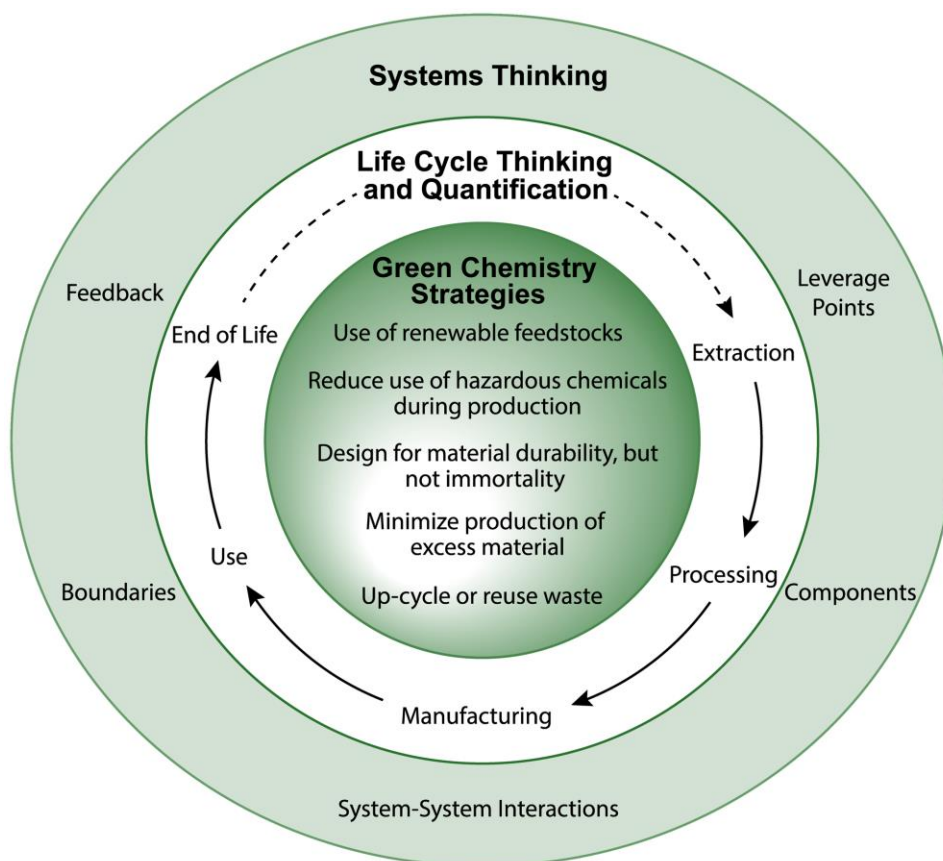


**Figure 6.1 Complementary lenses to practical sustainable product design.** Green chemistry is rooted in the 12 principles to reduce impacts. These principles can inspire change but require broader perspectives (life cycle and systems thinking) to assess tradeoffs and practicality.

A more holistic approach to designing and evaluating products and processes is necessary to achieve the aims of green chemistry. Although green chemistry principles

can be implemented to reduce environmental impacts, two additional approaches, life cycle thinking and systems thinking, are important to guide decision making for more sustainable solutions. Life cycle thinking considers material impacts for a specific technological solution at each stage of the life cycle - from cradle to grave (or ideally from cradle to cradle). This accounting of impacts at each stage of life can be performed qualitatively, where it is referred to as life cycle thinking, or quantitatively where it is referred to as a life cycle assessment. Systems thinking further expands the scope to consider how that specific technological solution impacts, and is influenced by, society, ecology and other technologies. The complementary relationship of green chemistry, life cycle thinking and systems thinking, is illustrated in Figure 6.1. In the figure, green chemistry is nested within life cycle thinking, and both of these are nested within systems thinking. In this context, the choice of green chemistry strategies can be informed by examining the relative impacts of competing solutions across the life cycle. By broadening the perspective out to the systems level, one can anticipate problems, challenges and opportunities as a technological solution interfaces with the commercial sector, the environment and society. We can use a children's car seat as an example product for thinking through these different lenses: green principles could drive exploration of the chemical hazards of the padding foam, life cycle thinking could expand on this to ask whether other types of foams have reduced end-of-life impacts or if the waste can be repurposed, and systems thinking could further expand the scope to consider if an alternative foam with better end-of-life impacts has performance advantages such as a reduced risk of accidental cracking during routine wear and tear. Using this combination of lenses can help students design and implement chemistry-based solutions

that increase product performance while anticipating tradeoffs and limiting unintended consequences.

The consideration of systems thinking in the chemistry curriculum has only recently received attention. Matlan et al. highlighted the need for modern chemistry education to use a systems approach in teaching, suggesting that students should work more broadly across disciplines and consider the relationships between chemistry and the rest of the world. The authors emphasized that chemistry is interconnected with a global future that is ethical and sustainable and that we need to stop treating it as a discipline that is isolated from human influence.<sup>8</sup> This call for a more integrated approach to chemistry pedagogy emphasized what we have also found to be true, students are seldom asked to think about how chemistry interacts with the world beyond the benchtop. Instead, chemistry is often reduced to the use or transformation of chemicals with little, or no, consideration of: resource depletion, waste generation, or impacts on stakeholders and the ecosystem. Outside of chemistry education, systems thinking has received attention in earth and life science education.<sup>9-11</sup> However, the goal there has typically been to increase students' ability to identify/understand complex ecological webs or earth cycles, not to use the knowledge of this interconnectedness to develop technical solutions. Since chemistry as a discipline is uniquely positioned to offer technical solutions to real-world challenges (*i.e.*, chemists introduce new chemicals and materials into the world), teaching chemistry students to think about innovation with a systems lens can be particularly advantageous. Higher education can help support this call to action by integrating activities into science courses where students are tasked to use a systems thinking framework to design technical solutions. More broadly, universities could require a general education course

that teaches systems thinking and has students practice applying it to a range of disciplines.

Although many excellent resources have been previously developed to help educators incorporate green chemistry into the undergraduate teaching curriculum,<sup>1,12-15</sup> few tools are available to help educators incorporate systems thinking or even life cycle thinking. Academic courses and labs in chemistry typically focus on reductionist problem solving skills as opposed to examining the bigger picture. Recently, there have been a few efforts to not only familiarize students with green chemistry, but to help students develop the tools to implement green principles on their own. In this light, Bode et al. developed lessons and discussion prompts aimed to teach students to understand and generalize technically challenging life cycle assessments.<sup>16</sup> A couple of universities have begun offering sustainable product design courses to train business students to evaluate scientific facts and assertions.<sup>17,18</sup> These types of practical approaches to teaching green chemistry are important for making chemistry concepts approachable to students with a variety of career interests and expertise. Inspired by the call for students to practice using chemistry for a broad multi-disciplinary purpose, we aimed to develop an immersive project that requires students to apply systems thinking to address a real-world problem. Herein, we describe a framework where students use systems thinking, along with life cycle thinking and green chemistry, to tackle a problem of industrial relevance. Our hope is that this framework can be used to guide future adapted versions of these workshops, potentially even leading to the design of general education courses where students from all disciplines practice using systems thinking to design sustainable solutions.

## Systems Thinking to Guide Green Chemistry

The basis for our approach is the realization that green chemistry principles can inspire innovation, but these principles alone do not give a perspective on the overall impacts of the changes made to a product or process. The multiple lenses needed for practical green product design (Figure 6.1) foster a holistic perspective that considers the impacts of an action on both the environment (through life cycle thinking) and societal and earth systems (through systems thinking). Life cycle thinking ensures that a green improvement at one stage of life does not have unrealized impacts elsewhere, and systems thinking considers the interconnections between *components* and anticipates ways in which action will be most beneficial for eliciting the desired system response.

This paper is not meant to give a comprehensive explanation of systems thinking concepts, but rather to showcase how to leverage the strengths of systems thinking (along with life cycle thinking) to guide greener product or process design. The terms that relate to Figure 6.1 are italicized and discussed below, but for a detailed guide to systems thinking we recommend *Thinking in Systems* by Donella Meadows.<sup>19</sup> A system is made up of a collection of *components* - people, things, infrastructure, etc. - that work together to influence the goal of the system. The scope of the components, and therefore of the system, is determined by the defined *boundaries*. No matter what the boundaries, a system's components are interconnected and influential. These casual connections between components are termed *feedback loops*. Feedback loops can be complex and have delays between system intervention and observed effect. Systems are also affected by *system-system interactions*. Feedback from other systems that will influence the

system of interest. Finally, systems have *leverage points* wherein a small intervention can cause a major shift in system behavior.

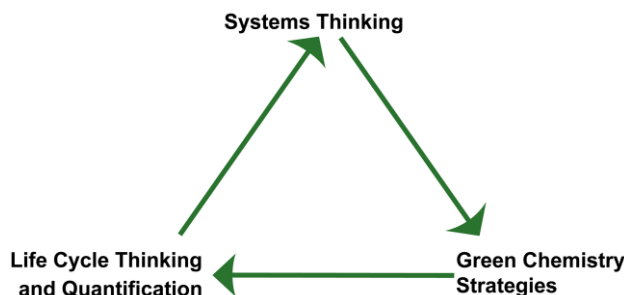


**Figure 6.2 The interplay between the three lenses introduced in Fig. 6.1: Green chemistry, life cycle and systems thinking.**

Innovation can start with a possible green chemistry strategy, be assessed through life cycle analysis and further evaluated from a systems perspective. On the other hand, the process can be initiated by the recognition of a significant life cycle impact or a new insight provided by systems thinking. Regardless of the starting point, multiple iterations are needed to identify the best strategies to reduce life cycle impacts, improve performance and gain leverage within the system.

In the context of greener consumer products, which provides the setting for the work described in this paper, some of the key components are: students, chemicals, product designers, corporate investment, and regulatory laws. Possible use scenarios for the product influence the boundaries of the system. For example, the material may just be of interest within a teaching lab, it could be studied for companywide R&D, or the entire industry sector in which that material is used could be the focus. The influence of other systems can have a significant impact, for example, changes in FDA regulations will influence a sunscreen company's R&D and activist bloggers often motivate innovation at consumer-facing companies.

Figure 6.2 focuses on the interconnection of the three complementary lenses from Figure 6.1. The benefits of using these approaches together are achieved through an iterative process as depicted in Fig. 6.2. This process is the equivalent of zooming in and

out between the lenses in Fig. 6.1, for example working outward from green chemistry to life cycle and systems thinking, then back inward to green chemistry solutions. There is no right level to start, but consideration of all of the perspectives is key to designing an innovative, and practical, solution that can prevent unintended consequences. For example, the motivation for innovation can come from safety concerns over a specific chemical (*e.g.*, a green chemistry starting point) or the motivation can come from a desire to enhance the product capabilities (*e.g.*, a systems starting point). No matter what the initial motivation for innovation, designers should consider the ripple effects such as changes to the manufacturing process, chemicals present in the final product, product performance and product disposal. We have provided a detailed example of this iterative thinking in Appendix E using sunscreen as an example product. Teaching students to intentionally integrate systems thinking with green chemistry and life cycle thinking provides a structure for helping to ensure that their sustainable solutions are carefully considered and have a net benefit.

### **Overview and Impact of Workshops**

We developed a series of workshops to provide students practical experience uniting green chemistry, life cycle thinking, and systems thinking to address an industrially relevant problem. Students were challenged to identify sustainable improvements or alternatives to a specific product under constraints related to product performance and viability. To test this approach, we piloted this project with an eco-friendly start-up company, WAYB. WAYB aims to create next generation children's products that have improved product performance and reduced environmental and health impacts. The project was carried out within the University of Oregon's Knight Campus

Internship Program's<sup>20</sup> polymer track that engages master's students in an intensive immersion lab wherein they work in small teams to solve a real-world problem. The challenge for the student team was to design a more environmentally conscious car seat for infants. The initial goal was to identify a greener polymer foam to replace the expanded polystyrene (EPS) used in a car seat, but, as the project developed, WAYB and the project team broadened the goal to greening all aspects of the product.

Based on the results from this project, we found that a series of three workshops was effective to introduce and implement the tiered strategy shown in Figures 6.1 and 6.2. Although we focused on the foam used in an infant car seat, we envision this framework being suitable for evaluating other types of products wherein a sustainable alternative material can be compared to an industry standard. The workshops were initiated with a framing lecture and a short summary of the project goals. Students did independent reading to familiarize themselves with the materials that were being studied and worked as a group to develop hypotheses that could be tested experimentally and/or supported with relevant literature. The duration of each workshop was typically a few days depending upon the workshop and breadth of data collected, however this can be tailored to the project and the student cohort. More information on the technical implementation, course format and timelines are provided in Appendix E.

Figure 6.3 outlines the key components of each workshop and illustrates the crosstalk between them. Workshop I focused on life cycle thinking and assessing the

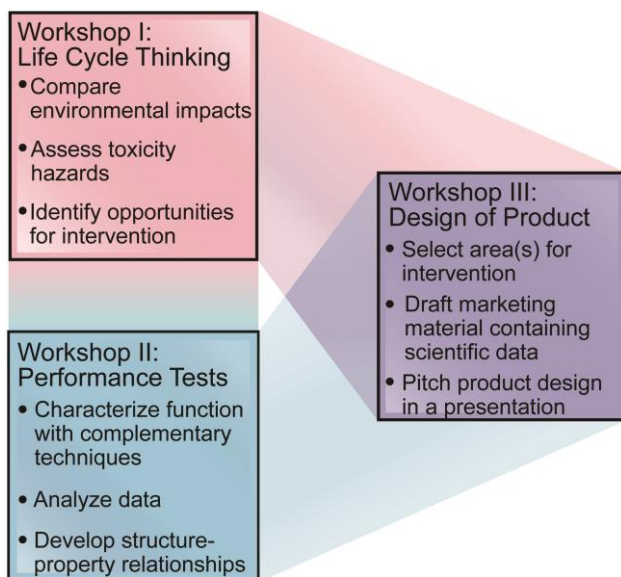


**Figure 6.3 Summary of Workshop Activities.**

Workshops I and II involved literature research and data collection, this knowledge then informed Workshop III where students moved forward to design and pitch their product.

impacts of a material of concern. The functional properties of that material were defined, tested and compared to potential alternatives in Workshop II. In Workshop III, the students synthesized the results from the first two workshops to design and present sustainable alternatives and innovations. As described below, each workshop was developed in response to key sets of learning outcomes that address systems thinking, life cycle thinking and green chemistry. The workshop format allows one to tailor the level of sophistication to different levels of student preparation, and we have suggested ways to adapt them to other student levels and venues.

Within our student cohort, these workshops were used to evaluate expanded polystyrene (EPS), which is the industry standard for high-impact absorbing materials in consumer products, and compare it to potential alternative foams.<sup>21</sup> In Workshop I students used life cycle assessments to document life cycle impacts of EPS . In Workshop II students defined functional needs and evaluated the performance of alternative foams by characterizing their relative energy dissipation ability and rigidity. Using data from Workshops I and II, students worked in small teams to evaluate alternative approaches and develop mock-product designs and marketing materials in Workshop III. The marketing material consisted of communications to the public as well as a verbal pitch to all the participants in the class. Workshop III required the students to use systems thinking as they considered how to design a next-generation car seat that does not compromise child safety, is more environmentally friendly, and has attributes that can be communicated to consumers in a compelling manner.

After the conclusion of the course, students reported that they were drawn to this lab project because they felt it provided an experience that better prepared them to solve real world problems. Students noted that this project was unusual because rather than having one correct solution there were many potential solutions that had to be quickly assessed to determine which one was the most feasible and compelling. The students said this decision-making process aided in their development as independent scientists. They also reported that the project forced them to work in teams in new ways. Although they had worked in teams before, those experiences consisted mostly of dividing up the responsibilities from a given set of tasks. Here, the interdisciplinary nature of the project motivated the students to discuss how to best utilize each team member's expertise and

undergraduate background. Finally, this lab was different from other teaching labs because they ultimately had to make conclusive decisions even though they didn't have all of the information they might have wanted.

Students reported that the experiential learning they engaged in during this project gave them a significantly improved appreciation for the importance of life cycle and systems thinking. This project taught students that starting with green chemistry principles is helpful, but you have to look beyond that to assess the practicality of a solution. One student specifically noted that despite being trained in environmental chemistry, she still found green washing<sup>6</sup> hard to discern and this type of project offered her a new way to critically analyze green claims. Students said that it was both frustrating and enlightening to get first-hand experience dealing with an interconnected system, where changing one element to be greener usually altered something else. They said knowing that there will inherently be tradeoffs, but that there are ways to anticipate these and think systematically about it, gives them strategies for implementing sustainable solutions in their future careers.

In evaluations conducted a few months after the students began working in industry, students reported that the problem-solving and material/time constraints that they experienced during the project prepared them for their current positions in ways that past teaching labs did not. The car seat project was especially constraining because the final product itself has safety requirements that must be addressed, including the use of child-safe materials and the necessity of passing a crash test. By working within these constraints, students discovered non-obvious leverage points, such as the foam manufacturing process.<sup>22,23</sup> Feedback provided by students is included in Appendix E.

## **Implementation of Workshops**

### Workshop I

Life cycle and Toxicity Analysis of the Material of Concern: Evaluating the Environmental Impacts of EPS. The purpose of this first workshop was to familiarize students with life cycle and toxicity assessments and to give students practice evaluating and comparing impacts for a specific material of interest. It was important to begin the project with life cycle thinking because it gave students the tools to evaluate and compare alternative materials in Workshop III. Students performed individual research to learn about the production and life cycle of the industry standard, EPS; then they combined their findings as a group to generate a summary document of the life cycle impacts. Students began by searching the primary literature for information regarding the production of EPS<sup>24</sup> and noting impacts at each stage of an EPS-based car seat's life. In the supplemental material we have provided a template for structured life cycle thinking that can be used to guide this process. Students worked together in class to discuss their findings and generate a group summary document. One effective way to do this is to have students use sticky notes to collaboratively develop a master life cycle summary on poster boards. Using the summary, students identified leverage points for improving greenness and weighed the pros and cons of innovating at various points. Students were directed to discuss ways to green the car seat in a scenario where they can replace EPS with a greener alternative foam, and a scenario where they can't replace EPS. Students also found articles on EPS toxicity and concluded that under normal use conditions, there are not any notable toxicity concerns for EPS use in a car seat.<sup>25,26</sup> Because it was determined that EPS did not have any major toxicity concerns, the students focused more

on the life cycle impacts when thinking about opportunities for innovation, however, if future cohorts of students study other materials that do have toxicity concerns then the toxicity reports would be more heavily emphasized.

After completing this workshop students were familiar with using life cycle assessments and toxicity reports to identify and compare the environmental impacts of materials. For instance, students found that the negative environmental impacts of EPS are primarily due to its petroleum-based raw ingredients,<sup>7</sup> organic blowing agents,<sup>24</sup> and poor reusability/recyclability.<sup>24,27</sup> Students noted that there are existing alternative foams that may be able to mitigate some of these impacts. However, the impacts of an alternative foam would also need to be assessed because it is likely that there would be some tradeoffs. For example, although it is tempting to recommend a biopolymer, students found that biopolymers can actually have higher impacts than petroleum sourced polymers in most major categories including: ozone depletion, acidification, eutrophication, carcinogens, and ecotoxicity.<sup>7,28</sup> This workshop also allowed students to identify areas for innovation that do not require replacing EPS, like the employment of a green blowing agent,<sup>29</sup> finding a secondary use for cracked/fatigued EPS, or reducing energy expenditure during foam shipping. Although EPS is not a toxicity concern due to its high MW and stability, residual monomer could be hazardous.<sup>25,26</sup> Testing of monomer leaching or off-gassing was noted as a potentially useful future research pursuit.

While our students evaluated EPS in this workshop, the approach can be easily tailored to examine other chemicals or materials of concern. Additionally, the scope and sophistication of this workshop can be adapted easily for other types of courses. For a

lower level course, instead of constructing a master life cycle summary, the instructor could give a lecture on what a life cycle assessment is. During this lecture there could be a class discussion on how public perception of a material may not accurately reflect the life cycle impacts and the instructor could guide students to consider hidden impacts encountered during production or transportation stages.

### Workshop II.

Defining and Measuring Performance: Evaluating Alternative Foams in a Simulated Crash Test. The purpose of this workshop is to compare the ability of an industry standard against potential alternatives to perform the key function of interest. We wanted to assess how EPS performed relative to other foam alternatives in protecting a child during a car crash. We challenged the students to compare the industrial performance of the materials on a benchtop scale without the need for specialized equipment. Because EPS has been the gold standard high-impact absorbing polymer foam for decades,<sup>21,24,30-32</sup> we used it as a point of reference during this workshop. Prior to beginning the lab work, alternatives to the industry standard material were acquired. In our case we worked with our industry partner, WAYB, to source specific alternative polymer foams of interest, but future labs can use any foams they think would be interesting to study. The results from one class can be used to inform the next class' selection so that each succession of this project allows for improved materials to be studied.

The students determined that they could simulate a small-scale crash test in lab by measuring a foam's ability to dissipate impact energy. Two experiments were performed to measure this, one ranked the foams' effectivity at absorbing instantaneous impact

energy and the other quantitatively characterized the foams' stress response to incremental increases in strain. To study a foam's response to instantaneous stress, ping pong balls and baseballs were dropped on a foam and the resulting ball bounce height was measured. The foams were ranked against one another to understand their relative energy dissipating ability under low impact and high impact collisions. Table 6.1 lists a summary of results from this experiment. The materials were ranked from best (1) to worst (6) impact absorption based on the ball rebound height (low height equals high absorption). The ping pong ball was dropped from a height of 1 ft and a baseball from a height of 2 ft. Of note, Alternative #1 could not be tested in this way due to a limited sample size. The students visually examined each foam before and after impact and noted any changes in appearance. They then discussed different mechanisms of energy dissipation<sup>33</sup> that may be occurring in each case based upon the foam performance and deformations (when applicable).

**Table 6.1 Student generated data ranking foam effectivity at energy dissipation from instantaneous impact.**

<b>Rank</b>	<b>Ping Pong Ball Bounce Dissipation Rank</b>	<b>Baseball Bounce Dissipation Rank</b>
1 (best)	Alternative #5	Alternative #6
2	Alternative #6	EPS
3	Alternative #4	Alternative #3
4	Alternative #3	Alternative #5
5	EPS	Alternative #2
6 (worst)	Alternative #2	Alternative #4

\*Note Alternative #1 was not included in this test due to the limited supply of this material.

These tests allowed students to relate material structure to performance in a simulated commercial function. It is interesting to note that under low impacts, simulated with the ping pong ball, EPS doesn't dissipate very much energy and it ranked #5 in performance, but at higher impacts it moved up to #2. Based on the rankings of the foams and the observed damage, students hypothesized at low impacts the primary mechanism of energy dissipation is compression. The foams with a macroscopically open web-like macroscopic structure (as opposed to foams with closed discrete beads) performed well in these tests. However, at high impacts, these foams likely reached a threshold of energy dissipation after full compression and thus they were not as effective. This hypothesis was supported by an absence of physical deformation for those foams. In contrast, the

foams that had a beaded structure that could be crushed, such as EPS, were very effective at energy dissipation under sudden high impacts. Students hypothesized that as the foam beads displace air and irreversibly deform they dissipate a substantial amount of energy,<sup>33</sup> thereby surpassing the non-beaded foam performance under high impact.

Students recognized that an important quality of safe foams is that they are neither too rigid nor too soft. Foams that exerted high stresses under low strains were said to be too rigid and provide minimal elastic storage of impact force, while foams that exerted small stresses at high strains were said to be too readily deformable and provide weak structural/conformational strength. First, qualitative descriptions of each foam's rigidity were recorded including details such as foam's response to a fingernail scratch. Foam rigidity was then measured with an INSTRON 4444, a mechanical testing instrument, to generate stress versus strain plots (representative results shown in Figure 6.4).

In this workshop the primary learning outcome was for students to learn how to evaluate the performance of alternative materials and relate the structural properties to the material function. Students characterized the rigid response and impact dissipation of

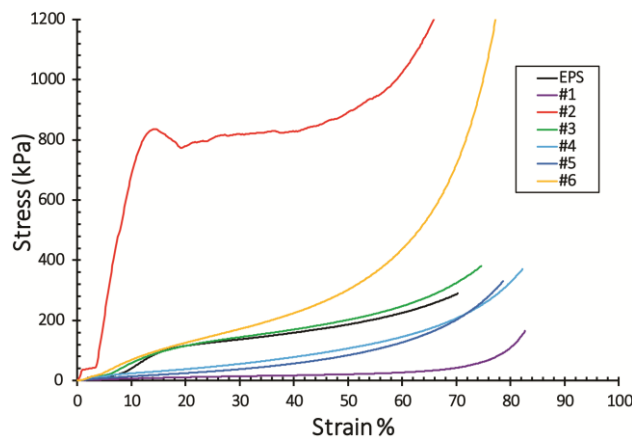


**Figure 6.4 Student-generated data measuring foam rigidity.**

The graph depicts the stress-strain relationship of each of the alternative foam samples, under quasi-static compression and at room temperature, compared to EPS.

alternative foams. They found that high rigidity and low dissipation ability were often related and hypothesized that this was because rigid materials were unable to cushion impacts effectively compared to more flexible materials. Students concluded that the best performing materials had moderate rigidity at low strain and readily deformed under high stress. This unique behavior was recognized in Figure 6.4 by the characteristic inflection observed at around 15% strain for EPS, Alternative #3, and Alternative #6.

The details of this workshop can be tailored to the material of interest, the level of preparation of the students, and the time available. Although the stress versus strain plots are helpful for mathematically ranking the foams, these results generally agreed with qualitative observations of rigidity and could be omitted for a lower level class or a more time constrained course. Additional metrics of material performance could also be included to scale the depth of this workshop. For example, under constant loading foams can deform/fatigue irreversibly over time.<sup>32</sup> To measure how EPS deformation compared to alternatives, students compressed all of the foams a uniform amount with a mechanical testing instrument and then let the foams conformationally equilibrate overnight. The foams were initially cut into 13 mm blocks and compressed to 4 mm, then the following day they were remeasured to determine the extent of irreversible deformation. The results of this study correlated with the qualitative observations from the high impact ball drops; the foams that were irreversibly damaged from the baseball drop also experienced a loss in thickness.

### Workshop III.

Design of a Greener Product: Proposed Infant Car Seat Design with Reduced Environmental Impacts and Uncompromised Safety: The final workshop synthesized

findings from Workshops I and II into a proposed product design with scientific and business merits. Students worked in small groups to decide how they wanted to innovate based upon: the life cycle impacts of the current industry standard, the performance of alternative materials, and the identified leverage points. Students developed a final presentation to present to the class, assuming the audience was composed of company stakeholders with a scientific background. Our students communicated directly with representatives at WAYB to advise on the marketing strategy for their innovation. In lieu of an industry partner, students could design accompanying marketing communications that articulate strategy and benefits of their innovation to general consumers.

Following the collection of experimental data, students generated a shared databank that everyone in the class had access to. They then worked in small groups to discuss whether they should use one of the EPS alternatives or use EPS, but decrease environmental impacts by innovating at a stage of EPS's life cycle. If we refer to Figure 6.1 to use multiple lenses for inspiring innovation, replacing EPS with a safer alternative represents a change that starts at the narrower green chemistry principles then works outward to evaluate these alternatives more comprehensively. Alternatively, starting by examining the life cycle of EPS to identify a place for improvement represents a midlevel starting point. Due to course constraints the students didn't have a chance to explore a third option; starting at the outermost lens and asking if there are other non-traditional ways to achieve the system goals. For example, removing the foam and reengineering a car seat's structure to achieve a new mechanism of energy dissipation would represent a change that starts from the system level. Achieving the same system goal by changing the mind-set about how to do so represents a fundamental change in the system and is known

as a *paradigm shift*.<sup>19</sup> Even if students do not have the time or expertise to explore redesign of a product entirely, we recommend a class discussion on what a paradigm shift would look like for a given product and how transformative this kind of systematic solution could be.

Once students decided on a product design, they prepared a twenty-minute presentation for the class, justifying their proposal with data from Workshops I and II that support the likely success of the product. These supporting data included a discussion on what green chemistry principles are satisfied, what impacts are expected to be improved at a particular stage of the life cycle, and any expected changes in the performance of the product. To help students prepare a marketing strategy, they were shown examples of marketing material for real-world green products that use scientific data to articulate claims to consumers (examples are provided in Appendix E). We recommend having students either write a company blog post or design a marketing pamphlet to practice communicating scientific concepts to a general audience. Either of these formats would encourage students to use illustrations, graphics, photographs, and/or data to support their reasoning.

In this workshop students learned how to use systems thinking to navigate the decision-making process around the selection of chemical and material alternatives. Students found that if they had prioritized green principles, they would have selected Alternative #3 to replace EPS because it has better reusability. However, a systems approach made students aware that the results of the impact analysis had to be prioritized over the green principles, and because EPS slightly outperformed Alternative #3 at high impacts, students ultimately decided that had to be prioritized. They ended up

recommending modifying the EPS production to eliminate the use of organic blowing agents and educating consumers on the hidden impacts of foam blowing agents. Additionally, they recommended exploring the performance of composite EPS foams in the future, with the hope that this may allow for the total amount of EPS to be reduced. In this decision making process students experienced the importance of fully evaluating how a material replacement affects product performance, which lead them to consider other possibilities for innovation such as affecting a life cycle change or creating a paradigm shift instead.

Studying a car seat was especially effective for teaching students to consider material performance because the students understood any car seat is going to have to pass regulatory safety testing before going on the market. Depending upon the foam alternatives selected for testing, the future outcomes of this workshop will vary; but in all cases, students should learn that systems thinking is needed to design a next generation product that is better from both an environmental and performance perspective. Although we did not identify a material that significantly outperformed EPS for car seat safety, we only selected six alternative foams to test for this pilot lab. We expect that future student cohorts could use these initial findings to tailor the alternatives selection to bias for more high performing foams, and each successive round of implementation of this project would allow for a more informed selection of materials for testing. Moreover, even for a set of materials with subpar performance, we could have asked students to identify an alternative application where it would make sense to switch from EPS to one of the tested alternatives. For example, we expect that some of the alternatives would have offered

sufficient impact absorbance for package padding material, with an improved end-of-life outcome over EPS.

This final workshop can also be easily adapted for lower level, or shorter, courses. For a short and easily accessible version of Workshop III, students could work in groups to identify their most promising material based upon the data from prior workshops. They would then individually describe their selection and the benefits of it in a post-lab writeup. If the original industry standard material is selected they should describe why they chose to keep it and how they could still meet the company goal to green their product. To practice articulating the benefits of a product to consumers, the students could also design a new product label that accurately communicates both a green and functional advantage of this product. Workshop III also provides an opportunity for implementing a systems thinking project in a lecture course without a lab. An instructor could provide students with a summary of life cycle impacts, toxicity, and performance measurements (*i.e.*, the data that would be gathered during Workshops I and II) and students could use this information to perform Workshop III.

### **Findings and Future Outlook**

Herein we have described an approach where students work at the interface of innovation, environmental stewardship and chemistry to design a next generation car seat. This project was developed with industry partners to provide an immersive learning experience for students that brings together tools from green chemistry, life cycle thinking, and systems thinking. By considering both the environmental impacts of a polymer foam and measuring the functional properties, students practiced using their chemistry toolbox for sustainable innovation. The project components were divided into

three workshops with each emphasizing different learning outcomes (detailed in Appendix E). In Workshop I students learned how to evaluate the greenness of a foam by engaging in structured life cycle thinking and using EPS as the model foam. Workshop II focused on functional performance. The students found that the ability of a foam to compress is one approach to dissipate energy, but it is not the major mechanism under high impact conditions. Additional mechanisms, such as irreversible foam deformation, are needed.<sup>33</sup> This knowledge was then built upon when students observed that irreversible deformation is desirable at high impacts, but not with the low impacts encountered during routine wear and tear. Finally, in Workshop III students synthesized their learnings from Workshops I and II to make a recommendation on the product design with the best performance and most reduced impacts. After integrating their learnings from green chemistry, life cycle thinking and systems thinking, students developed and optimized their proposed solutions and practiced marketing their alternative to both nonscientific and scientific audiences. It was important for students to discuss their proposals with people from a business background to see how the proposed technology was perceived and optimize the communication strategy. Our students had this opportunity during discussions with our industry collaborator; this impact can be maintained with future cohorts even in the absence of a collaborating company by having the students work with peers from a business discipline, ideally through a formal class collaboration.

These workshops have been intentionally designed to be flexible and adaptable for other contexts. While this project is written with senior level chemistry undergraduates or starting graduate students in mind, the workshops can be tailored

depending on the specific course and allotted time. Within each workshop we have included suggested methods of modifying the sophistication. For example, in Workshop II the material evaluation can range from methodically quantitative using polymer characterization techniques to rudimentary qualitative rankings with ball dropping and visual observations. Beyond tailoring the sophistication of these three specific workshops, we see this format as a portable framework for inspiring other systematic product evaluations. In all cases there would be a workshop focusing on material impacts (both biological and environmental), a workshop focused on comparing relevant performance metrics, and a marketing workshop where students communicate their innovation. Other suitable product candidates that we envision fitting well within this framework include food packaging, house paint, cooking skillets, and baby bottles. No matter what the product of interest, the larger purpose of this framework is to help students develop a fluency in systems thinking that transfers to future endeavors.

We have found that the increasing visibility of green products has made students interested in sustainable design, but they are often lacking in experience developing the technical implementation. To complement the widespread incorporation of green chemistry into many undergraduate chemistry curriculums, it is important to give students opportunities to practice implementing these principles to problem-solve (as opposed to just performing green labs). Having scientists that are trained this way is vital for green chemistry's successful adaptation outside of academia.<sup>34</sup> The cohort of master's students who participated in this lab noted that this was their first experience using green principles to address a problem when the solution was not provided, despite coming from a range of undergraduate universities with differing bachelor's degrees.

A key benefit of this project is that students begin to develop a habitual state of mind for using systems thinking when approaching green product design. Using a systems approach means that students are aware that green principles can be used to make irresponsible choices if too much attention is paid to only one piece of a puzzle.<sup>8</sup> We have found that this reductionist thinking is common when students are tasked with evaluating chemical sustainability. Students are likely to begin this project with an emphasized caution against EPS due to its well-known end of life impacts. However, after evaluating functional attributes in tandem with life cycle impacts, students are faced with tough systems decisions without an obviously correct answer; any innovation will have a benefit and associated side-effects, the students must decide how they can maximize the cost-benefit ratio. The marketing portion of this project gives students an opportunity to practice communicating sustainable design across disciplines, a key component of systems thinking training.<sup>8</sup> After completing this lab students report feeling empowered to strive for sustainable product design that advances past vague buzzwords to substantiated claims of environmental stewardship and superior functionality. Due to the inherent complexity and vagueness of systems thinking, we have observed that students need these types of hands-on immersive exercises to develop an intuition for thinking in systems. Future versions of this framework would benefit from having the students be active participants in the selection of the design problem. In this scenario we worked with an industry collaborator to achieve a company goal, so students were given the challenge of replacing EPS. The students noted that they would have enjoyed a component of preparatory work wherein they did literature research on a few potential problems and then selected one to target as a class, thereby allowing for them to practice

identifying leverage points and feel a greater personal investment in the problem. We hope that this project inspires others to design activities or courses where students are not just exposed to the benefits of green chemistry, but get to experience coming up with their own practical ways of implementing green chemistry. Successful, widespread implementation of green chemistry in commerce demands a systems thinking approach to design where both environmental impacts and product performance are weighed: It is up to educators to give the next generation of scientists the tools to do this.

### **Bridge to Chapter VII**

Chapter VI presented a pedagogical approach to sustainable product design aimed to help students avoid designs with unsubstantiated claims or unintended consequences. The framework presented integrated tools from systems thinking, life cycle thinking and green chemistry to teach students to consider not only the chemicals in their product, but how they got there, where they will go, and how they affect societal and earth systems. By giving students an immersive learning experience, they were able to develop generalizable strategies for innovating and approaching sustainable design. Chapter VII concludes this dissertation by discussing the takeaways from Chapters I-VI that can be used to inform future green product design and nanomaterial development.

## CHAPTER VII

### VII. CONCLUSION

#### **Concluding Remarks**

Product design is increasingly focused on sustainability. To maintain market interest in these products they must have substantiated sustainability claims and perform well. Compelling sustainability claims need to originate from design strategies that go beyond green chemistry principles to also investigate life cycle and societal impacts. Chapter VI presented a framework for integrating systems thinking and life cycle thinking into green product design. We implemented this framework in a master's level chemistry course and found that the students were not initially equipped to evaluate sustainability claims. Despite a strong technical background, the students were not familiar with greenwashing and assumed sustainable chemical inputs lead to sustainable products. We were able to demonstrate that this is not inherently true and can be more thoroughly evaluated using life cycle thinking and systems thinking. By working through product proposals with the students and helping them identify places where intervention led to nonobvious, secondary impacts, they became aware of the interconnectedness of all the elements (*i.e.*, systems thinking).

While the pilot lab was successful in achieving the project goals, future cohorts would further benefit from being a part of the planning stages rather than given a specific problem to solve. Many students will have opportunities in their career to influence the areas of focus for sustainable product development, and this project would have an

increased impact if students played an active role in the problem identification. Too often sustainable products are addressing a problem that is less important than an underlying issue; problem prioritization remains one of the greatest challenges in sustainable product design. For example, in Chapter V the decreasing toolbox of sunscreen actives is discussed. The recent industry focus has been on producing reef-safe products, leading to the phase out of some sunscreen chemicals, which while important, is likely less consequential in many scenarios than the lesser-known issue of sunscreen photodegradation. Having fewer chemicals available to work with further constrains scientists' ability to produce photostable formulations. This complex interplay between sunscreen regulatory control, consumer preferences, and data-driven innovation makes satisfying all three areas extremely challenging. Encouraging students who practice sustainable product design to think about these types of feedback loops, as relevant for their product of interest, and prioritize problems within the constraints of regulatory control and consumer interest is increasing important.

Designing technologies that advance upon existing alternatives, both in performance and sustainability, demands the employment of sophisticated chemistries. Materials with well-defined chemical structures are ideal starting points for achieving reliable products with maximum societal value. To this end, NPs have shown great promise as advanced materials capable of customizability and high performance. Developing well-defined NPs that have activity which can be related back to their structure, both as individual chemicals and in mixtures with chemicals relevant to their application, is at the forefront of NP research.

This dissertation focused on the study of commercially relevant NPs. A synthesis was presented to prepare versatile azide-functionalized AuNP building blocks for accessing hybrid nanomaterials through click reactions. NPs possessing functional groups that can be readily conjugated are important precursors for the preparation of customized nanohybrid products. A series of mixed-ligand NPs containing cationic and polyethylene glycol ligands were studied *in vivo*. By employing a polyethylene glycol diluent ligand the cationic ligands no longer induced AuNP toxicity. This provides a toxicity-reduction strategy for medicinal applications where cationic NPs are desired but their toxicity is not. Though NP safety is usually determined using solutions of individual particles that are free of additives, this dissertation identified multiple instances of NP safety changing in the presence of relevant mixtures. Mixtures of AuNPs and surfactants produced synergistic toxicity at concentrations where the individual components were benign. Besides considering relevant formula components, environmental use conditions can affect NP safety as well. UV irradiation significantly increased the *in vivo* toxicity of ZnO particles and organic sun filters mixtures, thus calling into question the appropriate way to evaluate sunscreen ingredient safety. These results demonstrate a need for additional, foundational studies to understand the effects of formula components on NP biocompatibility and challenge traditional models of NP safety where the matrix is assumed to have only additive effects on NP toxicity.

NPs offer the ability to advance so many products but their successful market integration relies on first developing a thorough understanding of properties and safety. There is an abundance of NP proof-of-concept studies; recently, efforts have been shifting to focus on syntheses that can be translated to industry. As we continue to

develop adaptable syntheses the field will have to continue evolving its understanding of NP safety to begin considering the effects of mixtures and use conditions. As high-throughput technologies and computing continue to advance in parallel to nanomaterials, thus expediting the identification of high-priority NPs, the widespread commercialization of sophisticated NP-containing products seems inevitable.

## APPENDICES

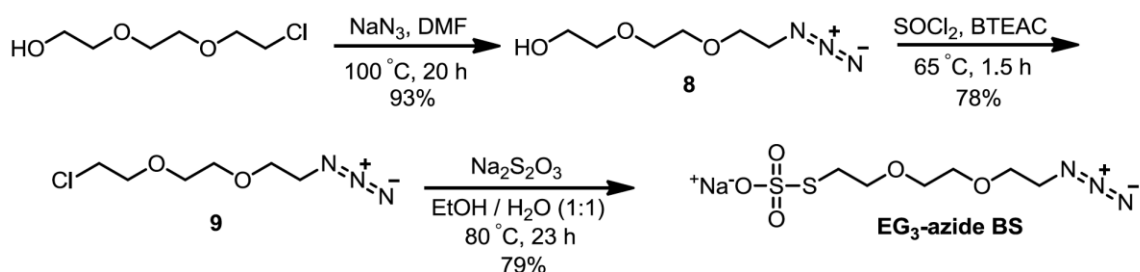
### A. SUPPORTING INFORMATION FOR CHAPTER II: SINGLE-STEP

#### SYNTHESIS OF SMALL, AZIDE-FUNCTIONALIZED GOLD

#### NANOPARTICLES: VERSATILE, WATER-DISPERSIBLE REAGENTS FOR

#### CLICK CHEMISTRY

#### Synthesis of sodium S-(2-(2-(2-azidoethoxy)ethoxy)ethyl) sulfthioate (N<sub>3</sub>-EG<sub>3</sub> BS)



#### Scheme A1. Synthetic route to a EG<sub>3</sub> tethered azide-functionalized Bunte salt 1-azido-2-(2-(2-chloroethoxy)ethoxy)ethane (**8**).

2-(2-(2-chloroethoxy)-ethoxy)ethanol (4.00 g, 0.0237 mol) was dissolved in anhydrous DMF (100 mL) under N<sub>2</sub>. Sodium azide (3.07 g, 0.0472 mol) was added and the mixture was heated to 100 °C for 20 h while stirring. The mixture was cooled down to r.t. and DMF was removed under reduced pressure in a rotary evaporator, and condensed over NaOH pellets to trap any HN<sub>3</sub> potentially produced. The crude residue was then suspended in diethyl ether (100 mL), filtered through a medium fritted funnel, and concentrated *in vacuo* to yield **8** (3.85 g, 93%) as a colorless liquid. <sup>1</sup>H-NMR (300 MHz, CDCl<sub>3</sub>): δ = 3.62-3.77 (m, 10H), 3.42 (t, 2H), 2.28 (t, 1H).

1-azido-2-(2-(2-chloroethoxy)ethoxy)ethane (**9**).<sup>1</sup> A mixture of azide **8** (3.50 g, 0.0200 mol) and benzyltriethylammonium chloride (BTEAC) (0.137 g, 0.0600 mmol) were heated in a 3-neck RB flask to 65 °C. Thionyl chloride (4.78 g, 0.0402) was then added dropwise from an addition funnel equipped with a pressure-equalization arm, and the reaction mixture was further stirred at 65 °C for 1.5 h while maintaining a continuous N<sub>2</sub> flow (to remove HCl generated). The mixture was let cool to r.t. and excess thionyl

chloride was removed by rotary evaporation. The crude product was suspended in phosphate buffer (50 mM, pH = 7.0, 15 mL) and extracted with EtOAc/hexane (1:1, 15 mL total). The organic layer was washed with phosphate buffer (4 x 15 mL), dried with Na<sub>2</sub>SO<sub>4</sub>, filtered using a coarse fritted funnel, and concentrated *in vacuo* to yield **9** (3.02 g, 78 %) as a yellow liquid. <sup>1</sup>H-NMR (300 MHz, CDCl<sub>3</sub>): δ = 3.64-3.81 (m, 10 H), 3.42 (t, 2H).

S-(2-(2-(2-azidoethoxy)ethoxy)ethyl)sulfothioate (N<sub>3</sub>-EG<sub>3</sub> BS). Chloro compound **9** (2.51 g, 0.0130 mol) was dissolved in EtOH/H<sub>2</sub>O (4:3, 70 mL total). Anhydrous sodium thiosulfate (2.47 g, 0.0156 mol) (dissolved in 10 mL deionized water) was added over ~ 2 min. The resulting mixture was heated at 80 °C for 23 h. Upon letting cool to r.t., EtOH and H<sub>2</sub>O were removed by rotary evaporation. The crude material was dissolved in CH<sub>3</sub>CN (20 mL) to precipitate salts that were subsequently removed by filtering using a medium fritted funnel. CH<sub>3</sub>CN was removed by rotary evaporation to produce a crude yellow liquid that was then redissolved in deionized H<sub>2</sub>O (10 mL) to separate unreacted starting material as a yellow oily residue. The water solution was decanted and subsequently filtered through a fine fritted funnel to remove residual trace starting material. Concentration *in vacuo* produced N<sub>3</sub>-EG<sub>3</sub> BS (2.99 g, 79%) as an oily pale yellow solid. <sup>1</sup>H-NMR (300 MHz, D<sub>2</sub>O): δ = 3.78 (t, 2H), 3.57-3.65 (m, 6H), 3.39 (t, 2H), 3.18 (t, 2H).

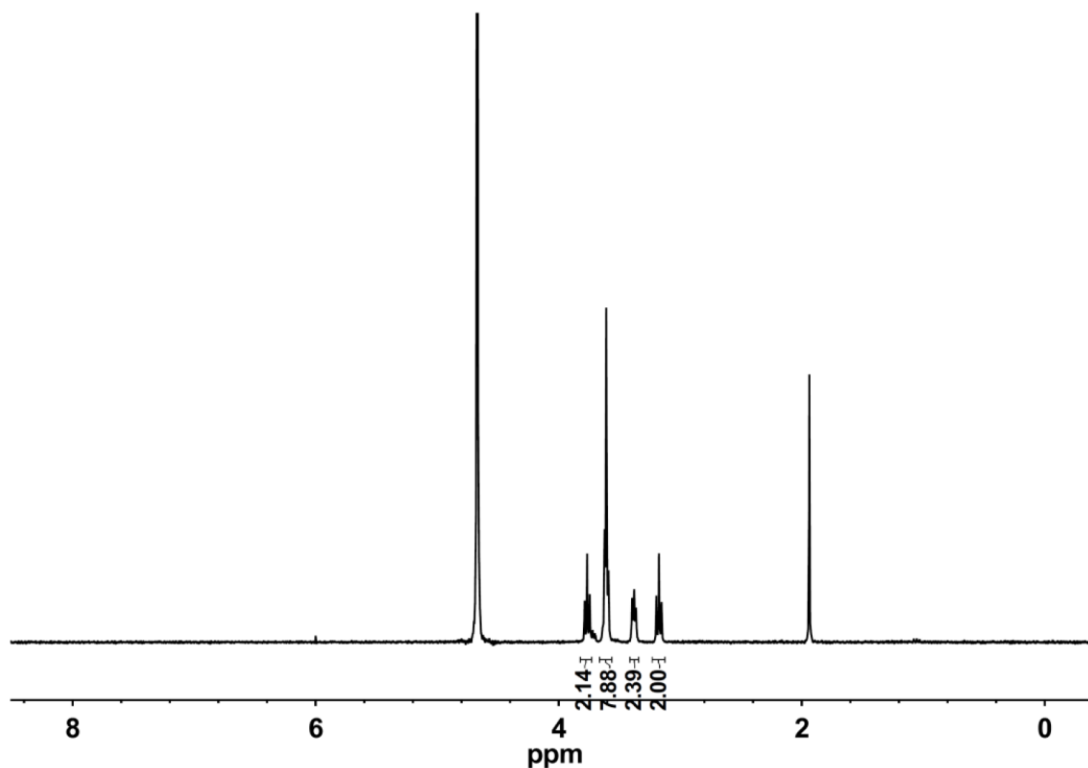


**Figure A1.  $^1\text{H-NMR}$  (300 MHz),  $\text{D}_2\text{O}$ , spectrum of  $\text{N}_3\text{-EG}_3$  BS**

### **$\text{N}_3\text{-EG}_3\text{-AuNP-EG}_3$ characterization**

*Calculation of moles of azide ligand for a given mass of  $\text{N}_3\text{-EG}_3\text{-AuNP-EG}_3$ .*

For a 3.5 nm AuNP, there are 1580 Au atoms (obtained from  $N_{\text{Au}} = 10^{(\text{LOG}(\text{diameter} - 0.2177) - \text{LOG}(0.225/0.3639))}$ ) and 180  $\text{EG}_3$  ligands ( $\# \text{EG}_3 \text{ ligands} = (\text{surface area} * 0.826_{\text{maximum packing density on a sphere}}) / (0.1775 \text{ nm}^2)_{\text{footprint of an EG}_3 \text{ molecule}}$ ).<sup>2,3</sup> Therefore, the average molecular weight for 3.5 nm  $\text{N}_3\text{-EG}_3\text{-AuNP-EG}_3$  [ $\text{Au}_{1580}(\text{N}_3\text{-EG}_3)_9(\text{EG}_3)_{171}$ ] is  $3.4 \times 10^5$  g/mol. The moles of AuNPs can then be calculated from  $g_{\text{AuNPs}} * (1 \text{ mol} / 3.41 \times 10^5 \text{ g}_{\text{AuNPs}})$ . For every mole of AuNPs, there are 9 molar equivalents of azide-ligand, therefore  $\text{mol}_{\text{AuNPs}} * 9 = \text{mol}_{\text{azides}}$ .

**Table A1. Multiple batches of N<sub>3</sub>-EG<sub>3</sub>-AuNP-EG<sub>3</sub>, core size determined by SAXS.**

	<b>Diameter (nm)</b>	<b>Polydispersity (nm)</b>	<b>% Polydispersity</b>
Batch 1	3.5	0.4	11%
Batch 2	3.7	0.3	8%
Batch 3	3.5	0.4	11%
Batch 4	3.4	0.5	15%
Batch 5	3.5	0.5	14%
Batch 6	3.5	0.5	14%
<b>Average</b>	<b>3.5</b>	<b>0.4</b>	<b>12%</b>
<i>Std Dev</i>	<i>0.09</i>	<i>0.07</i>	

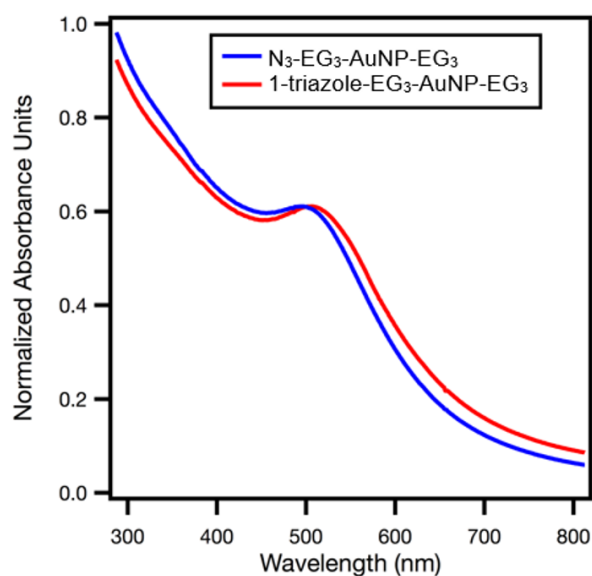


**Figure A2. UV-vis of AuNPs before (N<sub>3</sub>-EG<sub>3</sub>-AuNP-EG<sub>3</sub>) and after (1-triazole-EG<sub>3</sub>-AuNP-EG<sub>3</sub>) coupling reactions.**

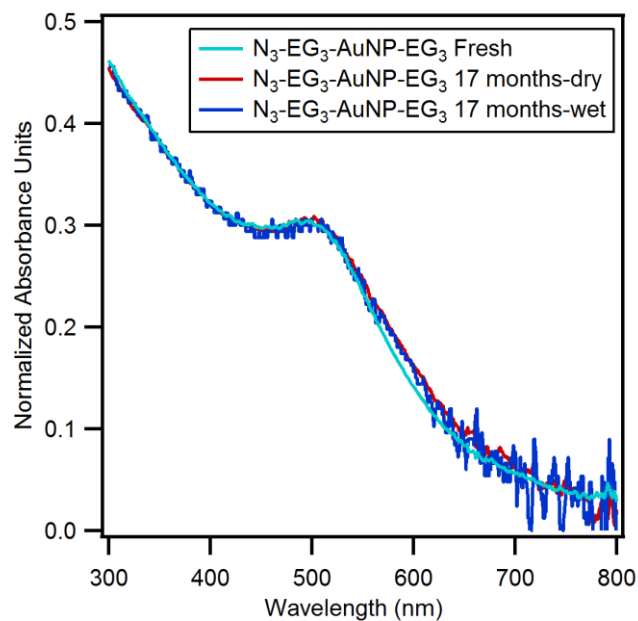


**Figure A3. UV-vis of N<sub>3</sub>-EG<sub>3</sub>-AuNP-EG<sub>3</sub> immediately following purification.** (“Fresh”), after 17 months of storage in the freezer as a dried powder (“17 months-dry”), and after 17 months of storage in water (“17 months-wet”).

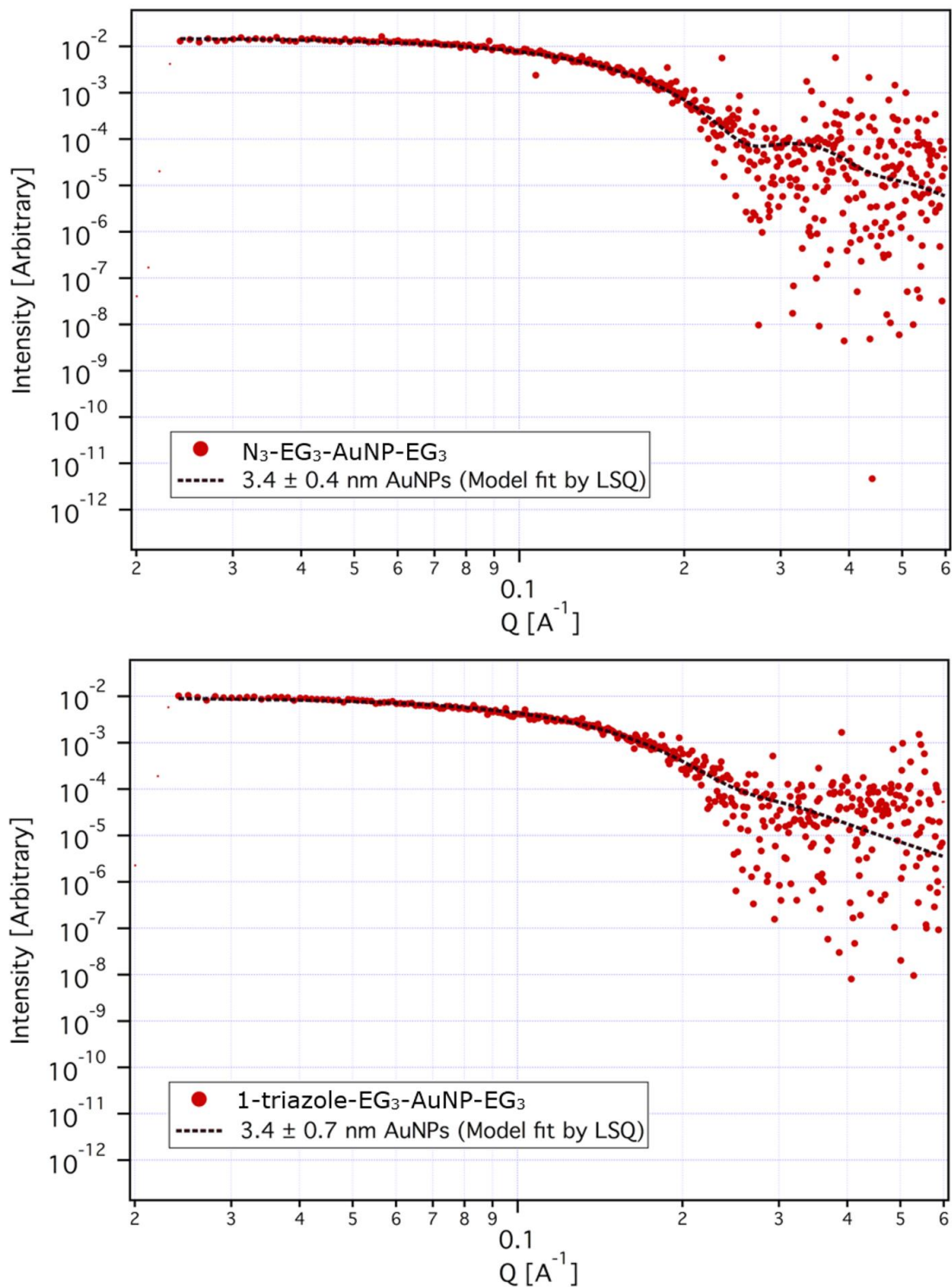


**Figure A4. Raw SAXS patterns and overlaid LSQ model fits for AuNPs.** Comparing before ( $N_3-EG_3-AuNP-EG_3$ ) and after ( $1-triazole-EG_3-AuNP-EG_3$ ) the coupling reaction shows no growth in average core size during the reaction or subsequent purification.

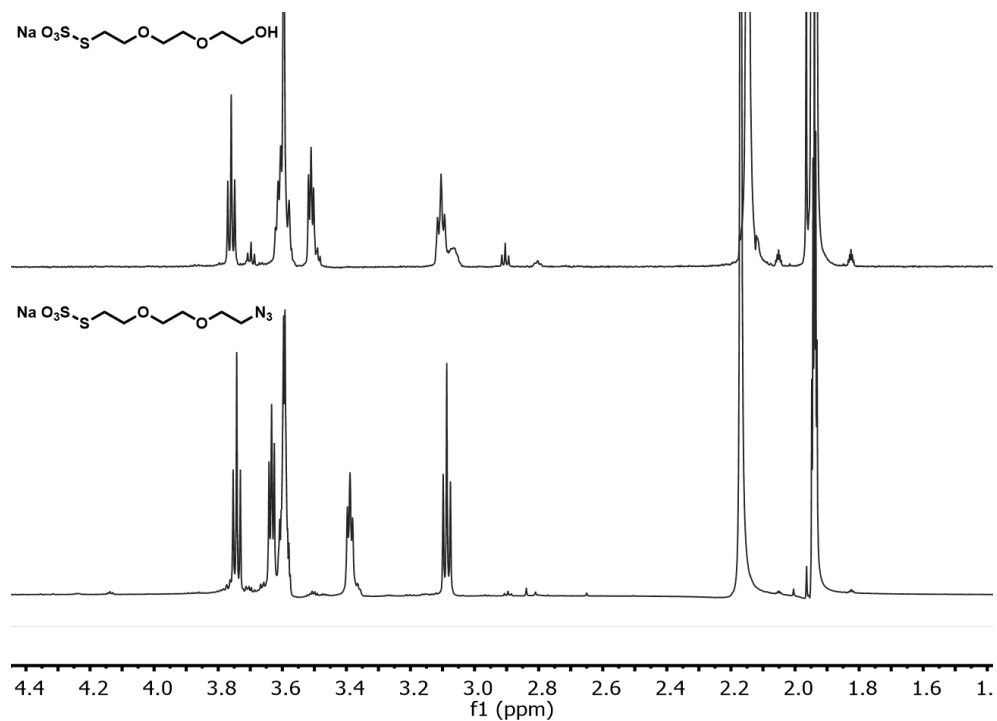


**Figure A5.**  $^1\text{H-NMR}$  (600 MHz),  $\text{CD}_3\text{CN}$ , stacked spectra of  $\text{EG}_3\text{-BS}$  and  $\text{N}_3\text{-EG}_3\text{-BS}$ .

Ligands demonstrate an upfield shift for the methylene signal  $\alpha$  to the azide group (relative to the methylene  $\alpha$  to the hydroxyl).

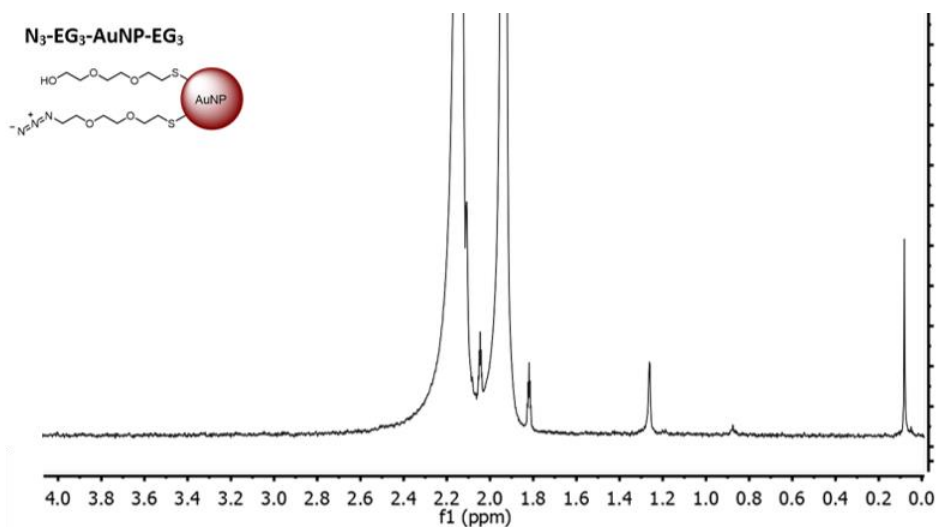


**Figure A6.**  $^1\text{H-NMR}$  (600 MHz),  $\text{CD}_3\text{CN}/\text{D}_2\text{O}$  (99:1),  $\text{N}_3\text{-EG}_3\text{-AuNP-EG}_3$  before decomposition.

The absence of signals between 2.9 and 4.0 ppm indicates all ligands are attached to the AuNPs and no free ligands are present (other peaks are due to residual solvent).

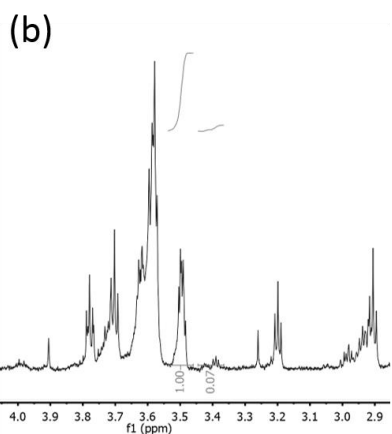
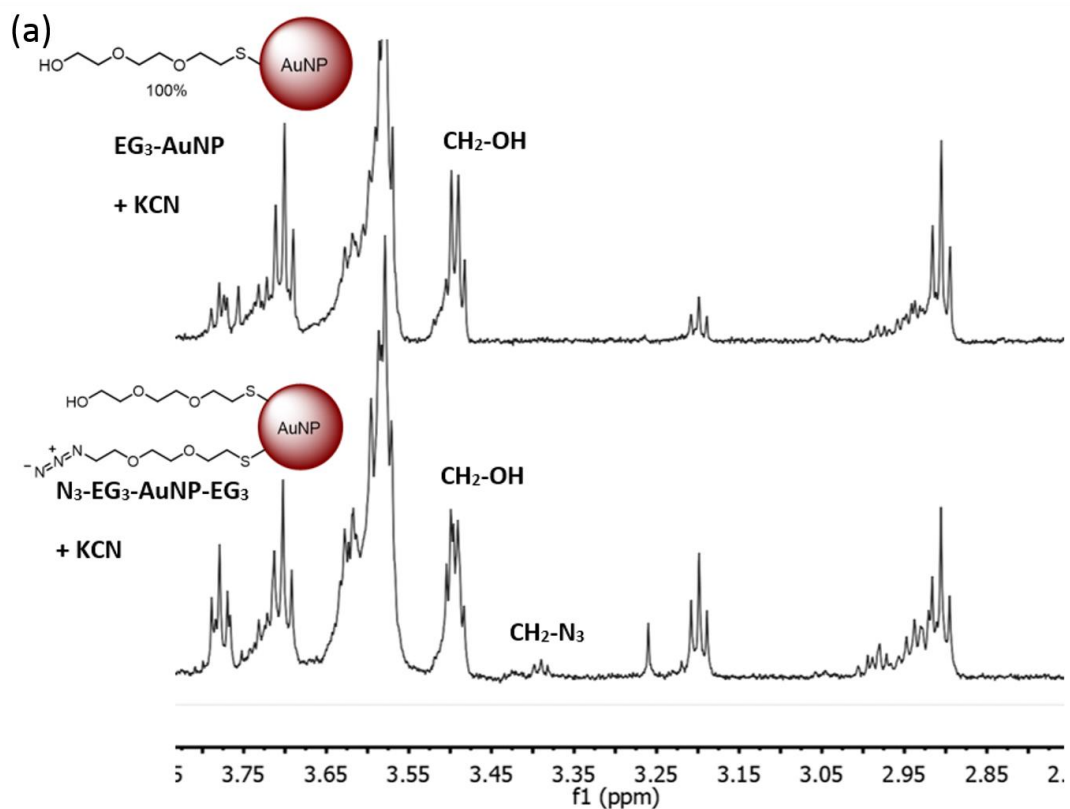


**Figure A7. <sup>1</sup>H-NMR (600 MHz), CD<sub>3</sub>CN/D<sub>2</sub>O (99:1), spectra after AuNP decomposition.**

The presence of sharp signals between 2.9 and 4.0 ppm indicates that the ligands are free in solution and no longer attached to AuNPs. (a) Stacked N<sub>3</sub>-EG<sub>3</sub>-AuNP-EG<sub>3</sub> and EG<sub>3</sub>-AuNP after cyanide decomposition, (b) Integrated signals of interest from N<sub>3</sub>-EG<sub>3</sub>-AuNP-EG<sub>3</sub> spectrum.

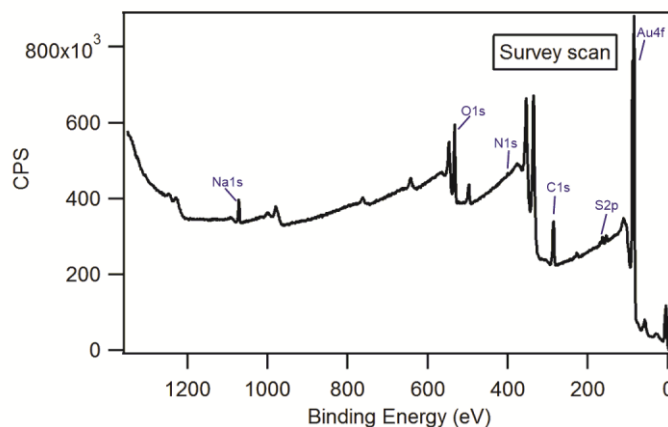


**Figure A8. XPS survey spectrum of 17-month-old N<sub>3</sub>-EG<sub>3</sub>-AuNP-EG<sub>3</sub> (stored dry) on a chromium coated silicon substrate.**

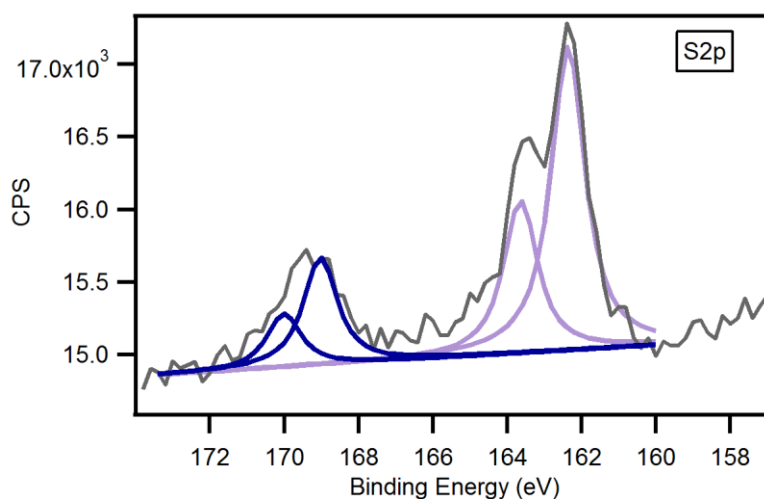


**Figure A9. A sulfur 2p XPS spectrum with peaks fit as the blue and purple traces (same sample as in Figure A8).**

The reduced sulfur at ~163 eV corresponds to the thiolate linkage on the AuNP surface, and oxidized sulfur is at ~169 eV.

**Copper-free strain promoted alkyne-azide cycloaddition (SPAAC) reactions with N<sub>3</sub>-EG<sub>3</sub>-AuNP-EG<sub>3</sub>.**

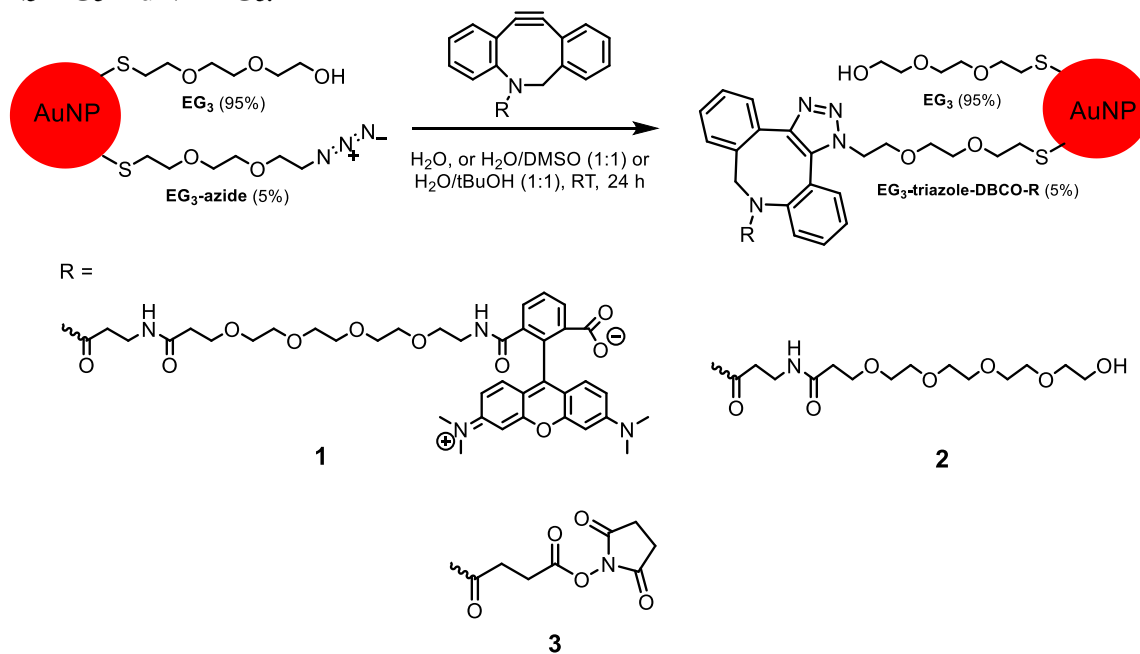


**Figure A10. Copper-free 1,3-dipolar cycloadditions of N<sub>3</sub>-EG<sub>3</sub>-AuNP-EG<sub>3</sub> and strained alkynes (1-3)**

**1-triazole-EG<sub>3</sub>-AuNP-EG<sub>3</sub>.** Lyophilized N<sub>3</sub>-EG<sub>3</sub>-AuNP-EG<sub>3</sub> (15.59 mg, 4.1 × 10<sup>-7</sup> mol EG<sub>3</sub>-azide) were dissolved in H<sub>2</sub>O (1.72 mL) in a scintillation vial. DBCO-PEG<sub>4</sub>-Fluor-545 (1.40 mg, 1.5 × 10<sup>-6</sup> mol) (dissolved in 0.28 mL H<sub>2</sub>O) was added to the vial, capped, and the mixture was stirred at room temperature for 24 hours to ensure a complete reaction. The reaction mixture was then purified and lyophilized to isolate **1-triazole-EG<sub>3</sub>-AuNP-EG<sub>3</sub>** as a black powder. Confirmation of the successful coupling reaction was obtained by I<sub>2</sub> decomposition followed by NMR analysis.

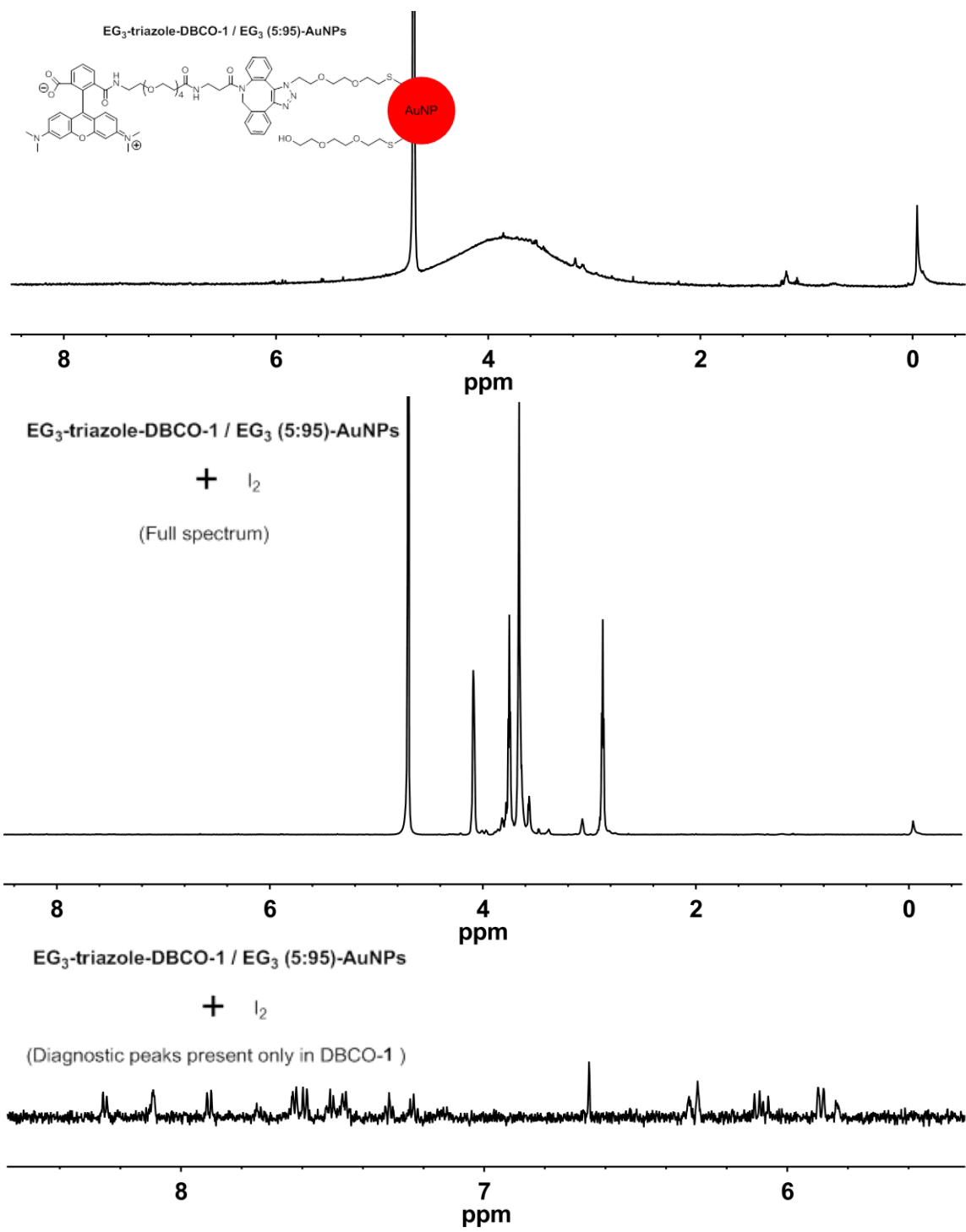


**Figure A11.** <sup>1</sup>H-NMR (600 MHz), D<sub>2</sub>O, characterization of 1-triazole-EG<sub>3</sub>-AuNP-EG<sub>3</sub> before and after I<sub>2</sub> decomposition.

Diagnostic peaks showing successful coupling shown enlarged.

**2-triazole-EG<sub>3</sub>-AuNP-EG<sub>3</sub>.** Lyophilized N<sub>3</sub>-EG<sub>3</sub>-AuNP-EG<sub>3</sub> (15.04 mg, 4.0 x 10<sup>-7</sup> mol EG<sub>3</sub>-azide) were dissolved in H<sub>2</sub>O (1 mL) in a scintillation vial. DBCO-PEG<sub>4</sub>-OH (1.53 mg, 3.0 x 10<sup>-6</sup> mol) (dissolved in 1 mL t-BuOH) was added to the vial, capped, and the mixture was stirred at room temperature for 24 hours. The reaction mixture was then purified and lyophilized to isolate **2-triazole-EG<sub>3</sub>-AuNP-EG<sub>3</sub>** as a black powder.

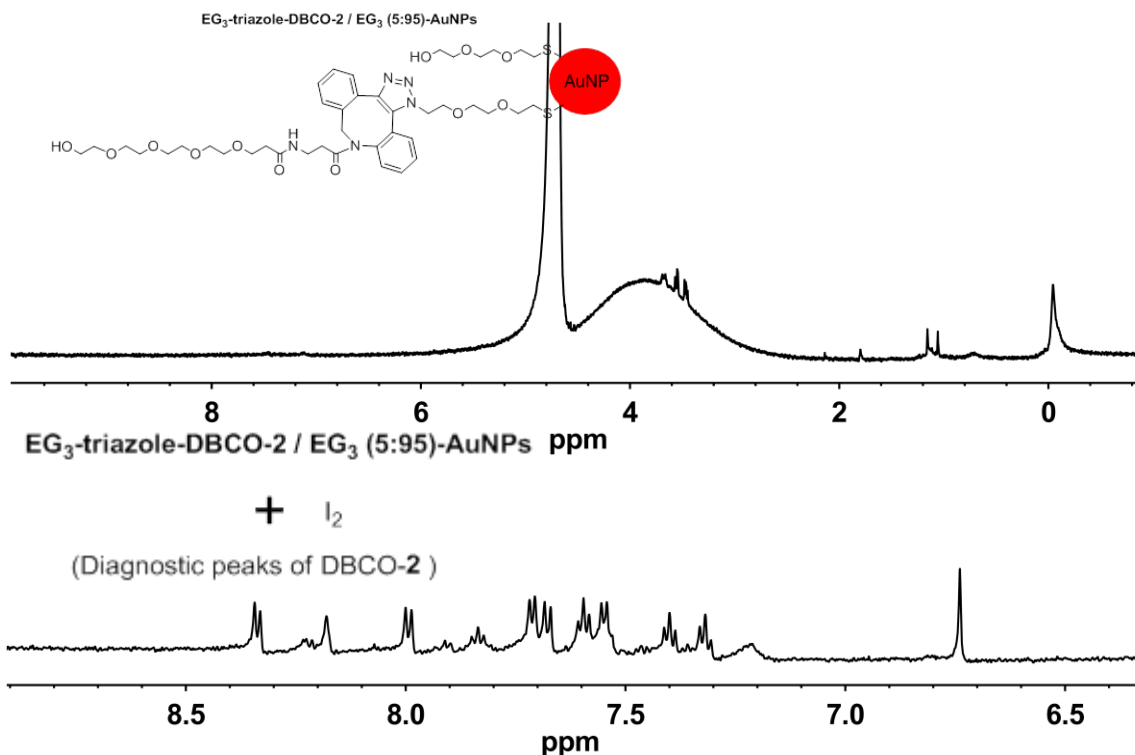


**Figure A12.** <sup>1</sup>H-NMR (600 MHz), D<sub>2</sub>O, characterization of **2-triazole-EG<sub>3</sub>-AuNP-EG<sub>3</sub>** before and after I<sub>2</sub> decomposition.

Diagnostic peaks showing successful coupling shown enlarged.

**3-triazole-EG<sub>3</sub>-AuNP-EG<sub>3</sub>.** Lyophilized N<sub>3</sub>-EG<sub>3</sub>-AuNP-EG<sub>3</sub> (16.70 mg, 4.4 x 10<sup>-7</sup> mol EG<sub>3</sub>-azide) were dissolved in H<sub>2</sub>O (1 mL) in a scintillation vial. DBCO-PEG<sub>4</sub>-NHS-ester (1.16 mg, 2.9 x 10<sup>-6</sup> mol) (dissolved in 1 mL DMSO) was added to the vial, capped, and the mixture was stirred at room temperature for 24 hours. The reaction mixture was then purified and lyophilized to isolate **3-triazole-EG<sub>3</sub>-AuNP-EG<sub>3</sub>** as a black powder.

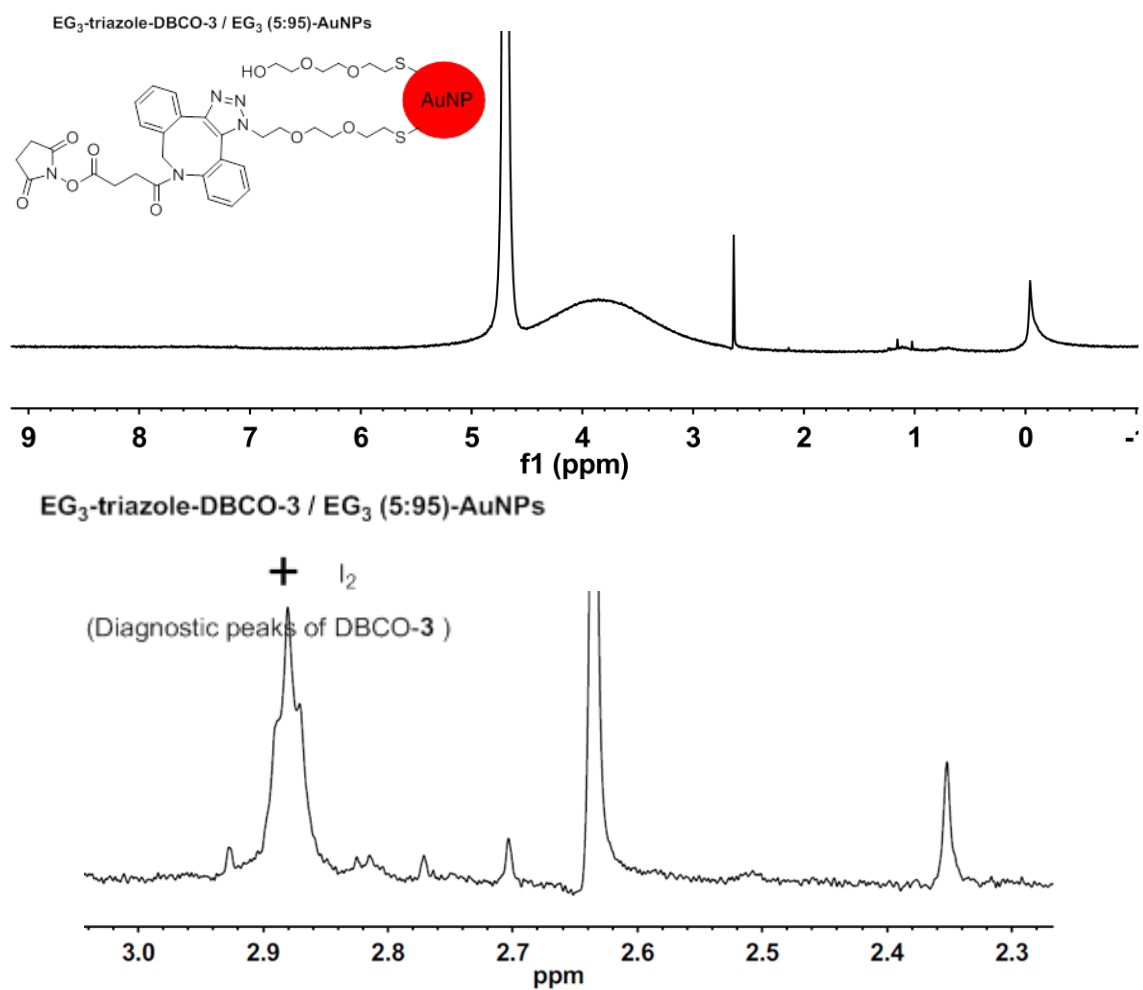


**Figure A13.** <sup>1</sup>H-NMR (600 MHz), D<sub>2</sub>O/DMSO-d<sub>6</sub> (80:20) characterization of 3-triazole-EG<sub>3</sub>-AuNP-EG<sub>3</sub> before and after I<sub>2</sub> decomposition. Diagnostic peaks showing successful coupling shown enlarged.

**Copper-catalyzed 1,3-dipolar cycloadditions with N<sub>3</sub>-EG<sub>3</sub>-AuNP-EG<sub>3</sub> and terminal alkynes (4-7)**

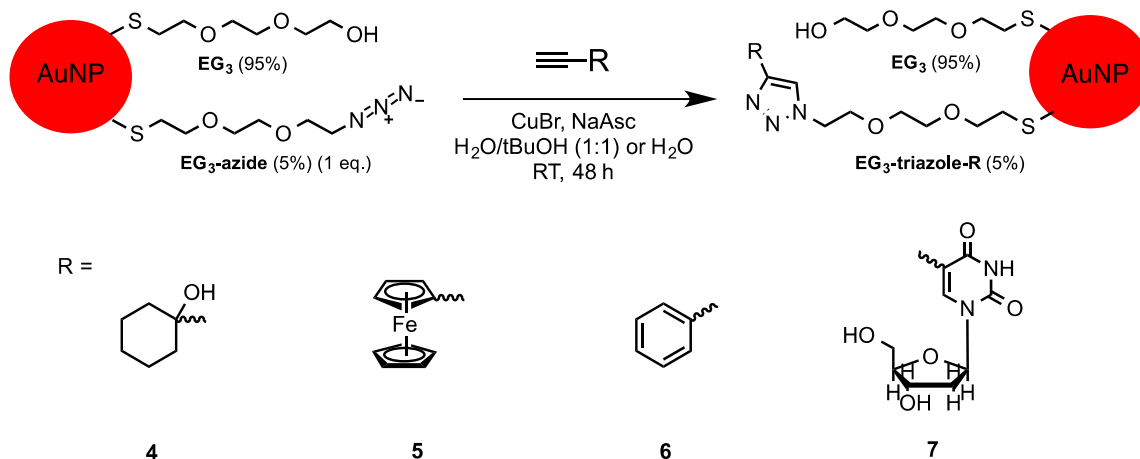


**Figure A14. Copper catalyzed 1,3-dipolar cycloadditions involving N<sub>3</sub>-EG<sub>3</sub>-AuNP-EG<sub>3</sub> and various terminal alkynes (4-7).**

**4-triazole-EG<sub>3</sub>-AuNP-EG<sub>3</sub>**. Lyophilized N<sub>3</sub>-EG<sub>3</sub>-AuNP-EG<sub>3</sub> (10.0 mg, 2.6 x 10<sup>-7</sup> mol N<sub>3</sub>-EG<sub>3</sub>) was dissolved in H<sub>2</sub>O (489 μL) in a scintillation vial. Sodium ascorbate (38 μL, 0.01 M in H<sub>2</sub>O, 3.8 x 10<sup>-7</sup> mol) was added to the vial, followed by tert-butyl alcohol as a co-solvent (985 μL), 1-ethynyl-1-cyclohexanol (15 μL, 0.1 M in tert-butyl alcohol, 1.5 x 10<sup>-6</sup> mol), and CuBr (474 μL, satd., aq. 3.8 x 10<sup>-8</sup> mol). The resulting solution was capped and stirred at room temperature for 48 hours. The reaction mixture was then purified and lyophilized to isolate **4-triazole-EG<sub>3</sub>-AuNP-EG<sub>3</sub>** as a black powder. For <sup>1</sup>H-NMR analysis, AuNPs were dissolved in D<sub>2</sub>O/DMSO-d<sub>6</sub> (80:20, 500 μL total) to confirm successful purification and decomposed with I<sub>2</sub>.

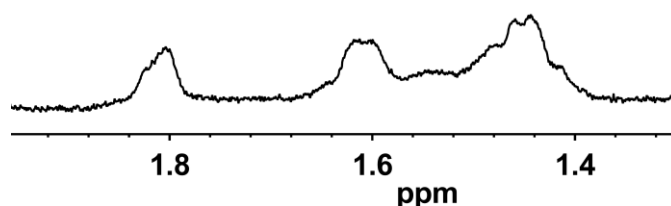


**Figure A15.**  $^1\text{H-NMR}$  (600 MHz),  $\text{D}_2\text{O}/\text{DMSO-d}_6$  (80:20), characterization of **4-triazole-EG<sub>3</sub>-AuNP-EG<sub>3</sub>** following  $\text{I}_2$  decomposition.

Diagnostic peaks showing successful coupling shown enlarged for clarity.

**5-triazole-EG<sub>3</sub>-AuNP-EG<sub>3</sub>.** Lyophilized  $\text{N}_3\text{-EG}_3\text{-AuNP-EG}_3$  (14.6 mg,  $3.9 \times 10^{-7}$  mol  $\text{N}_3\text{-EG}_3$ ) was dissolved in  $\text{H}_2\text{O}$  (489  $\mu\text{L}$ ) in a scintillation vial. Sodium ascorbate (37.5  $\mu\text{L}$ , 0.01 M in  $\text{H}_2\text{O}$ ,  $3.75 \times 10^{-7}$  mol) was added to the vial, followed by tert-butyl alcohol as a co-solvent (985  $\mu\text{L}$ ), ethynylferrocene (15  $\mu\text{L}$ , 0.1 M in tert-butyl alcohol,  $1.5 \times 10^{-6}$  mol), and  $\text{CuBr}$  (474  $\mu\text{L}$ , satd., aq.  $3.8 \times 10^{-8}$  mol). The resulting solution was capped and stirred at room temperature for 48 hours. The reaction mixture was then purified and lyophilized to isolate **5-triazole-EG<sub>3</sub>-AuNP-EG<sub>3</sub>** as a black powder. For  $^1\text{H-NMR}$  analysis, AuNPs were dissolved in  $\text{D}_2\text{O}/\text{DMSO-d}_6$  (80:20, 500  $\mu\text{L}$  total) to confirm successful purification and decomposed with  $\text{I}_2$ , then extracted into  $\text{CD}_2\text{Cl}_2$  (500  $\mu\text{L}$ ) and the organic phase was washed with brine (500  $\mu\text{L}$ ).

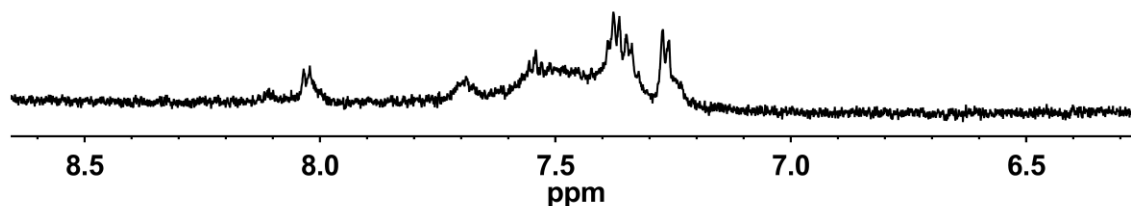


**Figure A16.**  $^1\text{H-NMR}$  (600 MHz),  $\text{CD}_2\text{Cl}_2$ , characterization of **5-triazole-EG<sub>3</sub>-AuNP-EG<sub>3</sub>** following  $\text{I}_2$  decomposition.

Diagnostic peaks showing successful coupling shown enlarged for clarity.

**6-triazole-EG<sub>3</sub>-AuNP-EG<sub>3</sub>.** Lyophilized  $\text{N}_3\text{-EG}_3\text{-AuNP-EG}_3$  (14.5 mg,  $3.8 \times 10^{-7}$  mol  $\text{N}_3\text{-EG}_3$ ) was dissolved in  $\text{H}_2\text{O}$  (489  $\mu\text{L}$ ) in a scintillation vial. Sodium ascorbate (37.5

$\mu\text{L}$ , 0.01 M in  $\text{H}_2\text{O}$ ,  $3.8 \times 10^{-7}$  mol) was added to the vial, followed by tert-butyl alcohol (985  $\mu\text{L}$ ), phenylacetylene (15  $\mu\text{L}$ , 0.1 M in tert-butyl alcohol,  $1.5 \times 10^{-6}$  mol), and  $\text{CuBr}$  (474  $\mu\text{L}$ , satd., aq.  $3.8 \times 10^{-8}$  mol). The resulting solution was capped and stirred at room temperature for 48 hours. The reaction mixture was then purified and lyophilized to isolate **6-triazole-EG<sub>3</sub>-AuNP-EG<sub>3</sub>** as a black powder. For  $^1\text{H-NMR}$  analysis, AuNPs were dissolved in  $\text{D}_2\text{O}/\text{DMSO-d}_6$  (80:20, 500  $\mu\text{L}$  total) to confirm successful purification, decomposed with  $\text{I}_2$ , then extracted into  $\text{CDCl}_3$  (500  $\mu\text{L}$ ) and the organic phase was washed with brine (500  $\mu\text{L}$ ).

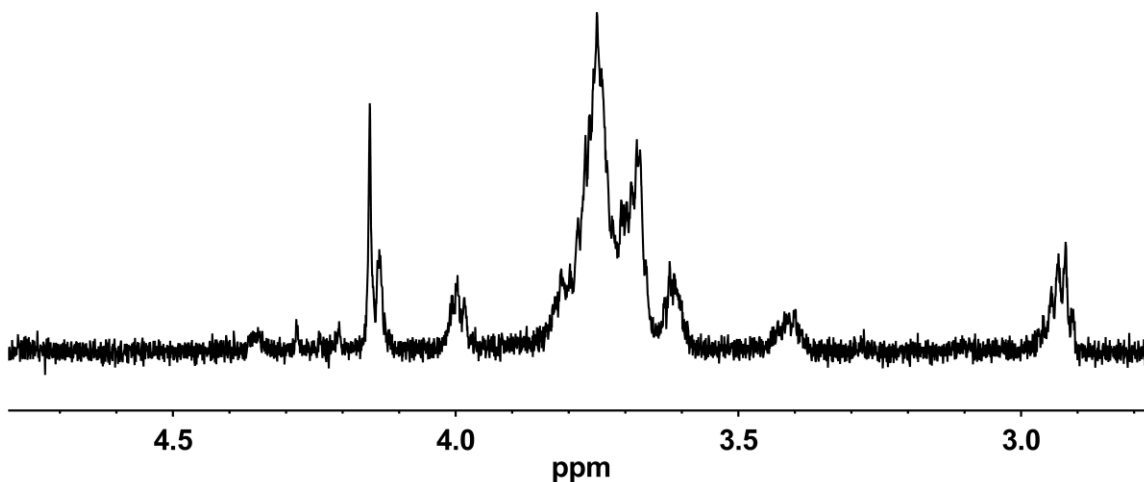


**Figure A17.**  $^1\text{H-NMR}$  (600 MHz),  $\text{CDCl}_3$ , characterization of **6-triazole-EG<sub>3</sub>-AuNP-EG<sub>3</sub>** AuNPs following  $\text{I}_2$  decomposition.

Diagnostic peaks showing successful coupling shown enlarged for clarity.

**7-triazole-EG<sub>3</sub>-AuNP-EG<sub>3</sub>**. Lyophilized **N<sub>3</sub>-EG<sub>3</sub>-AuNP-EG<sub>3</sub>** (13.1 mg,  $3.5 \times 10^{-7}$  mol **N<sub>3</sub>-EG<sub>3</sub>**) was dissolved in  $\text{H}_2\text{O}$  (489  $\mu\text{L}$ ) in a scintillation vial. Sodium ascorbate (37.5  $\mu\text{L}$ , 0.1 M in  $\text{H}_2\text{O}$ ,  $3.8 \times 10^{-7}$  mol) was added to the vial, followed by tert-butyl alcohol (985  $\mu\text{L}$ ), 5-ethynyl-2'-deoxyuridine<sup>4</sup> (15  $\mu\text{L}$ , 0.1 M in tert-butyl alcohol,  $1.5 \times 10^{-6}$  mol), and  $\text{CuBr}$  (474  $\mu\text{L}$ , satd., aq.  $3.8 \times 10^{-8}$  mol). The resulting solution was capped and stirred at room temperature for 48 hours. The reaction mixture was then purified and lyophilized to isolate **7-triazole-EG<sub>3</sub>-AuNP-EG<sub>3</sub>** as a black powder. For  $^1\text{H-NMR}$

analysis, AuNPs were dissolved in D<sub>2</sub>O/DMSO-d<sub>6</sub> (91:9, 550 μL total) to confirm successful purification and decomposed with I<sub>2</sub>

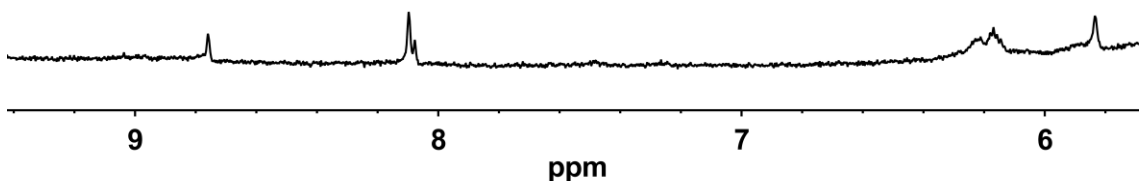


**Figure A18. <sup>1</sup>H-NMR (600 MHz), D<sub>2</sub>O/DMSO-d<sub>6</sub> (91:9), characterization of 7-triazole-EG<sub>3</sub>-AuNP-EG<sub>3</sub> following I<sub>2</sub> decomposition.**

Diagnostic peaks showing successful coupling shown enlarged for clarity.

### **Technical information for AuNP synthesis using computer-controlled pumps**

A detailed description of the mesofluidic reactor set-up, including part descriptions and assembly, is provided on page 11888 in our previous work.<sup>5</sup> In the present study we used a fourth pump to control addition of the second ligand so that direct mixed-ligand synthesis was possible. The four pumps were connected as shown in Figure 1. Each Bunte salt ligand flowed through 8 cm of tubing before they mixed at the first T-mixer, after which all tubing lengths were the same as those previously described.<sup>5</sup> The code to control the pumps was written in Kloehn Control 1.04 and is provided below for reference.

```
0 // Created by Ed Elliott
1 // Last Modified:
2 // 5-1-2015
3 // For use with 4 pumps, for mixed ligand synthesis. Set ligand A
percentage to 100 for single ligand NP synthesis
4 // There are hard coded fill values that depend on the current 25 mL x 10
mL x 10 mL x 10 mL syringe setup
5 // ... For a single ligand synthesis set laPer to 100 (ligand B pump will be
used for a water flush, don't panic
6 //
7 // THE ONLY SETTINGS TO BE CHANGED ARE IN THIS FIRST BLOCK
8 //
```

```

9      //          Set the totalFlowRate = to desired flow rate in mL per minute
10     VARIABLE <varName> = <float>    totalFlowRate, 60
11
12     //          Set laPer to a percentage of ligand A from 0 to 100 (Ligand B will be
calculated from this value)
13     VARIABLE <varName> = <float>    laPer, 100
14     //          No need to set this value for ligand B, it's calculated from the percent
of ligand A
15     VARIABLE <varName> = <float>    lbPer, 0
16
17     //          Prep reagent tubing Set prepTubing to 0 for NO, 1 for YES
18     CONSTANT <varName> = <float>    prepTubing, 1
19     //          Set nSynth = number of replicate runs
20     VARIABLE <varName> = <int>      nSynth, 3
21
22     //          Set maxAsp lower if of gassing is seen during aspiration
23     CONSTANT <varName> = <float>    maxAsp, 1200
24
25     //          START VARIABLE DECLARATION (Must be before any other
commands!)
26
27     //          Syringe Sizes in mL
28     CONSTANT <varName> = <float>    rSize, 25
29     CONSTANT <varName> = <float>    laSize, 10
30     CONSTANT <varName> = <float>    lbSize, 10
31     CONSTANT <varName> = <float>    auSize, 10
32
33     //          Valve numbers to names
34     CONSTANT <varName> = <float>    reaction, 1
35     CONSTANT <varName> = <float>    waste, 2
36     CONSTANT <varName> = <float>    reagent, 3
37     CONSTANT <varName> = <float>    water, 4
38
39     //          Calculate number of steps per mL for each of the syringes
40     VARIABLE <varName> = <float>    rmL, 0
41     VARIABLE <varName> = <float>    lamL, 0
42     VARIABLE <varName> = <float>    lbmL, 0
43     VARIABLE <varName> = <float>    aumL, 0
44
45     //          How much to fill each syringe (probably not going to be changed as
long as syringe sizes remain constant
46     //          Variable Names: rFillVol, lFillVol, and auFillVol
47     CONSTANT <varName> = <float>    rFillVol, 20
48     CONSTANT <varName> = <float>    lFillVol, 10
49     CONSTANT <varName> = <float>    auFillVol, 8
50
51     VARIABLE <varName> = <float>    laFillVol, 0
52     VARIABLE <varName> = <float>    lbFillVol, 1
53
54     //          Number of steps to fill each syringe
55     VARIABLE <varName> = <float>    rFillSteps, 0
56     VARIABLE <varName> = <float>    laFillSteps, 0
57     VARIABLE <varName> = <float>    lbFillSteps, 0

```

```

58          VARIABLE <varName> = <float>    auFillSteps, 0
59
60      //          Dispense Speed
61          VARIABLE <varName> = <float>    rDisp, 0
62          VARIABLE <varName> = <float>    laDisp, 0
63          VARIABLE <varName> = <float>    lbDisp, 500
64          VARIABLE <varName> = <float>    auDisp, 0
65
66      //          Aspirate Speed
67          VARIABLE <varName> = <float>    rAsp, 0
68          VARIABLE <varName> = <float>    laAsp, 0
69          VARIABLE <varName> = <float>    lbAsp, 0
70          VARIABLE <varName> = <float>    auAsp, 0
71
72      //          Loop counters
73          VARIABLE <varName> = <int>      rinseCount, 1
74          VARIABLE <varName> = <int>      nSynthCount, 0
75
76      //          END VARIABLE DECLARATION
77
78      //          Calculate percent of other ligand
79      ASSIGN <varName> = <int or float> lbPer, 100 - laPer
80
81      //          Calculate number of steps per mL for each of the syringes
82      ASSIGN <varName> = <int or float> rmL, 48000 / rSize
83      ASSIGN <varName> = <int or float> lamL, 48000 / laSize
84      ASSIGN <varName> = <int or float> lbmL, 48000 / lbSize
85      ASSIGN <varName> = <int or float> aumL, 48000 / auSize
86
87      //          Calculate ligand fill volume based on percent of each ligand desired
88      ASSIGN <varName> = <int or float> laFillVol, lFillVol * (laPer / 100)
89      IF <statement>    lbPer != 0
90      ASSIGN <varName> = <int or float> lbFillVol, lFillVol * (lbPer / 100)
91      ENDIF
92      //          Number of steps to fill each syringe based on above calculation
93      ASSIGN <varName> = <int or float> rFillSteps, rFillVol * rmL
94      ASSIGN <varName> = <int or float> laFillSteps, laFillVol * lamL
95      ASSIGN <varName> = <int or float> lbFillSteps, lbFillVol * lbmL
96      ASSIGN <varName> = <int or float> auFillSteps, auFillVol * aumL
97
98      //          Calculate dispense speed for each pump
99      ASSIGN <varName> = <int or float> rDisp, ((totalFlowRate / 2) * rmL) / 60
100     ASSIGN <varName> = <int or float> laDisp, (((totalFlowRate / 4) * (laPer / 100))
* lamL) / 60
101     IF <statement>    lbPer != 0
102     ASSIGN <varName> = <int or float> lbDisp, (((totalFlowRate / 4) * (lbPer / 100))
* lbmL) / 60
103     ENDIF
104     ASSIGN <varName> = <int or float> auDisp, ((totalFlowRate / 4) * aumL) / 60
105
106     //          Calculate aspirate speed for each pump
107     ASSIGN <varName> = <int or float> rAsp, maxAsp * (auSize / rSize)
108     ASSIGN <varName> = <int or float> laAsp, maxAsp * (auSize / laSize)

```

```

109          ASSIGN <varName> = <int or float> lbAsp, maxAsp * (auSize / lbSize)
110          ASSIGN <varName> = <int or float> auAsp, maxAsp
111
112      //          END OF CALCULATIONS
113
114      //          Initialize Pumps
115      //          PRINTF <text>   "Initializing Pumps"
116      //          1          INIT [IMM or SYNC]
117      //          2          INIT [IMM or SYNC]
118      //          3          INIT [IMM or SYNC]
119      //          4          INIT [IMM or SYNC]
120
121      //          Flush reagent tubing (up to 1 M long) uses 0.5 mL of each reagent
122      IF <statement>   prepTubing == 1
123      PRINTF <text>   "Flushing the reagent tubing..."
124
125      1          VALVE_PORT = <int> [CCW]          reagent
126      2          VALVE_PORT = <int> [CCW]          reagent
127      3          VALVE_PORT = <int> [CCW]          reagent
128      4          VALVE_PORT = <int> [CCW]          reagent
129
130      1          SET speed = <float>          rAsp
131      2          SET speed = <float>          laAsp
132      3          SET speed = <float>          lbAsp
133      4          SET speed = <float>          auAsp
134
135      1          ASPIRATE <float> [IMM or SYNC]   rmL / 2
136      2          ASPIRATE <float> [IMM or SYNC]   lamL / 2
137      IF <statement>   lbPer != 0
138      3          ASPIRATE <float> [IMM or SYNC]   lbmL / 2
139      ENDIF
140      4          ASPIRATE <float> [IMM or SYNC]   aumL / 2
141
142      1          VALVE_PORT = <int> [CCW]          waste, CCW
143      2          VALVE_PORT = <int> [CCW]          waste, CCW
144      3          VALVE_PORT = <int> [CCW]          waste, CCW
145      4          VALVE_PORT = <int> [CCW]          waste, CCW
146
147      1          DISPENSE <float> [IMM or SYNC]   rmL / 2
148      2          DISPENSE <float> [IMM or SYNC]   lamL / 2
149      IF <statement>   lbPer != 0
150      3          DISPENSE <float> [IMM or SYNC]   lbmL / 2
151      ENDIF
152      4          DISPENSE <float> [IMM or SYNC]   aumL / 2
153
154      PRINTF <text>   "Finished flushing reagent tubing..."
155      ENDIF
156
157      //          SYNTHESIS LOOP (number of runs set by nSynth)
158      DO
159      PRINTF <text>   "Performing synthesis..."
160      PRINTF <text>   "PRESS RUN TO START SYNTHESIS"
161      1          HALT

```

```

162          PRINTF <text>   "This is one synthesis happening"
163
164          1      SET speed = <float>      rAsp
165          2      SET speed = <float>      laAsp
166          3      SET speed = <float>      lbAsp
167          4      SET speed = <float>      auAsp
168
169          1      VALVE_PORT = <int> [CCW]      reagent
170          2      VALVE_PORT = <int> [CCW]      reagent
171          3      VALVE_PORT = <int> [CCW]      reagent
172          4      VALVE_PORT = <int> [CCW]      reagent
173
174          2      ASPIRATE <float> [IMM or SYNC] laFillSteps, IMM
175          IF <statement> lbPer != 0
176          3      ASPIRATE <float> [IMM or SYNC] lbFillSteps, IMM
177          ELSE
178          3      VALVE_PORT = <int> [CCW]      water
179          3      ASPIRATE <float> [IMM or SYNC] 10 * lbmL, IMM
180          ENDIF
181          4      ASPIRATE <float> [IMM or SYNC] auFillSteps, IMM
182          1      ASPIRATE <float> [IMM or SYNC] rFillSteps
183
184          1      DELAY <float>   5
185
186          1      SET speed = <float>      rDisp
187          2      SET speed = <float>      laDisp
188          IF <statement> lbPer != 0
189          3      SET speed = <float>      lbDisp
190          ENDIF
191          4      SET speed = <float>      auDisp
192
193          1      VALVE_PORT = <int> [CCW]      reaction, CCW
194          2      VALVE_PORT = <int> [CCW]      reaction, CCW
195          3      VALVE_PORT = <int> [CCW]      reaction, CCW
196          4      VALVE_PORT = <int> [CCW]      reaction, CCW
197
198          1      DISPENSE <float> [IMM or SYNC] rFillSteps, IMM
199          2      DISPENSE <float> [IMM or SYNC] laFillSteps, IMM
200          IF <statement> lbPer != 0
201          3      DISPENSE <float> [IMM or SYNC] lbFillSteps, IMM
202          ENDIF
203          1      DELAY <float>   3
204          4      DISPENSE <float> [IMM or SYNC] auFillSteps
205          IF <statement> lbPer == 0
206          3      SET speed = <float>      laDisp // Flushing with water as ligand A speed after
run
207          3      DISPENSE <float> [IMM or SYNC] 10 * lbmL
208          ENDIF
209          1      DELAY <float>   10
210
211          ASSIGN <varName> = <int or float> nSynthCount, nSynthCount + 1
212
213 //          3x water rinses to clear the lines

```

```

214 DO
215 IF <statement> rinseCount == 1
216 PRINTF <text> "Starting 1st Rinse"
217 ENDIF
218 IF <statement> rinseCount == 2
219 PRINTF <text> "Move reaction tubing to the water only waste and"
220 PRINTF <text> "PRESS RUN TO CONTINUE"
221 1 HALT
222 PRINTF <text> "Starting 2nd Rinse"
223 ENDIF
224 IF <statement> rinseCount == 3
225 PRINTF <text> "Starting 3rd (and final) Rinse"
226 ASSIGN <varName> = <int or float> rinseCount, 0 // Reset rinse count
227 ENDIF
228
229 // Rinse syringes with water
230 PRINTF <text> "This is one rinse happening"
231
232 1 SET speed = <float> rAsp * 2
233 2 SET speed = <float> laAsp
234 3 SET speed = <float> lbAsp
235 4 SET speed = <float> auAsp
236
237 1 VALVE_PORT = <int> [CCW] water, CCW
238 2 VALVE_PORT = <int> [CCW] water, CCW
239 3 VALVE_PORT = <int> [CCW] water, CCW
240 4 VALVE_PORT = <int> [CCW] water, CCW
241
242 2 ASPIRATE <float> [IMM or SYNC] laSize * lamL, IMM
243 IF <statement> lbPer != 0
244 3 ASPIRATE <float> [IMM or SYNC] lbSize * lbmL, IMM
245 ENDIF
246 4 ASPIRATE <float> [IMM or SYNC] auSize * aumL, IMM
247 1 ASPIRATE <float> [IMM or SYNC] rFillSteps + rmL
248
249 1 DELAY <float> 3
250
251 1 SET speed = <float> rDisp
252 2 SET speed = <float> maxAsp
253 3 SET speed = <float> maxAsp
254 4 SET speed = <float> auDisp
255
256 1 VALVE_PORT = <int> [CCW] reaction, CCW
257 2 VALVE_PORT = <int> [CCW] reaction, CCW
258 3 VALVE_PORT = <int> [CCW] reaction, CCW
259 4 VALVE_PORT = <int> [CCW] reaction, CCW
260
261 2 DISPENSE <float> [IMM or SYNC] laSize * lbmL, IMM
262 IF <statement> lbPer != 0
263 3 DISPENSE <float> [IMM or SYNC] lbSize * lbmL
264 ENDIF
265 4 DISPENSE <float> [IMM or SYNC] auSize * aumL, IMM
266 1 DISPENSE <float> [IMM or SYNC] rFillSteps + rmL

```

```
267         1      DELAY <float>    10
268
269         ASSIGN <varName> = <int or float> rinseCount, rinseCount + 1
270
271     //             END OF RINSE LOOP
272     LOOP <int>      3
273
274     //             END OF SYNTHESIS LOOP
275     LOOP <int>      nSynth
276
```

B. SUPPORTING INFORMATION FOR CHAPTER III: PROTECTIVE  
EFFECT OF PEG LIGANDS ON CATIONIC GOLD NANOPARTICLE  
TOXICITY

**AuNP characterization data**

AuNP<sub>31% MEEE</sub> is shown as a representative example of all the AuNP sets. The data was generally consistent between AuNP sets, with the exception of the UV-Vis stability study. AuNP<sub>31% MEEE</sub> had the most significant destabilization over the 5 day assay; the other AuNP sets exhibited minor decreases in absorbance but to a lesser extent than the shown example.

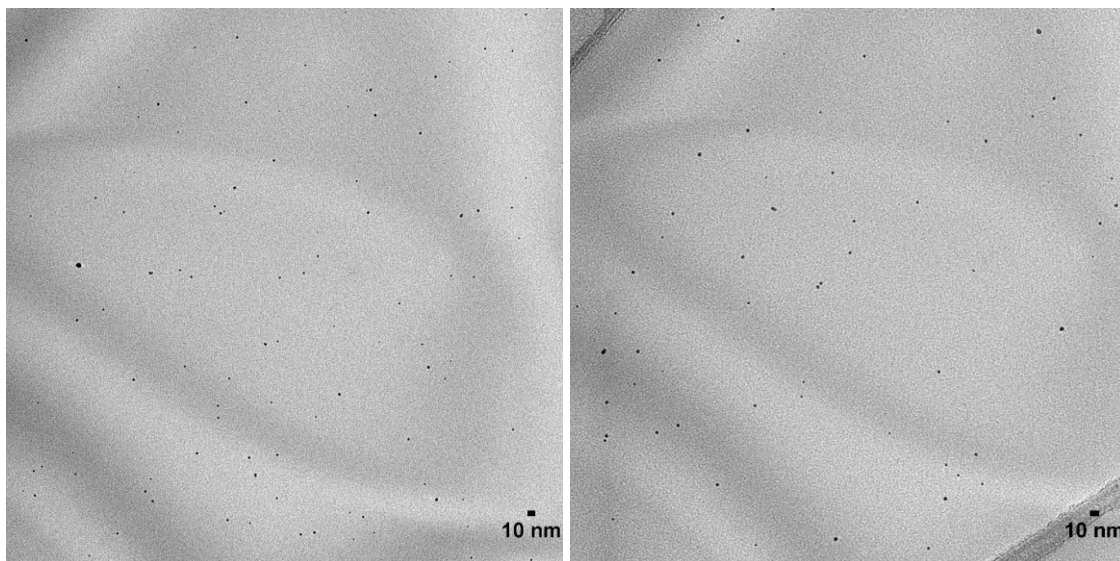


**Figure B1. TEM images showing spherical AuNP<sub>31% MEEE</sub> morphology.**

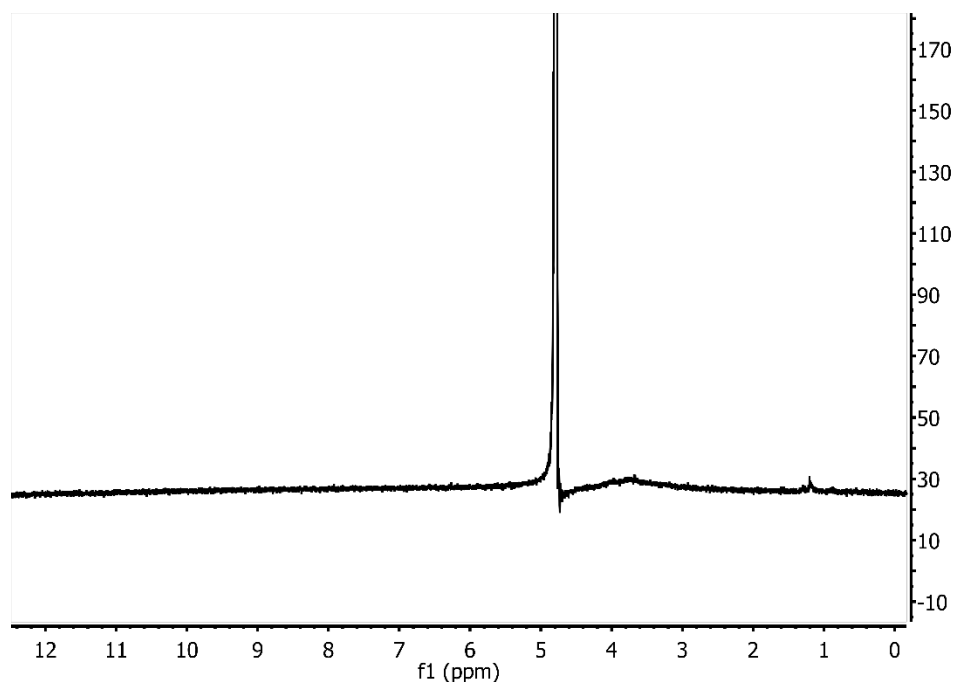


**Figure B2.  $^1\text{H-NMR}$  spectrum of  $\text{AuNP}_{31\% \text{ MEEE}}$  indicating successful column purification.**

The peak at 4.79 ppm is due to residual protonated water in the  $\text{D}_2\text{O}$  solvent. The broad signal at 3.8 ppm corresponds to the AuNP ligands which are characteristically broadened due to their slow molecular tumbling when attached to the NP surface.<sup>1</sup>

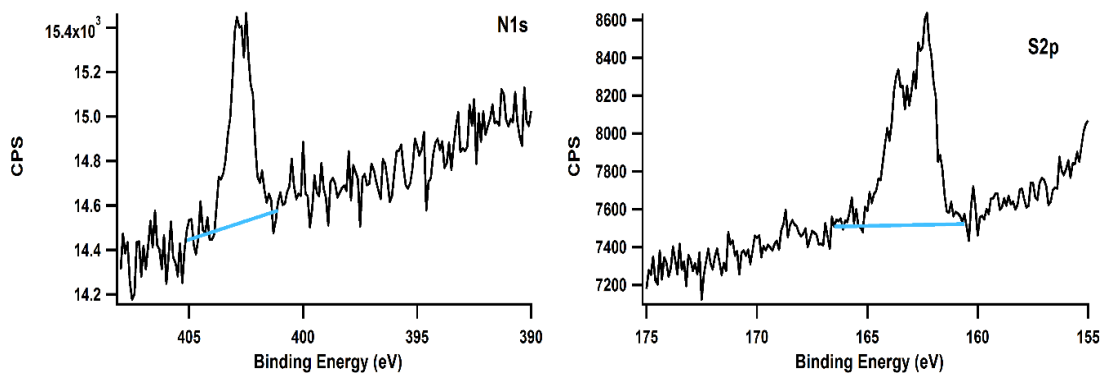


**Figure B3. XPS spectra (black trace) and background subtractions (blue trace) of  $\text{AuNP}_{31\% \text{ MEEE}}$  on boron doped diamond.**

The accuracy of these background subtractions was validated using free TMAT ligand. All backgrounds were set to be linear and peak fitting was not used.

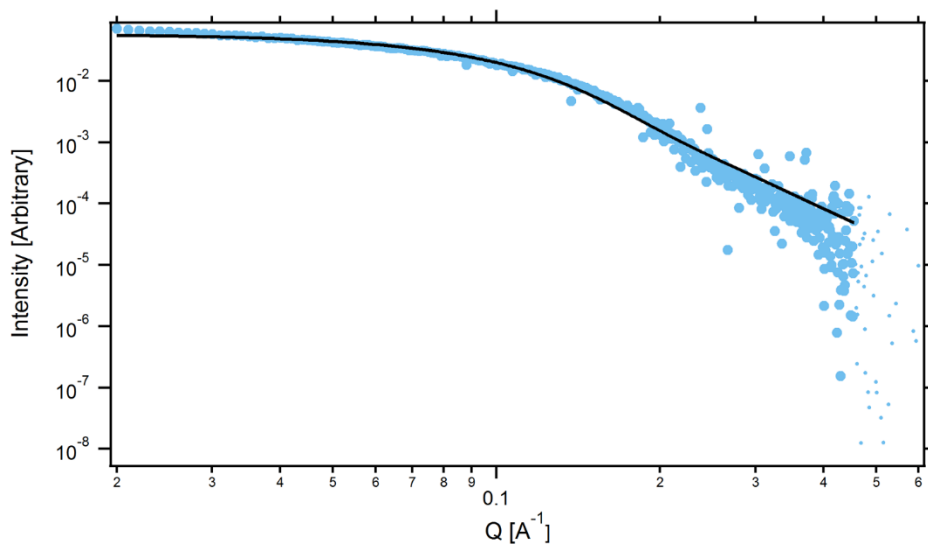


**Figure B4. Small-angle X-ray scattering pattern of AuNP<sub>31%</sub> MEEE.**  
 The fitted data (black trace) is mapped on top of the raw data (blue dots) to determine a core size of 3.7 $\pm$  1.1 nm.

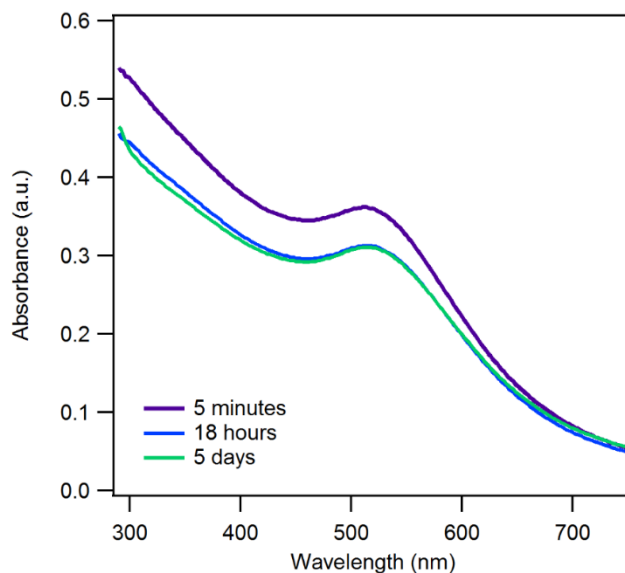


**Figure B5. UV-Vis stability study of AuNP<sub>31%</sub> MEEE at 50 ppm.**  
 Even at the highest AuNP concentration the majority of the particles remain dispersed in solution over the 5 day toxicity assay.

## Toxicity Results

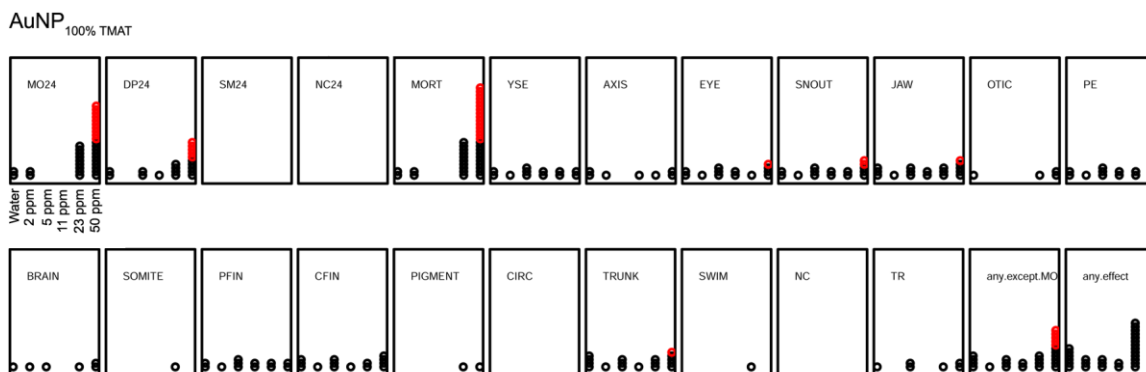


**Figure B6. Developmental effects caused by AuNP<sub>100% TMAT</sub>.**

All endpoints studied are shown here including morphological malformations and mortality. Red signifies a statistically significant response.

Key to endpoints: Mortality (MO24), developmental progress delayed (DP24), Spontaneous Movement: absent tail flexions by visual check (SM24) and deformities in the notochord (NC24) at 24 hpf. At 120 hpf, Mortality (MORT), excess fluid accumulation around yolk sac (YSE), body axis curvature (AXIS), abnormal eye placement or size (EYE), visibly malformed snout (SNOUT), jaw (JAW), ear malformed (OTIC), excessive fluid accumulation around pericardial edema (PE), absent or malformed brain (BRAIN), abnormal trunk muscle organization (SOMITE), under developed or malformed caudal fin (CFIN), hyper- or hypo-developmental of melanocytes (PIGMENT), visibly slower/faster or less developed circulation (CIRC), body length shorter than normal (TRUNK), not present or not inflated swim bladder (SWIM), curvy or otherwise abnormal notochord (NC), gentle touch of head or tail region fails to elicit an escape response (TR). Summary of all endpoints without mortality (any.except.MO), and any effects observed at each concentration (any.effect).

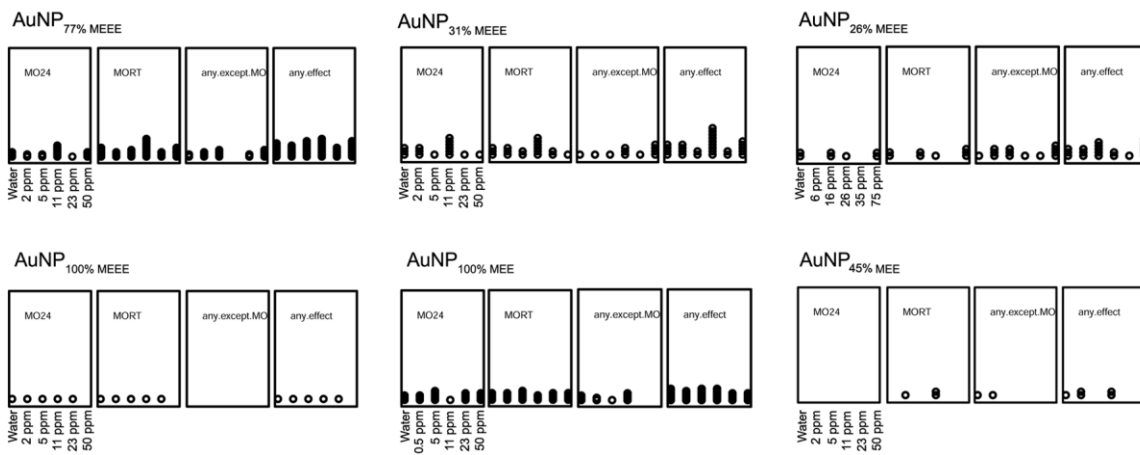


**Figure B7. Developmental effects caused by mixed-ligand MEEE/TMAT-AuNPs ( $\text{AuNP}_{X\% \text{ MEEE}}$ ), MEE(E)-AuNPs ( $\text{AuNP}_{100\% \text{ MEE(E)}}$ ), and MEE/TMAT-AuNPs ( $\text{AuNP}_{45\% \text{ MEE}}$ ).**

The four endpoints shown for each AuNP set are a summary of the 22 endpoints examined in total. “Any except MO” and “any effect” are summations of morphological, and morphological + mortality data, respectively. There are no statistically significant adverse effects observed.

### Analysis of AuNPs with BSA

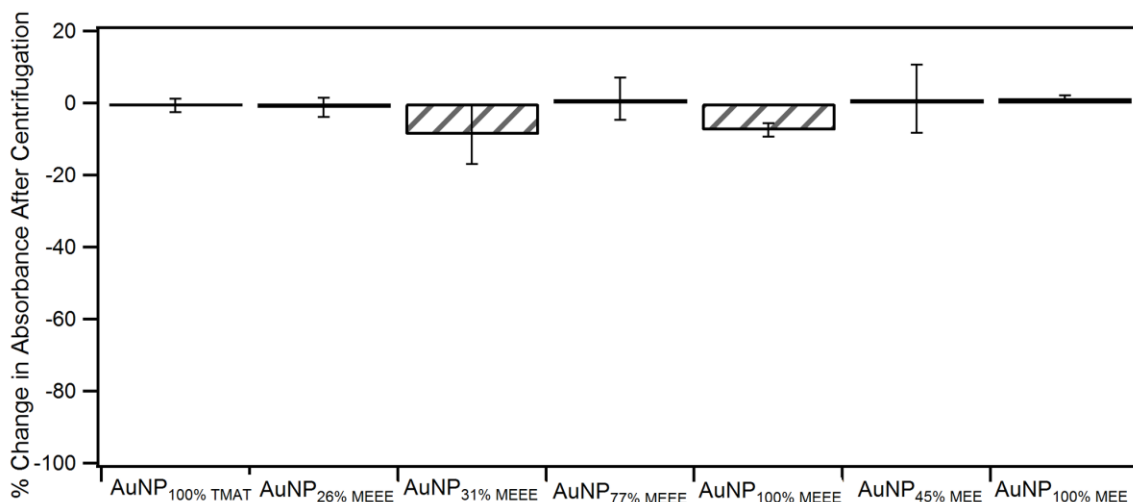


**Figure B8. Control of centrifuged AuNPs without BSA.**

Only minor differences are observed in AuNP stability after centrifuging with NaCl. This indicates that the sedimentation observed with BSA (Figure 3.4) is significantly different than the sedimentation observed just due to centrifugation under these conditions.

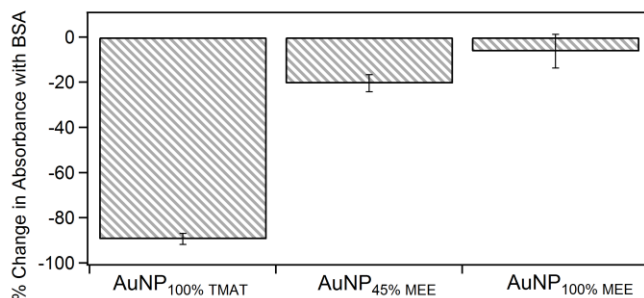


**Figure B9. Extent of BSA/AuNP Aggregation for AuNPs with shortened PEG chains.**

Error bars represent the range of three triplicate measurements.

C. SUPPORTING INFORMATION FOR CHAPTER IV: SYNERGISTIC TOXICITY  
 PRODUCED BY MIXTURES OF BIOCOMPATIBLE GOLD NANOPARTICLES  
 AND WIDELY USED SURFACTANTS

**Table C1. Definition of particle notation and corresponding core sizes determined by SAXS.**

AuNPs Used in Toxicity Assays	Measured core diameter (nm)
AuNP <sub>1.0 nm</sub> <sup>a</sup>	1.0 ± 0.8 <sup>a</sup>
AuNP <sub>2.8 nm</sub> <sup>b</sup>	2.8 ± 0.5 <sup>b</sup>
AuNP <sub>3.1 nm</sub> <sup>b</sup>	3.1 ± 0.5 <sup>b</sup>
AuNP <sub>3.6 nm</sub> <sup>b</sup>	3.6 ± 0.5 <sup>b</sup>
AuNP <sub>3.9 nm</sub> <sup>b</sup>	3.9 ± 0.5 <sup>b</sup>

<sup>a</sup>AuNPs were synthesized *via* ligand exchange of thiols with triphenylphosphine-passivated AuNPs as described in the manuscript. <sup>b</sup>AuNPs were synthesized directly in a flow reactor by gold salt reduction in the presence of masked thiol ligands. The method has been previously described in detail.<sup>1</sup>

**Toxicity assay set-up and representative results for all AuNP sizes**

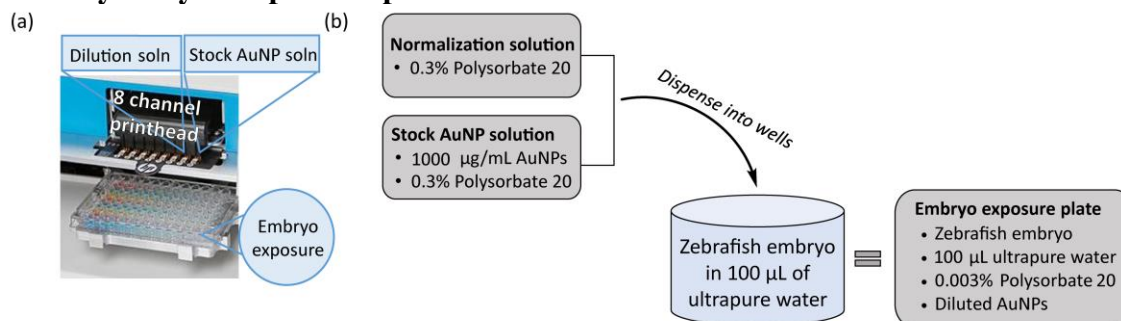


**Figure C1. Assay Set-up.**

(a) Picture of the BioPrinter set-up. (b) Schematic of the order of reagent dispersal with the Bioprinter method. In the Bioprinter, the concentrated stock solution of AuNPs contains surfactant in order to break surface tension in the dispersal syringe. Since the concentration of AuNPs varies between zebrafish wells, a second stock solution, containing only PS20 is also used to ensure that all wells contain 0.003% PS20.

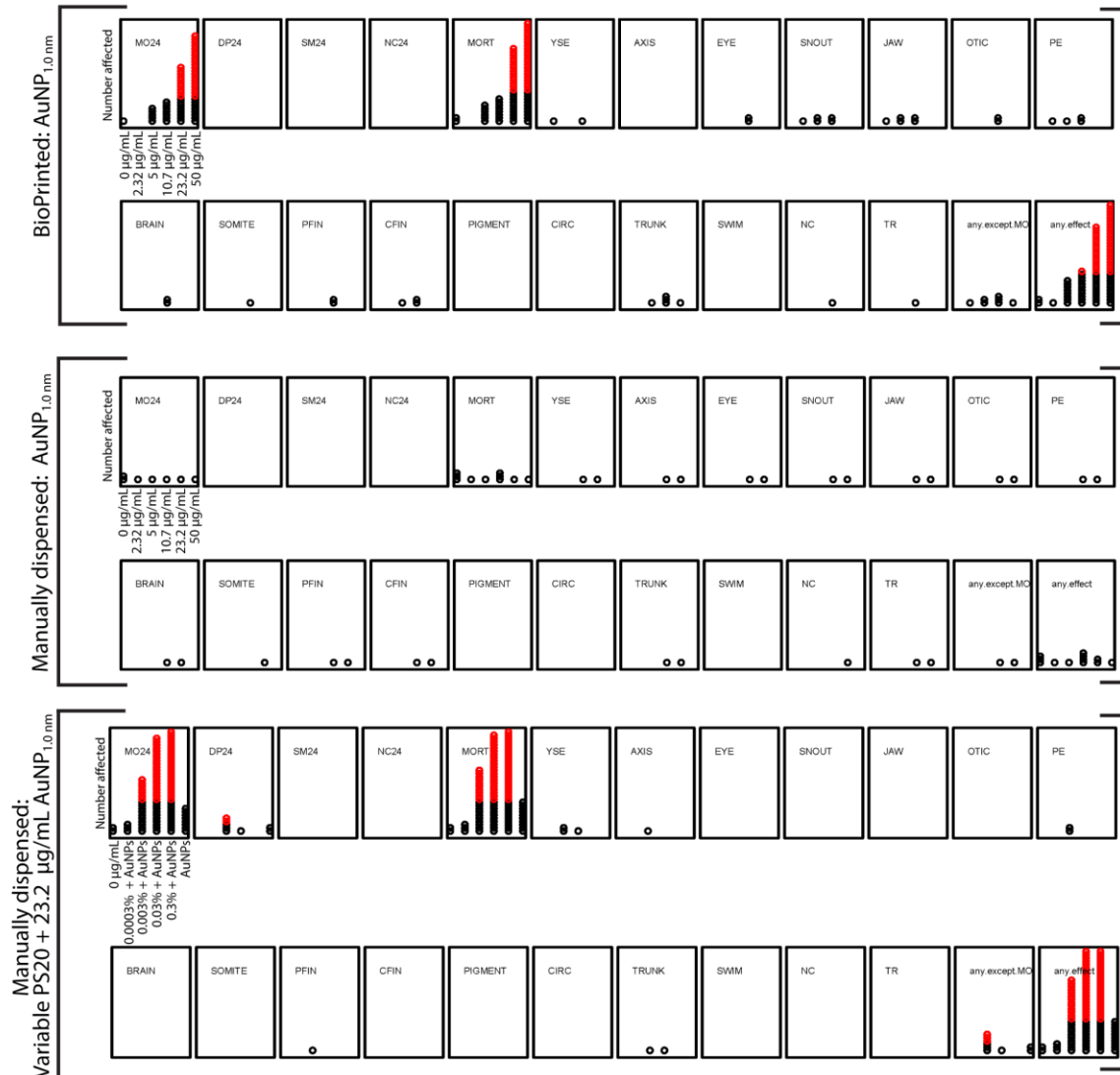


**Figure C2. Representative results of the entire set of endpoints examined for all toxicity assays.**

In this case, BioPrinted AuNPs contain 0.003% PS20 and are toxic, and manually dispensed AuNPs are non-toxic until PS20 is added. PS20 is non-toxic by itself until 0.3% (see Figure S11).

Key to endpoints: Mortality (MO24), developmental progress delayed (DP24), Spontaneous Movement: absent tail flexions by visual check (SM24) and deformities in the notochord (NC24) at 24 hpf. At 120 hpf, Mortality (MORT), excess fluid accumulation around yolk sac (YSE), body axis curvature (AXIS), abnormal eye placement or size (EYE), visibly malformed snout (SNOUT), jaw (JAW), ear malformed (OTIC), excessive fluid accumulation around pericardial edema (PE), absent or malformed brain (BRAIN), abnormal trunk muscle organization (SOMITE), under developed or malformed caudal fin (CFIN), hyper- or hypo-developmental of melanocytes (PIGMENT), visibly slower/faster or less developed circulation (CIRC), body length shorter than normal (TRUNK), not present or not inflated swim bladder (SWIM), curvy or otherwise abnormal notochord (NC), gentle touch of head or tail

region fails to elicit an escape response (TR). Summary of all endpoints without mortality (any.excep.MO), and any effects observed at each concentration (any.effect).

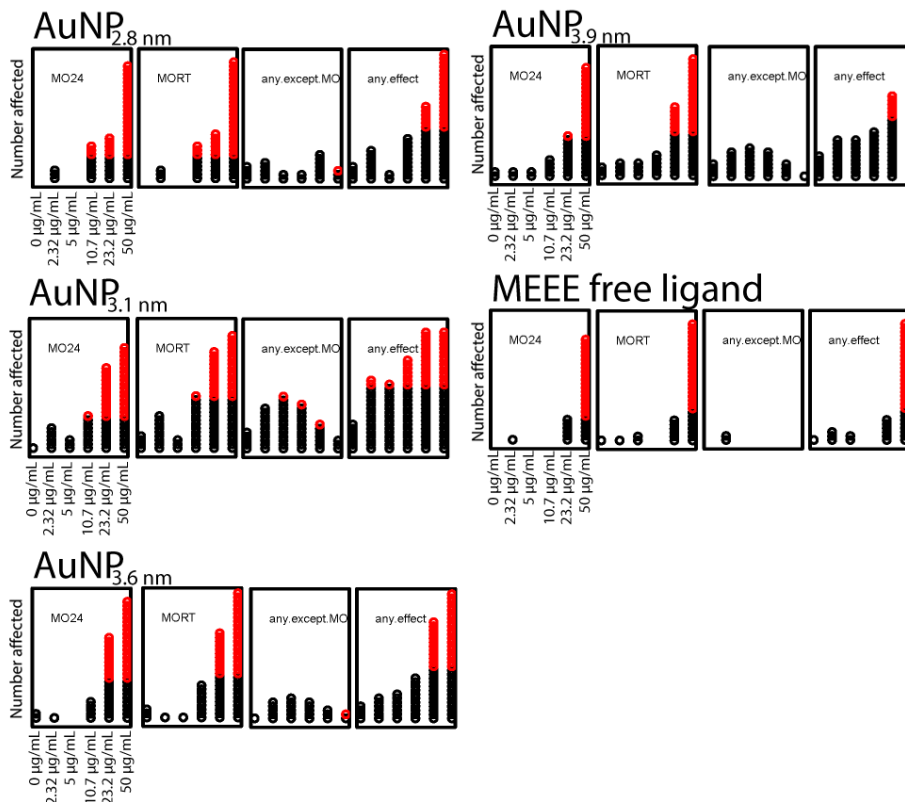


**Figure C3. Summary of zebrafish developmental endpoints in the presence of each size of AuNPs, and the free ligand, when dispensed with the BioPrinter.**

All samples contain 0.003% PS20 because they were dispensed using the BioPrinter. These endpoints are selected as representative data because they encompass all acute (MO24) and chronic effects [both lethal (MORT) and non-lethal (any.except.MO)] studied. All AuNP sizes cause mortality using this dispensing method, with the smaller NPs tending to be the most toxic. Note that 50 µg/mL of MEEE-AuNPs only contains 4-15 µg/mL of MEEE ligand (varies by NP size).

## Characterization of AuNPs in solution with PS20

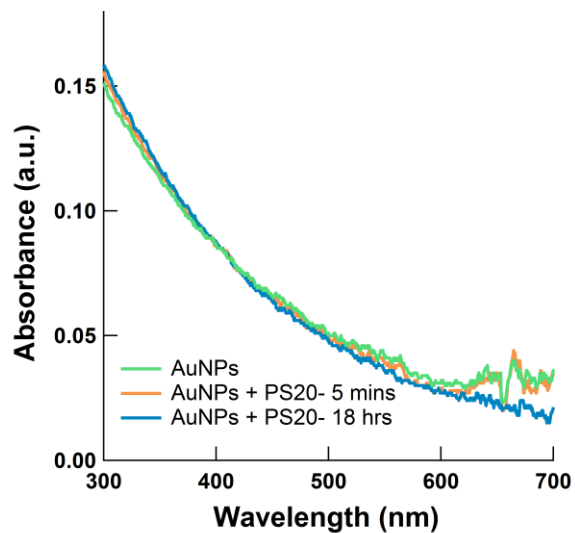


**Figure C4. UV-Vis measurements demonstrating the stability of the smallest AuNPs.** (AuNP<sub>1.0 nm</sub>, 50  $\mu\text{g}/\text{mL}$ ), in the presence of PS20, in water. There is no change in the absorbance over 18 hours, indicating AuNPs remain in solution and the average core size is constant.

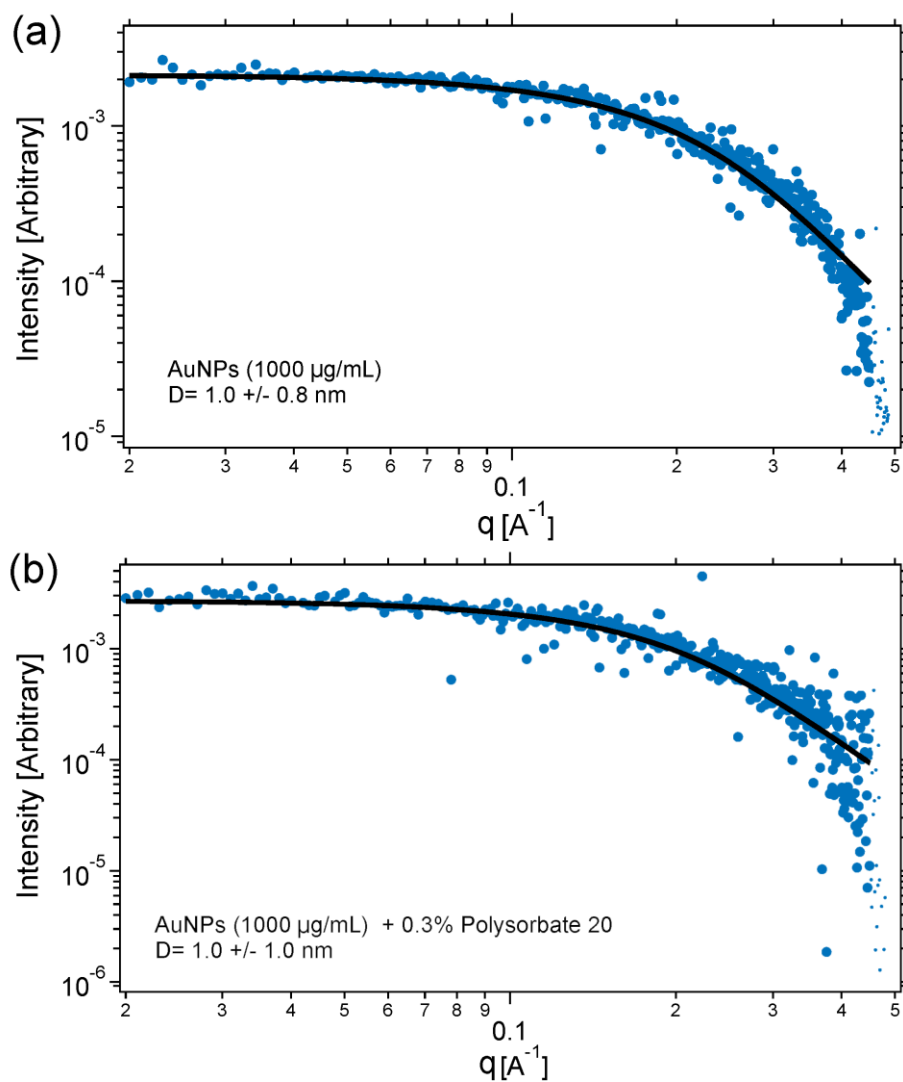


**Figure C5. SAXS of smallest AuNPs (AuNP<sub>1.0 nm</sub>) in (a) water and (b) with PS20 after 18 hours.**

The blue points represent the scattering data and the solid black line is the fit to the modeled size of these particles. The data suggest that addition of PS20 does not change the average core size or lead to multiple size populations.

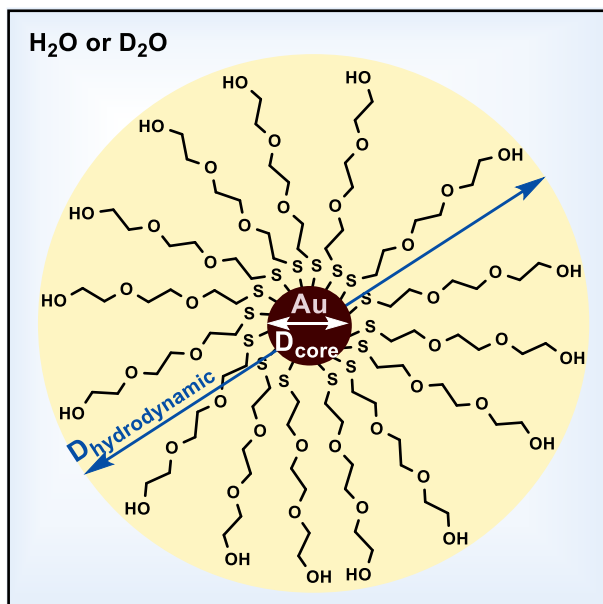


**Figure C6. Structure of MEEE-AuNPs differentiating the core size ( $D_{\text{core}}$ ) from the solvation size ( $D_h$ ).**

## **NMR processing information, supplemental spectra and calculations**

### Processing the DOSY spectra in MestReNova

When processing data acquired on a Bruker NMR within MestReNova software, some of the metadata can be imported incorrectly and must be checked and adjusted. The “arrayed data” subwindow needs to be set to accurately reflect the nucleus observed, the instrument unit output, and the probe employed.  $\Delta$  and  $\delta$  were verified (0.1 and 0.0034 s, respectively),  $k$  (the gradient calibration number) was changed to 6.57, to be consistent with the probe used,  $\gamma$  (the gyromagnetic ratio) was set to 4257.7 because we are observing a  $^1\text{H}$  nucleus and MestReNova requires  $\gamma$  in  $\text{G}^{-1}\text{s}^{-1}$ . The  $G'$  field was set to “ $G*k*100$ ” to convert the metadata to the correct units of  $\text{G}^{-1}\text{s}^{-1}$  because the data collected on a Bruker imports in  $\text{MHzT}^{-1}$ . The spectra were referenced to residual HDO ( $\delta = 4.79$  ppm) and had manual phase adjustments. The phase adjustments were performed to improve aesthetics and typically caused around 0.02 nm difference in the

$D_h$ . The spectra were plotted in 2D using Bayesian DOSY Transform with the default parameters (resolution factor 1, 1 repetition, 128 points in diffusion dimension). This method of processing DOSY data in MestReNova was first verified by running a mannose standard and obtaining a diffusion coefficient consistent with the known value.

### Supplemental NMR spectra

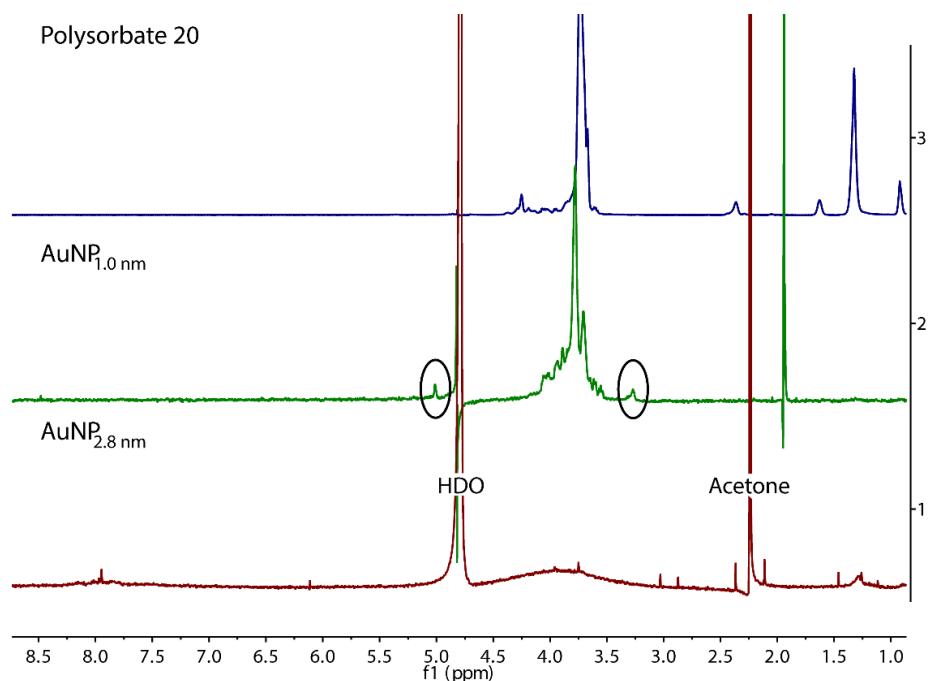


**Figure C7. Comparison of <sup>1</sup>H-NMR spectra of PS20 and the two smallest sizes of AuNPs.**

For the 1.0 nm AuNPs the peaks at 4.97 and 3.24 ppm are well-enough resolved to track the AuNP population without interference from any PS20 signals. The larger AuNPs ( $D_{\text{core}} = 2.8$  nm) have significantly more signal broadening due to the reduced molecular tumbling of the ligands, making it impossible to track AuNP specific peaks.<sup>2</sup>

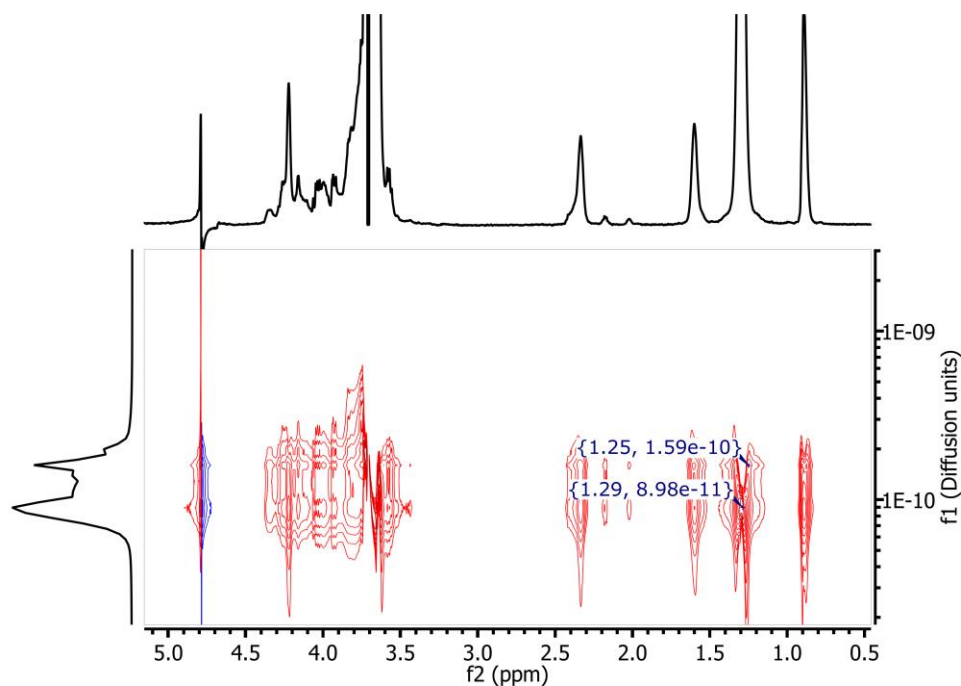


**Figure C8. 2D spectrum of PS20 (0.3%) in D<sub>2</sub>O.**

At this concentration, two size populations exist for PS20, 3.1 nm and 5.4 nm in diameter. It should be noted that DOSY experimental parameters were the same as those used to measure AuNP diffusion. These parameters are therefore not optimal for measuring the full PS20 decay curve, but reflect the diffusion spectrum expected for PS20 in our studies containing AuNPs.

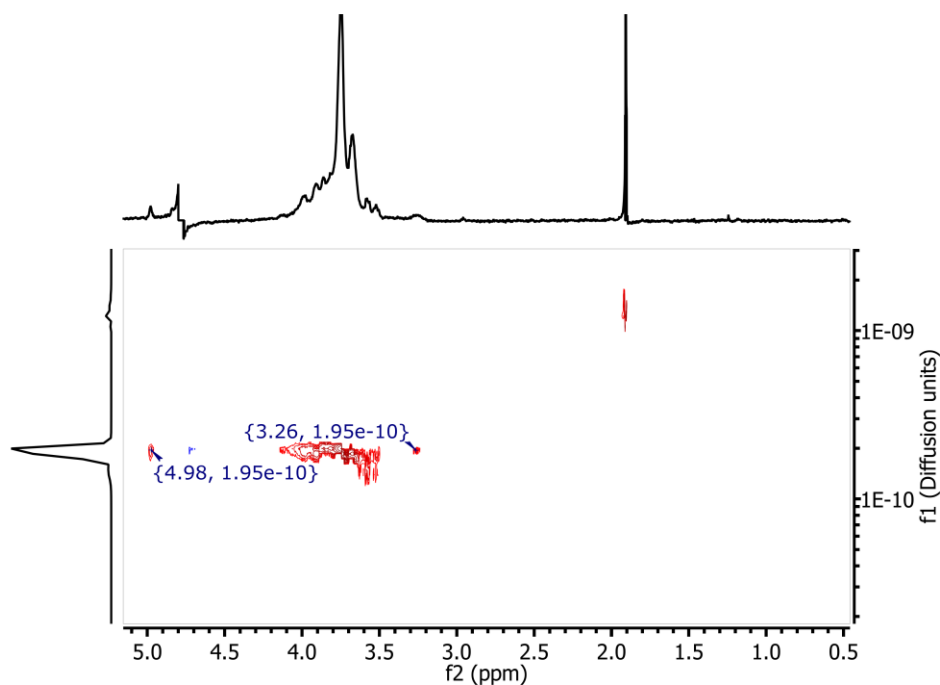


**Figure C9. 2D spectrum of AuNPs before 0.3% PS20 is added.**

The spectrum shows that in the absence of PS20 only one population of AuNP sizes exist.

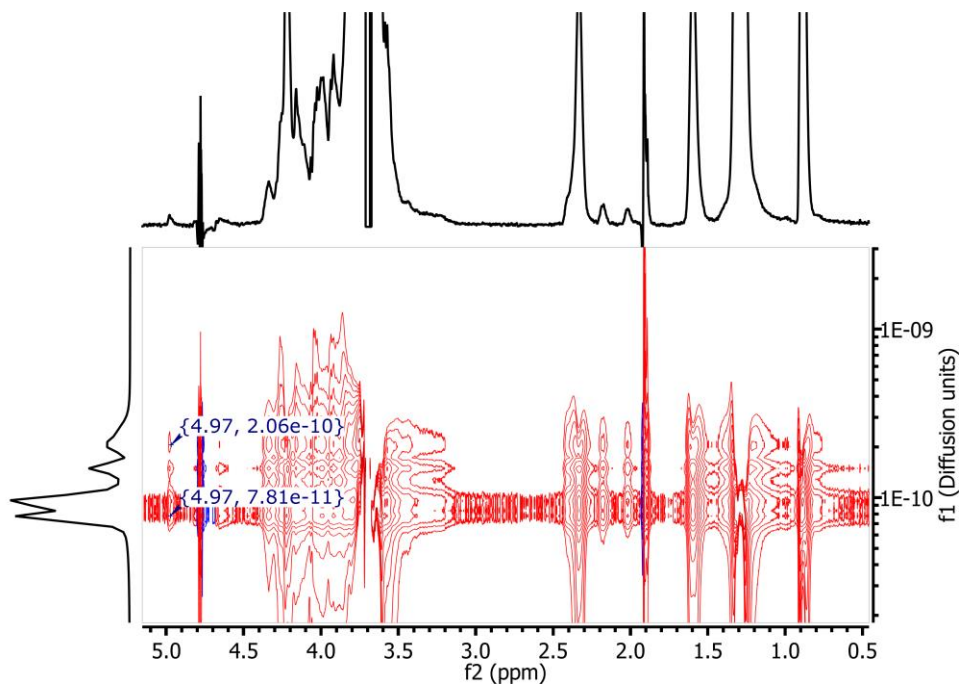


**Figure C10. 2D spectrum of AuNPs + PS20 (0.3%) after 30 mins.**

The spectrum shows that the diffusing species are not representative of PS20 or AuNPs alone, rather, they are assemblies of the two species.

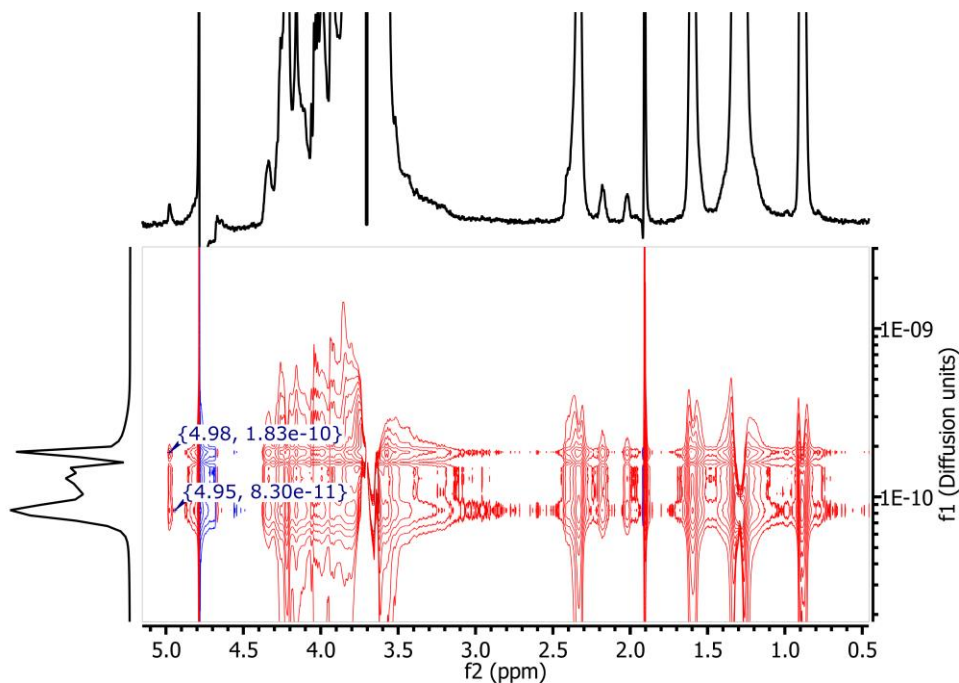


**Figure C11. 2D spectrum of AuNPs + PS20 (0.3%) after 2 hours.**

The assembly process is dynamic between 30 mins and 2 hours, as evidenced by the difference in the distribution of populations and diffusion coefficients.

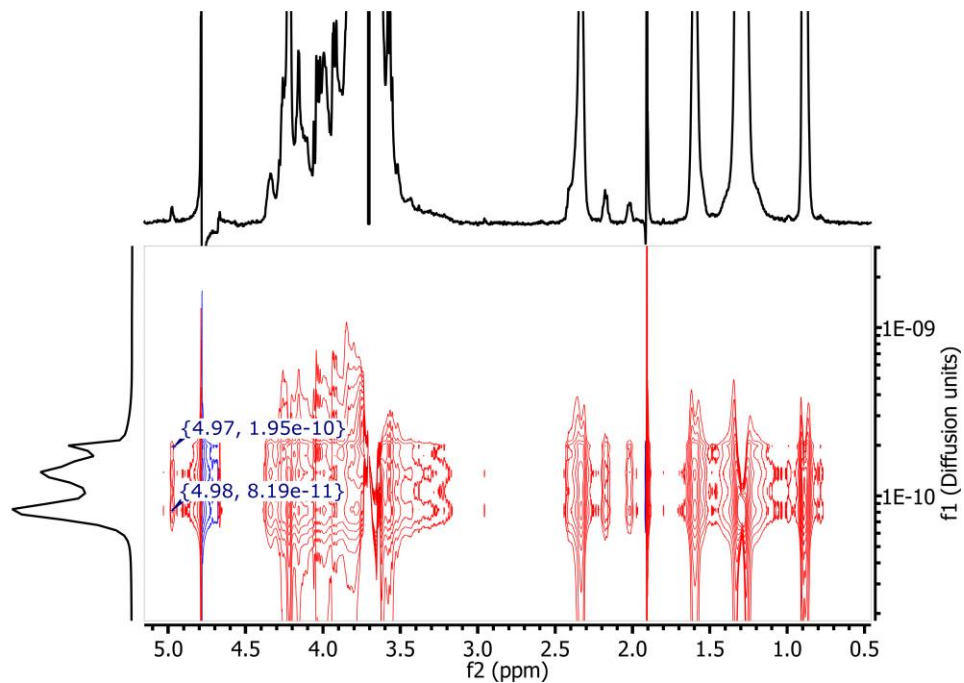


**Figure C12. 2D spectrum of AuNPs + PS20 (0.3%) after 13 hours.**  
The assemblies are similar in size and distribution to the 2 hour timepoint.

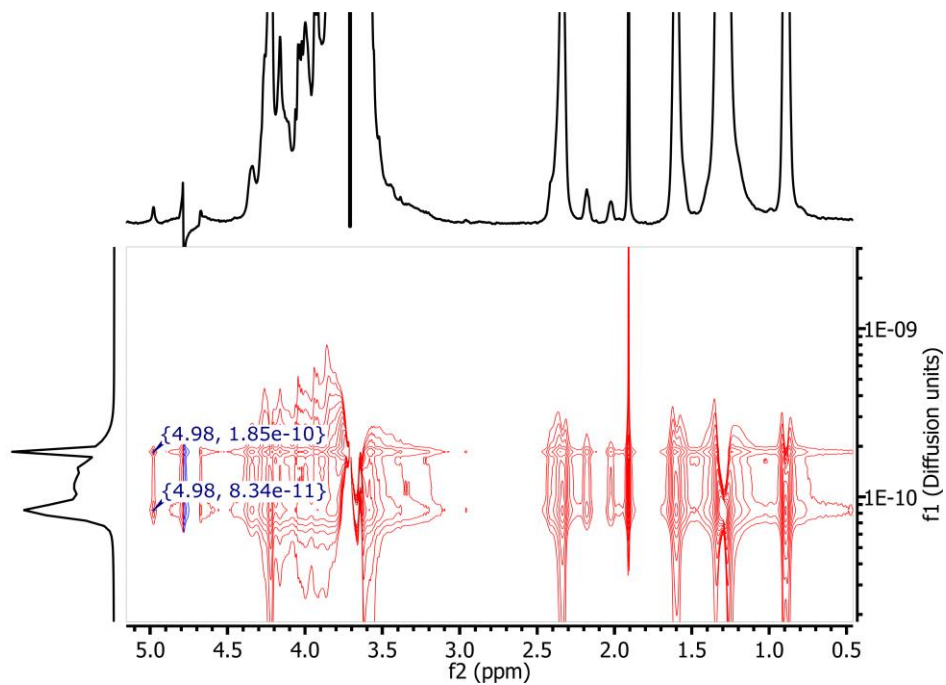


**Figure C13. 2D spectrum of AuNPs + PS20 (0.3%) after 18 hours.**  
Comparing this spectrum to the other timepoints shows that over 18 hours most of the change in solution composition occurs within the first 2 hours of mixing.

### **Consideration of variation between mixture viscosities and temperatures**

It is important to consider that the Stokes-Einstein equation includes viscosity as one of the parameters that affect particle radius. We verified, both experimentally and theoretically, that  $D_h$  measurements were not influenced by changes to the mixture viscosity due to the addition of PS20. The Refutas equation<sup>3</sup> provides a method for estimating a binary mixture's viscosity, which can then be related back to the  $D_h$  via the Stokes-Einstein equation. At a 0.3% concentration of PS20 the expected mixture viscosity is 0.000902 N-s/m<sup>2</sup> as compared to 0.000894 N-s/m<sup>2</sup> for pure water. Employing the Stokes-Einstein equation, this change in viscosity corresponds to less than a 0.02 nm decrease in  $D_h$ . A DOSY spectrum of mannose was collected in D<sub>2</sub>O, then again after the addition of 0.3% PS20. The measured  $D_h$  decreased by 0.09 nm. Both 0.09 and 0.02 nm are within our reported experimental variation of  $D_h$  (0.1 nm), as determined by triplicate experiments. Therefore, under the conditions used within this study, differences between mixture viscosities have a negligible impact on reported  $D_h$  values.

Variations in temperature could also affect the measured values of  $D_h$ . The probe temperature was maintained at 25 °C throughout these experiments. Even a temperature variation of 5 °C would only result in a 0.05 nm difference in  $D_h$ . Therefore, minor differences in temperature are not a concern for this work.

### **Calculation of size of AuNPs containing a complete monolayer of PS20**

There are several ways to calculate the theoretical size of MEEE-AuNPs with a full monolayer of PS20. Using distances obtained computationally it is possible to predict the expected size for a monolayer of fully extended PS20. We employed Spartan 10 to determine the range of molecule lengths (a range occurs because of the variable

distribution of w,x,y and z units within PS20). By adding the shortest and longest lengths of PS20 to the size of the MEEE-AuNPs we know that the  $D_h$  should range between 7.2 and 15.9 nm for a fully extended monolayer of PS20 on MEEE-AuNPs. Another way of calculating the expected size of a PS20 monolayer is to assume that the monolayer contains aggregates of surfactant equivalent in size to the populations observed in the absence of AuNPs (Figure S5). This method reveals that a monolayer of PS20 aggregates around an MEEE-AuNP would result in a maximum  $D_h$  around 13.3 nm, corresponding to the NPs alone (2.5 nm) plus the size of the larger PS20 population (5.4 nm x 2), and a minimum  $D_h$  of 8.7 nm. Since the maximum AuNP size observed with the DOSY studies was 6.3 nm, it is unlikely that PS20 forms a complete monolayer; instead, it likely interdigitates into the MEEE shell or forms a partial monolayer.

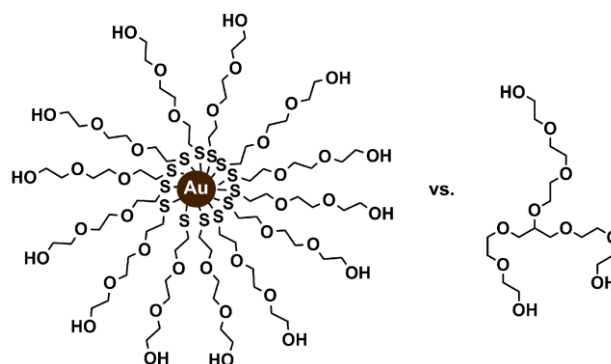


**Figure C14. Structural comparison of MEEE-AuNPs to polyethylene glycol dendrimers.**

## Structural information on dendrimers and representative toxicity data

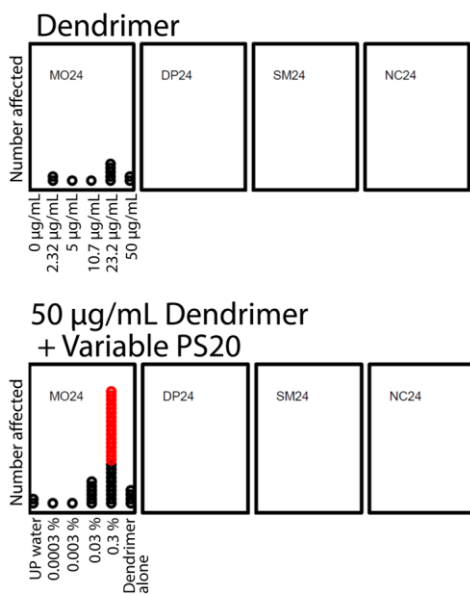


**Figure C15. Summary of zebrafish developmental endpoints in the presence of a PEG dendrimer and PS20/dendrimer mixtures.**

The dendrimer, a metal-free structure with approximately the same dimensions and surface chemistry as MEEE-AuNPs, does not cause a synergistic toxicity in the presence of PS20.

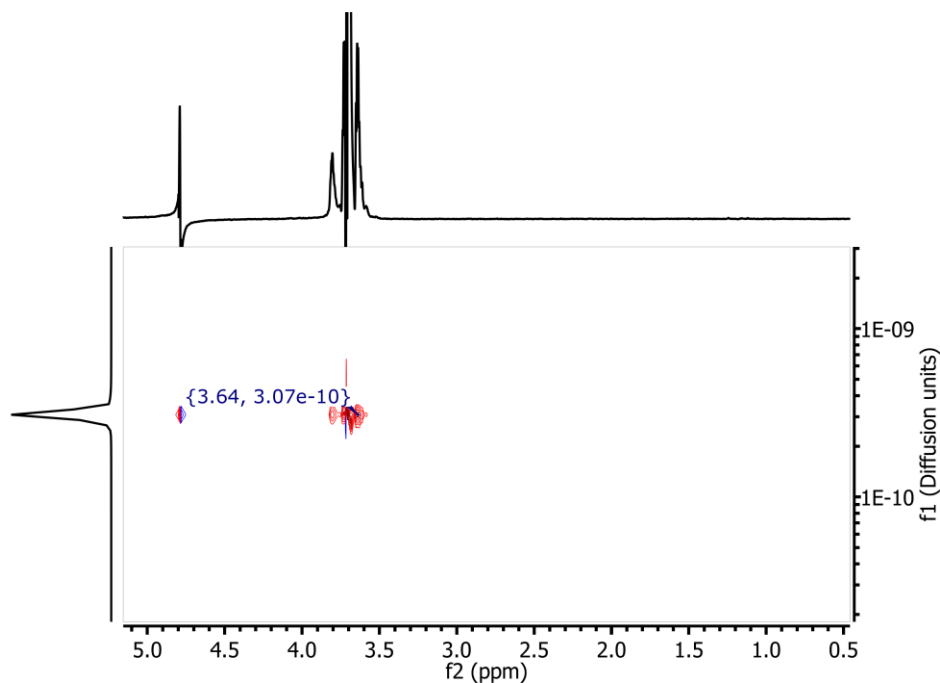


**Figure C16. 2D spectrum of dendrimers alone in D<sub>2</sub>O; dendrimers are 1.6 nm in hydrodynamic diameter at 1000 µg/mL.**

Dendrimer size was also measured at more dilute concentrations that reflect the range used for toxicity assays, and under those conditions the diameter was measured as 1.5 nm.

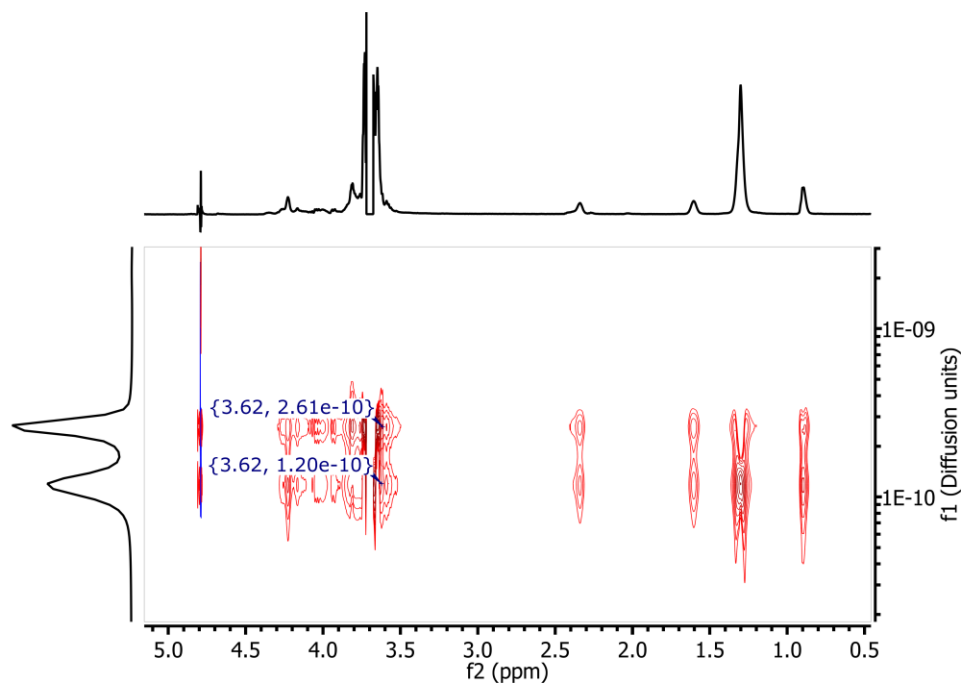


**Figure C17. 2D spectrum of dendrimers (1000 µg/mL) + PS20 (0.3%) after 30 minutes.**

Although the proton signals from PS20 overlap with the dendrimer proton signals, the diffusion signals (vertical axis peaks) show that the initial 1.6 nm population is gone. The diffusion populations do not represent either the dendrimers or the PS20 alone. Therefore, there is evidence of dendrimer/PS20 assembly formation. These assemblies are 1.9 nm and 4.1 nm in diameter. \*Similar results were obtained using the dilute samples of dendrimer. The concentrated result is shown because the ratio of dendrimer to PS20 is sufficiently high that diffusion signals for the dendrimers alone should still appear if assemblies were not forming.

## Representative toxicity data from various surfactant mixtures

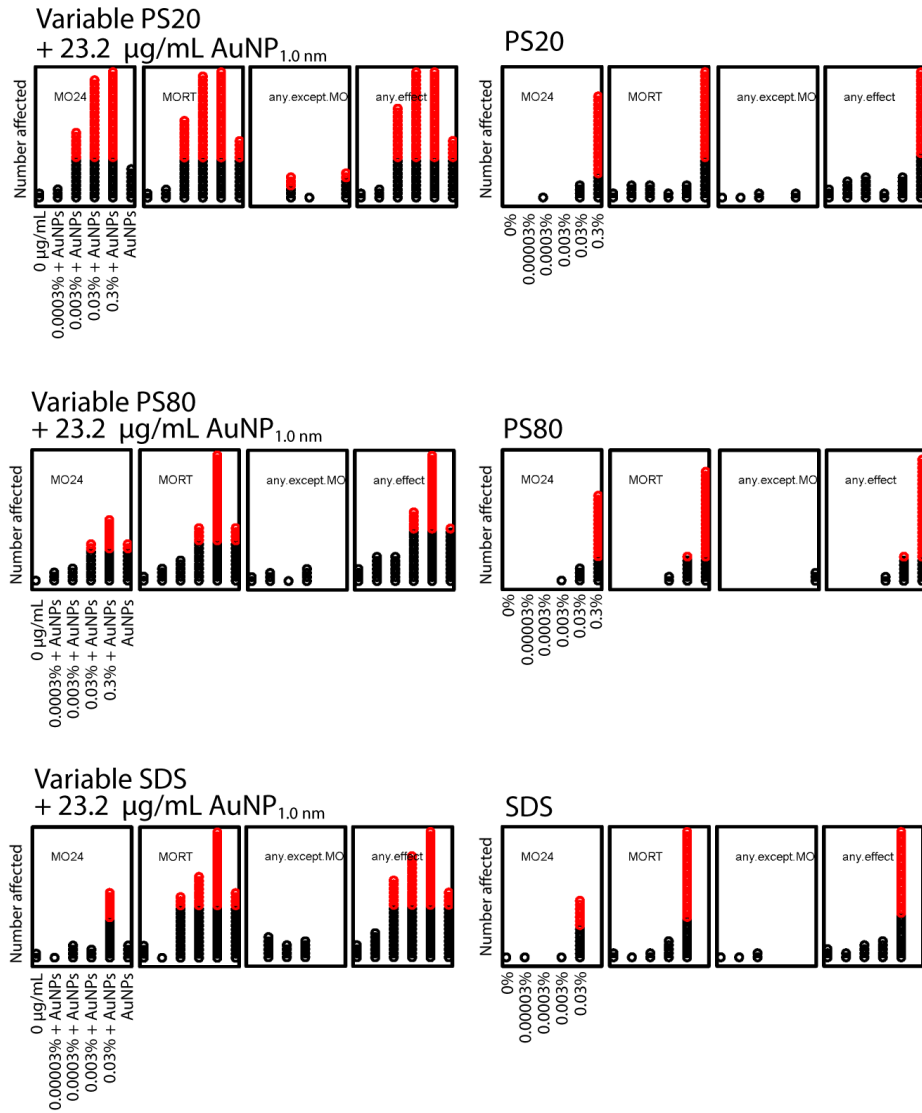


**Figure C18. Summary of zebrafish developmental endpoints in the presence of various surfactants, and the corresponding surfactant/AuNP mixtures.** All surfactant/AuNP mixtures demonstrate a synergistic toxicity by the end of the assay, although to varying extents and on different timeframes.

## TEM images of AuNPs

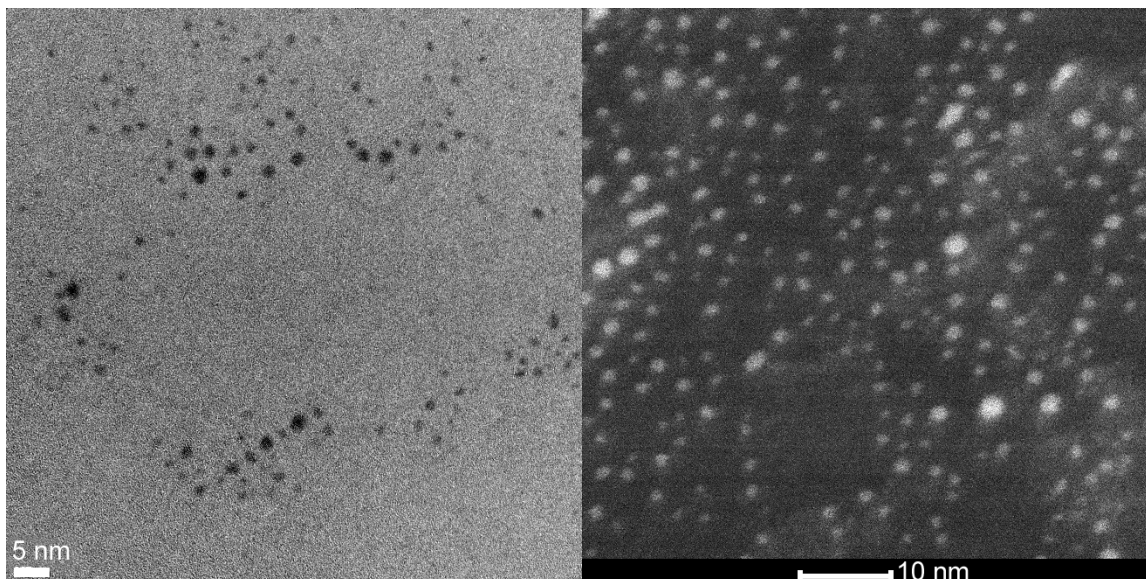


**Figure C19. Bright-field and dark-field TEM images of AuNPs corroborating the 1.0 nm core size.**

The smaller spheres are consistent with the size of the single NP population observed by SAXS, the larger spheres are an agglomeration of NPs due to drying effects.

D. SUPPORTING INFORMATION FOR CHAPTER V: ZINC OXIDE  
INDUCED CHANGES TO SUNSCREEN EFFICACY AND TOXICITY  
UNDER UV IRRADIATION

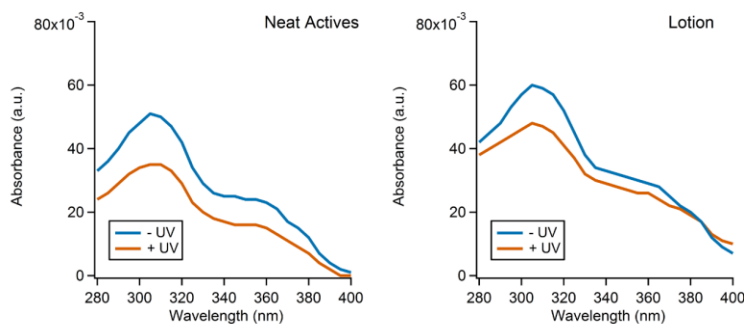


**Figure D1. UV-Vis spectra of a moderately stable sun filter mixture formulated with just neat actives in DMSO versus actives into a lotion.**

The neat actives spectrum is measured in 99:1 IPA/DMSO and the lotion spectrum is measured in 99:1 Water/DMSO. Both mixtures were exposed to UV irradiation for 2 hrs and the lotion film was dissolved into DMSO following exposure. The results are comparable, suggesting that exposure in DMSO and measurement in IPA is an informative and simple way of simplifying the testing of sun lotion stability.

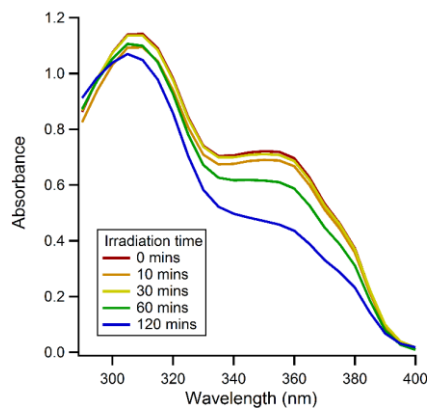


**Figure D2. Irradiation of a moderately stable sun filter mixture over 2 hrs.**

Measured in 99:1 IPA/DMSO. The data show that photodegradation begins within 30 mins and continues occurring throughout the 2 exposure hr window.

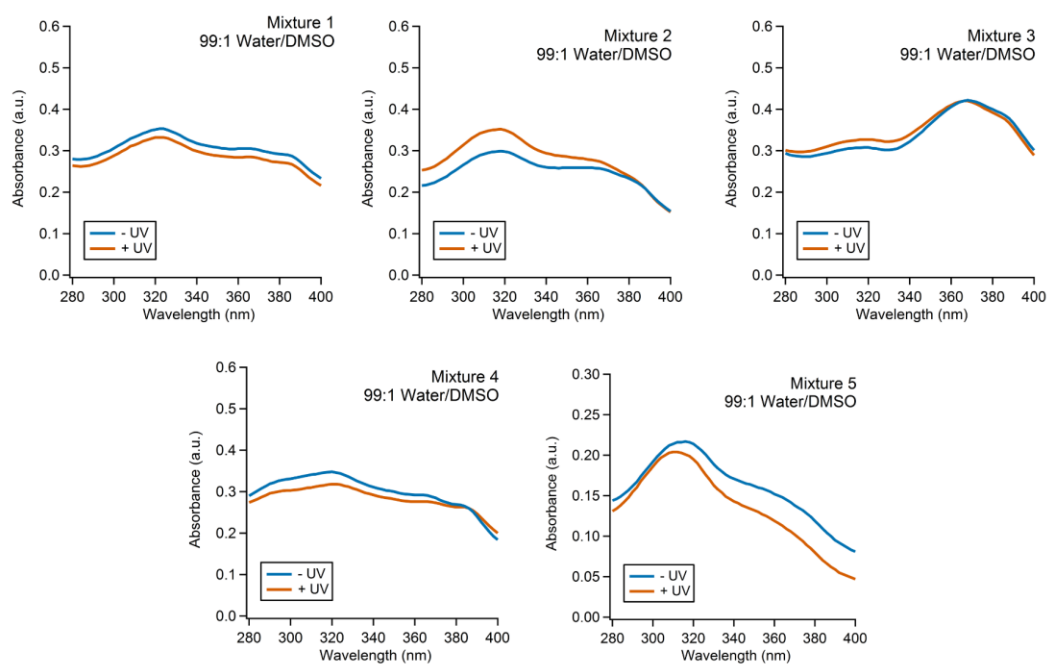


**Figure D3. UV-Vis spectra showing photodegradation of Mixtures 1-5. Measured in 99:1 Water/DMSO.**

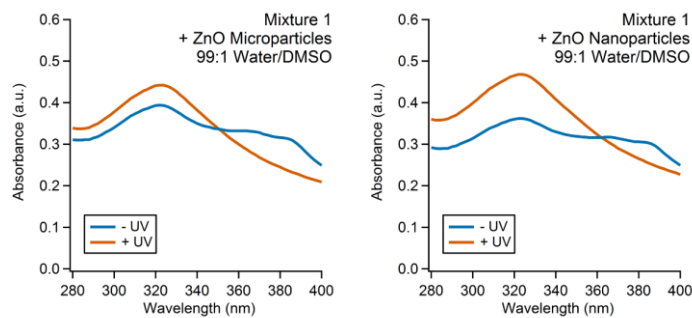


**Figure D4. UV-Vis spectra showing photodegradation of Mixtures 1 + ZnO. Measured in 99:1 Water/DMSO.**

**Table D1. Concentrations used for *in vivo* toxicity testing**

<b>Sample name</b>	<b>Final concentration (%organic filters)</b>	<b>Final concentration (%ZnO)</b>
Mixture 1 - UV	0.0014	0.0000
Mixture 1 + UV	0.0014	0.0000
Mixture 2 - UV	0.0015	0.0000
Mixture 2 + UV	0.0015	0.0000
Mixture 3 - UV	0.0030	0.0000
Mixture 3 + UV	0.0030	0.0000
Mixture 4 - UV	0.0015	0.0000
Mixture 4 + UV	0.0015	0.0000
Mixture 5 - UV	0.0015	0.0000
Mixture 5 + UV	0.0015	0.0000
DMSO with UV	0.0000	0.0000
(Mixture 1 + ZnO microparticles) - UV	0.0014	0.0005
(Mixture 1 + ZnO microparticles) + UV	0.0014	0.0005
(Mixture 1 + ZnO nanoparticles) - UV	0.0014	0.0005
(Mixture 1 + ZnO nanoparticles) + UV	0.0014	0.0005
(ZnO microparticles) - UV	0.0000	0.0005
(ZnO microparticles) + UV	0.0000	0.0005
(ZnO nanoparticles) - UV	0.0000	0.0005
(ZnO nanoparticles) + UV	0.0000	0.0005

E. SUPPORTING INFORMATION FOR CHAPTER VI: EXPERIENTIAL  
LEARNING TO PROMOTE SYSTEMS THINKING IN CHEMISTRY:  
EVALUATING AND DESIGNING SUSTAINABLE PRODUCTS IN A  
POLYMER IMMERSION LAB

**Student Feedback**

Although all 19 of the master's class students were familiar with the project and had the opportunity to provide intellectual insights during semiweekly recap meetings, the course is structured to have multiple immersion projects running in parallel. The four students that worked most intimately on the data collection and interpretation for this project provided the feedback below. Feedback was requested *via* email six months after they completed the lab. At the time of the survey, each student was completing a paid internship with an industrial partner.

1. Did your experience on this project contrast with other lab projects you have been part of?

Student #1: "The WAYB project was certainly a unique experience, both personally and compared to the other projects in the course (which is why it was my top choice). The scope of the project encompassed many impactful elements - from product development and engineering, to green chemistry, to marketing and economic analysis. Our team was also given a lot of freedom to construct our own goals and deliverables in conjunction with some of WAYB's expectations. This made the project more exciting and representative of industry and engineering development. The project challenged our team to think outside

of our chemistry-based curriculum and to consider more macro-structural, physics-based thinking. My favorite part was developing the model detailing the important physical impact reactions characteristic to padding materials.”

Student #2: “This project was so different for me because of how much creativity WAYB allowed us to have. They had two goals in mind: test the mechanical properties of the foams to recommend one of the given samples, and to have this recommendation align with green chemistry standards. They also challenged us to possibly come up with a foam of our own. This was unique because after these goals were communicated to us, they gave us full reign and responsibility to do any test we wanted to prove the mechanical properties. Most other projects I have been a part of had strict deadlines with specific tests or data that were due. This allowed to fail (a lot) to learn the best tests that we could do, which I believe really helped me grow as an independent chemist.”

Student #3: “It did in the sense that I have never been part of a project in which we had to design our own methods for testing the properties of our samples. Previously there have always been structured tests and guidelines, but for this project we had to get very creative to comprehend the properties of the foams on impact while staying within time and money budgets.”

Student #4: “This project was driven more by analysis of already existing materials rather than a desire to create a new material. I liked this approach because there are a lot of materials available and it is very difficult to create a new material. For example, in my internship I have been working with a

material that we are working on developing and it is very difficult to optimize and especially to scale up the production process. With the scale of the projects that we were doing in the Industrial Projects lab, it is much more feasible to focus on understanding what sort of properties the material we currently use has and what other materials have comparable properties.”

2. What was the most beneficial part of this project? What was the most frustrating?

Student #1: “The most beneficial part of this project was learning how to really think outside the box. The equipment immediately available to us had very limited ability to simulate impact (especially at the magnitude of car collisions). We had to isolate and test several deformational reactions using an assortment of different instruments, which we then consolidated in an overall assessment of material compatibility. One such experiment involved a field trip to [a collaborating lab at a neighboring university]; another simply involved dropping balls onto sheets of foam material and recording rebound (and setting off emergency alarms!). The most frustrating aspect of the project was the combination of limited time and limited equipment capabilities, but that's what made it exciting!”

Student #2: “Similar to my last answer, the most beneficial part was the most frustrating part as well, the amount of times we failed. These failures were due to instrument capabilities, instrument availability, sample amounts, etc., that allowed the entire group to really hone our critical thinking and to not panic

under stress. It allowed us to make the best out of what we had where we were still very confident with the series of experiments that we performed and the conclusions that arose from them. It was also frustrating at the end of the project that we ended up recommending Styrofoam as the best foam. Although we were very confident in that conclusion, it seemed like a bit of a dead end. The green chemistry aspect allowed us to recommend other possibilities for Styrofoam, such as composite foams, and even some changes to the manufacturing process to limit the environmental impact of Styrofoam.”

Student #3: “I learned how to be extremely creative in my thinking to overcome obstacles. I also saw how practical it is to have a well rounded team. We all came from different scientific backgrounds and were able to solve problems quickly by combining our skillsets. The frustrating part for me was how little time we had on this project. We had a very short amount of time to design, complete, and analyze our experiments, and while I feel that my team and I did a good job it still feels like there was so much I would have liked to do. For example, how fun would it have been to try and synthesize new foams? The answer is extremely fun.”

Student #4: “Simultaneously the most beneficial and most frustrating parts of this project were our lack of resources. We were doing a lot of different mechanical tests using DMA, TMA, Instron, and the rheometer and none of the instruments were able to mimic even the force of a 30 mph collision, which is

typically the speed that car seats are tested at. Because of this, we were forced to figure out how to utilize the instruments to give us the data we needed and how to read the data and extrapolate the behavior of the material at higher impact. One of our most important tests was the ball bounce using a ping pong ball and a baseball and comparing the results of the two as a way to consider how the materials would react with different forces.”

3. How do you think this experience will influence your approach to product innovation in the future?

Student #1: “The project was a great opportunity to apply creative thinking under pressure of a tight deadline. Additionally, undertaking the project with a big-picture business perspective was an experience I valued greatly for my professional growth.”

Student #2: “This experience really helped me see the relationship between green chemistry and a finished product. Reading LCA after LCA shed so much light into how much of the processes can be improved (one large example being taking the distance from factory to supplier into consideration to limit environmental effects from large delivery trucks). I had never really thought of all the improvements to products that can be made from a green chemistry initiative, so this project really changed the way I think about product manufacturing and process improvements. In terms of an overall approach,

green chemistry is an amazing place to start, because it can give a best case scenario, that a scientist/developer can try to fit a finished product.”

Student #3: “Ultimately, I feel much more prepared to tackle things I have never seen before. As a student, it has been very rare to face obstacles on my own. In undergrad my professors always had new ideas for me to try or some vision on how they wanted a project to turn out. In this case we were on our own. This project forced me to think both on my own and as a team to generate new ideas. In addition, with the help of [student], I learned how to think things through from an engineering perspective. Currently, reformulating and designing new products in a significant part of my job and now I have a much more structured process to do that. If there is a test or piece of equipment I don’t have I will just design a way around it.”

Student #4: “Working on this project really forced me to consider the utility of the material itself and not just whether or not it was "green". Growing up in Eugene, I was surrounded by people who really only focus on how environmentally conscious something is, but especially when we performed the mechanical tests on the different foam samples, I realized that there is often a good reason why we use materials that do not recycle well or are manufactured using toxic chemicals - they are simply better. A lot of money, research, and development goes into creating a more environmentally friendly material that also matches the performance. Also, these materials are typically have inferior

performance AND are more expensive, making them undesirable to consumers. Something I will implement in my future with product design is the idea of making changes to parts of the material's life cycle that will make it more environmentally friendly. For example, we found literature on the use of different, less toxic, blowing agents for EPS. Another idea would be to take used car seats (since they cannot be used again once they have experienced some sort of collision because of EPS's permanent deformation) and donating the EPS as packing material. I think there are a lot of ways to improve on little things like this and still be marketable to the environmentally conscious community, which is obviously an important part of product innovation as well!”

4. How did your perspective regarding green chemistry change during work on this project?

Student #1: “I initially became familiar with the concepts of green chemistry during my undergraduate engineering curriculum. However, this project provided insight into how the principles of green chemistry can be specifically applied to product development. It was also interesting to consider how green chemistry could be strategically marketed to add consumer value to a product. Given more time, we probably would've delved a great deal further into the green chemistry and marketing aspect of the project.”

Student #2: “This project showed me that there really is room for improvement in green chemistry initiatives in many manufacturing processes. I previously thought that processes were performed because there was no other feasible way, but diving into green chemistry helped me make recommendation for improvements on 3-4 different foam productions. The only caveat is that these new green processes are much more expensive, but, it allowed me to see hope in the future where these green processes could be affordable and widely used.”

Student #3: “Luckily, I came into this project with an environmental science minor and spent a significant time in environmental chemistry courses before my time at the University of Oregon. The science aspect remained constant and I felt capable of knowing what to look out for regarding the environmental impacts of the foam samples. However, I was surprised by the marketing aspect of green chemistry following the presentation given by Aurora. I’ve always been so focused on the science that it never occurred to me how many misconceptions and false claims were out there regarding green chemistry and environmental practices. How can the general public know what is true or false when even I needed a presentation to learn what to look out for and I studied environmental science? Overall, I feel more obliged to support companies who genuinely want to find better products and be transparent about their practices and I hope to be the type of chemist who works consistently with the environmental implications of my work on my mind.”

Student #4: “I realized how difficult it is to integrate greener materials into already existing products. Our results showed us that EPS had superior mechanical properties over the other foam materials that we tested, indicating that there is a good safety reason why EPS is commonly used in car seats. In order to replace EPS with a greener alternative, much more research and development would be necessary. One of the promising alternatives was [Alternative #1].

Since there is no layering, the final part has the same mechanical properties in all directions. This allows the company to print parts with customizable mechanical properties. Theoretically, this would be ideal for our application, along with use of a more environmentally friendly material for printing.”

**Structured Life Cycle Thinking Template (with Example Entries for EPS)<sup>1-5</sup>**

Extraction	Processing	Manufacturing	Use	End of Life
Crude oil and natural gas refined into primary and secondary petrochemicals	Petrochemicals polymerized and then transformed into EPS foam	Car seat is made with EPS foam	Consumer uses car seat	Consumer gets rid of car seat
	Expansion of polystyrene beads <ul style="list-style-type: none"> <li>• Uses organic blowing agents and heat</li> </ul>		Most car seats expire after 6 years <ul style="list-style-type: none"> <li>• The longer a seat can stay in the use phase the better for reducing lifecycle impacts</li> </ul>	EPS is typically incinerated or put into a landfill <ul style="list-style-type: none"> <li>• EPS is unlikely to be separated from car seat shell by consumers</li> </ul>

## **Key Learning Outcomes**

### **Overarching outcomes:**

Students will demonstrate an understanding of the interrelationship between systems thinking, life cycle thinking and green chemistry.

Students will be able to develop innovative strategies for product development starting at the systems, life cycle or green chemistry level of analysis.

### **Workshop I:**

Students will be able to use life cycle assessments and toxicity data to identify and explain the impacts of materials.

Students will be able to apply life cycle thinking to compare materials and select alternatives that minimize impacts.

### **Workshop II:**

Students will be able to combine data from complementary analysis techniques to thoroughly characterize materials and relate their structural properties to performance.

Students will be able to relate experimental lab-scale results to commercial product function.

### **Workshop III**

Students will demonstrate knowledge about systems thinking principles and give examples of how these principles can guide innovation.

Students will be able to distill technical experimental data for product marketing that can be understood by nonscientists.

Students will be able to develop a product design with both scientific and business merits.

### **Additional Details on Workshop Implementation**

The three workshops were piloted in a master's level immersion lab course within the Polymer Science track of the University of Oregon's Knight Campus for Accelerating Scientific Impact. This laboratory course is required for all students within the track and 19 students were enrolled. The course takes place for three weeks during the summer and students work approximately 40 hours a week to complete industrially-relevant lab projects. The students work in small groups (3-5 students) on specific projects within the lab but share their experience and progress with the whole class in semiweekly recap meetings. The cohort working on this project performed all three of the workshops back-to-back. There was also some overlap between the timing of the workshops because students continued researching lifecycle impacts of various foams as they learned more about their performance during Workshop II. We have suggested this interplay in Figure 3 by having a gradient between Workshops I and II.

The course instructor, Dr. Casey Check and four teaching assistants allowed students to design their own experiments, utilize instrumentation, interpret data and maintain a safe lab environment with minimal interference. The mentors also provided feedback during the course to help guide progress. The final presentation was graded and students received feedback on areas of strength and areas for improvement.

To prepare students for this project, they were given an initial framing lecture to introduce them to concepts they were not likely to have learned in prior courses (*e.g.*, systems thinking, green marketing, and life cycle thinking). They were also given a one-page summary of the project goals and expectations. The goals were intentionally broad

so that they had the opportunity to practice scientific creativity and process design. For example, one goal was to design an in-house quasi-crash test to compare the foam function. From this they developed the ping pong and baseball tests. The students trialed a number of experimental methods for testing the foams before arriving on the ones documented in this manuscript: these were the most informative. The students also performed extensive thermal and mechanical analysis that was good preparation for their careers as polymer chemists, but was not included in this manuscript because it isn't necessary for achieving the learning outcomes described herein.

Given the difference in experimental depth, and the dependence on effective task delegation during group work, the time requirements for each workshop are only estimates of the amount of time needed for students to complete them. The life cycle thinking lesson in Workshop I required students to do preparatory reading outside of class and 3-4 hours of group work to summarize life cycle impacts and agree upon areas with good opportunities for intervention. Students estimate that they spent about 13 hours developing Workshop II but think it could be repeated by future students in 3-4 lab hours now that the test conditions have been optimized. The data analysis would take another few hours and can be done outside of lab. Students estimate that they spent around 15 hours on Workshop III, and although they did this during lab hours it does not require lab space. We recommend having students start Workshop III during a 3-4 hour lab and then having them continue work outside of class. We expect that this workshop series could be successfully implemented over five lab days with each period lasting 3-4 hours. Day one would be an initial framing lecture and independent student reading for Workshop I, day two would be group life cycle thinking (Workshop I), day three would be performance

testing (Workshop II), day four would be composition of a final product pitch and marketing material (Workshop III) and day five would be group presentations. There would be additional homework required between lab days to complete the analysis.

### **Useful Resources for Introducing Students to Green Marketing**

- (1) Dahl, R. Green Washing: Do You Know What You're Buying? *Environ. Health Perspect.* **2010**, 118, 246–252.

This article presents an approachable overview of green washing and describes seven common signs of it.

- (2) Patagonia Materials and Technologies. Patagonia [Online], <https://www.patagonia.com/materials-tech.html> (accessed Apr 1, 2019).

The textile company, Patagonia, is renowned for their compelling green marketing. Their blog posts describing the environmental and performance benefits of their products are excellent examples for students to study. The post describing Yulex<sup>®</sup> replacement for neoprene is especially interesting because it showcases a systems approach to product innovation including: challenging preconceptions about certain chemicals, quantitatively assessing lifecycle impacts, and a description of performance enhancements (*e.g.*, increased wetsuit elasticity) achieved.

- (3) Defunkify Active Wash Laundry Detergent. Defunkify [Online], <https://defunkify.com/collections/main/products/active-wash-laundry-detergent> (accessed Apr 1, 2019).

Defunkify is a company that uses green chemistry to formulate safe and effective laundry products. Their hallmark product, the active wash, has evidence of both safety and efficacy on the box. They show scanning electron microscope images of

textile fibers cleaned with this wash to demonstrate a microscopically effective clean. The green formulation earned the detergent an EPA Safer Choice label and the minimal list of ingredients includes a functional purpose for each chemical.

(4) Allbirds: The World's Most Comfortable Shoes. Allbird [Online],

<https://www.allbirds.com/pages/our-materials-wool> (accessed Apr 1, 2019).

Allbirds is a sustainable shoe manufacturer that provides many specific examples of how they reduce environmental impacts and create comfortable shoes. Their website has pages dedicated to the benefits of their materials, for example, they explain that the small diameter of the wool they use allows it to be breathable but not itchy. To ensure the wool they use comes from ethically managed farms and animals they have partnerships with a wool environmental stewardship company. They also have numerous strategies for extending the use phase of the shoe including selling affordable replacement soles and partnering with a reuse program where communities in need receive their lightly used shoes.

### **Specific Example of Integrating Green Chemistry, Life Cycle Thinking and Systems Thinking (shown in Fig. 6.2)**

Here we provide a detailed example of the iterative process shown in Figure 6.2 to illustrate sustainable product design using sunscreen as an example product.

There is currently substantial consumer concern over coral reef-damage due to sunscreens.<sup>6,7</sup> Using this concern as motivation for innovation, one could start with a green chemistry approach, using UV absorbers that are less toxic and/or that rapidly degrade into less toxic byproducts. Life cycle thinking would allow for an evaluation of the different possible chemicals and their effects on humans and the environment. A

systems approach could explore the overall formula performances (*e.g.*, the relative SPFs of different formulations) and possible regulatory aspects of sunscreen ingredients. From these data, one can refer back to green chemistry principles and life cycle analysis to consider additional strategies for improvement.

Instead of starting at the green chemistry level, it is also possible to start with systems thinking and think of a bigger picture solution. One may ask the question of whether sunscreens are even needed for a specific use scenario. Is it possible to use more protective clothing when swimming over coral reefs and avoid UV exposure? Will people use clothing they already own or buy specific clothing for this purpose? If new clothing is the most likely way to change people's behavior, then what are the life cycle impacts of manufacturing new clothing for this purpose? From a green chemistry perspective, can a manufacturing process for the clothing be used that prevents dye pollution that commonly plagues the textile industry?<sup>8</sup> By starting at the systems level and working from the outside in we came up with an entirely different result within this example. Both example solutions would represent impactful innovations but are useful for different types of companies. It is also possible to start by addressing a hotspot (an impact that represents an especially fruitful opportunity for corrective action) identified in a life cycle assessment.

## REFERENCES CITED

### CHAPTER I

- (1) Tumbleston, J. R.; Shirvanyants, D.; Ermoshkin, N.; Januszewicz, R.; Johnson, A. R.; Kelly, D.; Chen, K.; Pinschmidt, R.; Rolland, J. P.; Ermoshkin, A.; Samulski, E. T.; DeSimone, J. M. Continuous Liquid Interface Production of 3D Objects. *Science* **2015**, *347*, 1349–1352.
- (2) Carbon 3D. Carbon Lattice Innovation — The Adidas Story <https://www.carbon3d.com/white-papers/carbon-lattice-innovation-the-adidas-story/> (accessed Jul 23, 2019).
- (3) Hosseini, P.; Wright, C. D.; Bhaskaran, H. An Optoelectronic Framework Enabled by Low-Dimensional Phase-Change Films. *Nature* **2014**, *511*, 206–211.
- (4) Bodle. Core Technology <https://www.bodletechnologies.com/node/19> (accessed Jul 30, 2019).
- (5) Carson, R. *Silent Spring*; Houghton Mifflin Company: Boston, 1962.
- (6) Lee, B. M.; Kwon, S.; Cho, Y. M.; Kim, K. B.; Seo, K.; Min, C. S.; Kim, K. Perspectives on Trace Chemical Safety and Chemophobia: Risk Communication and Risk Management. *J. Toxicol. Environ. Heal. - Part A Curr. Issues* **2019**, *82*, 186–199.
- (7) Francl, M. How to Counteract Chemophobia. *Nat. Chem.* **2013**, *5*, 439–440.
- (8) Anastas, P.; Eghbali, N. Green Chemistry: Principles and Practice. *Chem. Soc. Rev.* **2010**, *39*, 301–312.
- (9) Gilbertson, L. M.; Zimmerman, J. B.; Plata, D. L.; Hutchison, J. E.; Anastas, P. T. Designing Nanomaterials to Maximize Performance and Minimize Undesirable Implications Guided by the Principles of Green Chemistry. *Chem. Soc. Rev.* **2015**, *44*, 5758–5777.
- (10) National Research Council. *A Framework to Guide Selection of Chemical Alternatives*; The National Academies Press: Washington, D.C., 2014.
- (11) Winkler, D. A. Recent Advances, and Unresolved Issues, in the Application of Computational Modelling to the Prediction of the Biological Effects of Nanomaterials. *Toxicol. Appl. Pharmacol.* **2016**, *299*, 96–100.
- (12) Kumar, A.; Kumar, P.; Anandan, A.; Fernandes, T. F.; Ayoko, G. A.; Biskos, G. Engineered Nanomaterials: Knowledge Gaps in Fate, Exposure, Toxicity, and Future Directions. *J. Nanomater.* **2014**.

- (13) Voutchkova, A. M.; Osimitz, T. G.; Anastas, P. T. Toward a Comprehensive Molecular Design Framework for Reduced Hazard. *Chem. Rev.* **2010**, *110*, 5845–5882.
- (14) Van der Veen, I.; de Boer, J. Phosphorus Flame Retardants: Properties, Production, Environmental Occurrence, Toxicity and Analysis. *Chemosphere* **2012**, *88*, 1119–1153.
- (15) Nohynek, G. J.; Borgert, C. J.; Dietrich, D.; Rozman, K. K. Endocrine Disruption: Fact or Urban Legend? *Toxicol. Lett.* **2013**, *223*, 295–305.
- (16) Nohynek, G. J.; Antignac, E.; Re, T.; Toutain, H. Safety Assessment of Personal Care Products/Cosmetics and Their Ingredients. *Toxicol. Appl. Pharmacol.* **2010**, *243*, 239–259.
- (17) Winkler, D. A.; Mombelli, E.; Pietroiusti, A.; Tran, L.; Worth, A.; Fadeel, B.; McCall, M. J. Applying Quantitative Structure-Activity Relationship Approaches to Nanotoxicology: Current Status and Future Potential. *Toxicology* **2013**, *313*, 15–23.
- (18) Devito, S. C. On the Design of Safer Chemicals: A Path Forward. *Green Chem.* **2016**, *18*, 4332–4347.
- (19) Rana, S.; Bajaj, A.; Mout, R.; Rotello, V. M. Monolayer Coated Gold Nanoparticles for Delivery Applications. *Adv. Drug Deliv. Rev.* **2012**, *64*, 200–216.
- (20) Lee, D.-E.; Koo, H.; Sun, I.-C.; Ryu, J. H.; Kim, K.; Kwon, I. C. Multifunctional Nanoparticles for Multimodal Imaging and Theragnosis. *Chem. Soc. Rev.* **2012**, *41*, 2656–2672.
- (21) Ng, S. M.; Koneswaran, M.; Narayanaswamy, R. A Review on Fluorescent Inorganic Nanoparticles for Optical Sensing Applications. *RSC Adv.* **2016**, *6*, 21624–21661.
- (22) Qu, X.; Alvarez, P. J. J.; Li, Q. Applications of Nanotechnology in Water and Wastewater Treatment. *Water Res.* **2013**, *47*, 3931–3946.
- (23) Guo, S.; Zhang, S.; Sun, S. Tuning Nanoparticle Catalysis for the Oxygen Reduction Reaction. *Angew. Chemie - Int. Ed.* **2013**, *52*, 8526–8544.
- (24) Mieszawska, A. J.; Mulder, W. J. M.; Fayad, Z. A.; Cormode, D. P. Multifunctional Gold Nanoparticles for Diagnosis and Therapy of Disease. *Mol. Pharm.* **2013**, *10*, 831–847.

- (25) Cheng, Z.; Al Zaki, A.; Hui, J. Z.; Muzykantov, V. R.; Tsourkas, A. Multifunctional Nanoparticles: Cost versus Benefit of Adding Targeting and Imaging Capabilities. *Science* **2012**, *338*, 903–910.
- (26) Gao, J.; Gu, H.; Xu, B. Multifunctional Magnetic Nanoparticles : Design , Synthesis , and Biomedical Applications. **2009**, *42*.
- (27) Ahn, S.; Jung, S. Y.; Lee, S. J. Gold Nanoparticle Contrast Agents in Advanced X-Ray Imaging Technologies. *Molecules* **2013**, *18*, 5858–5890.
- (28) Ali, Z.; Abbasi, A. Z.; Zhang, F.; Arosio, P.; Lascialfari, A.; Casula, M. F.; Wenk, A.; Kreyling, W.; Plapper, R.; Seidel, M.; Niessner, R.; Knöll, J.; Seubert, A.; Parak, W. J. Multifunctional Nanoparticles for Dual Imaging. *Anal. Chem.* **2011**, *83*, 2877–2882.
- (29) Saha, K.; Agasti, S.; Kim, C.; Li, X.; Rotello, V. Gold Nanoparticles in Chemical and Biological Sensing. *Chem. Rev.* **2012**, *112*, 2739–2779.
- (30) Vines, J. B.; Yoon, J.-H.; Ryu, N.-E.; Lim, D.-J.; Park, H. Gold Nanoparticles for Photothermal Cancer Therapy. *Front. Chem.* **2019**, *7*, 1–16.
- (31) Vance, M. E.; Kuiken, T.; Vejerano, E. P.; McGinnis, S. P.; Hochella, M. F.; Hull, D. R. Nanotechnology in the Real World: Redeveloping the Nanomaterial Consumer Products Inventory. *Beilstein J. Nanotechnol.* **2015**, *6*, 1769–1780.
- (32) Richman, E. K.; Hutchison, J. E. The Nanomaterial Characterization Bottleneck. *ACS Nano* **2009**, *3*, 2441–2446.
- (33) Bobo, D.; Robinson, K. J.; Islam, J.; Thurecht, K. J.; Corrie, S. R. Nanoparticle-Based Medicines: A Review of FDA-Approved Materials and Clinical Trials to Date. *Pharm. Res.* **2016**, *33*, 2373–2387.
- (34) Björnmalm, M.; Faria, M.; Caruso, F. Increasing the Impact of Materials in and beyond Bio-Nano Science. *J. Am. Chem. Soc.* **2016**, *138*, 13449–13456.
- (35) Feynman, R. P. There’s Plenty of Room at the Bottom. *Eng. Sci.* **1960**, *23*, 22–36.
- (36) Ferrando, R.; Jellinek, J.; Johnston, R. L. Nanoalloys: From Theory to Applications of Alloy Clusters and Nanoparticles. *Chem. Rev.* **2008**, *108*, 845–910.
- (37) Shew, A. Nanotech’s History: An Interesting, Interdisciplinary, Ideological Split. *Bull. Sci. Technol. Soc.* **2008**, *28*, 390–399.
- (38) Kroto, H. W.; Heath, J. R.; O’Brien, S. C.; Curl, R. F.; Smalley, R. E. C<sub>60</sub> : Buckminsterfullerene. *Nature* **1985**, *318*, 162–163.

- (39) Roco, M. C. The US National Nanotechnology Initiative after 3 Years (2001-2003). *J. Nanoparticle Res.* **2004**, *6*, 1–10.
- (40) Hulla, J. E.; Sahu, S. C.; Hayes, A. W. Nanotechnology: History and Future. *Hum. Exp. Toxicol.* **2015**, *34*, 1318–1321.
- (41) Wood, J. The Top Ten Advances in Materials Science. *Materials Today*, 2008, *11*, 40–45.
- (42) Drexler, K. E. Nanotechnology: From Feynman to Funding. *Bull. Sci. Technol. Soc.* **2004**, *24*, 21–27.
- (43) Kaur, I. P.; Kakkar, V.; Deol, P. K.; Yadav, M.; Singh, M.; Sharma, I. Issues and Concerns in Nanotech Product Development and Its Commercialization. *J. Control. Release* **2014**, *193*, 51–62.
- (44) Roco, M. C. The Long View of Nanotechnology Development: The National Nanotechnology Initiative at 10 Years. *J. Nanoparticle Res.* **2011**, *13*, 427–445.
- (45) Desai, N. Challenges in Development of Nanoparticle-Based Therapeutics. *AAPS J.* **2012**, *14*, 282–295.
- (46) Alkilany, A. M.; Murphy, C. J. Toxicity and Cellular Uptake of Gold Nanoparticles: What We Have Learned so Far? *J. Nanoparticle Res.* **2010**, *12*, 2313–2333.
- (47) Oliveri, A. F.; Elliott, E. W.; Carnes, M. E.; Hutchison, J. E.; Johnson, D. W. Elucidating Inorganic Nanoscale Species in Solution: Complementary and Corroborative Approaches. *ChemPhysChem* **2013**, *14*, 2655–2661.
- (48) Casals, E.; Pfaller, T.; Duschl, A.; Oostingh, G. J.; Puentes, V. Time Evolution of the Nanoparticle Protein Corona. *ACS Nano* **2010**, *4*, 3623–3632.
- (49) Mensch, A. C.; Hernandez, R. T.; Kuether, J. E.; Torelli, M. D.; Feng, Z. V.; Hamers, R. J.; Pedersen, J. A. Natural Organic Matter Concentration Impacts the Interaction of Functionalized Diamond Nanoparticles with Model and Actual Bacterial Membranes. *Environ. Sci. Technol.* **2017**, *51*, 11075–11084.
- (50) Harkness, K. M.; Balinski, A.; McLean, J. A.; Cliffel, D. E. Nanoscale Phase Segregation of Mixed Thiolates on Gold Nanoparticles. *Angew. Chemie - Int. Ed.* **2011**, *50*, 10554–10559.
- (51) Nel, A. E.; Mädler, L.; Velegol, D.; Xia, T.; Hoek, E. M. V.; Somasundaran, P.; Klaessig, F.; Castranova, V.; Thompson, M. Understanding Biophysicochemical Interactions at the Nano-Bio Interface. *Nat. Mater.* **2009**, *8*, 543–557.

- (52) Busquets, M. A.; Estelrich, J.; Sánchez-Martín, M. J. Nanoparticles in Magnetic Resonance Imaging: From Simple to Dual Contrast Agents. *Int. J. Nanomedicine* **2015**, 1727.
- (53) Cooper, S. R.; Plummer, L. K.; Cosby, A. G.; Lenox, P.; Jander, A.; Dhagat, P.; Hutchison, J. E. Insights into the Magnetic Properties of Sub-10 Nm Iron Oxide Nanocrystals through the Use of a Continuous Growth Synthesis. *Chem. Mater.* **2018**, 30, 6053–6062.
- (54) Diroll, B. T.; Gordon, T. R.; Gauding, E. A.; Klein, D. R.; Paik, T.; Yun, H. J.; Goodwin, E. D.; Damodhar, D.; Kagan, C. R.; Murray, C. B. Synthesis of N-Type Plasmonic Oxide Nanocrystals and the Optical and Electrical Characterization of Their Transparent Conducting Films. *Chem. Mater.* **2014**, 26, 4579–4588.
- (55) Crockett, B. M.; Jansons, A. W.; Koskela, K. M.; Sharps, M. C.; Johnson, D. W.; Hutchison, J. E. Influence of Nanocrystal Size on the Optoelectronic Properties of Thin, Solution-Cast Sn-Doped In<sub>2</sub>O<sub>3</sub> Films. *Chem. Mater.* **2019**, 31, 3370–3380.
- (56) Truong, L.; Zaikova, T.; Baldock, B. L.; Balik-meisner, M.; To, K.; Reif, D. M.; Kennedy, Z. C.; Hutchison, J. E.; Tanguay, L. Systematic Determination of the Relationship between Nanoparticle Core Diameter and Toxicity for a Series of Structurally Analogous Gold Nanoparticles in Zebrafish. *Nanotoxicology* **2019**, ASAP.
- (57) Cho, E. C.; Zhang, Q.; Xia, Y. The Effect of Sedimentation and Diffusion on Cellular Uptake of Gold Nanoparticles. *Nat Nanotechnol.* **2011**, 6, 385–391.
- (58) Levard, C.; Hotze, E. M.; Lowry, G. V.; Brown, G. E. Environmental Transformations of Silver Nanoparticles: Impact on Stability and Toxicity. *Environ. Sci. Technol.* **2012**, 46, 6900–6914.
- (59) Valencia, P. M.; Farokhzad, O. C.; Karnik, R.; Langer, R. Microfluidic Technologies for Accelerating the Clinical Translation of Nanoparticles. *Nat. Nanotechnol.* **2012**, 7, 623–629.
- (60) Nightingale, A. M.; Phillips, T. W.; Bannock, J. H.; De Mello, J. C. Controlled Multistep Synthesis in a Three-Phase Droplet Reactor. *Nat. Commun.* **2014**, 5, 1–8.
- (61) Elliott, E. W.; Haben, P. M.; Hutchison, J. E. Subnanometer Control of Mean Core Size During Mesofluidic Synthesis of Small ( $D_{\text{core}} < 10$  Nm) Water-Soluble, Ligand-Stabilized Gold Nanoparticles. *Langmuir* **2015**, 31, 11886–11894.
- (62) Crockett, B. M.; Jansons, A. W.; Koskela, K. M.; Johnson, D. W.; Hutchison, J. E. Radial Dopant Placement for Tuning Plasmonic Properties in Metal Oxide Nanocrystals. *ACS Nano* **2017**, 11, 7719–7728.

- (63) Jansons, A. W.; Hutchison, J. E. Continuous Growth of Metal Oxide Nanocrystals: Enhanced Control of Nanocrystal Size and Radial Dopant Distribution. *ACS Nano* **2016**, *10*, 6942–6951.
- (64) Kellon, J. E.; Young, S. L.; Hutchison, J. E. Engineering the Nanoparticle-Electrode Interface. *Chem. Mater.* **2019**, *31*, 2685–2701.
- (65) Pyrżyńska, K.; Bystrzejewski, M. Comparative Study of Heavy Metal Ions Sorption onto Activated Carbon, Carbon Nanotubes, and Carbon-Encapsulated Magnetic Nanoparticles. *Colloids Surfaces A Physicochem. Eng. Asp.* **2010**, *362*, 102–109.
- (66) Truong, L.; Reif, D. M.; Mary, L. S.; Geier, M. C.; Truong, H. D.; Tanguay, R. L. Multidimensional *in Vivo* Hazard Assessment Using Zebrafish. *Toxicol. Sci.* **2014**, *137*, 212–233.
- (67) Boyd, W. A.; McBride, S. J.; Rice, J. R.; Snyder, D. W.; Freedman, J. H. A High-Throughput Method for Assessing Chemical Toxicity Using A *Caenorhabditis Elegans* Reproduction Assay. *Toxicol Appl Pharmacol.* **2010**, *245*, 153–159.
- (68) Wang, H.; Wick, R. L.; Xing, B. Toxicity of Nanoparticulate and Bulk ZnO, Al<sub>2</sub>O<sub>3</sub> and TiO<sub>2</sub> to the Nematode *Caenorhabditis Elegans*. *Environ. Pollut.* **2009**, *157*, 1171–1177.
- (69) Kim, H.; Park, K.; Lee, M.-Y. Biocompatible Dispersion Methods for Carbon Black. *Toxicol. Res.* **2012**, *28*, 209–216.
- (70) *Surfactants in Personal Care Products and Decorative Cosmetics*; Rhein, L. D.; Schlossman, M.; O'Lenick, A.; Somasundaran, P., Eds.; 3rd ed.; CRC Press: Boca Raton, 2007.
- (71) Glover, R. D.; Miller, J. M.; Hutchison, J. E. Generation of Metal Nanoparticles from Silver and Copper Objects: Nanoparticle Dynamics on Surfaces and Potential Sources of Nanoparticles in the Environment. *ACS Nano* **2011**, *5*, 8950–8957.
- (72) Nel, A. E.; Mädler, L.; Velegol, D.; Xia, T.; Hoek, E. M. V.; Somasundaran, P.; Klaessig, F.; Castranova, V.; Thompson, M. Understanding Biophysicochemical Interactions at the Nano-Bio Interface. *Nat. Mater.* **2009**, *8*, 543–557.
- (73) You, D. G.; Deepagan, V. G.; Um, W.; Jeon, S.; Son, S.; Chang, H.; Yoon, H. I.; Cho, Y. W.; Swierczewska, M.; Lee, S.; Pomper, M. G.; Kwon, I. C.; Kim, K.; Park, J. H. ROS-Generating TiO<sub>2</sub> Nanoparticles for Non-Invasive Sonodynamic Therapy of Cancer. *Sci. Rep.* **2016**, *6*, 1–12.

- (74) Dayem, A. A.; Hossain, M. K.; Lee, S. Bin; Kim, K.; Saha, S. K.; Yang, G. M.; Choi, H. Y.; Cho, S. G. The Role of Reactive Oxygen Species (ROS) in the Biological Activities of Metallic Nanoparticles. *Int. J. Mol. Sci.* **2017**, *18*, 1–21.
- (75) Templeton, A. C.; Hostetler, M. J.; Kraft, C. T.; Murray, R. W. Reactivity of Monolayer-Protected Gold Cluster Molecules: Steric Effects. *J. Am. Chem. Soc.* **1998**, *120*, 1906–1911.
- (76) Feliu, N.; Docter, D.; Heine, M.; Del Pino, P.; Ashraf, S.; Kolosnjaj-Tabi, J.; Macchiarini, P.; Nielsen, P.; Alloyeau, D.; Gazeau, F.; Stauber, R. H.; Parak, W. J. *In Vivo* Degeneration and the Fate of Inorganic Nanoparticles. *Chem. Soc. Rev.* **2016**, *45*, 2440–2457.
- (77) Lundqvist, M.; Stigler, J.; Elia, G.; Lynch, I.; Cedervall, T.; Dawson, K. A. Nanoparticle Size and Surface Properties Determine the Protein Corona with Possible Implications for Biological Impacts. *Proc. Natl. Acad. Sci.* **2008**, *105*, 14265–14270.
- (78) Choi, K.; Riviere, J. E.; Monteiro-Riviere, N. A. Protein Corona Modulation of Hepatocyte Uptake and Molecular Mechanisms of Gold Nanoparticle Toxicity. *Nanotoxicology* **2017**, *11*, 64–75.
- (79) Cao, Y.; Roursgaard, M.; Kermanizadeh, A.; Loft, S.; Møller, P. Synergistic Effects of Zinc Oxide Nanoparticles and Fatty Acids on Toxicity to Caco-2 Cells. *Int. J. Toxicol.* **2015**, *34*, 67–76.
- (80) Cedergreen, N. Quantifying Synergy: A Systematic Review of Mixture Toxicity Studies within Environmental Toxicology. *PLoS One* **2014**, *9*, e96580.
- (81) SCHER; SCCS; SCENIHR. *Opinion on the Toxicity and Assessment of Chemical Mixtures*; European Commission, 2012.

## CHAPTER II

- (1) Kim E. Sapsford, W. Russ Algar, L. B. Functionalizing Nanoparticles with Biological Molecules: Developing Chemistries That Facilitate Nanotechnology. *Chem. Rev.* **2013**, *113*, 1904–2074.
- (2) Stankus, D. P.; Lohse, S. E.; Hutchison, J. E.; Nason, J. A. Interactions between Natural Organic Matter and Gold Nanoparticles Stabilized with Different Organic Capping Agents. *Environ. Sci. Technol.* **2011**, *45*, 3238–3244.
- (3) Lee, D.-E.; Koo, H.; Sun, I.-C.; Ryu, J. H.; Kim, K.; Kwon, I. C. Multifunctional Nanoparticles for Multimodal Imaging and Theragnosis. *Chem. Soc. Rev.* **2012**, *41*, 2656–2672.

- (4) Rana, S.; Bajaj, A.; Mout, R.; Rotello, V. M. Monolayer Coated Gold Nanoparticles for Delivery Applications. *Adv. Drug Deliv. Rev.* **2012**, *64*, 200–216.
- (5) Alkilany, A. M.; Murphy, C. J. Toxicity and Cellular Uptake of Gold Nanoparticles: What We Have Learned so Far? *J. Nanoparticle Res.* **2010**, *12*, 2313–2333.
- (6) Zhu, Y.; Fan, L.; Yang, B.; Du, J. Multifunctional Homopolymer Vesicles for Facile Immobilization of Gold Nanoparticles and Effective Water Remediation. *ACS Nano* **2014**, *8*, 5022–5031.
- (7) Mieszawska, A. J.; Mulder, W. J. M.; Fayad, Z. A.; Cormode, D. P. Multifunctional Gold Nanoparticles for Diagnosis and Therapy of Disease. *Mol. Pharm.* **2013**, *10*, 831–847.
- (8) Kim, C.; Ghosh, P.; Rotello, V. M. Multimodal Drug Delivery Using Gold Nanoparticles. *Nanoscale* **2009**, *1*, 61–67.
- (9) Saha, K.; Agasti, S.; Kim, C.; Li, X.; Rotello, V. Gold Nanoparticles in Chemical and Biological Sensing. *Chem. Rev.* **2012**, *112*, 2739–2779.
- (10) Cheng, Z.; Al Zaki, A.; Hui, J. Z.; Muzykantov, V. R.; Tsourkas, A. Multifunctional Nanoparticles: Cost versus Benefit of Adding Targeting and Imaging Capabilities. *Science* **2012**, *338*, 903–910.
- (11) Wicki, A.; Witzigmann, D.; Balasubramanian, V.; Huwyler, J. Nanomedicine in Cancer Therapy: Challenges, Opportunities, and Clinical Applications. *J. Control. Release* **2015**, *200*, 138–157.
- (12) Desai, N. Challenges in Development of Nanoparticle-Based Therapeutics. *AAPS J.* **2012**, *14*, 282–295.
- (13) Li, N.; Binder, W. H. Click-Chemistry for Nanoparticle-Modification. *J. Mater. Chem.* **2011**, *21*, 16717–16734.
- (14) Buckley, H. L.; Rubin, L. K.; Chromiński, M.; McNicholas, B. J.; Tsen, K. H. Y.; Gryko, D. T.; Arnold, J. Corroles That “click”: Modular Synthesis of Azido- and Propargyl-Functionalized Metalloporphyrin Complexes and Convergent Synthesis of a Bis-Corrole Scaffold. *Inorg. Chem.* **2014**, *53*, 7941–7950.
- (15) Kolb, H. C.; Finn, M. G.; Sharpless, K. B. Click Chemistry: Diverse Chemical Function from a Few Good Reactions. *Angew. Chemie - Int. Ed.* **2001**, *40*, 2004–2021.

- (16) Fleming, D. A.; Thode, C. J.; Williams, M. E. Triazole Cycloaddition as a General Route for Functionalization of Au Nanoparticles. *Chem. Mater.* **2006**, *18*, 2327–2334.
- (17) Zhao, P.; Grillaud, M.; Salmon, L.; Ruiz, J.; Astruc, D. Click Functionalization of Gold Nanoparticles Using the Very Efficient Catalyst copper(I) (Hexabenzyl)tris(2-Aminoethyl)-Amine Bromide. *Adv. Synth. Catal.* **2012**, *354*, 1001–1011.
- (18) Brennan, J. L.; Hatzakis, N. S.; Tshikhudo, T. R.; Dirvianskyte, N.; Razumas, V.; Patkar, S.; Vind, J.; Svendsen, A.; Nolte, R. J. M.; Rowan, A. E.; et al. Bionanoconjugation via Click Chemistry: The Creation of Functional Hybrids of Lipases and Gold Nanoparticles. *Bioconjug. Chem.* **2006**, *17*, 1373–1375.
- (19) Li, N.; Zhao, P.; Salmon, L.; Ruiz, J.; Zabawa, M.; Hosmane, N. S.; Astruc, D. “Click” star-Shaped and Dendritic PEGylated Gold Nanoparticle-Carborane Assemblies. *Inorg. Chem.* **2013**, *52*, 11146–11155.
- (20) Boisselier, E.; Salmon, L.; Ruiz, J.; Astruc, D. How to Very Efficiently Functionalize Gold Nanoparticles By “click” chemistry. *Chem. Commun.* **2008**, 5788–5790.
- (21) Chen, Q.; Kaneko, T.; Hatakeyama, R. Rapid Synthesis of Water-Soluble Gold Nanoparticles with Control of Size and Assembly Using Gas-Liquid Interfacial Discharge Plasma. *Chem. Phys. Lett.* **2012**, *521*, 113–117.
- (22) Gao, J.; Huang, X.; Lui, H.; Zan, F.; Ren, J. Colloidal Stability of Gold Nanoparticles Modified with Thiol Compounds: Bioconjugation and Application in Cancer Cell Imaging. *Langmuir* **2012**, *28*, 4464–4471.
- (23) Oh, E.; Delehanty, J. B.; Sapsford, K. E.; Susumu, K.; Goswami, R.; Blanco-canosa, J. B.; Dawson, P. E.; Granek, J.; Shoff, M.; Zhang, Q.; et al. Cellular Uptake and Fate of PEGylated Gold Nanoparticles Is Dependent on Both Cell-Penetration Peptides and Particle Size. *ACS Nano* **2011**, *5*, 6434–6448.
- (24) Gole, A.; Murphy, C. J. Azide-Derivatized Gold Nanorods: Functional Materials For “click” chemistry. *Langmuir* **2008**, *24*, 266–272.
- (25) Zhang, M. X.; Huang, B. H.; Sun, X. Y.; Pang, D. W. Clickable Gold Nanoparticles as the Building Block of Nanobioprobes. *Langmuir* **2010**, *26*, 10171–10176.
- (26) Wang, X.; Gobbo, P.; Suchy, M.; Workentin, M. S.; Hudson, R. H. E. Peptide-Decorated Gold Nanoparticles via Strain-Promoted Azide–alkyne Cycloaddition and Post Assembly Deprotection. *RSC Adv.* **2014**, *4*, 43087–43091.

- (27) Gobbo, P.; Novoa, S.; Biesinger, M. C.; Workentin, M. S. Interfacial Strain-Promoted Alkyne-Azide Cycloaddition (I-SPAAC) for the Synthesis of Nanomaterial Hybrids. *Chem. Commun.* **2013**, *49*, 3982–3984.
- (28) Brust, M.; Walker, M.; Bethell, D.; Schiffrin, D. J.; Whyman, R. Synthesis of Thiol-Derivatized Gold Nanoparticles in a Two-Phase Liquid-Liquid System. *J. Chem. Soc. Chem. Commun.* **1994**, No. 7, 801–802.
- (29) Zhao, P.; Li, N.; Astruc, D. State of the Art in Gold Nanoparticle Synthesis. *Coord. Chem. Rev.* **2013**, *257*, 638–665.
- (30) Foos, E. E.; Snow, A. W.; Twigg, M. E.; Ancona, M. G. Thiol-Terminated Di-, Tri-, and Tetraethylene Oxide Functionalized Gold Nanoparticles: A Water-Soluble, Charge-Neutral Cluster. *Chem. Mater.* **2002**, *14*, 2401–2408.
- (31) Elliott, E. W.; Haben, P. M.; Hutchison, J. E. Subnanometer Control of Mean Core Size During Mesofluidic Synthesis of Small ( $D_{\text{core}} < 10 \text{ Nm}$ ) Water-Soluble, Ligand-Stabilized Gold Nanoparticles. *Langmuir* **2015**, *31*, 11886–11894.
- (32) Lohse, S. E.; Dahl, J. A.; Hutchison, J. E. Direct Synthesis of Large Water-Soluble Functionalized Gold Nanoparticles Using Bunte Salts as Ligand Precursors. *Langmuir* **2010**, *26*, 7504–7511.
- (33) Amaral, S. P.; Fernandez-villamarin, M.; Correa, J.; Riguera, R.; Fernandez-megia, E. Efficient Multigram Synthesis of the Repeating Unit of Gallic Acid-Triethylene Glycol Dendrimers. *Org. Lett.* **2011**, *13*, 4522–4525.
- (34) Terrill, R. H.; Postlethwaite, T. A.; Chen, C.; Poon, C.-D.; Terzis, A.; Chen, A.; Hutchison, J. E.; Clark, M. R.; Wignall, G. Monolayers in Three Dimensions: NMR, SAXS, Thermal, and Electron Hopping Studies of Alkanethiol Stabilized Gold Clusters. *J. Am. Chem. Soc.* **1995**, *117*, 12537–12548.
- (35) Templeton, A. C.; Hostetler, M. J.; Kraft, C. T.; Murray, R. W.; Hill, C.; Carolina, N. Reactivity of Monolayer-Protected Gold Cluster Molecules: Steric Effects. *J. Am. Chem. Soc.* **1998**, *120*, 1906–1911.
- (36) Demers, L. M.; Mirkin, C. A.; Mucic, R. C.; Reynolds, R. A.; Letsinger, R. L.; Elghanian, R.; Viswanadham, G. A Fluorescence-Based Method for Determining the Surface Coverage and Hybridization Efficiency of Thiol-Capped Oligonucleotides Bound to Gold Thin Films and Nanoparticles. *Anal. Chem.* **2000**, *72*, 5535–5541.
- (37) Ilavsky, J.; Jemian, P. R. Irena: Tool Suite for Modeling and Analysis of Small-Angle Scattering. *J. Appl. Crystallogr.* **2009**, *42*, 347–353.

- (38) Harper, S. L.; Carriere, J. L.; Miller, J. M.; Hutchison, J. E.; Maddux, B. L. S.; Tanguay, R. L. Systematic Evaluation of Nanomaterial Toxicity: Utility of Standardized Materials and Rapid Assays. *ACS Nano* **2011**, *5*, 4688–4697.
- (39) Karakoti, A. S.; Das, S.; Thevuthasan, S.; Seal, S. PEGylated Inorganic Nanoparticles. *Angew. Chemie - Int. Ed.* **2011**, *50*, 1980–1994.
- (40) Kennedy, Z. C.; Lisowski, C. E.; Mitaru-Berceanu, D. S.; Hutchison, J. E. Influence of Ligand Shell Composition upon Interparticle Interactions in Multifunctional Nanoparticles. *Langmuir* **2015**, *31*, 12742–12752.
- (41) Thode, C. J.; Williams, M. E. Kinetics of 1,3-Dipolar Cycloaddition on the Surfaces of Au Nanoparticles. *J. Colloid Interface Sci.* **2008**, *320*, 346–352.
- (42) Fringuelli, F.; Pizzo, F.; Vaccaro, L. Cobalt(II) Chloride-Catalyzed Chemoselective Sodium Borohydride Reduction of Azides in Water. *Synthesis (Stuttg.)* **2000**, *2000*, 646–650.
- (43) Villermaux, J. Mixing Effects on Complex Chemical Reactions in a Stirred Reactor. *Rev. Chem. Eng.* **1991**, *7*, 51–108.
- (44) Hartman, R. L.; McMullen, J. P.; Jensen, K. F. Deciding Whether to Go with the Flow: Evaluating the Merits of Flow Reactors for Synthesis. *Angew. Chemie - Int. Ed.* **2011**, *50*, 7502–7519.
- (45) Sweeney, S. F.; Woehrle, G. H.; Hutchison, J. E. Rapid Purification and Size Separation of Gold Nanoparticles via Diafiltration. *J. Am. Chem. Soc.* **2006**, *128*, 3190–3197.
- (46) McKenzie, L. C.; Haben, P. M.; Kevan, S. D.; Hutchison, J. E. Determining Nanoparticle Size in Real Time by Small-Angle X-Ray Scattering in a Microscale Flow System. *J. Phys. Chem. C* **2010**, *114*, 22055–22063.
- (47) *Practical Surface Analysis by Auger and X-Ray Photoelectron Spectroscopy*; Briggs, D., Seah, M. P., Eds.; John Wiley & Sons, 1985.
- (48) Ali, Z.; Abbasi, A. Z.; Zhang, F.; Arosio, P.; Lascialfari, A.; Casula, M. F.; Wenk, A.; Kreyling, W.; Plapper, R.; Seidel, M.; et al. Multifunctional Nanoparticles for Dual Imaging. *Anal. Chem.* **2011**, *83*, 2877–2882.
- (49) Kreuter, J. Drug Delivery to the Central Nervous System by Polymeric Nanoparticles: What Do We Know? *Adv. Drug Deliv. Rev.* **2014**, *71*, 2–14.
- (50) Salic, A.; Mitchison, T. J. A Chemical Method for Fast and Sensitive Detection of DNA Synthesis in Vivo. *Proc. Natl. Acad. Sci. U. S. A.* **2008**, *105*, 2415–2420.

- (51) Zhang, X.-Q.; Xu, X.; Lam, R.; Giljohann, D.; Ho, D.; Mirkin, C. A. Strategy for Increasing Drug Solubility and Efficacy through Covalent Attachment to Polyvalent DNA–Nanoparticle Conjugates. *ACS Nano* **2011**, *5*, 6962–6970.

### CHAPTER III

- (1) Winkler, D. A.; Mombelli, E.; Pietroiusti, A.; Tran, L.; Worth, A.; Fadeel, B.; McCall, M. J. Applying Quantitative Structure–Activity Relationship Approaches to Nanotoxicology: Current Status and Future Potential. *Toxicology* **2013**, *313*, 15–23.
- (2) Voutchkova, A. M.; Osimitz, T. G.; Anastas, P. T. Toward a Comprehensive Molecular Design Framework for Reduced Hazard. *Chem. Rev.* **2010**, *110*, 5845–5882.
- (3) Mieszawska, A. J.; Mulder, W. J. M.; Fayad, Z. A.; Cormode, D. P. Multifunctional Gold Nanoparticles for Diagnosis and Therapy of Disease. *Mol. Pharm.* **2013**, *10*, 831–847.
- (4) Suk, J. S.; Xu, Q.; Kim, N.; Hanes, J.; Ensign, L. M. PEGylation as a Strategy for Improving Nanoparticle-Based Drug and Gene Delivery. *Adv. Drug Deliv. Rev.* **2016**, *99*, 28–51.
- (5) Cheng, Z.; Al Zaki, A.; Hui, J. Z.; Muzykantov, V. R.; Tsourkas, A. Multifunctional Nanoparticles: Cost versus Benefit of Adding Targeting and Imaging Capabilities. *Science* **2012**, *338*, 903–910.
- (6) Ong, Q.; Luo, Z.; Stellacci, F. Characterization of Ligand Shell for Mixed-Ligand Coated Gold Nanoparticles. *Acc. Chem. Res.* **2017**, *50*, 1911–1919.
- (7) Bobo, D.; Robinson, K. J.; Islam, J.; Thurecht, K. J.; Corrie, S. R. Nanoparticle-Based Medicines: A Review of FDA-Approved Materials and Clinical Trials to Date. *Pharm. Res.* **2016**, *33*, 2373–2387.
- (8) Harper, S. L.; Carriere, J. L.; Miller, J. M.; Hutchison, J. E.; Maddux, B. L. S.; Tanguay, R. L. Systematic Evaluation of Nanomaterial Toxicity: Utility of Standardized Materials and Rapid Assays. *ACS Nano* **2011**, *5*, 4688–4697.
- (9) Truong, L.; Zaikova, T.; Schaeublin, N. M.; Kim, K.-T.; Hussain, S. M.; Hutchison, J. E.; Tanguay, R. L. Residual Weakly Bound Ligands Influence Biological Compatibility of Mixed Ligand Shell, Thiol-Stabilized Gold Nanoparticles. *Environ. Sci. Nano* **2017**, *4*, 1634–1646.
- (10) Ginzburg, A. L.; Truong, L.; Tanguay, R. L.; Hutchison, J. E. Synergistic Toxicity Produced by Mixtures of Biocompatible Gold Nanoparticles and Widely Used Surfactants. *ACS Nano* **2018**, *12*, 5312–5322.

- (11) Li, S.-D.; Huang, L. Stealth Nanoparticles: High Density but Sheddable PEG Is a Key for Tumor Targeting. *J Control Release* **2011**, *145*, 178–181.
- (12) Perry, J. L.; Reuter, K. G.; Kai, M. P.; Herlihy, K. P.; Jones, S. W.; Luft, J. C.; Napier, M.; Bear, J. E.; Desimone, J. M. PEGylated PRINT Nanoparticles: The Impact of PEG Density on Protein Binding, Macrophage Association, Biodistribution, and Pharmacokinetics. *Nano Lett.* **2012**, *12*, 5304–5310.
- (13) Link, C.; Alexis, F.; Pridgen, E.; Molnar, L. K. Factors Affecting the Clearance and Biodistribution of Polymeric Nanoparticles. *Mol. Pharm.* **2015**, *5*, 505–515.
- (14) Zuckerman, J. E.; Choi, C. H. J.; Han, H.; Davis, M. E. Polycation-SiRNA Nanoparticles Can Disassemble at the Kidney Glomerular Basement Membrane. *Proc. Natl. Acad. Sci.* **2012**, *109*, 3137–3142.
- (15) Gold, A. A.; Ghosh, P. S.; Kim, C.; Han, G.; Forbes, N. S.; Rotello, V. M. Surface Charge Density of Amino Acid- Efficient Gene Delivery Vectors by Tuning the Surface Charge Density Of. *ACS Nano* **2008**, *2*, 2213–2218.
- (16) Rana, S.; Bajaj, A.; Mout, R.; Rotello, V. M. Monolayer Coated Gold Nanoparticles for Delivery Applications. *Adv. Drug Deliv. Rev.* **2012**, *64*, 200–216.
- (17) Bilensoy, E. Cationic Nanoparticles for Cancer Therapy. *Expert Opin Drug Deliv.* **2010**, *7*, 795–809.
- (18) Fröhlich, E. The Role of Surface Charge in Cellular Uptake and Cytotoxicity of Medical Nanoparticles. *Int. J. Nanomedicine* **2012**, *7*, 5577–5591.
- (19) Leroueil, P. R.; Berry, S. A.; Duthie, K.; Han, G.; Rotello, V. M.; McNerny, D. Q.; Baker, J. R.; Orr, B. G.; Holl, M. M. B. Wide Varieties of Cationic Nanoparticles Induce Defects in Supported Lipid Bilayers. *Nano Lett.* **2008**, *8*, 420–424.
- (20) Hwang, T.-L.; Aljuffali, I. A.; Lin, C.-F.; Chang, Y.-T.; Fang, J.-Y. Cationic Additives in Nanosystems Activate Cytotoxicity and Inflammatory Response of Human Neutrophils: Lipid Nanoparticles versus Polymeric Nanoparticles. *Int. J. Nanomedicine* **2015**, 371–385.
- (21) Lv, H.; Zhang, S.; Wang, B.; Cui, S.; Yan, J. Toxicity of Cationic Lipids and Cationic Polymers in Gene Delivery. *J. Control. Release* **2006**, *114*, 100–109.
- (22) Malek, A.; Merkel, O.; Fink, L.; Czubayko, F.; Kissel, T.; Aigner, A. In Vivo Pharmacokinetics, Tissue Distribution and Underlying Mechanisms of Various PEI(-PEG)/SiRNA Complexes. *Toxicol. Appl. Pharmacol.* **2009**, *236*, 97–108.

- (23) Luong, D.; Kesharwani, P.; Deshmukh, R.; Mohd Amin, M. C. I.; Gupta, U.; Greish, K.; Iyer, A. K. PEGylated PAMAM Dendrimers: Enhancing Efficacy and Mitigating Toxicity for Effective Anticancer Drug and Gene Delivery. *Acta Biomater.* **2016**, *43*, 14–29.
- (24) Bugel, S. M.; Tanguay, R. L.; Planchart, A. Zebrafish: A Marvel of High-Throughput Biology for 21st Century Toxicology. *Curr Environ Health Rep.* **2014**, *1*, 341–352.
- (25) Elliott, E. W.; Haben, P. M.; Hutchison, J. E. Subnanometer Control of Mean Core Size During Mesofluidic Synthesis of Small ( $D_{\text{core}} < 10 \text{ Nm}$ ) Water-Soluble, Ligand-Stabilized Gold Nanoparticles. *Langmuir* **2015**, *31*, 11886–11894.
- (26) Elliott, E. W.; Ginzburg, A. L.; Kennedy, Z. C.; Feng, Z.; Hutchison, J. E. Single-Step Synthesis of Small, Azide-Functionalized Gold Nanoparticles: Versatile, Water-Dispersible Reagents for Click Chemistry. *Langmuir* **2017**, *33*, 5796–5802.
- (27) Woehrle, G. H.; Warner, M. G.; Hutchison, J. E. Molecular-Level Control of Feature Separation in One-Dimensional Nanostructure Assemblies Formed by Biomolecular Nanolithography. *Langmuir* **2004**, *20*, 5982–5988.
- (28) Warner, M. G.; Hutchison, J. E. Linear Assemblies of Nanoparticles Electrostatically Organized on DNA Scaffolds. *Nat. Mater.* **2003**, *2*, 272–277.
- (29) Marbella, L. E.; Millstone, J. E. NMR Techniques for Noble Metal Nanoparticles. *Chem. Mater.* **2015**, *27*, 2721–2739.
- (30) Oliveri, A. F.; Elliott, E. W.; Carnes, M. E.; Hutchison, J. E.; Johnson, D. W. Elucidating Inorganic Nanoscale Species in Solution: Complementary and Corroborative Approaches. *ChemPhysChem* **2013**, *14*, 2655–2661.
- (31) McKenzie, L. C.; Haben, P. M.; Kevan, S. D.; Hutchison, J. E. Determining Nanoparticle Size in Real Time by Small-Angle X-Ray Scattering in a Microscale Flow System. *J. Phys. Chem. C* **2010**, *114*, 22055–22063.
- (32) Truong, L.; Zaikova, T.; Baldock, B. L.; Balik-meisner, M.; To, K.; Reif, D. M.; Kennedy, Z. C.; Hutchison, J. E.; Tanguay, L. Systematic Determination of the Relationship between Nanoparticle Core Diameter and Toxicity for a Series of Structurally Analogous Gold Nanoparticles in Zebrafish. *Nanotoxicology* **2019**, ASAP.
- (33) Zhu, ZJ; Carboni, R; Quercio, MJ Jr; Yan, B; Miranda, OR; Anderton, DL; Arcaro, KF; Rotello, VM; Vachet, R. Surface Properties Dictate Uptake, Distribution, Excretion, and Toxicity of Nanoparticles in Fish. **2010**, *6*, 2261–2265.

- (34) Kim, S. T.; Saha, K.; Kim, C.; Rotello, V. M. The Role of Surface Functionality in Determining Nanoparticle Cytotoxicity. *Acc. Chem. Res.* **2013**, *46*, 681–691.
- (35) Pillai, P. P.; Huda, S.; Kowalczyk, B.; Grzybowski, B. A. Controlled PH Stability and Adjustable Cellular Uptake of Mixed-Charge Nanoparticles. *J. Am. Chem. Soc.* **2013**, *135*, 6392–6395.
- (36) Goodman, C. M.; McCusker, C. D.; Yilmaz, T.; Rotello, V. M. Toxicity of Gold Nanoparticles Functionalized with Cationic and Anionic Side Chains. *Bioconjug. Chem.* **2004**, *15*, 897–900.
- (37) Ehrenberg, M. S.; Friedman, A. E.; Finkelstein, J. N.; Oberdörster, G.; McGrath, J. L. The Influence of Protein Adsorption on Nanoparticle Association with Cultured Endothelial Cells. *Biomaterials* **2009**, *30*, 603–610.
- (38) Aggarwal, P.; Hall, J. B.; McLeland, C. B.; Dobrovolskaia, M. A.; McNeil, S. E. Nanoparticle Interaction with Plasma Proteins as It Relates to Particle Biodistribution, Biocompatibility and Therapeutic Efficacy. *Adv. Drug Deliv. Rev.* **2009**, *61*, 428–437.
- (39) Bekdemir, A.; Stellacci, F. A Centrifugation-Based Physicochemical Characterization Method for the Interaction between Proteins and Nanoparticles. *Nat. Commun.* **2016**, *7*, 1–8.
- (40) Alisar, S. Z.; Cheryl, A. D.; Michael, V. P. Macrophage Uptake of Core-Shell Nanoparticles Surface Modified with Poly(Ethylene Glycol). *Langmuir* **2006**, *22*, 8178–8185.
- (41) Chan, W. C. W.; Guo, H.; Emili, A.; Walkey, C. D.; Olsen, J. B. Nanoparticle Size and Surface Chemistry Determine Serum Protein Adsorption and Macrophage Uptake. *J. Am. Chem. Soc.* **2011**, *134*, 2139–2147.
- (42) Yang, C.; Gao, S.; Dagnæs-Hansen, F.; Jakobsen, M.; Kjems, J. Impact of PEG Chain Length on the Physical Properties and Bioactivity of PEGylated Chitosan/SiRNA Nanoparticles in Vitro and in Vivo. *ACS Appl. Mater. Interfaces* **2017**, *9*, 12203–12216.
- (43) Libutti, S. K.; Paciotti, G. F.; Byrnes, A. A.; Alexander, H. R.; Gannon, W. E.; Walker, M.; Seidel, G. D.; Yuldasheva, N.; Tamarkin, L. Phase I and Pharmacokinetic Studies of CYT-6091, a Novel PEGylated Colloidal Gold-RhTNF Nanomedicine. *Clin Cancer Res.* **2010**, *16*, 6139–6149.
- (44) Wang, S.; Huang, P.; Chen, X. Stimuli-Responsive Programmed Specific Targeting in Nanomedicine. *ACS Nano* **2016**, *10*, 2991–2994.

- (45) Kimmel, C. B.; Ballard, W. W.; Kimmel, S. R.; Ullmann, B.; Schilling, T. F. Stages of Embryonic Development of the Zebrafish. *Dev. Dyn.* **1995**, *203*, 253–310.
- (46) Mandrell, D.; Truong, L.; Jephson, C.; Sarker, M. R.; Moore, A.; Lang, C.; Simonich, M. T.; Tanguay, R. L. Automated Zebrafish Chorion Removal and Single Embryo Placement: Optimizing Throughput of Zebrafish Developmental Toxicity Screens. *J Lab Autom* **2012**, *17*, 66–74.
- (47) Truong, L.; Bugel, S. M.; Chlebowski, A.; Usenko, C. Y.; Simonich, M. T.; Simonich, S. L. M.; Tanguay, R. L. Optimizing Multi-Dimensional High Throughput Screening Using Zebrafish. *Reprod. Toxicol.* **2016**, *65*, 139–147.
- (48) Truong, L., Harper, S.L., Tanguay, R. L. Evaluation of Embryotoxicity Using the Zebrafish Model. In *Drug Safety Evaluation: Methods and Protocols*; Humana, Press: Totowa, NJ, 2010; pp. 271–279.
- (49) Truong, L.; Reif, D. M.; Mary, L. S.; Geier, M. C.; Truong, H. D.; Tanguay, R. L. Multidimensional in Vivo Hazard Assessment Using Zebrafish. *Toxicol. Sci.* **2014**, *137*, 212–233.

#### CHAPTER IV

- (1) Coe-Sullivan, S. Quantum Dot Developments. *Nat. Photonics* **2009**, *3*, 315–316.
- (2) Qu, X.; Alvarez, P. J. J.; Li, Q. Applications of Nanotechnology in Water and Wastewater Treatment. *Water Res.* **2013**, *47*, 3931–3946.
- (3) Nohynek, G. J.; Lademann, J.; Ribaud, C.; Roberts, M. S. Grey Goo on the Skin? Nanotechnology, Cosmetic and Sunscreen Safety. *Crit. Rev. Toxicol.* **2007**, *37*, 251–277.
- (4) Ki, H. Y.; Kim, J. H.; Kwon, S. C.; Jeong, S. H. A Study on Multifunctional Wool Textiles Treated with Nano-Sized Silver. *J. Mater. Sci.* **2007**, *42*, 8020–8024.
- (5) Wicki, A.; Witzigmann, D.; Balasubramanian, V.; Huwyler, J. Nanomedicine in Cancer Therapy: Challenges, Opportunities, and Clinical Applications. *J. Control. Release* **2015**, *200*, 138–157.
- (6) Kim, C.; Ghosh, P.; Rotello, V. M. Multimodal Drug Delivery Using Gold Nanoparticles. *Nanoscale* **2009**, *1*, 61–67.

- (7) Hwu, J. R.; Lin, Y. S.; Josephrajan, T.; Hsu, M.; Cheng, F.; Yeh, C.; Su, W.; Shieh, D. Targeted Paclitaxel by Conjugation to Iron Oxide and Gold Nanoparticles Targeted Paclitaxel by Conjugation to Iron Oxide and Gold Nanoparticles. *J. Am. Chem. Soc.* **2009**, *131*, 66–68.
- (8) Reed, R. B.; Zaikova, T.; Barber, A.; Simonich, M.; Lankone, R.; Marco, M.; Hristovski, K.; Herckes, P.; Passantino, L.; Fairbrother, D. H.; Tanguay, R.; Ranville, J. F.; Hutchison, J. E.; Westerhoff, P. K. Potential Environmental Impacts and Antimicrobial Efficacy of Silver- and Nanosilver-Containing Textiles. *Environ. Sci. Technol.* **2016**, *50*, 4018–4026.
- (9) Wang, Y.; Yuan, L.; Yao, C.; Ding, L.; Li, C.; Fang, J.; Sui, K.; Liu, Y.; Wu, M. A Combined Toxicity Study of Zinc Oxide Nanoparticles and Vitamin C in Food Additives. *Nanoscale* **2014**, *6*, 15333–15342.
- (10) Papakostas, D.; Rancan, F.; Sterry, W.; Blume-Peytavi, U.; Vogt, A. Nanoparticles in Dermatology. *Arch. Dermatol. Res.* **2011**, *303*, 533–550.
- (11) *Surfactants in Personal Care Products and Decorative Cosmetics*; Rhein, L. D.; Schlossman, M.; O'Lenick, A.; Somasundaran, P., Eds.; 3rd ed.; CRC Press: Boca Raton, 2007.
- (12) *Mixture Toxicity: Linking Approaches from Ecological and Human Toxicology*; Gestel, C. A. M. van; Jonker, M.; Kammenga, J. E.; Laskowski, R.; Svendsen, C., Eds.; 1st ed.; CRC Press: Boca Raton, 2010.
- (13) Cedergreen, N. Quantifying Synergy: A Systematic Review of Mixture Toxicity Studies within Environmental Toxicology. *PLoS One* **2014**, *9*, e96580.
- (14) Rodea-Palomares, I.; González-Pleiter, M.; Martín-Betancor, K.; Rosal, R.; Fernández-Piñas, F. Additivity and Interactions in Ecotoxicity of Pollutant Mixtures: Some Patterns, Conclusions, and Open Questions. *Toxics* **2015**, *3*, 342–369.
- (15) Alassane-Kpembé, I.; Kolf-Clauw, M.; Gauthier, T.; Abrami, R.; Abiola, F. A.; Oswald, I. P.; Puel, O. New Insights into Mycotoxin Mixtures: The Toxicity of Low Doses of Type B Trichothecenes on Intestinal Epithelial Cells Is Synergistic. *Toxicol. Appl. Pharmacol.* **2013**, *272*, 191–198.
- (16) Gauthier, P. T.; Norwood, W. P.; Prepas, E. E.; Pyle, G. G. Metal-PAH Mixtures in the Aquatic Environment: A Review of Co-Toxic Mechanisms Leading to More-than-Additive Outcomes. *Aquat. Toxicol.* **2014**, *154*, 253–269.

- (17) European Food Safety Authority. *Harmonisation of Risk Assessment Methodologies for Human Health and Ecological Risk Assessment of Combined Exposure to Multiple Chemicals*; Public consultation on the terms of reference of the Scientific Committee Working Group, EFSA Technical Report, European Union, 2016.
- (18) European Food Safety Authority. *Harmonisation of Human and Ecological Risk Assessment of Combined Exposure to Multiple Chemicals*; Scientific Colloquium 21, EFSA Summary Report, European Union, 2015.
- (19) Nohynek, G. J.; Antignac, E.; Re, T.; Toutain, H. Safety Assessment of Personal Care Products/cosmetics and Their Ingredients. *Toxicol. Appl. Pharmacol.* **2010**, *243*, 239–259.
- (20) SCHER; SCCS; SCENIHR. *Opinion on the Toxicity and Assessment of Chemical Mixtures*; European Commission, 2012.
- (21) Nel, A. E.; Mädler, L.; Velegol, D.; Xia, T.; Hoek, E. M. V.; Somasundaran, P.; Klaessig, F.; Castranova, V.; Thompson, M. Understanding Biophysicochemical Interactions at the Nano-Bio Interface. *Nat. Mater.* **2009**, *8*, 543–557.
- (22) Stankus, D. P.; Lohse, S. E.; Hutchison, J. E.; Nason, J. A. Interactions between Natural Organic Matter and Gold Nanoparticles Stabilized with Different Organic Capping Agents. *Environ. Sci. Technol.* **2011**, *45*, 3238–3244.
- (23) Maiorano, G.; Sabella, S.; Sorce, B.; Brunetti, V.; Malvindi, M. A.; Cingolani, R.; Pompa, P. P. Effects of Cell Culture Media on the Dynamic Formation of Protein-Nanoparticle Complexes and Influence on the Cellular Response. *ACS Nano* **2010**, *4*, 7481–7491.
- (24) Hvolbæk, B.; Janssens, T. V. W.; Clausen, B. S.; Falsig, H.; Christensen, C. H.; Nørskov, J. K. Catalytic Activity of Au Nanoparticles. *Nanotoday* **2007**, *2*, 14–18.
- (25) Lundqvist, M.; Stigler, J.; Elia, G.; Lynch, I.; Cedervall, T.; Dawson, K. A. Nanoparticle Size and Surface Properties Determine the Protein Corona with Possible Implications for Biological Impacts. *Proc. Natl. Acad. Sci.* **2008**, *105*, 14265–14270.
- (26) Casals, E.; Pfaller, T.; Duschl, A.; Oostingh, G. J.; Puentes, V. Time Evolution of the Nanoparticle Protein Corona. *ACS Nano* **2010**, *4*, 3623–3632.
- (27) Mensch, A. C.; Hernandez, R. T.; Kuether, J. E.; Torelli, M. D.; Feng, Z. V.; Hamers, R. J.; Pedersen, J. A. Natural Organic Matter Concentration Impacts the Interaction of Functionalized Diamond Nanoparticles with Model and Actual Bacterial Membranes. *Environ. Sci. Technol.* **2017**, *51*, 11075–11084.

- (28) Derfus, A. M.; Chan, W. C. W.; Bhatia, S. N. Probing the Cytotoxicity of Semiconductor Quantum Dots. *Nano Lett.* **2004**, *4*, 11–18.
- (29) Contado, C. Nanomaterials in Consumer Products: A Challenging Analytical Problem. *Front. Chem.* **2015**, *3*, 1–20.
- (30) Karakoti, A. S.; Das, S.; Thevuthasan, S.; Seal, S. PEGylated Inorganic Nanoparticles. *Angew. Chem. Int. Ed.* **2011**, *50*, 1980–1994.
- (31) Harper, S. L.; Carriere, J. L.; Miller, J. M.; Hutchison, J. E.; Maddux, B. L. S.; Tanguay, R. L. Systematic Evaluation of Nanomaterial Toxicity: Utility of Standardized Materials and Rapid Assays. *ACS Nano* **2011**, *5*, 4688–4697.
- (32) Som, I.; Bhatia, K.; Yasir, M. Status of Surfactants as Penetration Enhancers in Transdermal Drug Delivery. *J. Pharm. Bioallied Sci.* **2012**, *4*, 2–9.
- (33) Qian, C.; McClements, D. J. Formation of Nanoemulsions Stabilized by Model Food-Grade Emulsifiers Using High-Pressure Homogenization: Factors Affecting Particle Size. *Food Hydrocoll.* **2011**, *25*, 1000–1008.
- (34) Kim, H.; Park, K.; Lee, M.-Y. Biocompatible Dispersion Methods for Carbon Black. *Toxicol. Res.* **2012**, *28*, 209–216.
- (35) Cao, Y.; Roursgaard, M.; Kermanizadeh, A.; Loft, S.; Møller, P. Synergistic Effects of Zinc Oxide Nanoparticles and Fatty Acids on Toxicity to Caco-2 Cells. *Int. J. Toxicol.* **2015**, *34*, 67–76.
- (36) Belden, J. B.; Gilliom, R. J.; Lydy, M. J. How Well Can We Predict the Toxicity of Pesticide Mixtures to Aquatic Life? *Integr. Environ. Assess. Manag.* **2007**, *3*, 364–372.
- (37) Westerfield, M. *The Zebrafish Book: A Guide for the Laboratory Use of Zebrafish (Danio Rerio)*; 5th ed.; University of Oregon Press: Eugene, OR, 2007.
- (38) Harper, S. L.; Dahl, J. A.; Maddux, B. L. S.; Tanguay, R. L.; Hutchison, J. E. Proactively Designing Nanomaterials to Enhance Performance and Minimise Hazard. *Int. J. Nanotechnol.* **2008**, *5*, 124–142.
- (39) United States Environmental Protection Agency. Safer Chemical Ingredients List <https://www.epa.gov/saferchoice/safer-ingredients> (accessed Feb 17, 2018).
- (40) U.S. Food and Drug Administration. CFR - Code of Federal Regulations Title 21 <https://www.accessdata.fda.gov/scripts/cdrh/cfdocs/cfcfr/cfrsearch.cfm> (accessed Feb 17, 2018).

- (41) United States Environmental Protection Agency. United States High Production Volume Challenge Program List  
[https://iaspub.epa.gov/sor\\_internet/registry/substreg/LandingPage.do](https://iaspub.epa.gov/sor_internet/registry/substreg/LandingPage.do) (accessed Feb 17, 2018).
- (42) Food Safety Commission. *Evaluation Report of Food Additives “Polysorbate 20, Polysorbate 60, Polysorbate 65 and Polysorbate 80”*; 2007.
- (43) Brown, D. M.; Johnston, H. J.; Gaiser, B.; Pinna, N.; Caputo, G.; Culha, M.; Kelestemur, S.; Altunbek, M.; Stone, V.; Roy, J. C.; Kinross, J. H.; Fernandes, T. F. A Cross-Species and Model Comparison of the Acute Toxicity of Nanoparticles Used in the Pigment and Ink Industries. *NanoImpact* **2018**, *11*, 20–32.
- (44) Gu, Y.-J.; Cheng, J.; Lin, C.-C.; Lam, Y. W.; Cheng, S. H.; Wong, W.-T. Nuclear Penetration of Surface Functionalized Gold Nanoparticles. *Toxicol. Appl. Pharmacol.* **2009**, *237*, 196–204.
- (45) Alkilany, A. M.; Murphy, C. J. Toxicity and Cellular Uptake of Gold Nanoparticles: What We Have Learned so Far? *J. Nanoparticle Res.* **2010**, *12*, 2313–2333.
- (46) Lowry, G. V.; Gregory, K. B.; Apte, S. C.; Lead, J. R. Transformation of Nanomaterials in the Environment. *Environ. Sci. Technol.* **2012**, *46*, 6893–6899.
- (47) Negishi, Y.; Nobusada, K.; Tsukuda, T. Glutathione-Protected Gold Clusters Revisited: Bridging the Gap between Gold (I) -Thiolate Complexes and Nanocrystals, Thiolate-Protected Gold Nanocrystals. *J. Am. Chem. Soc.* **2005**, *127*, 5261–5270.
- (48) McKenzie, L. C.; Haben, P. M.; Kevan, S. D.; Hutchison, J. E. Determining Nanoparticle Size in Real Time by Small-Angle X-Ray Scattering in a Microscale Flow System. *J. Phys. Chem. C* **2010**, *114*, 22055–22063.
- (49) Kennedy, Z. C.; Lisowski, C. E.; Mitaru-Berceanu, D. S.; Hutchison, J. E. Influence of Ligand Shell Composition upon Interparticle Interactions in Multifunctional Nanoparticles. *Langmuir* **2015**, *31*, 12742–12752.
- (50) Oliveri, A. F.; Elliott, E. W.; Carnes, M. E.; Hutchison, J. E.; Johnson, D. W. Elucidating Inorganic Nanoscale Species in Solution: Complementary and Corroborative Approaches. *ChemPhysChem* **2013**, *14*, 2655–2661.
- (51) Oliveri, A. F.; Carnes, M. E.; Baseman, M. M.; Richman, E. K.; Hutchison, J. E.; Johnson, D. W. Single Nanoscale Cluster Species Revealed by <sup>1</sup>H NMR Diffusion-Ordered Spectroscopy and Small-Angle X-Ray Scattering. *Angew. Chem. Int. Ed.* **2012**, *51*, 10992–10996.

- (52) Marbella, L. E.; Millstone, J. E. NMR Techniques for Noble Metal Nanoparticles. *Chem. Mater.* **2015**, *27*, 2721–2739.
- (53) Kerssebaum, R.; Salnikov, G. DOSY and Diffusion by NMR. In *A Tutorial for TopSpin 2.0*; Bruker BioSpin GmbH: Rheinstetten, Germany, 2006; pp. 1–32.
- (54) Kim, K. T.; Zaikova, T.; Hutchison, J. E.; Tanguay, R. L. Gold Nanoparticles Disrupt Zebrafish Eye Development and Pigmentation. *Toxicol. Sci.* **2013**, *133*, 275–288.
- (55) Truong, L.; Zaikova, T.; Schaeublin, N. M.; Kim, K.-T.; Hussain, S. M.; Hutchison, J. E.; Tanguay, R. L. Residual Weakly Bound Ligands Influence Biological Compatibility of Mixed Ligand Shell, Thiol-Stabilized Gold Nanoparticles. *Environ. Sci. Nano* **2017**, *4*, 1634–1646.
- (56) Sambandan, D. R.; Ratner, D. Sunscreens: An Overview and Update. *J. Am. Acad. Dermatol.* **2011**, *64*, 748–758.
- (57) Muller, J.; Huaux, F.; Moreau, N.; Misson, P.; Heilier, J.-F.; Delos, M.; Arras, M.; Fonseca, A.; Nagy, J. B.; Lison, D. Respiratory Toxicity of Multi-Wall Carbon Nanotubes. *Toxicol. Appl. Pharmacol.* **2005**, *207*, 221–231.
- (58) Ivanković, T.; Hrenović, J. Surfactants in the Environment. *Arh. Hig. Rada Toksikol.* **2010**, *61*, 95–110.
- (59) Maurer-Jones, M. A.; Gunsolus, I. L.; Murphy, C. J.; Haynes, C. L. Toxicity of Engineered Nanoparticles in the Environment. *Anal. Chem.* **2013**, *85*, 3036–3049.
- (60) Kuhn, B.; Guba, W.; Hert, J.; Banner, D.; Bissantz, C.; Ceccarelli, S.; Haap, W.; Körner, M.; Kuglstatter, A.; Lerner, C.; Mattei, P.; Neidhart, W.; Pinard, E.; Rudolph, M. G.; Schulz-Gasch, T.; Woltering, T.; Stahl, M. A Real-World Perspective on Molecular Design. *J. Med. Chem.* **2016**, *59*, 4087–4102.
- (61) Gilbertson, L. M.; Zimmerman, J. B.; Plata, D. L.; Hutchison, J. E.; Anastas, P. T. Designing Nanomaterials to Maximize Performance and Minimize Undesirable Implications Guided by the Principles of Green Chemistry. *Chem. Soc. Rev.* **2015**, *44*, 5758–5777.
- (62) Truong, L.; Bugel, S. M.; Chlebowski, A.; Usenko, C. Y.; Simonich, M. T.; Simonich, S. L. M.; Tanguay, R. L. Optimizing Multi-Dimensional High Throughput Screening Using Zebrafish. *Reprod. Toxicol.* **2016**, *65*, 139–147.
- (63) Valencia, P. M.; Farokhzad, O. C.; Karnik, R.; Langer, R. Microfluidic Technologies for Accelerating the Clinical Translation of Nanoparticles. *Nat. Nanotechnol.* **2012**, *7*, 623–629.

- (64) Bugel, S. M.; Tanguay, R. L.; Planchart, A. Zebrafish: A Marvel of High-Throughput Biology for 21st Century Toxicology. *Curr Environ Health Rep.* **2014**, *1*, 341–352.
- (65) Woehrle, G. H.; Warner, M. G.; Hutchison, J. E. Molecular-Level Control of Feature Separation in One-Dimensional Nanostructure Assemblies Formed by Biomolecular Nanolithography. *Langmuir* **2004**, *20*, 5982–5988.
- (66) Woehrle, G. H.; Brown, L. O.; Hutchison, J. E. Thiol-Functionalized, 1.5-Nm Gold Nanoparticles through Ligand Exchange Reactions: Scope and Mechanism of Ligand Exchange. *J. Am. Chem. Soc.* **2005**, *127*, 2172–2183.
- (67) Elliott, E. W.; Haben, P. M.; Hutchison, J. E. Subnanometer Control of Mean Core Size During Mesofluidic Synthesis of Small ( $D_{\text{core}} < 10$  nm) Water-Soluble, Ligand-Stabilized Gold Nanoparticles. *Langmuir* **2015**, *31*, 11886–11894.
- (68) Sweeney, S. F.; Woehrle, G. H.; Hutchison, J. E. Rapid Purification and Size Separation of Gold Nanoparticles via Diafiltration. *J. Am. Chem. Soc.* **2006**, *128*, 3190–3197.
- (69) Kimmel, C. B.; Ballard, W. W.; Kimmel, S. R.; Ullmann, B.; Schilling, T. F. Stages of Embryonic Development of the Zebrafish. *Dev. Dyn.* **1995**, *203*, 253–310.
- (70) Mandrell, D.; Truong, L.; Jephson, C.; Sarker, M. R.; Moore, A.; Lang, C.; Simonich, M. T.; Tanguay, R. L. Automated Zebrafish Chorion Removal and Single Embryo Placement: Optimizing Throughput of Zebrafish Developmental Toxicity Screens. *J. Lab Autom.* **2012**, *17*, 66–74.
- (71) Tecan. Rapid Generation of Dose-Response Curves for High Throughput Screening. *Tecan J.* **2015**, 26–27.
- (72) Truong, L., Harper, S.L., Tanguay, R. L. Evaluation of Embryotoxicity Using the Zebrafish Model. In *Drug Safety Evaluation: Methods and Protocols*; Humana, Press: Totowa, NJ, 2010; pp. 271–279.
- (73) Truong, L.; Reif, D. M.; Mary, L. S.; Geier, M. C.; Truong, H. D.; Tanguay, R. L. Multidimensional *In Vivo* Hazard Assessment Using Zebrafish. *Toxicol. Sci.* **2014**, *137*, 212–233.
- (74) Truong, L.; Tilton, S. C.; Zaikova, T.; Richman, E.; Waters, K. M.; Hutchison, J. E.; Tanguay, R. L. Surface Functionalities of Gold Nanoparticles Impact Embryonic Gene Expression Responses. *Nanotoxicology* **2013**, *7*, 192–201.

## CHAPTER V

- (1) LaMotte, S. Sunscreen Enters Bloodstream After Just One Day of Use, Study Says. *CNN* [Online] **2019**, <https://www.cnn.com/2019/05/06/health/sunscreen-bloodstream-fda-study/index.html> (accessed Aug 7, 2019).
- (2) Bever, L. Hawaii Just Banned Your Favorite Sunscreen to Protect its Coral Reefs. *The Washington Post* [Online] **2018**, [https://www.washingtonpost.com/news/energy-environment/wp/2018/07/02/hawaii-is-about-to-ban-your-favorite-sunscreen-to-protect-its-coral-reefs/?noredirect=on&utm\\_term=.ea3fd711bc41](https://www.washingtonpost.com/news/energy-environment/wp/2018/07/02/hawaii-is-about-to-ban-your-favorite-sunscreen-to-protect-its-coral-reefs/?noredirect=on&utm_term=.ea3fd711bc41) (accessed Apr 1, 2019).
- (3) Matta, M. K.; et al. Effect of Sunscreen Application under Maximal Use Conditions on Plasma Concentration of Sunscreen Active Ingredients: A Randomized Clinical Trial. *JAMA* **2019**, *321*, 2082–2091.
- (4) Downs, C. A.; et al. Toxicopathological Effects of the Sunscreen UV Filter, Oxybenzone (Benzophenone-3), on Coral Planulae and Cultured Primary Cells and Its Environmental Contamination in Hawaii and the U.S. Virgin Islands. *Arch. Environ. Contam. Toxicol.* **2016**, *70*, 265–288.
- (5) U.S. Food and Drug Administration. Enforcement Policy - OTC Sunscreen Drug Products Marketed Without an Approved Application. *Center for Drug Evaluation and Research, Guideline for Industry* [Online] **2018**, <https://www.fda.gov/regulatory-information/search-fda-guidance-documents/enforcement-policy-otc-sunscreen-drug-products-marketed-without-approved-application> (accessed Aug 1, 2019).
- (6) Canadian Centre for Occupational Health and Safety. Ultraviolet Radiation. *Government of Canada* [Online] **2016**, [https://www.ccohs.ca/oshanswers/phys\\_agents/ultravioletradiation.html](https://www.ccohs.ca/oshanswers/phys_agents/ultravioletradiation.html) (accessed Aug 2, 2019).
- (7) Kerr, J. B.; Fioletov, V. E. Surface Ultraviolet Radiation. *Atmos. - Ocean* **2008**, *46*, 159–184.
- (8) State of Hawaii. *Senate Bill No. 2571*; 2018; p. Twenty-Ninth Legislature.
- (9) Environmental Working Group. EWG's 13th Annual Guide to Sunscreens. [Online] **2019**, <https://www.ewg.org/sunscreen/report/executive-summary/> (accessed Aug 7, 2019).
- (10) Lewicka, Z. A.; Yu, W. W.; Oliva, B. L.; Contreras, E. Q.; Colvin, V. L. Photochemical Behavior of Nanoscale TiO<sub>2</sub> and ZnO Sunscreen Ingredients. *J. Photochem. Photobiol. A Chem.* **2013**, *263*, 24–33.

- (11) Bar-Ilan, O.; Louis, K. M.; Yang, S. P.; Pedersen, J. A.; Hamers, R. J.; Peterson, R. E.; Heideman, W. Titanium Dioxide Nanoparticles Produce Phototoxicity in the Developing Zebrafish. *Nanotoxicology* **2012**, *6*, 670–679.
- (12) Kim, E. J.; Kim, M. J.; Im, N. R.; Park, S. N. Photolysis of the Organic UV Filter, Avobenzone, Combined with Octyl Methoxycinnamate by Nano-TiO<sub>2</sub> Composites. *J. Photochem. Photobiol. B Biol.* **2015**, *149*, 196–203.
- (13) Regulation (EC) No 1223/2009 of The European Parliament and of The Council of 30 November 2009 on Cosmetic Products. *Off. J. Eur. Union* **2009**, Annex VI, List of UV Filters Allowed in Cosmetic Products.
- (14) Kockler, J.; Oelgemöller, M.; Robertson, S.; Glass, B. D. Photostability of Sunscreens. *J. Photochem. Photobiol. C Photochem. Rev.* **2012**, *13*, 91–110.
- (15) Butt, S. T.; Christensen, T. Toxicity and Phototoxicity of Chemical Sun Filters. *Radiat. Prot. Dosimetry* **2000**, *91*, 283–286.
- (16) Sayre, R. M.; Dowdy, J. C.; Gerwig, A. J.; Shields, W. J.; Lloyd, R. V. Unexpected Photolysis of the Sunscreen Octinoxate in the Presence of the Sunscreen Avobenzone. *Photochem. Photobiol.* **2005**, *81*, 452–456.
- (17) Crovara Pescia, A.; Astolfi, P.; Puglia, C.; Bonina, F.; Perrotta, R.; Herzog, B.; Damiani, E. On the Assessment of Photostability of Sunscreens Exposed to UVA Irradiation: From Glass Plates to Pig/Human Skin, Which Is Best? *Int. J. Pharm.* **2012**, *427*, 217–223.
- (18) Hojerová, J.; Medovčíková, A.; Mikula, M. Photoprotective Efficacy and Photostability of Fifteen Sunscreen Products Having the Same Label SPF Subjected to Natural Sunlight. *Int. J. Pharm.* **2011**, *408*, 27–38.
- (19) Forestier, S. Rationale for Sunscreen Development. *J. Am. Acad. Dermatol.* **2008**, *58*, s133–s138.
- (20) Gonzalez, S.; Gilaberte, Y.; Philips, N.; Juarranz, A. Current Trends in Photoprotection-A New Generation of Oral Photoprotectors. *Open Dermatol. J.* **2011**, *5*, 6–14.
- (21) Afonso, S.; Horita, K.; Sousa E Silva, J. P.; Almeida, I. F.; Amaral, M. H.; Lobão, P. A.; Costa, P. C.; Miranda, M. S.; Esteves Da Silva, J. C. G.; Sousa Lobo, J. M. Photodegradation of Avobenzone: Stabilization Effect of Antioxidants. *J. Photochem. Photobiol. B Biol.* **2014**, *140*, 36–40.

- (22) Kockler, J.; Oelgemöller, M.; Robertson, S.; Glass, B. Influence of Titanium Dioxide Particle Size on the Photostability of the Chemical UV-Filters Butyl Methoxy Dibenzoylmethane and Octocrylene in a Microemulsion. *Cosmetics* **2014**, *1*, 128–139.
- (23) Karlsson, I.; Hillerström, L.; Stenfeldt, A. L.; Mårtensson, J.; Börje, A. Photodegradation of Dibenzoylmethanes: Potential Cause of Photocontact Allergy to Sunscreens. *Chem. Res. Toxicol.* **2009**, *22*, 1881–1892.
- (24) Dondi, D.; Albini, A.; Serpone, N. Interactions between Different Solar UVB/UVA Filters Contained in Commercial Suncreams and Consequent Loss of UV Protection. *Photochem. Photobiol. Sci.* **2006**, *5*, 835–843.
- (25) Truong, L.; Bugel, S. M.; Chlebowski, A.; Usenko, C. Y.; Simonich, M. T.; Simonich, S. L. M.; Tanguay, R. L. Optimizing Multi-Dimensional High Throughput Screening Using Zebrafish. *Reprod. Toxicol.* **2016**, *65*, 139–147.
- (26) BASF Sunscreen Simulator [Online], [https://www.sunscreensimulator.basf.com/Sunscreen\\_Simulator/](https://www.sunscreensimulator.basf.com/Sunscreen_Simulator/) (accessed Jul 21, 2019).
- (27) Kimmel, C. B.; Ballard, W. W.; Kimmel, S. R.; Ullmann, B.; Schilling, T. F. Stages of Embryonic Development of the Zebrafish. *Dev. Dyn.* **1995**, *203*, 253–310.
- (28) Westerfield, M. *The Zebrafish Book: A Guide for the Laboratory Use of Zebrafish (Danio Rerio)*; 5th ed.; University of Oregon Press: Eugene, OR, 2007.
- (29) Mandrell, D.; Truong, L.; Jephson, C.; Sarker, M. R.; Moore, A.; Lang, C.; Simonich, M. T.; Tanguay, R. L. Automated Zebrafish Chorion Removal and Single Embryo Placement: Optimizing Throughput of Zebrafish Developmental Toxicity Screens. *J Lab Autom* **2012**, *17*, 66–74.
- (30) Truong, L., Harper, S.L., Tanguay, R. L. Evaluation of Embryotoxicity Using the Zebrafish Model. In *Drug Safety Evaluation: Methods and Protocols*; Humana, Press: Totowa, NJ, 2010; pp. 271–279.
- (31) Making Skincare. How To Make a Lotion. [Online], <http://makingskincare.com/how-to-make-a-lotioncream-part-1-equipment-and-ingredients/> (accessed Aug 2, 2019).
- (32) Moloney, F. J.; Collins, S.; Murphy, G. M. Sunscreens: Safety, Efficacy and Appropriate Use. *Am. J. Clin. Dermatol.* **2002**, *3*, 185–191.

- (33) Fukui, H.; Horie, M.; Endoh, S.; Kato, H.; Fujita, K.; Nishio, K.; Komaba, L. K.; Maru, J.; Miyauhi, A.; Nakamura, A.; Kinugasa, S.; Yoshida, Y.; Hagihara, Y.; Iwahashi, H. Association of Zinc Ion Release and Oxidative Stress Induced by Intratracheal Instillation of ZnO Nanoparticles to Rat Lung. *Chem. Biol. Interact.* **2012**, *198*, 29–37.
- (34) U.S. Food and Drug Administration. PART 352 -- SUNSCREEN DRUG PRODUCTS FOR OVER-THE-COUNTER HUMAN USE.
- (35) Shamoto, Y.; Yagi, M.; Oguchi-Fujiyama, N.; Miyazawa, K.; Kikuchi, A. Photophysical Properties of Hexyl Diethylaminohydroxybenzoylbenzoate (Uvinul A Plus), a UV-A Absorber. *Photochem. Photobiol. Sci.* **2017**, *16*, 1449–1457.
- (36) Reisch, M. S. After More Than A Decade, FDA Still Won't Allow New Sunscreens. *Chemical and engineering news*. May 2015, pp. 10–15.
- (37) Shahbandeh, M. Forecasted market value of sun care worldwide from 2018 to 2024. [Online] **2019**, <https://www.statista.com/statistics/812522/sun-care-market-value-global/> (accessed Aug 7, 2019).
- (38) Maugh, T. H. FDA Issues New Rules for Sunscreen Labeling. *Los Angeles Times* [Online] **2011**, <https://www.latimes.com/health/la-xpm-2011-jun-15-la-0615-sunscreens-20110615-story.html> (accessed Aug 7, 2019).

## CHAPTER VI

- (1) Anastas, P. T.; Warner, J. C. *Green Chemistry: Theory and Practice*; Oxford University Press: Oxford, 1998.
- (2) Betts, K. How Industrial Applications in Green Chemistry Are Changing Our World. *American Chemical Society* [Online] **2015**, <https://www.acs.org/content/dam/acsorg/membership/acs/benefits/extra-insights/green-chemistry-applications.pdf> (accessed Apr 1, 2019).
- (3) Erythropel, H. C.; Zimmerman, J. B.; De Winter, T. M.; Petitjean, L.; Melnikov, F.; Lam, C. H.; Lounsbury, A. W.; Mellor, K. E.; Janković, N. Z.; Tu, Q.; Pincus, L. N.; Falinski, M. M.; Shi, W.; Coish, P.; Plata, D. L.; Anastas, P. T. The Green ChemisTREE: 20 Years after Taking Root with the 12 Principles. *Green Chem.* **2018**, *20*, 1929–1961.
- (4) Haack, J. A.; Hutchison, J. E. Green Chemistry Education: 25 Years of Progress and 25 Years Ahead. *ACS Sustain. Chem. Eng.* **2016**, *4*, 5889–5896.
- (5) Anastas, P.; Eghbali, N. Green Chemistry: Principles and Practice. *Chem. Soc. Rev.* **2010**, *39*, 301–312.

- (6) Dahl, R. Green Washing: Do You Know What You're Buying? *Environ. Health Perspect.* **2010**, *118*, 246–252.
- (7) Tabone, M. D.; Cregg, J. J.; Beckman, E. J.; Landis, A. E. Sustainability Metrics : Life Cycle Assessment and Green Design in Polymers. *Environ. Sci. Technol.* **2010**, *44*, 8264–8269.
- (8) Matlin, S. A.; Mehta, G.; Hopf, H.; Krief, A. One-World Chemistry and Systems Thinking. *Nat. Chem.* **2016**, *8*, 393–398.
- (9) Assaraf, O. B. Z.; Orion, N. Development of System Thinking Skills in the Context of Earth System Education. *J. Res. Sci. Teach.* **2005**, *42*, 518–560.
- (10) Hogan, K. Assessing Students' Systems Reasoning in Ecology. *J. Biol. Educ.* **2000**, *35*, 22–28.
- (11) Libarkin, J. C.; Kurdziel, J. P. Ontology and the Teaching of Earth System Science. *J. Geosci. Educ.* **2006**, *54*, 408–413.
- (12) Guron, M.; Paul, J. J.; Roeder, M. H. Incorporating Sustainability and Life Cycle Assessment into First-Year Inorganic Chemistry Major Laboratories. *J. Chem. Educ.* **2016**, *93*, 639–644.
- (13) Marteel-Parrish, A. E. Teaching Green and Sustainable Chemistry: A Revised One-Semester Course Based on Inspirations and Challenges. *J. Chem. Educ.* **2014**, *91*, 1084–1086.
- (14) Vervaeke, M. Life Cycle Assessment Software for Product and Process Sustainability Analysis. *J. Chem. Educ.* **2012**, *89*, 884–890.
- (15) Waddell, D. C.; Ringo, J. M.; Das, A.; Hopgood, H.; Denlinger, K. L.; Haley, R. A. Graduate Student Designed and Delivered: An Upper-Level Online Course for Undergraduates in Green Chemistry and Sustainability. *J. Chem. Educ.* **2018**, *95*, 560–569.
- (16) Bode, C. J.; Chapman, C.; Pennybaker, A.; Subramaniam, B. Developing Students' Understanding of Industrially Relevant Economic and Life Cycle Assessments. *J. Chem. Educ.* **2017**, *94*, 1798–1801.
- (17) Bouldin, R. M.; Folchman-Wagner, Z. Chemistry of Sustainable Products: Filling the Business Void in Green-Chemistry Curricula. *J. Chem. Educ.* **2019**, ASAP.
- (18) Salvia, V. Problem Solvers United. *Eugene Weekly* [Online] **2013**, <https://www.eugeneweekly.com/2013/10/03/problem-solvers-united/> (accessed Apr 1, 2019).

- (19) Meadows, D. H. *Thinking in Systems*; Wright, D., Ed.; Earthscan: London, UK, 2009.
- (20) Master's Industrial Internship Program at the University of Oregon  
<https://internship.uoregon.edu/> (accessed Apr 1, 2019).
- (21) Di Landro, L.; Sala, G.; Olivieri, D. Deformation Mechanisms and Energy Absorption of Polystyrene Foams for Protective Helmets. *Polym. Test.* **2002**, *21*, 217–228.
- (22) Kostal, J.; Voutchkova-Kostal, A.; Anastas, P. T.; Zimmerman, J. B. Identifying and Designing Chemicals with Minimal Acute Aquatic Toxicity. *Proc. Natl. Acad. Sci.* **2014**, *112*, 6289–6294.
- (23) Gilbertson, L. M.; Zimmerman, J. B.; Plata, D. L.; Hutchison, J. E.; Anastas, P. T. Designing Nanomaterials to Maximize Performance and Minimize Undesirable Implications Guided by the Principles of Green Chemistry. *Chem. Soc. Rev.* **2015**, *44*, 5758–5777.
- (24) Price Waterhouse Coopers. Life Cycle Assessment of the Industrial Use of Expanded Polystyrene Packaging in Europe. [Online] **2001**,  
[http://www.anape.es/pdf/gabinete\\_oi.pdf](http://www.anape.es/pdf/gabinete_oi.pdf)  
(accessed Apr 1, 2019).
- (25) Lithner, D.; Larsson, A.; Dave, G. Environmental and Health Hazard Ranking and Assessment of Plastic Polymers Based on Chemical Composition. *Sci. Total Environ.* **2011**, *409*, 3309–3324.
- (26) Ahmad, M.; Bajahlan, A. S. Leaching of Styrene and Other Aromatic Compounds in Drinking Water from PS Bottles. *J. Environ. Sci.* **2007**, *19*, 421–426.
- (27) Tan, R. B. H.; Khoo, H. H. Life Cycle Assessment of EPS and CPB Inserts: Design Considerations and End of Life Scenarios. *J. Environ. Manage.* **2005**, *74*, 195–205.
- (28) Searchinger, T.; Heimlich, R.; Houghton, R. A.; Dong, F.; Elobeid, A.; Fabiosa, J.; Tokgoz, S.; Hayes, D.; Yu, T. Use of U.S. Croplands for Biofuels Increases Greenhouse Gases Through Emissions from Land-Use Change. *Science* **2008**, *319*, 1238–1240.
- (29) Schut, J. H. Water-Blown EPS Will Help You and the Environment. *Plastics Technology*  
[Online] **2010**, <https://www.ptonline.com/articles/water-blown-eps-will-help-you-and-the-environment> (accessed Apr 1, 2019).

- (30) Medding, J. A.; Love, B. J. Evaluation of Collisional Damage in Polystyrene Foam Constructions Using a Dual Hammer Impact Test. *Polym. Eng. Sci.* **1996**, *36*, 1286–1289.
- (31) Krundaeva, A.; Bruyne, G. De; Gagliardi, F.; Paepegem, W. Van. Dynamic Compressive Strength and Crushing Properties of Expanded Polystyrene Foam for Different Strain Rates and Different Temperatures. *Polym. Test.* **2016**, *55*, 61–68.
- (32) Mills, N. J.; Fitzgerald, C.; Gilchrist, A.; Verdejo, R. Polymer Foams for Personal Protection: Cushions, Shoes and Helmets. *Compos. Sci. Technol.* **2003**, *63*, 2389–2400.
- (33) Qiao, P.; Yang, M.; Bobaru, F. Impact Mechanics and High-Energy Absorbing Materials : Review. *J. Aerosp. Eng.* **2008**, *21*, 235–248.
- (34) Bomgardner, M.; Baum, R. Empowering a sustainable world. *Chemical & Engineering News* [Online] **2018**, <https://cen.acs.org/environment/green-chemistry/Empowering-sustainable-world/96/web/2018/07> (accessed Apr 1, 2019).

## APPENDIX A

- (1) Amaral, S. P.; Fernandez-villamarin, M.; Correa, J.; Riguera, R.; Fernandez-megia, E. Efficient Multigram Synthesis of the Repeating Unit of Gallic Acid-Triethylene Glycol Dendrimers. *Org. Lett.* **2011**, *13*, 4522–4525.
- (2) Woehrle, G. H.; Brown, L. O.; Hutchison, J. E. Thiol-Functionalized, 1.5-Nm Gold Nanoparticles through Ligand Exchange Reactions: Scope and Mechanism of Ligand Exchange. *J. Am. Chem. Soc.* **2005**, *127*, 2172–2183.
- (3) Haben, P. M. Controlling the Synthesis of Bunte Salt Stabilized Gold Nanoparticles Using a Microreactor Platform in Concert with Small Angle X-Ray Scattering Analysis, The University of Oregon, 2013.
- (4) Yu, C.-S.; Oberdorfer, F. Synthesis of (E)-5-[2-(Tri-N-Butylstannyl)vinyl] Substituted 2'-Deoxyuridine Derivatives for Use in Halogenation and Radiohalogenation Reactions. *Synlett* **2000**, No. 1, 86–88.
- (5) Elliott, E. W.; Haben, P. M.; Hutchison, J. E. Subnanometer Control of Mean Core Size During Mesofluidic Synthesis of Small ( $D_{\text{core}} < 10 \text{ Nm}$ ) Water-Soluble, Ligand-Stabilized Gold Nanoparticles. *Langmuir* **2015**, *31*, 11886–11894.

## APPENDIX B

- (1) Marbella, L. E.; Millstone, J. E. NMR Techniques for Noble Metal Nanoparticles. *Chem. Mater.* **2015**, *27*, 2721–2739.

## APPENDIX C

- (1) Elliott, E. W.; Haben, P. M.; Hutchison, J. E. Subnanometer Control of Mean Core Size During Mesofluidic Synthesis of Small ( $D_{\text{core}} < 10$  nm) Water-Soluble, Ligand-Stabilized Gold Nanoparticles. *Langmuir* **2015**, *31*, 11886–11894.
- (2) Marbella, L. E.; Millstone, J. E. NMR Techniques for Noble Metal Nanoparticles. *Chem. Mater.* **2015**, *27*, 2721–2739.
- (3) Zhmud, B. Viscosity Blending Equations. *Lube: The European Lubricants Industry Magazine* **2014**, No. 121, 22–27.

## APPENDIX E

- (1) Price Waterhouse Coopers. Life Cycle Assessment of the Industrial Use of Expanded Polystyrene Packaging in Europe. [Online] **2001**, [http://www.anape.es/pdf/gabinete\\_oi.pdf](http://www.anape.es/pdf/gabinete_oi.pdf) (accessed Apr 1, 2019)
- (2) Tan, R. B. H.; Khoo, H. H. Life Cycle Assessment of EPS and CPB Inserts: Design Considerations and End of Life Scenarios. *J. Environ. Manage.* **2005**, *74*, 195–205.
- (3) Tabone, M. D.; Cregg, J. J.; Beckman, E. J.; Landis, A. E. Sustainability Metrics : Life Cycle Assessment and Green Design in Polymers. *Environ. Sci. Technol.* **2010**, *44*, 8264–8269.
- (4) Lithner, D.; Larsson, A.; Dave, G. Environmental and Health Hazard Ranking and Assessment of Plastic Polymers Based on Chemical Composition. *Sci. Total Environ.* **2011**, *409*, 3309–3324.
- (5) Schut, J. H. Water-Blown EPS Will Help You and the Environment. *Plastics Technology* [Online] **2010**, <https://www.ptonline.com/articles/water-blown-eps-will-help-you-and-the-environment> (accessed Apr 1, 2019).
- (6) Bever, L. Hawaii just banned your favorite sunscreen to protect its coral reefs. *The Washington Post* [Online] **2018**, [https://www.washingtonpost.com/news/energy-environment/wp/2018/07/02/hawaii-is-about-to-ban-your-favorite-sunscreen-to-protect-its-coral-reefs/?noredirect=on&utm\\_term=.3ceb90cd4171](https://www.washingtonpost.com/news/energy-environment/wp/2018/07/02/hawaii-is-about-to-ban-your-favorite-sunscreen-to-protect-its-coral-reefs/?noredirect=on&utm_term=.3ceb90cd4171) (accessed Apr 1, 2019).
- (7) Schneider, S. L.; Lim, H. W. Review of Environmental Effects of Oxybenzone and Other Sunscreen Active Ingredients. *J. Am. Acad. Dermatol.* **2019**, *80*, 266–271.

- (8) Natarajan, S.; Bajaj, H. C.; Tayade, R. J. Recent Advances Based on the Synergetic Effect of Adsorption for Removal of Dyes from Waste Water Using Photocatalytic Process. *J. Environ. Sci.* **2018**, *65*, 201–222.